"TECTONIC" MAGNETIC FABRICS IN PURE AND SIMPLE SHEAR: EXPERIMENTAL INVESTIGATIONS

by

CRAIG STEVEN ALFORD©

Submitted in partial fulfillment
of the requirements for the degree
of

Master of Science

Geology Department
Lakehead University
Thunder Bay, Ontario, Can.

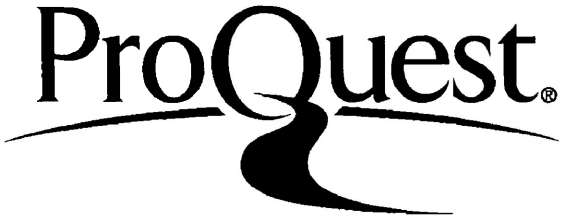

ISBN 0-315-44785-0

ABSTRACT

Triaxial compression tests were preformed such that changes in the magnetic susceptibility anisotropy with strain would be represented by experimental approximations of simple shear and pure shear. Both types of tests were performed on artificial materials of high magnetic susceptibility at room temperature and atmospheric pore fluid pressure. Experimental displacement-rates and strain-rates were computer controlled during testing.

Two different shear zone materials were employed for the "simple shear" testing, a sand-cement mixture and a calcite-cement mixture. Three series of simple shear tests were conducted on the sand-cement material at various confining pressures; Series A, at 0.689 kbars, Series B at 1.0 kbar and Series C at 1.5 kbars. Two series of simple shear tests were conducted on the calcite-cement material, Series 1, at 1.0 kbar confining pressure and Series 2 at 1.5 kbars P_C. For both materials a constant axial displacement-rate of 5.0×10^{-6} inches. s^{-1} (corresponding to a slip displacement-rate on the shear zone walls of 8.7×10^{-6} inches. s^{-1}) was employed. Final

shear strain values ranged from 0.025 γ to 0.378 γ.

One series of pure shear deformation was conducted on the calcite-cement material at 1.5 kbars confining pressure employing a constant natural strain-rate of 5.0×10^{-6} s^{-1}. Final axial strain values ranged from 4.42% to 18.3% shortening.

The development of simulated "tectonic" magnetic fabrics in both pure and simple shear has been achieved. Principal directions of susceptibility rotate sometimes in complex patterns toward 'tectonically' significant stable orientations. Magnitudes of susceptibility show progressive changes consonant with the intensity of strain such that there appears to exist a consistent relation between the change in the degree of anisotropy of susceptibility ($\Delta P'$) and the bulk strain ratio (ln X/Z) for both the pure and simple shear experiments.

ACKNOWLEDGEMENTS

The author gratefully acknowledges Dr. Graham Borradaile who supervised and provided financial support for this study from NSERC grant A6861. His perception, constructive criticisms, guidance, and enthusiasm were highly valued.

Most of the rock deformation equipment was purchased from a grant provided by the Board of Industrial Leadership and Developement (BILD) of Ontario.

Dr. W. Keeler and Dr. M. Hawton of the physics department of Lakehead Universtiy are acknowledged for their valuable insight, criticisms and assistance.

Technical assistance was generously provided by Don Lough, Dianne Crothers, Anne Hammond, Maureen Artist and Sam Spivak. Many thanks go out to each one of them for their contributions to this work.

Thanks are extended to all my fellow graduate students, in particular Perry Sarvas and Owen Steele for their help and camaraderie.

A special note of thanks goes to Carol Lormand, for her love, assistance and understanding, without whom my life would be a little less unpredictable but all that much more boring.

Finally I acknowledge with gratitude the receipt of a Lakehead University Graduate Entrance Scholarship and a Ontario Graduate Scholarship during my studies.

TABLE OF CONTENTS

CHAPTER ONE

Introduction

Recently, the uses of magnetic susceptibility anisotropy (MSA) have received considerable attention in structural and tectonic geology. The orientations of the principal susceptibility directions have been shown to correspond to the orientations of sedimentary, magnetic and tectonic fabrics (Hrouda 1982; ref. therein).

In the case of tectonically deformed rocks, the principal susceptibilities, which define the magnetic susceptibility magnitude ellipsoid, often correspond to the principal strain directions determined from conventional strain markers (ie. Rathore 1979; Wood et al., 1976). Thus, in the absence of conventional strain or fabric markers, the cryptic fabric of the magnetic minerals in the rock may provide information on the principal strain orientations.

Furthermore, it has been suggested by Rathore (1979; with Henry 1982) that the axial ratios of the magnetic susceptibility magnitude ellipsoid may correspond with the axial ratios of the strain ellipsoid. However, a follow up study of this idea (Borradaile and Mothersill 1984) has shown that the method by which such correlations were obtained is invalid.

Recently, in a study of experimentally deformed materials (Borradaile and Alford 1987) a correlation between strain and

magnetic susceptibility was discovered by correlating the macroscopically determined strain with the change in the anisotropy of magnetic susceptibility.

Aims and Scope of the Thesis

This investigation focusses upon the bulk strain effects during pure and simple shear on two multigranular, multimineralic materials with disseminated ferrimagnetic marker grains.

In order to refine our knowledge on the correlations between susceptibility and strain in deformed rocks, attention must be focussed on the following:

(i) From which minerals does the magnetic susceptibility originate?

(ii) What was the state of the primary or pre-tectonic susceptibility anisotropy?

(iii) What are the various processes affecting the rock that alter the original susceptibility (K_{ij}) to the final susceptibility (K'_{ij}) ?

(iv) What is the state of the finite strain of the rock (e_{ij})?

Problems invariably arise in determining these four items in naturally deformed rocks. While this does not altogether undermine the value of MSA studies, it does leave questions unanswered in linking the four items.

This investigation attempts to address these problems by observing the results of laboratory experiments using artificial materials;

(a) of known magnetic mineralogy

(b) of known original susceptibility, and

(c) subjected to progressive increments of experimental deformation such that the bulk finite strains (e_{ij}) are known

Using such a method, something of three (i, ii and iv) of the previous four items in question are known. In addition, the artificial materials can be subjected to stress relaxation testing and microscopic thin-section examination in the deformed and undeformed state such that (iii), the deformation processes affecting the original susceptibility may be investigated.

Experiments of a similar nature have been previously conducted (Borradaile and Alford 1987). This earlier work will provide an invaluable guideline for the experiments of this investigation. However, the previous tests were all conducted under conditions of pure shear, where the finite and incremental strain ellipse are coaxial. This investigation will attempt to produce a non-coaxial strain history by employing a shear zone configuration in order to deform the specimens in simple shear. Furthermore, two compositionally different materials will be deformed such that the effect of differing predominant deformation mechanisms may be observed in the changes of susceptibility. For similar purposes, one series of pure shear tests will be conducted using a material compositionally different than the material in Borradaile and Alford (1987) .

CHAPTER TWO
PREVIOUS WORK

It has only been very recently that a study of the observed changes in the anisotropy and shape of the magnetic susceptibility magnitude ellipsoid in experimentally deformed materials has been undertaken (Borradaile & Alford 1987). A considerable amount of work has been conducted, however, in the fields of experimental deformation of rocks, stress relaxation, deformation mechanisms, magnetic susceptibility and magnetic susceptibility anisotropy studies. This thesis intends to integrate some of this work, thus a brief review of the results and the related work in these fields is necessary.

Experimental Deformation of Rock:

The study of experimentally deformed rocks has provided innumerable contributions to our understanding of the mechanical behaviour of rocks within the Earth's crust. Observations on the macroscopic scale (scale of the specimen) provide knowledge of the effects of physical conditions on the rheological behaviour of rocks, while microscopic observations describe how the rock accommodates strain.

The experimental deformation of rocks, minerals and synthetic analogues have been achieved generally by three types of tests:

1) Creep Tests: where a constant axial load is maintained on

the material after the initial, almost instantaneous loading.

2) Compression Tests: where the axial load is initially progressively increased, and thereafter adjusted, usually to maintain a constant rate of strain. Compression is normally along the long axis of the specimen with $\sigma_1 > \sigma_2 = \sigma_3$ in 'triaxial' tests.

3) Extension Tests: much like compression tests, however the rock is extended in the direction of the long axis of the specimen and $\sigma_1 = \sigma_2 > \sigma_3$ for 'triaxial' tests.

An understanding of the physical conditions to which deformed rocks have been exposed within the crust and upper mantle has been essential in the development and progression of laboratory apparatus and experimentation. Since any specific geological structure is the result of both fundamental processes and incidental conditions (Dahlstrom 1970), it has been the effort of the experimentalist not to attempt to reproduce exact geologic circumstances or specific metamorphic textures, but instead toward the testing of fundamental processes. Therefore tests are deliberately unrealistic as, for any forcast of the mechanical behaviour of rocks, the relative contributions of each process must be separately investigated and understood.

At present, all regionally consistent temperatures and confining pressures within the crust and upper mantle can be experimentally simulated. With computer-assistance, precise measurement and control of the experimental strain-rates and

differential stresses can be made during testing.

The current study used a Donath-type triaxial compression testing apparatus (see Chapter 3). A brief review of the mechanical effects of the major physical parameters discovered in the compression testing of materials is presented. Only those variable with the present experimental deformation apparatus will be discussed.

Confining Pressure- From a mechanical standpoint, the chief function of increasing confining pressure is to inhibit macroscopic shear failures in the material by subsequently increasing the stress normal to all potential fracture planes (Carter 1976). The increase in confining pressure has three important effects; 1) the strain reached before macroscopic failure increases markedly, 2) it enhances the possibility of ductile flow and 3) there is a greater extent and degree of strain hardening in the ductile deformation at higher pressures (Paterson 1978). Figure 2-1 displays a stress vs. strain graph which illustrates these three effects.

Macroscopically the effects can be considered in terms of dilatancy, which is defined as the inelastic increase in volume during deformation under applied differential stress (Paterson 1978). With increased confining pressure, the magnitude of the dilatancy decreases (Figure 2-2), subsequently increasing the range of truly elastic behaviour, the 'strength' of the material and promoting work hardening.

Figure 2-1. Progression in the nature of the stress-strain curve in triaxial compression tests as confining pressure is increased. The differential stress before yield is increased with higher confining pressures, as well as the resistance to failure in the rock.

(from Paterson 1978)

Figure 2-2. Volume changes (Dilatancy) versus strain for various confining pressures. Higher confining pressures inhibit dilatancy.

(from Paterson 1978)

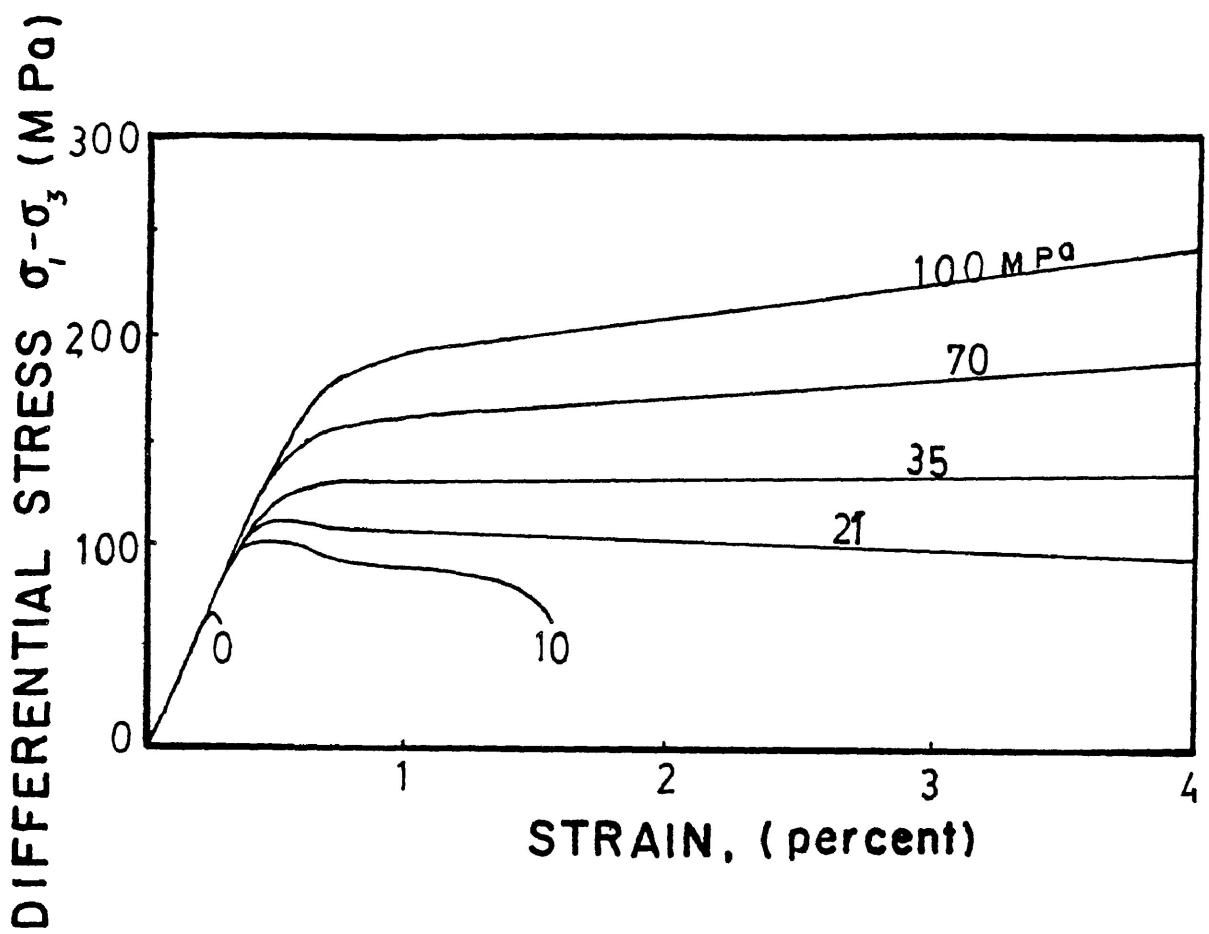
DIFFERENTIAL STRESS $\sigma_1-\sigma_3$ (MPa)
300
200
100
0
100 MPa
70
35
21
0
10
1
2
3
4
STRAIN, (percent)

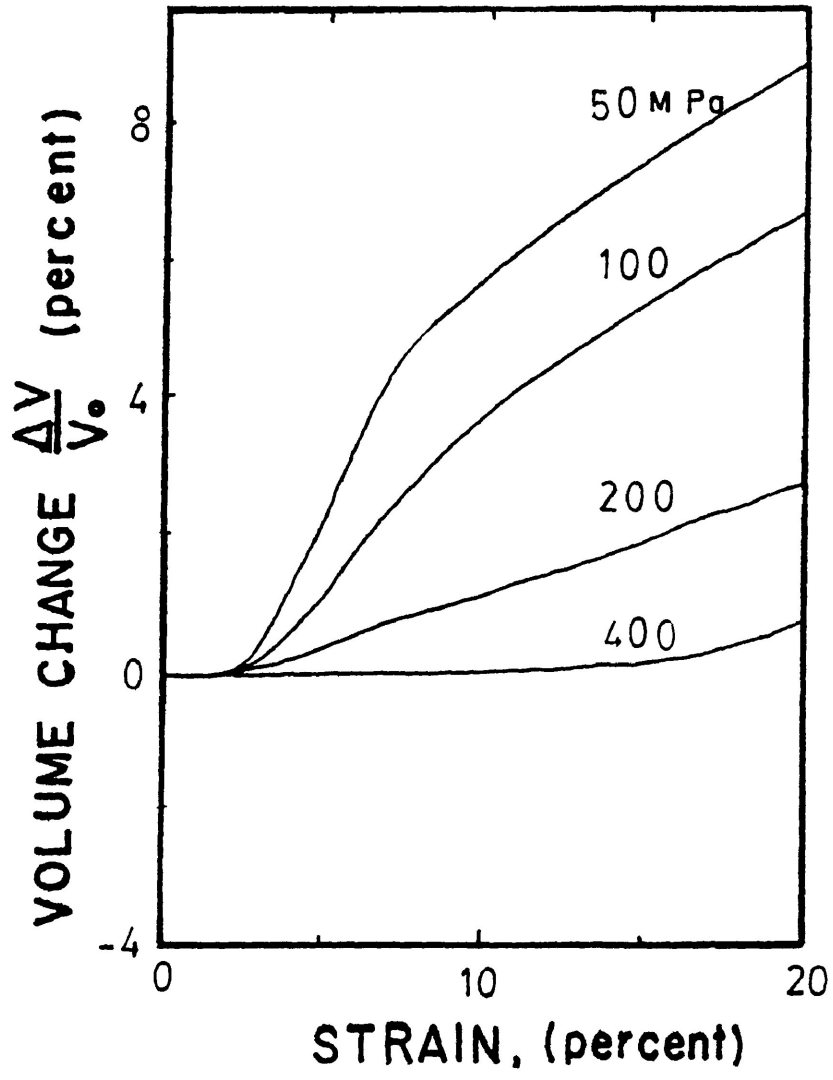
VOLUME CHANGE $\frac{\Delta V}{V_o}$ (percent)
8
4
0
-4
50 MPa
100
200
400
0
10
20
STRAIN, (percent)

Pore Fluid Pressure- The mechanical effect of increasing pore fluid pressure is to enhance fracturing by reducing the normal stress on potential fracture planes. Figure 2-3 illustrates the role of pore fluid pressure in reducing the stress normal between grain contacts. When pore fluid pressures are low, this same effect has been noted to enhance the macroscopic ductility of a specimen (Rutter 1972) (Figure 2-4)

Temperature- Mechanically, the increase of temperature enhances ductility and decreases the differential stress required for the rock to yield, hence it 'weakens' the rock. Experimentally, it has been noted that some confining pressure is required to enhance ductility as the increase in temperature alone is usually ineffective in doing so, even when the constituent minerals would normally be ductile at such temperatures. Reasons for this include the suppression of grain boundary parting resulting from anisotropic thermal expansion, the avoidance of decomposition or other phase changes leading to disintegration (when the ambient temperature becomes close to the melting temperature) and the inadequacy of easily activated slip systems to satisfy intergranular strain compatibility requirements (Paterson 1978).

Strain Rate- Estimates of geologic strain-rates have been made by various processes; geodetic measurements of surface displacements, rebound from ancient water and ice loads and estimated rates of shortening in orogenic regions (Carter 1976). The rates calculated fall in the range of 10^{-13} to 10^{-15} s^{-1},

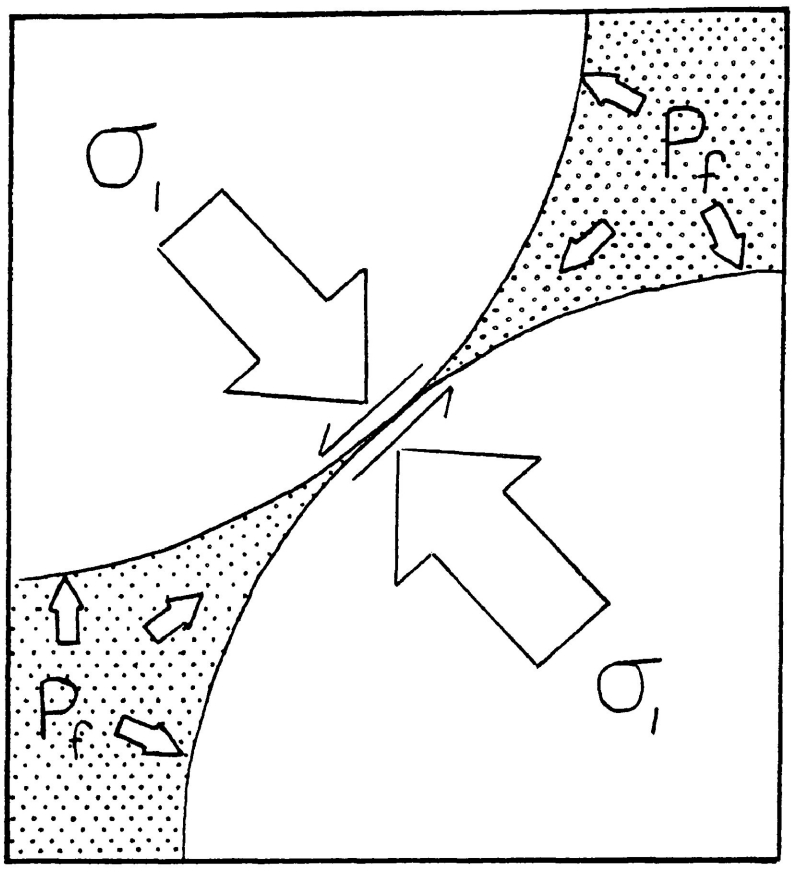

Figure 2-3. Diagram illustrating how pore fluid pressure acts to reduce the stress value at grain contacts. If the pore fluid pressure is large enough the grains may slide past each other.

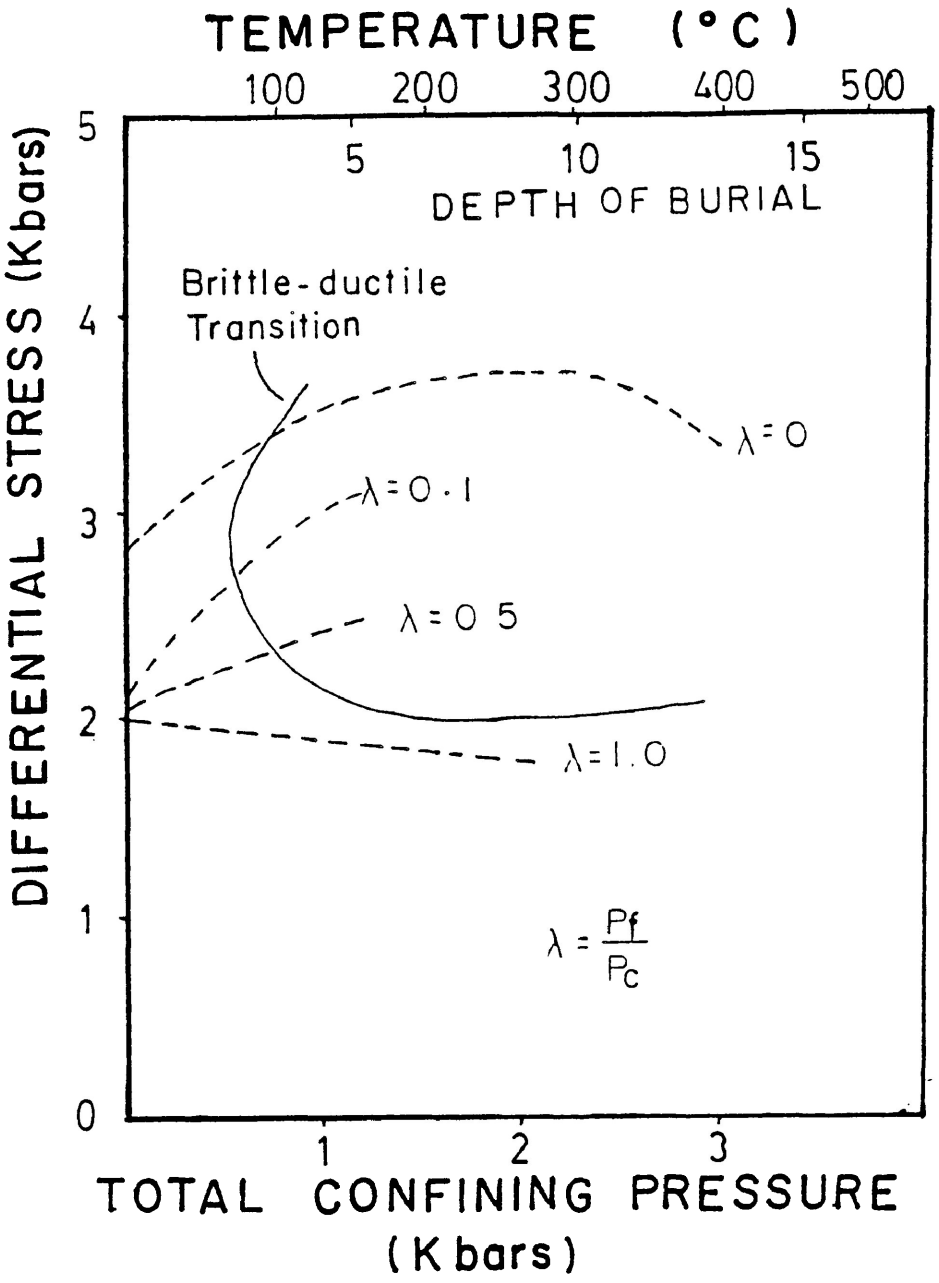

Figure 2-4. Synoptic diagram showing the effects of a barothermal gradient of 135o C/Kbar on the ultimate strength (or strength at 10% strain) on Solnhofen limestone tested dry and 'wet' with various λ values. Note how the differential stress required for ductile behaviour becomes less for for λ>0. However, for large λ values the rock behaves in a brittle manner.

after Rutter (1972)

however, much faster rates (i.e. 10^{-8} s^{-1}) have been estimated for the formation of mylonites (White 1976). Nevertheless, experimental operation at such strain-rates would be impossible, given the necessary time required to accumulate an appreciable amount of strain. Experimental strain-rates are therefore much faster, ranging in value from 10^{-2} to 10^{-6}.

Mechanically the increase in the rate of strain has the same effects as decreasing temperature (Figure 2-5). Thus one can imagine that to create the same mechanical behaviour in a rock as is produced by geological temperatures and strain-rates, one could increase the temperatures to unrealistic levels to account for the experimentally necessary strain-rates (Figure 2-6).

Differential Stress- Experimental differential stresses are commonly much higher than actual crustal differential stress values.

Measured stress differences from various surface mine and borehole methods yield values much lower than 1 kilobar (i.e. Sbar & Sykes 1972; Haimson 1975) as do seismic methods (i.e. Wyss 1970). Thus the range of differential stress values in the lithosphere are probably within a few hundred bars to one kilobar at most, while experimental differential stresses are generally above 1 kilobar. The high stresses are necessary with the high strain-rates in order that the rock is able to flow within the time scale of the laboratory test. As noted earlier, temperatures can be raised to offset the high strain-rates, however, the relevance of

Figure 2-5. Effect of temperature and strain-rate on the stress-strain curve during a triaxial compression test. T1>T2 and e1>e2. Note how by either increasing the temperature or decreasing the strain-rate cause the differential stress at the yield point to decrease. Thus they have a 'weaking' effect on the rock.

(from Paterson 1978)

Figure 2-6. If the geologic mechanical behaviour of a rock is to be simulated in the lab, the temperature must be raised due to the fast laboratory strain-rates.

(from Paterson 1978)

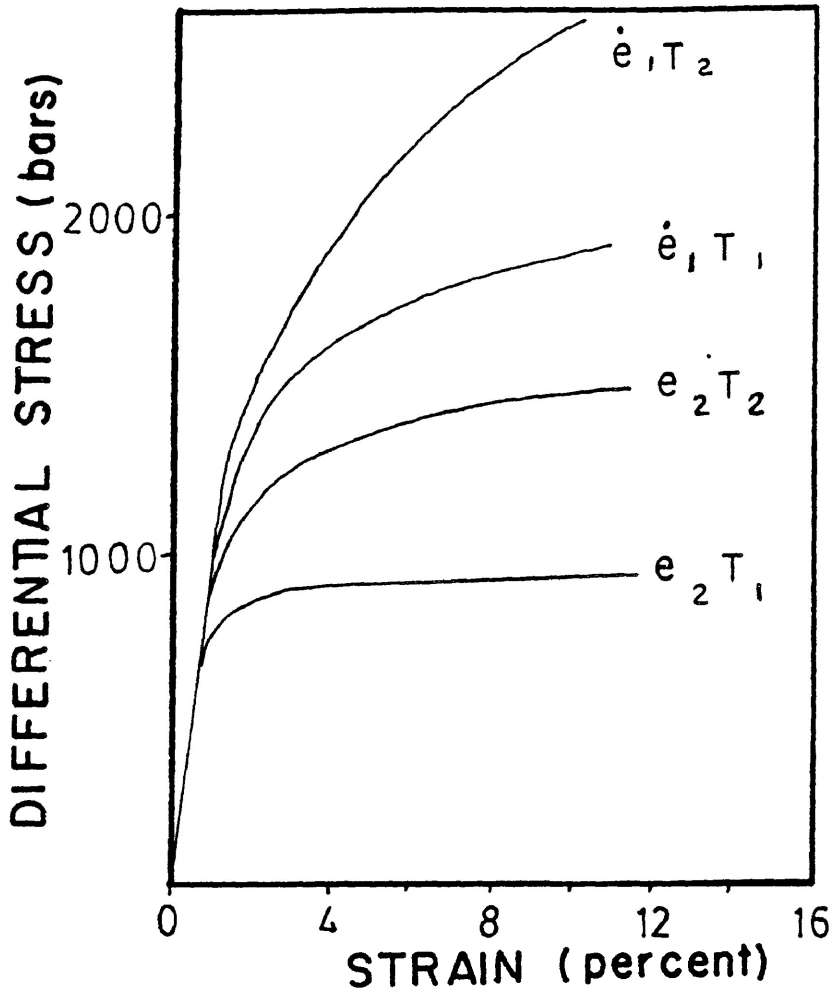
DIFFERENTIAL STRESS (bars)
2000
1000
0
4
8
12
16
STRAIN (percent)
$\dot{e}_1 T_2$
$\dot{e}_1 T_1$
$\dot{e}_2 T_2$
$\dot{e}_2 T_1$

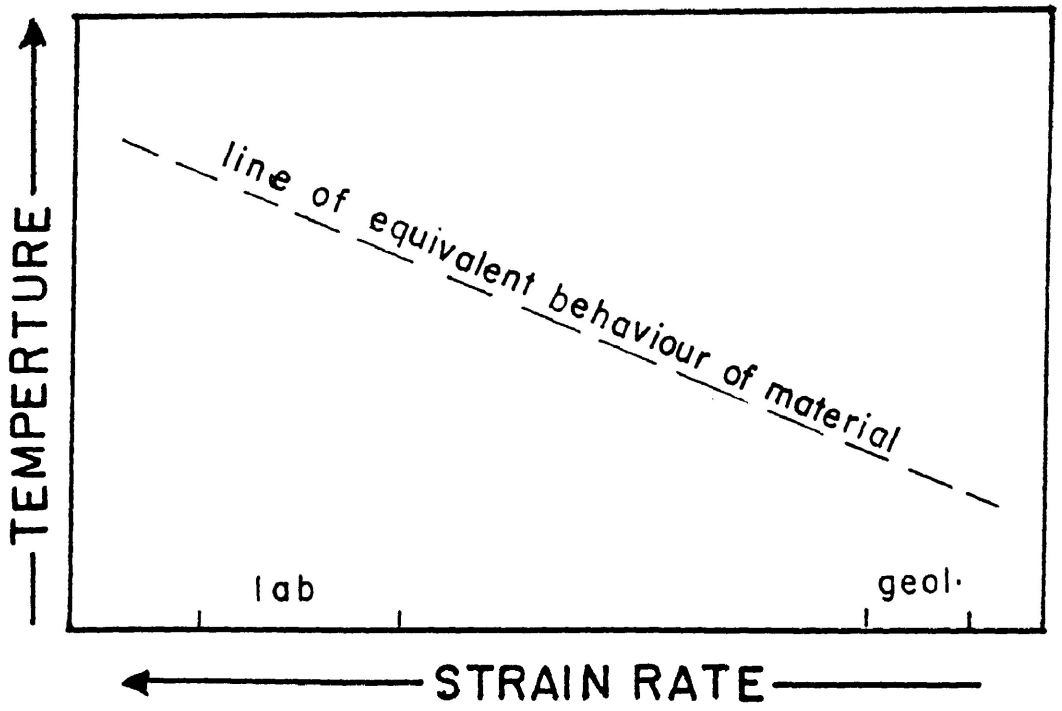
TEMPERTURE
line of equivalent behaviour of material
lab
geol.
STRAIN RATE

such tests would inevitably involve questions on the mechanisms of deformation (Paterson 1987). Thus the experimentalist must be able to demonstrate in some way what the flow processes involved in the experiments are and be aware of those involved in the geologic time scale.

Stress Relaxation:

The stress relaxation or load relaxation test, has been shown to be a relatively quick and useful method for providing the constitutive relations governing a materials inelastic behaviour (i.e. Guiu & Pratt 1964). It was first used, and has been widely accepted in the testing of materials for engineering purposes (i.e. ASTM STP 676) and the relaxation testing of geological materials is now widespread (i.e. Griggs & Blacic 1965; Hobbs 1968, Gupta & Li 1970; Schmid 1976; Rutter & Mainprice 1978; Borradaile & Alford 1987; etc.).

Stress relaxation testing can be conducted at any point in the history of a compression or creep test. After an arbitrary amount of strain, the specimens length is held constant by locking the pistons adjacent to the sample into place. As a result, the stored elastic strain energy in the specimen is dissipated into permanent deformation of the specimen at a rate which is determined by the rheological characteristics of the material (Rutter et al.,1978). The general form of the constitutive flow law is;

$$\dot{e} = A \exp(-H/RT) f_1(\sigma) f_2(S)$$

where $\dot{e}$ is the strain-rate, A a constant, H an activation enthalpy, R the gas constant and T is the absolute temperature. $f_1(\sigma)$ is a function of stress and $f_2(S)$ a function which describes the effect of specimen structure. The form of the equation follows from the experimental fact that the relationships between strain rate and any one of temperature, stress or structure can be determined while holding the other two constant (Dorn 1957). Commonly, the temperature and structure of the material are constant during relaxation and the equation becomes,

$$\dot{e} \propto \sigma^n$$

The stress exponent, n, is determined experimentally by the stress relaxation method, as it is equivalent to the slope of the data determined on a log (stress) versus -log (strain rate) plot by:

$$n = (\dot{e}_2 - \dot{e}_1)/(\sigma_2 - \sigma_1)$$

In this way any significant change in slope of the data, or the n value, will suggest a change from one power flow-law for the material to another, hence a change in the predominant mechanism

of deformation. Composite flow laws, which have the advantage of being able to represent a smooth transition from one dominant deformation mechanism to another may be more applicable when the stress relaxation data fits a curve (Ferguson 1983). However, the value of n can be important in qualitatively determining the predominant deformation mechanism.

Deformation Mechanisms:

The metamorphic textures present in a deformed rock will depend mainly on the relative contributions of the various mechanisms of deformation, which in turn are dependent on the particular physical conditions (T, P_c, $\dot{e}$, etc.) present during deformation.

Crystalline matter may deform by several inter- and intra-granular processes, termed deformation mechanisms. Intergranular deformation, termed particulate flow (Borradaile 1981), encompasses deformation which occurs between grains by slip on grain boundaries and/or by the rotation of grains. Intragranular deformation processes are those responsible for the deformation which occurs within the grains of a rock, resulting in a change of grain shape (op. cit.). Four main independent classes of intragranular deformation mechanisms have been defined:

1) Cataclasis

2) Intracrystalline Plasticity

3) Diffusive Mass Transfer, and

4) Recrystallization

It is important to note that no one mechanism operates solely during deformation. This fact is readily demonstrated in the 'look through' experiments of Means (1977). Thus, reference is often made to mechanisms being either dependent or independent.

Two events, A and B, are said to be dependent if A cannot proceed until B has taken place, so that the processes occur in sequence. The two events are said to be independent if they are not related in any manner and may proceed, each at their own speed (Elliot 1973). Whether a particular mechanism predominates, or is 'rate-controlling' depends upon it being either a dependent or independent process. For independent processes, the overall deformation rate is simply the sum of all the independent rates, the process with the fastest rate effectively dominates. For the dependent processes the overall rate is dominated by the slowest mechanism.

The characteristics of the predominant deformation mechanisms (cataclasis and intracrystalline plasticity) expected to occur under the physical conditions present in the experimental method (high differential stress-low temperature-zero pore fluid pressure) (see the deformation mechanism map of Rutter 1976) will be briefly discussed along with the condition necessary for

the mechanism and the associated microstructures developed by each mechanism.

Cataclastic processes: Cataclasis refers to the permanent straining achieved by the fracturing of grains within the rock and usually results in dilatancy. Fracture results from the extensive or catastrophic growth of microcracks having an orientation such that the applied stress is concentrated at their tips (Tullis 1978). As deformation proceeds, cataclasis may continue causing a progressive reduction in grain size (by fragmentation), these rock fragments may slide past and roll over each other on old and new grain surfaces. This combination of fracture and sliding (Figure 2-7) has been termed cataclastic flow (Borg et al., 1960). Cataclastic flow, however, is not a distinctive mechanism in itself as it involves both cataclasis and particulate flow. The fracturing of grains and grain displacement and rotation have been shown to depend on stress in different and characteristic ways (Borradaile 1981) and may occur independently, which by definition (Ashby 1972) makes them distinguishable mechanisms.

Cataclasis is important at low confining pressure and high strain rates. It is insensitive to temperature, however the occurrence of cataclasis may be a lower temperature effect, since crystal plasticity is more effective in deforming grains at higher temperatures (Borradaile 1981).

Cataclasis as a predominant deformation mechanism in

Figure 2-7. Cataclastic flow, by which granular material can deform by fracturing and rolling or sliding of granules or fragments over each other.
after Ashby and Verrall (1978)

Figure 2-8. Graph illustrating how the stress-rate is extremely fast during the initial phase of a compressive test at constant strain-rate.

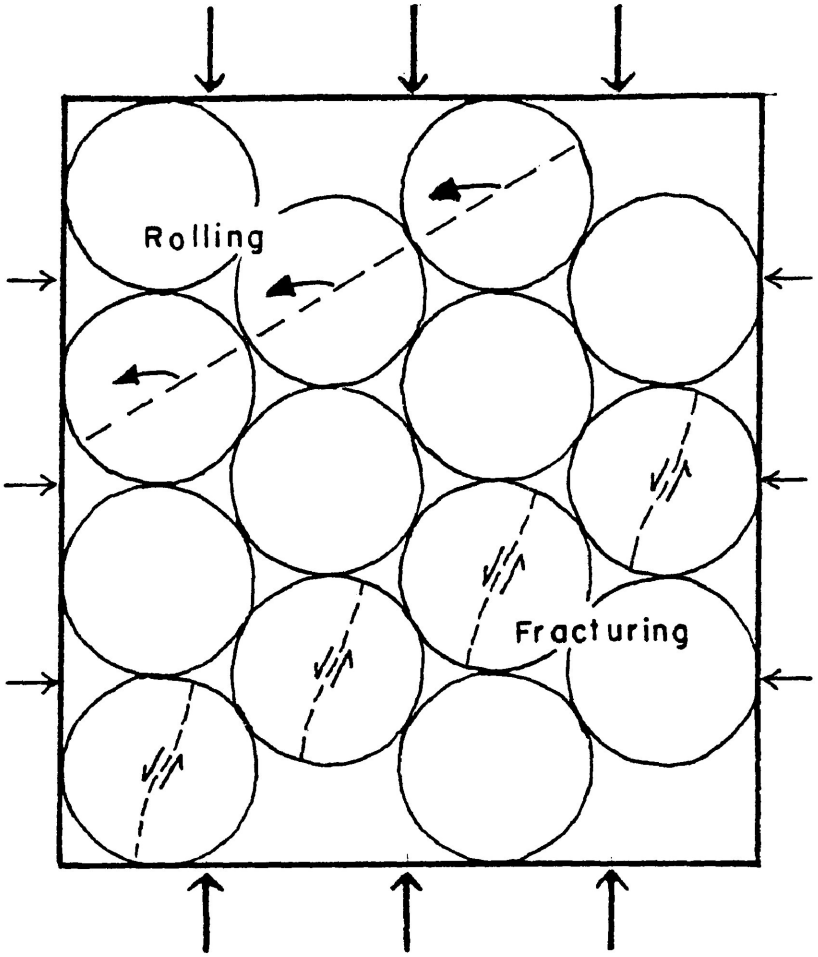
Rolling
Fracturing

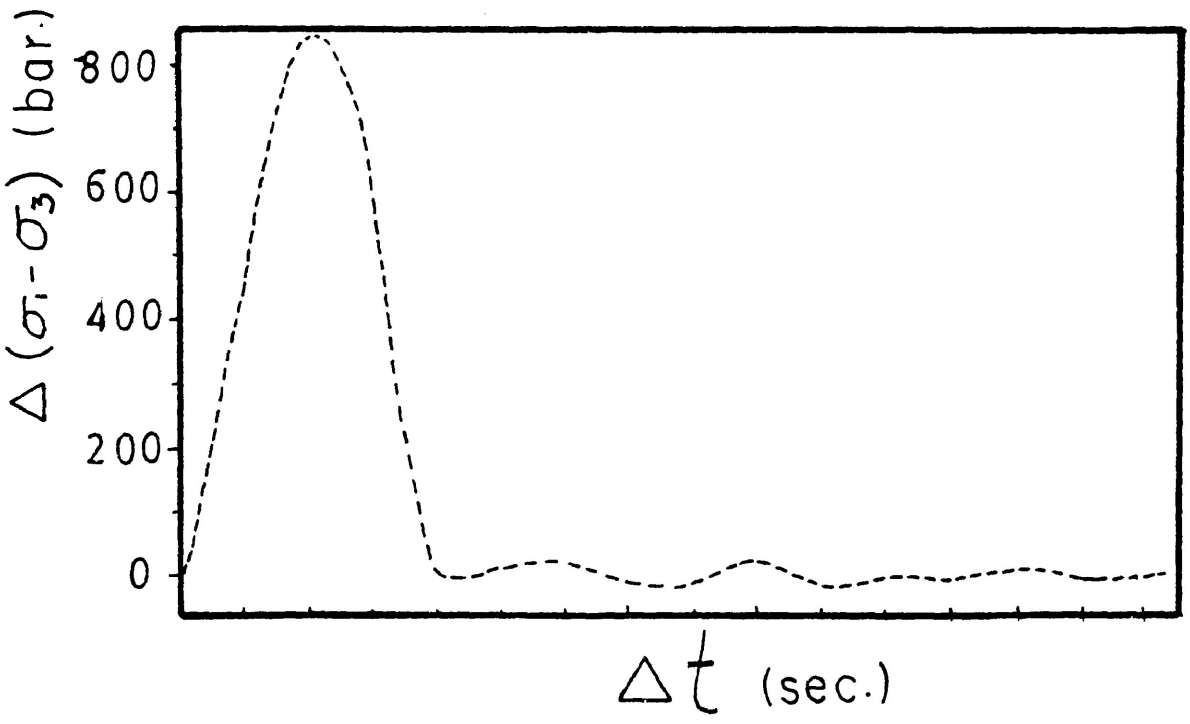
800
600
400
200
0
Δ (σ1 - σ3) (bar.)
Δt (sec.)

experimentally deformed aggregates is quite common (i.e. Borg et al., 1960; Friedman 1963; Donath & Fruth 1971; Hadizadeh & Rutter 1983). Its major role in the experimental deformation of rocks may be due to insufficiently high temperatures that are necessary with laboratory strain-rates (Paterson 1976). Donath and Fruth (1971) have suggested that cataclasis is not so much a function of the strain-rate but of the differential stress-rate, which is usually extremely fast during the initial stage of a constant strain-rate experiment (Figure 2-8).

Microfracture orientations within grains appears to relate to the principal orientations of stress if grain to grain contacts are numerous or to the orientations of grain contacts if there are but few grains that touch (Friedman 1963).

Intracrystalline Plasticity : Crystal plasticity refers to any change of shape achieved predominately by the glide motion of dislocations, as expressed by slip on crystallographic and/or twin planes (Paterson 1976). Dislocations are defects in the lattice of a crystal which occur as the crystal grows. When an external stress is applied, new dislocations are formed and the dislocations may glide (or slip) through the crystal producing small displacements of the lattice (see Hull 1975; Nicolas & Poirrer 1976).

Intracrystalline plasticity processes are both temperature- and stress-sensitive. No substantial volume changes are involved in the deformation of a grain by dislocation motion, thus, only relatively small effects of confining pressure are to be expected.

At low temperatures, the mobility of dislocations is limited and the dislocation density increases with increasing strain due to the continuous formation of dislocations and their inhibited movement by obstacles such as point defects, impurities, tangles and grain boundaries. Thus greater stresses are required by the dislocations to overcome these obstructions and produce a net strain, a process termed strain or work hardening. With higher temperatures dislocations have the ability to 'climb' over obstructions, thus distinguishing two mechanisms of dislocation motion, the gliding motion (Dislocation Glide) and the climbing and gliding motion of dislocations (Dislocation Creep).

Results from the deformation of an almost dislocation free peridotite (Phakey et al., 1972) indicate that slip initially occurs on favourably oriented planes of low critical resolved shear stress, primarily by the motion of edge dislocations. At higher temperatures, the disparity in the velocities of edge and screw components is reduced and slip tends not to be constrained to one plane.

Crystal-plasticity processes produce ductile textures and crystallographic preferred orientations. Dislocation processes have been related to such optical features as undulatory extinction, deformation lamellae, deformation bands, mechanical twinning and kinking.

Magnetic Susceptibility and Magnetic Susceptibility Anisotropy:

The magnetic susceptibility (k) relates the applied field (H) to the intensity of magnetization (J) produced in many materials, at low field strengths by:

$$J = k\ H$$

In many rocks and minerals it has been noted that the strength of the internal magnetization varies with the orientation of the rock or mineral respective to an external magnetic field of constant strength and direction. Thus the magnetic susceptibility displays a directional variability referred to as magnetic susceptibility anisotropy (Ising 1942). The magnetic susceptibility anisotropy, or MSA, of a rock may result from 1) the preferred orientation of elongate magnetic minerals, 2) the alignment of magnetocrystalline axes within magnetic minerals, 3) the alignment of magnetic domains, and 4) exchange anistropy (see Hrouda 1982).

The three dimensional variation in magnetic susceptibility of a rock or mineral can be described by a second order tensor, referred to as the magnetic susceptibility tensor. It is represented by:

$$\begin{matrix} k_{11} & k_{12} & k_{13} \\ k_{21} & k_{22} & k_{23} \\ k_{31} & k_{32} & k_{33} \end{matrix}$$

Completely defined, the magnetic susceptibility tensor describes the magnitude and anisotropy of the magnetic susceptibility's ellipsoid. The components k_{11}, k_{22} and k_{33} of the tensor are called the principal susceptibilities and their directions the principal susceptibility directions when k_{11}= the maximum (k_{max}), k_{22}= the intermediate (k_{int}) and k_{33}= the minimun (k_{min}) susceptibility directions. The orientations of the principal susceptibility directions will, in this study, be plotted on a lower hemisphere equal area stereonet.

The shape and anistropy of the susceptibility's magnitude ellipsoid can be described by means of suitably chosen ratios or differences between susceptibilities (see Hrouda 1982). The present study will employ two methods of graphically describing both the anisotropy and shape of the susceptibility ellipsoid using 1) a 'susceptibility plot' comparable to the deformation plot of Flinn (1962) and 2) a 'Hrouda-Jelinek plot' using the anisotropy and shape parameters, P' and T of Jelinek (1981).

The susceptibility plot (Figure 2-9) illustrates the susceptibility ellipsoid in a manner similar to how the strain ellipsoid may described in the deformation plot of Flinns' (1962) where:

$$L = k_{max} / k_{int}$$

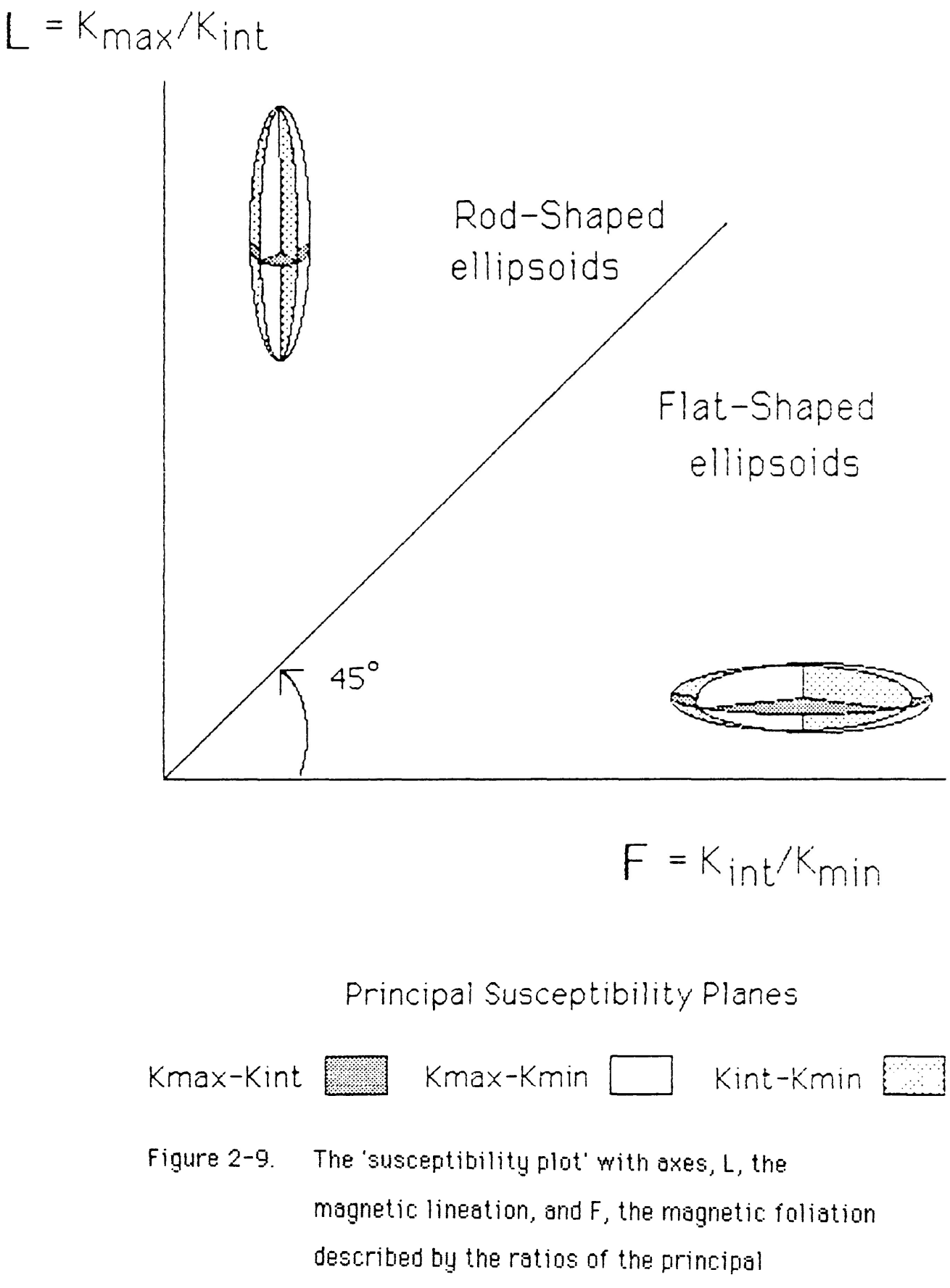

Figure 2-9. The 'susceptibility plot' with axes, L, the magnetic lineation, and F, the magnetic foliation described by the ratios of the principal susceptibility directions.

is used as the ordinate. L is the magnetic lineation, describing the extent to which the magnetic fabric is linear. The abscissa is the magnetic foliation, F, where:

$$F = k_{int} / k_{min}$$

describes the extent to which the magnetic fabric is planar. In this manner, a line with a slope of 1 separates the prolate or rod-shaped susceptibility ellipsoids from those which are oblate or flat-shaped (see Figure 2-9). This type of plot is convenient as it resembles the deformation plot and hence qualitative correlations of the magnetic anisotropy paths with the strain paths, along with the shapes of the strain and susceptibility ellipsoids can be made.

The P' parameter of Jelinek (1981) is an expression of the total degree of anisotropy given by:

$$P' = \exp [2(a_1^2 + a_2^2 + a_3^2)]^{1/2}$$

where $a_1 = \ln(k_{11} / \bar{k})$ etc. and:

$$\bar{k} = (k_{11} \cdot k_{22} \cdot k_{33})^{1/3}; \text{ where } k_{11} = k_{max} \text{ etc.}$$

The way in which P' varies with the magneic lineation and foliation is shown on the susceptibility plot (Figure 2-10).

Figure 2-10. Illustrating the variation of the anisotropy parameter, P', in terms of the ratios of the pricipal susceptibilities.

(From Borradaile and Alford 1987)

Figure 2-11. Illustrating the variation of the shape parameter, T, in terms of the ratios of the principal susceptibilities.

(From Borradaile and Alford 1987)

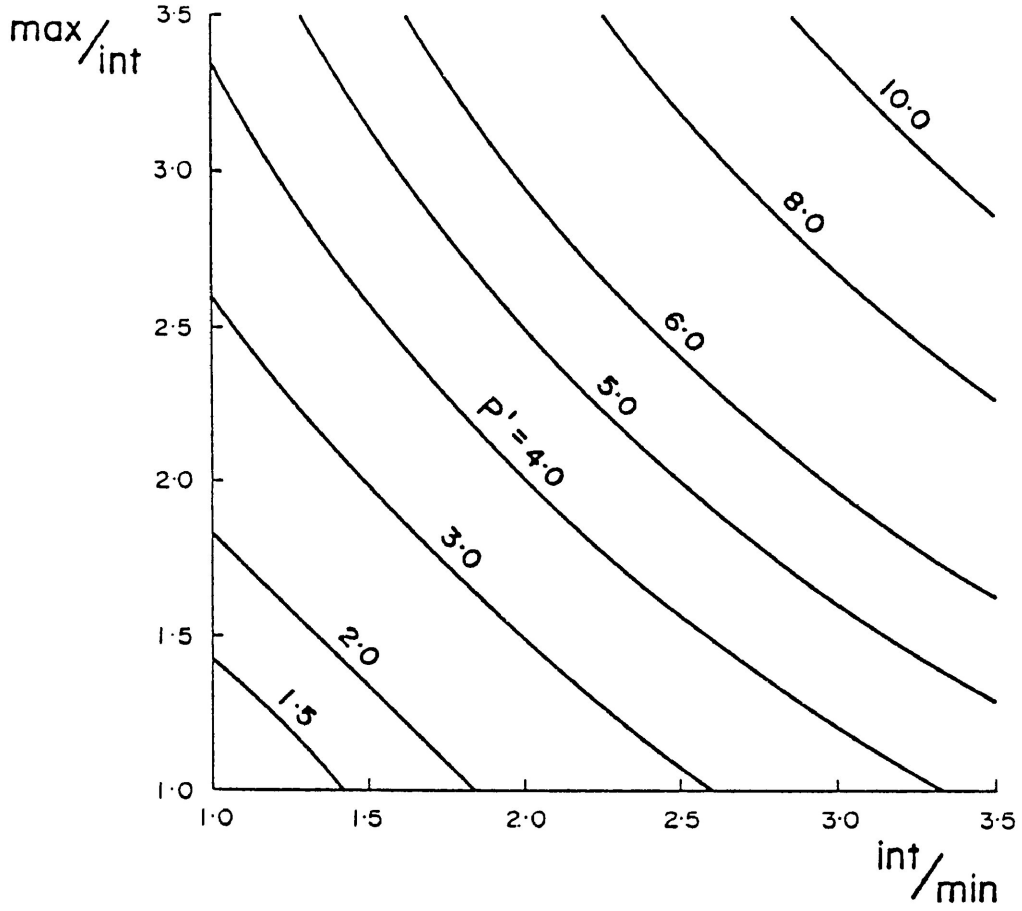
max/int
3·5
3·0
2·5
2·0
1·5
1·0
1·0
1·5
2·0
2·5
3·0
3·5
int/min
P' = 4·0
1·5
2·0
3·0
5·0
6·0
8·0
10·0

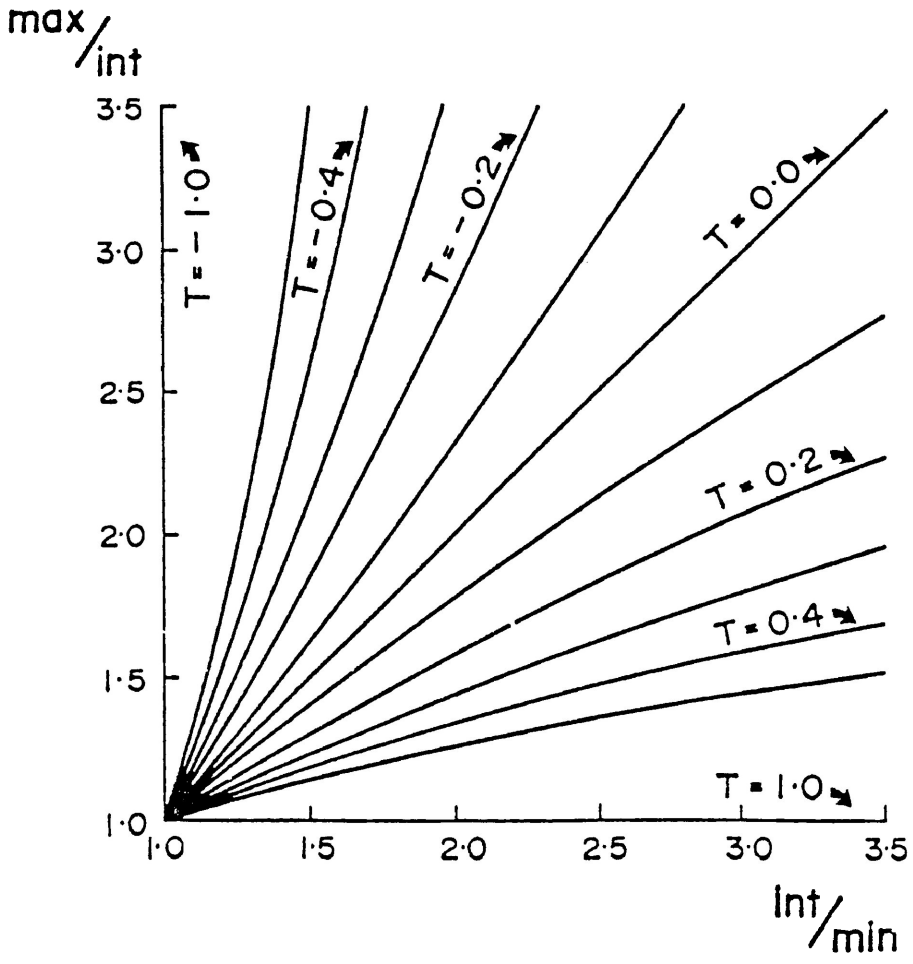
max/int
3·5
3·0
2·5
2·0
1·5
1·0
1·0
1·5
2·0
2·5
3·0
3·5
int/min
T = −1·0
T = −0·4
T = −0·2
T = 0·0
T = 0·2
T = 0·4
T = 1·0

The shape of the magnetic susceptibility ellipsoid is represented by Jelinek's T parameter where:

$$T = [2 (\ln k_{11} - \ln k_{22}) / (\ln k_{22} - \ln k_{33})] - 1$$

The variation of the T parameter in the susceptibility plot is shown in Figure 2-11.

The Hrouda-Jelinek diagram, using T, the shape parameter, as the ordinate and P' as the abscissa (Figure 2-12) is a convenient representation as it distinguishes the degree of anisotropy from shape more clearly than the conventional susceptibility Flinn plot.

Magnetic Susceptibility Anisotropy Studies:

The use of a rocks magnetic susceptibility anisotropy as a method of petrofabric analysis was suggested by Graham (1954). Since then, the use of this relatively rapid and reliable technique in investigating rock fabrics has become widespread in the geologic literature (ie. Hrouda 1982, references therein). The study of MSA evolved from the realization that, in most geological environments, the principal planes of the susceptibility ellipsoid are generally oriented parallel to some geologic fabric and hence can be related to a given geologic process. This is understandable since orientation, shape and anisotropy of the magnetic susceptibility ellipsoid stems from the spatial or cystallographic arrangement of the magnetic minerals present in a rock.

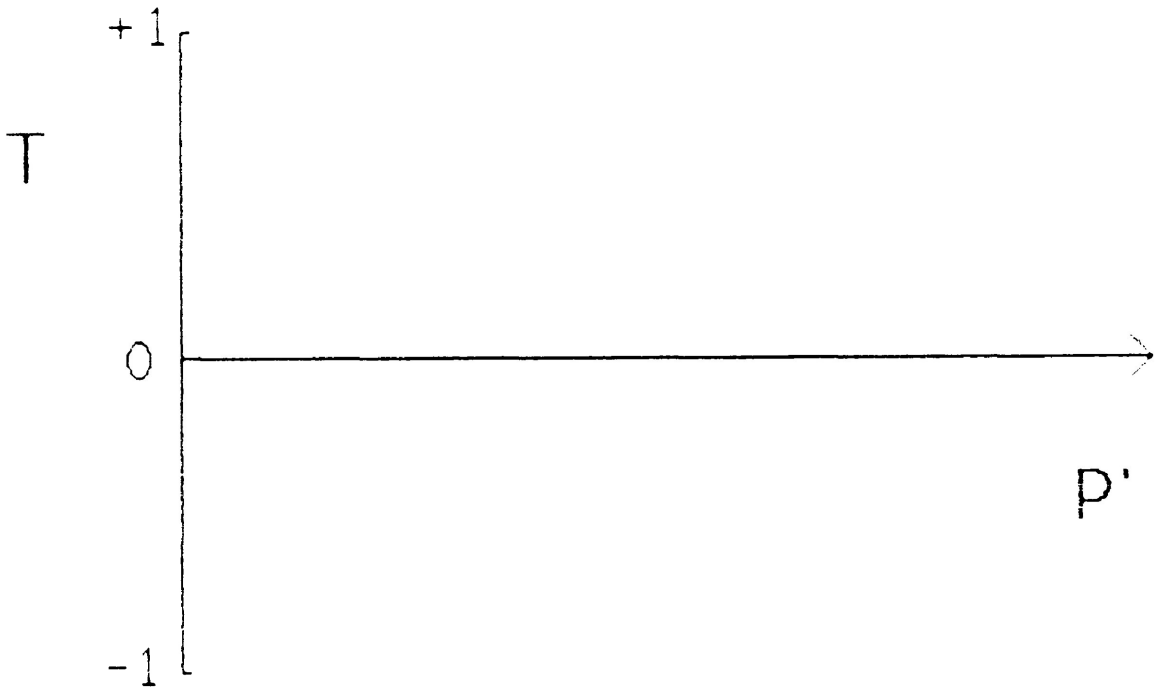

Figure 2-12. The 'Hrouda-Jelinek diagram', wherein the shape and anisotropy of the magnetic susceptibility's magnitude ellipsoid are plotted against each other. The T=0 line separates rod-shaped and flat-shaped ellipsoids.

There are many applications of MSA in geological and geophysical studies. Some of the geological applications of MSA studies include:

1) determing the paleocurrent direction and information on the depositional processes of sedimentary rocks in natural (ie. Hamilton & Rees 1971; Elwood & Ledbetter 1979) and experimental studies (ie. Rees 1966; Hamilton et al., 1968; Rees & Woodall 1975)

2) detecting the fabric of massive ores to advance the knowledge of genetic and post-genetic evolution of the ores (ie. Porath 1968; Schwarz 1974).

3) determing the flow direction of lava (ie. Kolofikova 1976), sills (ie. Halvorsen 1974) and magma (ie. Chlupacova et al.,1975) as well inferences on the formation (Ellwood 1975,1979) of igneous rocks

4) examing the character and intensity of deformaton in metamorphic tectonites

It is this last use of MSA to which the present study concentrates, thus review will be primarily concerned with the results of work in this field.

The Magnetic Susceptibility Anisotropy of Metamorphic Tectonites:

When igneous or sedimentary rocks are subjected to even a weak deformation and/or metamorphism, the susceptibility

ellipsoid changes from its primary shape as planar and linear fabrics are produced (Graham 1966; Hrouda 1976) and the magnitude of the MSA has been shown to quickly increase (i.e. Janak 1972; Hrouda et al., 1978). Any further progressive deformation/metamorphism only slightly affects the degree of MSA beyond this initial transition (Hrouda 1982).

This rapid transition from a relatively weak to strong MSA in low metamorphic grade rocks must, in part, reflect an effective re-orienting of the magnetic minerals by some deformation mechanism. Indeed, experimental deformation of a magnetite-enhanced artificial sand-cement mixture at room temperature (Borradaile & Alford 1987), has shown that, for relatively small strains, the magnetic susceptibility ellipsoid may re-orientate, relative to the principal strain directions, much more rapidly than would be expected by the active rotation of a material line. However, deformation by particulate flow and pressure solution may predominate in weakly deformed rocks of low grade metamorphism (Borradaile 1981). Such mechanisms have been shown to be relatively ineffective in aligning the ferrimagnetic minerals (Borradaile & Tarling 1981; 1984).

Thus the strong MSA of some metamorphic rocks may be related to the preferred crystallographic growth of common matrix-forming metamorphic minerals. Commonly, a rock's bulk magnetic susceptibility and anisotropy are credited to the ferrimagnetic mineral component even when the amounts of the

ferrimagnetic minerals are small (ie. Singh et al., 1975, Rathore 1979). However, within metamorphic rocks it has been shown that the large quantities of the more weakly magnetic minerals may constitute the source of the susceptibilities' bulk value and anisotropy (Borradaile et al., 1985). Minerals typically comprising a significant proportion of metamorphic rocks such as biotite, muscovite, amphibole and chlorite possess relatively weak paramagnetic susceptibilities but have been shown to possess strong magnetocrystalline anisotropies (Borradaile et al., 1987). Combined with the preferred dimensional orientation of the metamorphic minerals this would produce rocks with relatively low susceptibility but high degrees of anisotropy, a state commonly observed in natural metamorphic rocks.

Studies of the relations between the directions of the principal susceptibilities and the principal strain directions have shown that the shape, anisotropy and orientation of the suscetpibility's magnitude ellipsoid often correspond to local strains as would conventional strain markers (ie. Graham 1966; Hrouda & Janak 1976; Rathore 1979; etc).

Within areas of progressive deformation in regionally deformed schists, the primary susceptibility ellipsoids have been shown to become more anisotropic and flat-shaped with strain (Hrouda & Janak 1976). Principal susceptibility directions closely related to the primary-fabric elements in the undeformed rocks become related to the deformational-fabric elements with increasing

strain. The principal magnetic susceptibility directions (k_{max}, k_{int}, k_{min}) are noted to correspond with the principal strain directions (X, Y, Z) with; k_{min} parallel to maximum shortening direction (Z), and k_{max} parallel to maximum extension direction (X) (ie. Rathore, 1980; Wood et al., 1976; Kligfield et al., 1982).

Correlation between Magnetic Susceptibility Aniostropy and Strain:

There have been some attempts to quantitatively correlate magnitudes of principal magnetic susceptibilities and principal strains (Wood et al., 1976; Rathore 1979; Rathore & Henry 1982). It was hoped that determination of the magnetic susceptibility ellipsoid could directly provide, not only the directions of the principal strain axes, but an estimate of the amount of strain experienced by the rock.

Detailed examination of the magnetic fabric of a deformed lapilli tuff by Borradaile and Mothersill (1984) have indicated that the method of quantitative correlation between the magnitudes of the principal susceptibility axes and strain is invalid. The contribution to the susceptibility anisotropy by such complex factors as the source or sources of the susceptibility, the operating deformation mechanisms and the history of finite strain within the rock must be addressed.

Magnetic Fabric Studies by Experimental Deformation:

Experimental work in the elastic field by Kern (1961) and also by Nagata (1964; 1970) showed that under uniaxial compression the magnetic susceptibility of a rock decreases along the axis of compression and increases perpendicular to the axis of compression. Thus, the magnetic susceptibility of a compressed rock was noted to become anisotropic.

Owens and Rutter (1978) investigated the changes in the diamagnetic susceptibility of experimentally deformed marble and single calcite crystalls. For these materials a correlation was noted between the susceptiblity and the accompanying crystallographic fabrics.

Focusing on the bulk strain effects of a magnetite enriched sand-cement material deformed in pure shear, Borradaile and Alford (1987) observed a power-law correlation between the change in degree of anisotropy ($\Delta P'$) and the strain ratio (X/Z).

CHAPTER THREE

Apparatus

The apparatus employed in the present investigation consisted of a Donath type triaxial rig, an SI-1 Magnetic Susceptibility and Anisotropy unit, a drill press with a diamond core drill, several micrometers for measuring sample size and a measuring magnifier (graticule) for measuring shear displacements. For the preparation of specimens, non-ferrous metal mesh sieves were used to retain the specific grain sizes of the sands and crushed magnetite. Finally, a wooden setting tray was used as a mold for the sand-cement aggregate blocks.

The principal apparatus to be described are the triaxial rig and the SI-1 MSA unit.

Triaxial Rig- Both the pure shear and simple shear specimens were deformed in a triaxial rig (Plate 3-1), designed and manufactured by Dr. F. Donath of Earth Technology Corporation, 3777 Long Beach Boulevard, Long Beach, California, 90807 (c.f. 1970), which was controlled by a micro-computer system, the hardware for which was supplied by Dr. J. Holder of C.G.S., 2405 Spring Creek, Austin, Texas 78704.

The entire triaxial rig-computer system consists of the following components:

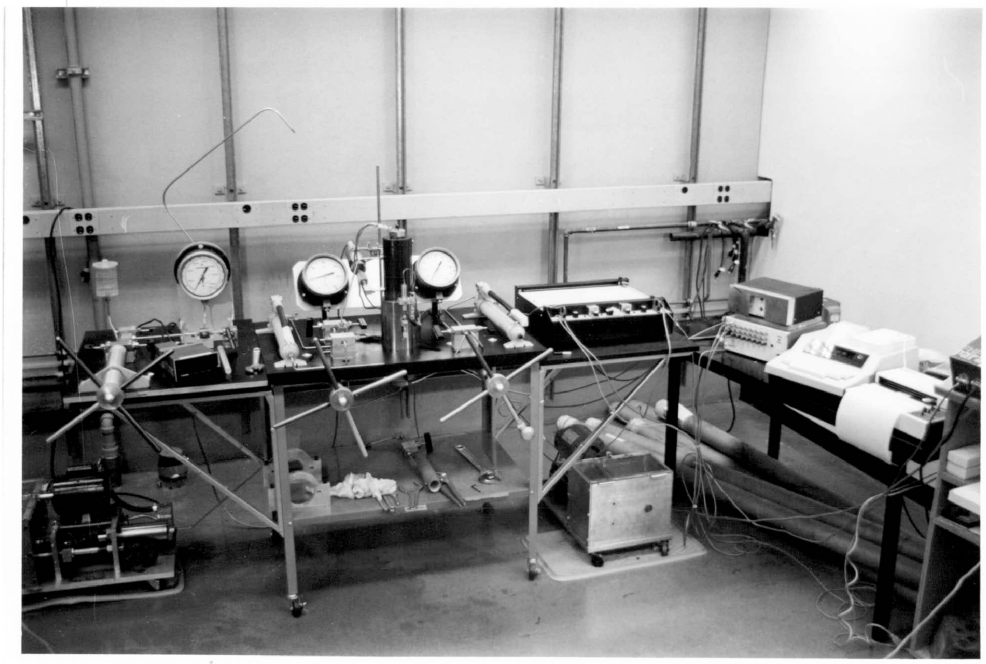

Plate 3-1. The triaxial rig, chart recorders and computer system as was used during this investigation.

1) Pressure Vessel
2) Force and Displacement measuring/recording System
3) Loading Ram System
4) Confining Pressure System
5) Pore Fluid pressure equipment
6) Computer and Analog-Digital Converter for the control of loading

The individual equipment will be discussed separately.

The pressure vessel (Figure 3-1) consists of a cylindrical piece of tool steel machined to provide a pressure chamber with a wall ratio (outside to inside diameter) permitting operation up to at least 30,000 p.s.i. Upper and lower pressure seals and retaining plugs act to contain the confining pressure medium. The lower seal and retaining plug are bored to permit movement of the lower piston into the vessel while confining pressure is maintained.

The specimen-piston assembly consists of an upper piston, jacketed sample and anvil which are placed into the pressure vessel from the top and held in place by the upper retaining plug, which houses the load cell.

Differential axial load is measured with strain gauges affixed to the load cell, the power supply to which is adjusted such that a

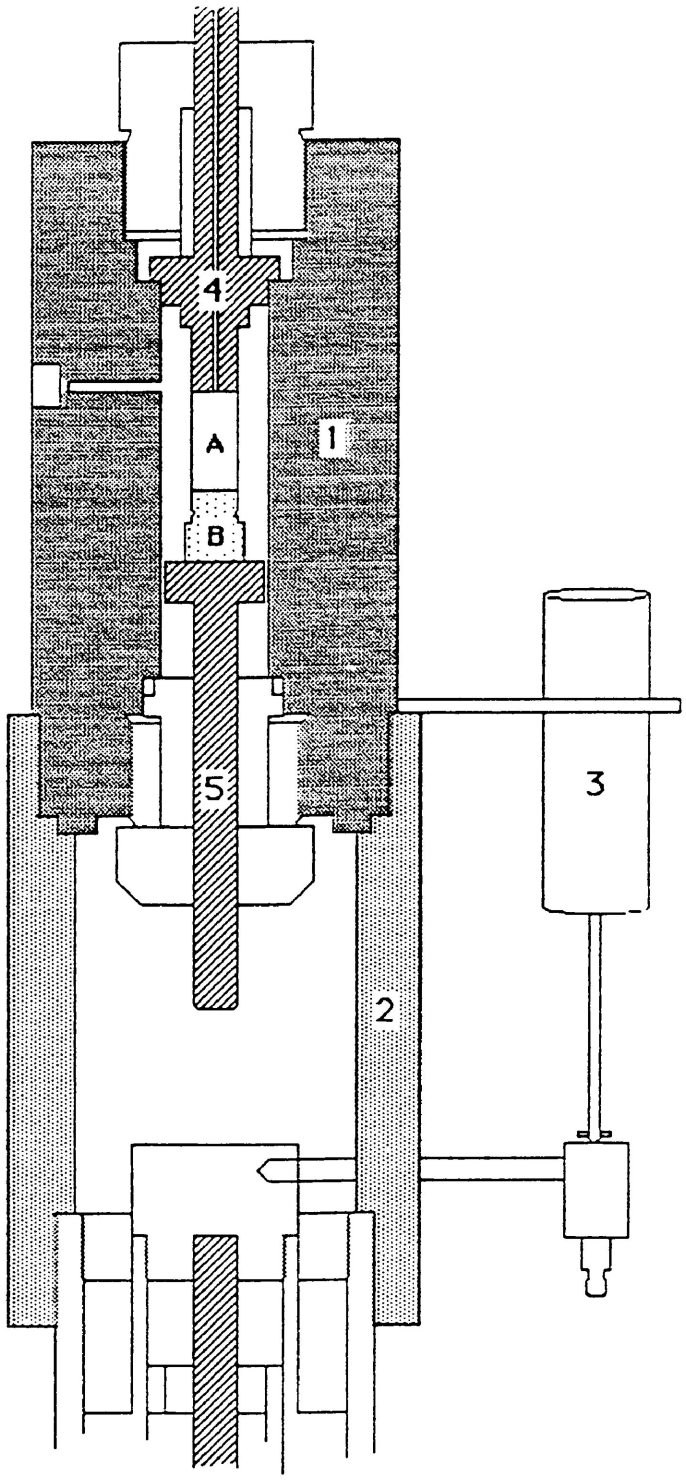

Figure 3-1. Schematic diagram of the pressure vessel (1), the coupling collar (2) and the LVDT (3). The specimen (A) and anvil (B) are located within the pressure vessel and are seated against the upper (4) and lower pistons (5).

change of 1,000 pounds force produces a change of 1 millivolt in the output signal.

Axial shortening of the specimen is determined from the movement of the Ram Piston relative to the vessel body. A linear variable differential transformer (LVDT) is affixed to the outside of the pressure vessel. The transformer stem is in contact with an arm extending from the top of the Ram Piston through a slot in the coupling collar (see Figure 3-1). The piston displacement, after suitable corrections for apparatus distortion, is used to calculate specimen shortening (See Appendix A).

An X-Y chart recorder continually receives the output from the load cell and LVDT and thus monitors the differential load versus displacement. The chart recorder is calibrated so that a one millivolt signal from the load cell gives a displacement of one centimeter, equivalent to 1000 lbs of force, along the Y-axis. The X-axis is calibrated so that a piston displacement of 0.01 inches produces a movement of the recorder arm by one centimeter.

A strip chart recorder was occasionally used to monitor the displacement or differential load versus time. This was used either to examine the LVDT or the load cell noise with respect to time, or as a visual check on strain-rates or displacement-rates.

Differential load on the specimen is produced by the thrust of the ram, which is determined by the pressure of the hydraulic fluid (a hydraulic jack oil) pumped into it. The 20-ton ram is primed via

a 10,000 p.s.i. hand pump which is used to seat the lower piston against the specimen. Further hydraulic pressure is provided by a syringe pump driven by an electric motor through a multi-rate gear box (Figure 3-2).

Confining pressures of up to 30,000 p.s.i can be generated by either a hand-turned pressure generator or, as in later tests, by a motor driven syringe pump in series with a pressure intensifier (Figure 3-3). The system is primed by means of a 10,000 p.s.i. hand pump which drives the confining pressure medium, a very low viscosity silicon oil (vacuum pump oil), into the pressure vessel.

The triaxial rig is so designed that the lower piston is pushed by the ram, which is driven by both the confining pressure and the pressure of hydraulic oil in the ram system. Therefore, the confining pressure acts on the bottom as well as on the sides of the specimen. In this manner the differential load is zero, thus the specimen is subjected to hydrostatic pressure.

The upper piston stem is bored such that fluids can be discharged from the specimen (in the case of a confining pressure leak into the specimen by jacket failure) or received, if a pore fluid pressure is desired. Thus, pore fluid pressures may be introduced by coupling the pore pressure control equipment's extension tube to the external section of the emplaced upper piston. Once attached, pore pressures can be increased to those of the surrounding confining pressures by means of a hand-turned

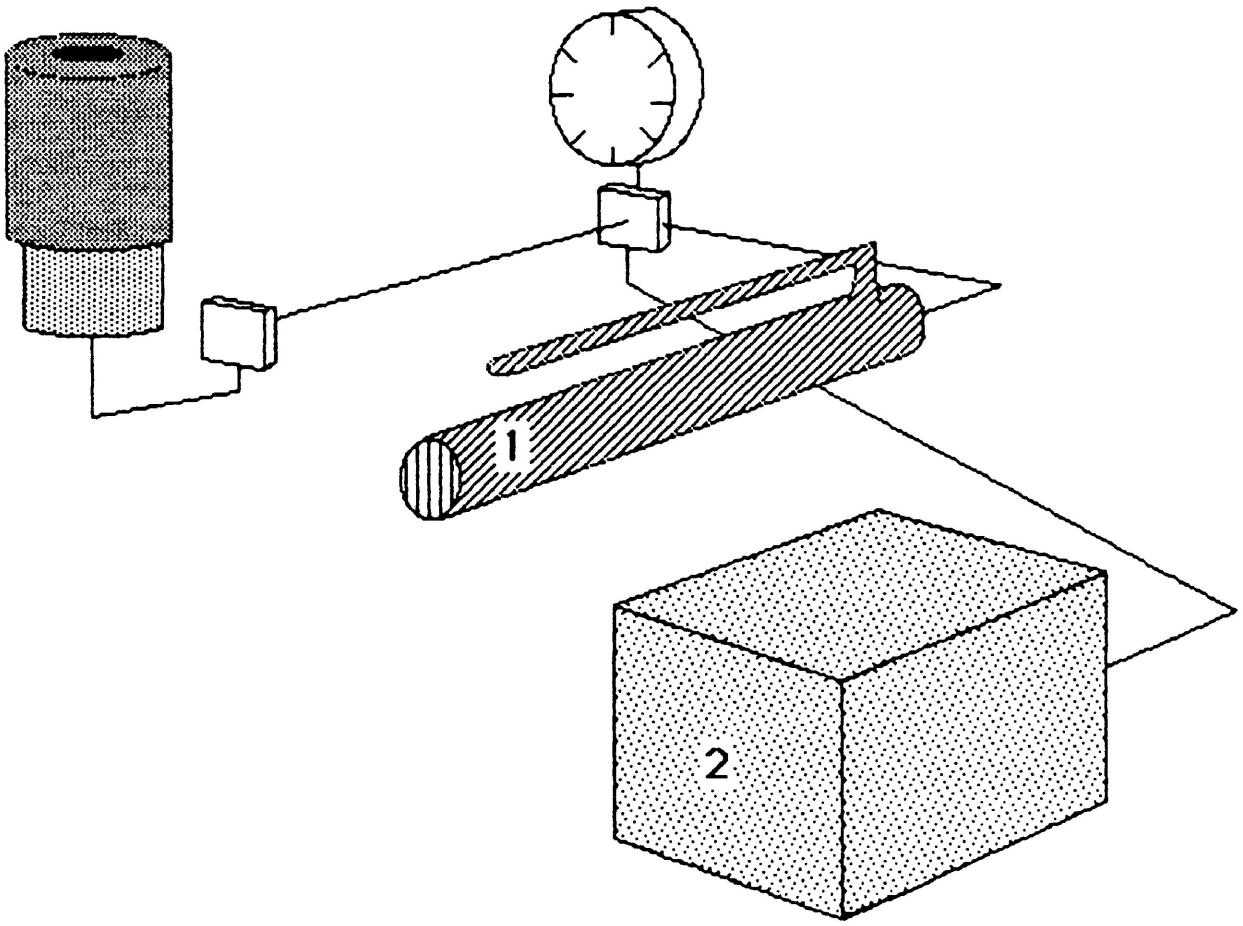

LOADING SYSTEM

Figure 3-2. Differential load can be produced by either a 10,000 p.s.i. hand pump (1) or through a syringe pump driven by a multi-rate gear box (2).

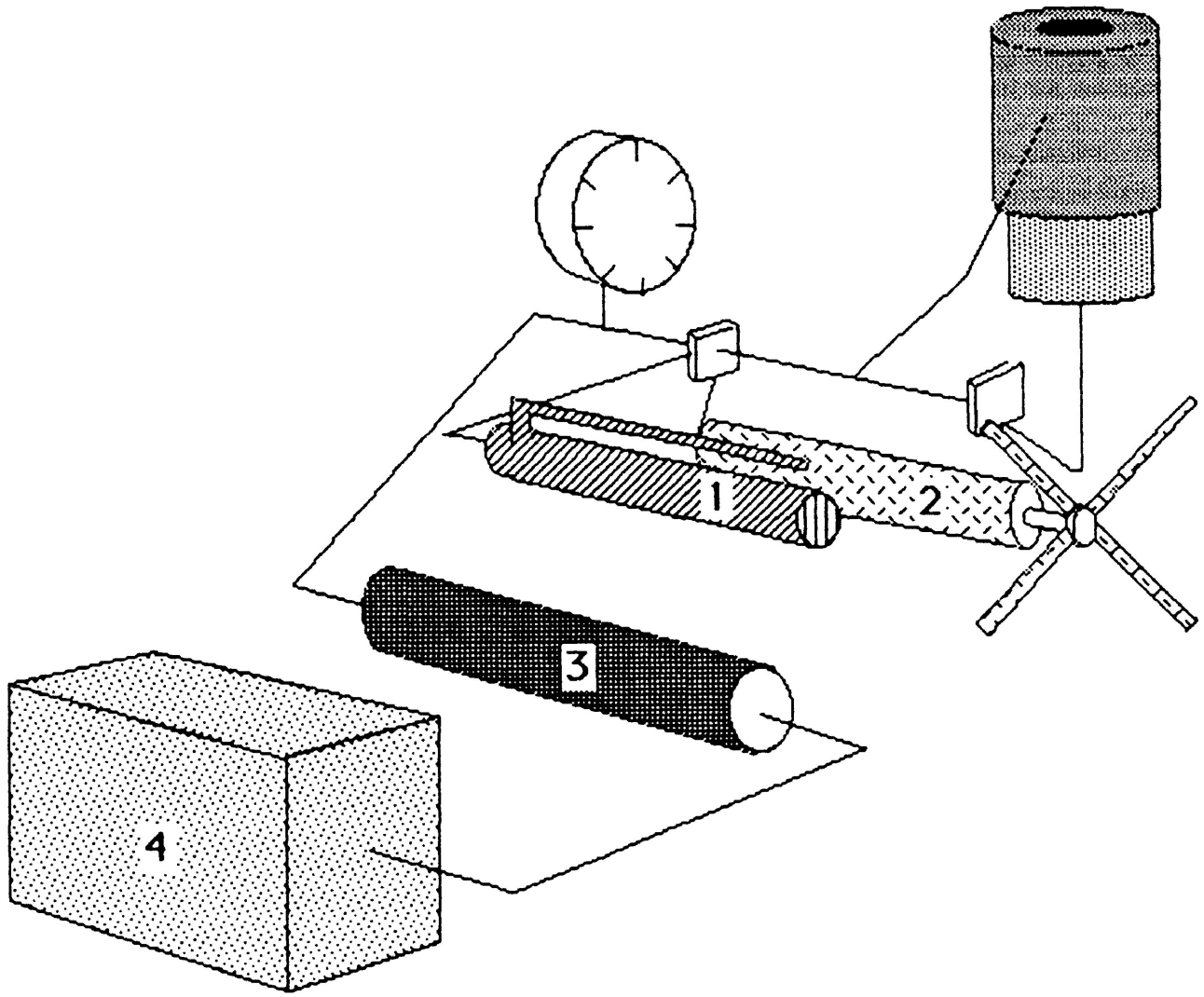

CONFINING PRESSURE SYSTEM

Figure 3-3. Confining pressures of up to 10,000 p.s.i. can be achieved using the hand pump (1). For confining pressures beyond this a hand turned pressure generator (2) may be used or pressure may be increased by a pressure intensifier (3) driven by multi-rate gear box (4).

pressure generator (Figure 3-4).

The system controlling the strain-rate consists essentially of a computer receiving the load and displacement signals and outputing signals to the multi-rate pump driving the ram (Figure 3-5). The Direct Current signals, from the load cell and the LVDT, are supplied via an analog to digital converter to the computer, which by using data reduction techniques similar to those of Donath and Guven (1971), in either a constant displacement-rate or a constant strain-rate program (See Appendix A), determines the required piston advance rate at that time. The computer then sends a Direct Current analog output to the motor speed control unit ('Parajust') which regulates the speed of the multi-rate pump to that necessary for the desired strain-rate.

SI-1 MSA UNIT- The SI-1 Magnetic Susceptibility and Anisotropy Instrument is capable of measuring both the bulk susceptibility and the magnetitic susceptibility anisotropy (MSA) of rocks, minerals and other materials. The unit was developed by Dr. M. Stupavsky of Saphire Instruments, Ruthven, Ontario, and consists of four basic components:

1) A Sensing Coil of inner volume 160 cm^3
2) Precision digital circuitry for measuring the inductance of the sensing coil to seven significant figures.

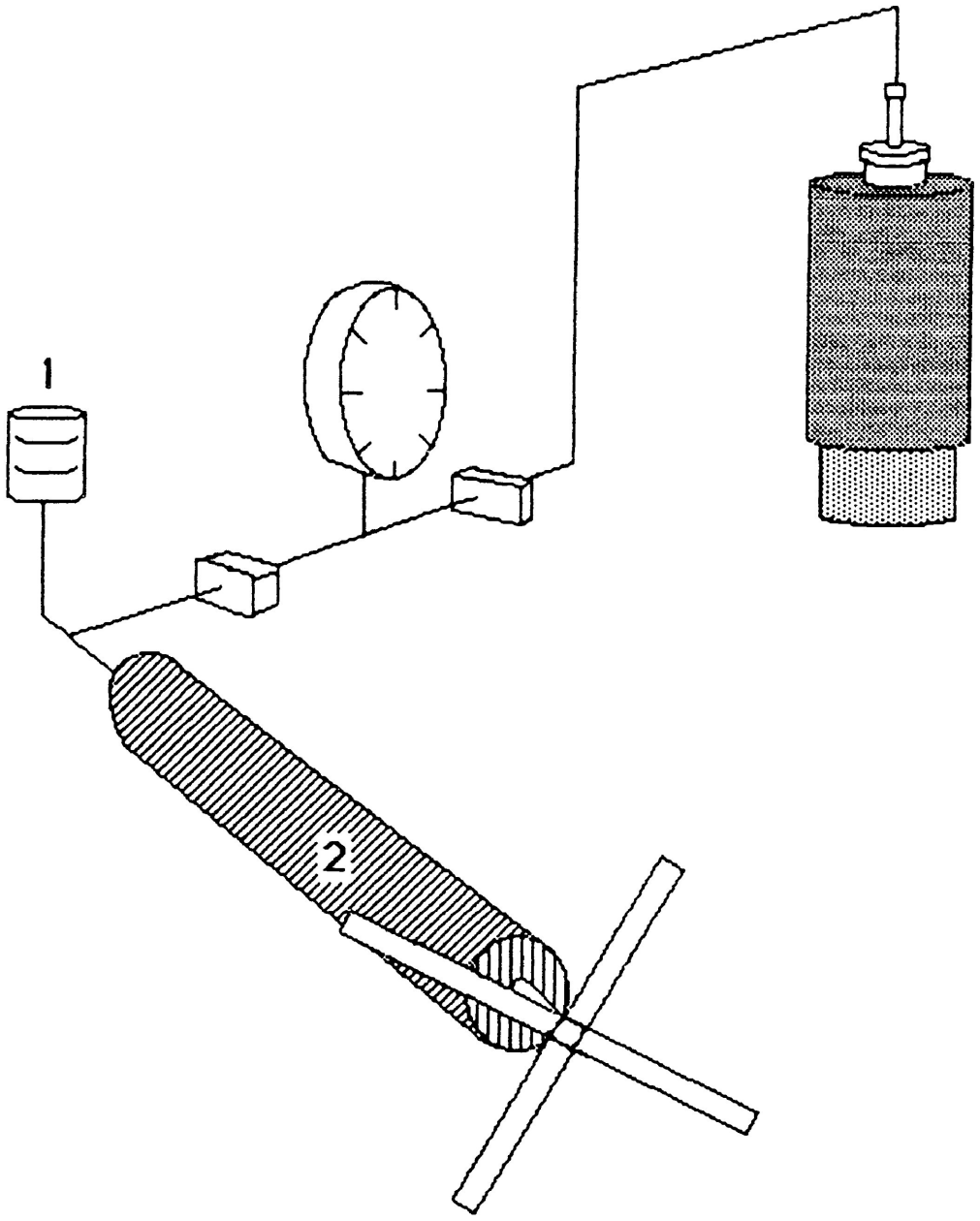

PORE FLUID PRESSURE SYSTEM

Figure 3-4. The fluid in the container (1) is drawn into the hand turned pressure generator (2) by turning the wheel counter-clockwise, the fluid is then sent into the sample via tubing which is conected to the upper piston (3) by turning the wheel clockwise.

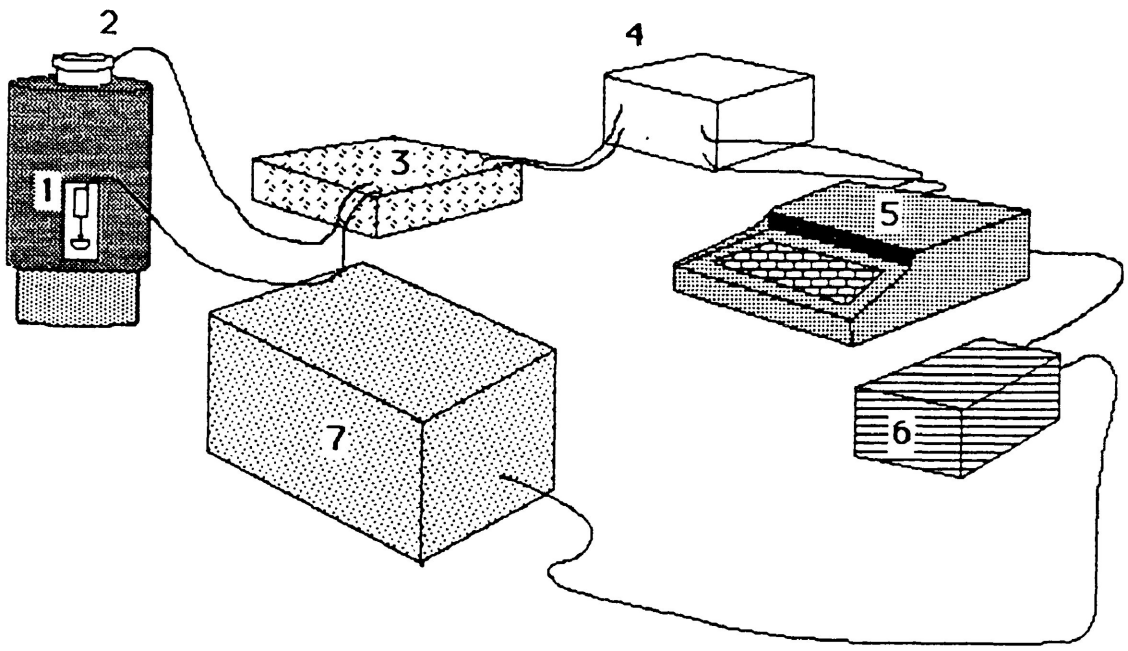

DATA PROCESSING AND STRAIN-RATE CONTROL SYSTEM

Figure 3-5 Displacements from the LVDT (1) and the amount of load on the sample from the load cell (2) are read as voltages and are recorded on the X-Y chart recorder (3). From the chart recorder the voltages are converted to digital numbers ranging from 1 to 4096 by the analog to digital converter (4). The computer (5) records the readings and computes the current amount of strain and the present strain-rate, if alterations in the rate of deformation are required the computer sends a signal to the 'Parajust' (6) a motor speed contol unit which sends a voltage to the multi-rate gear box (7) which controls the ram pressure.

3) Interface circuitry that enters the measured value into a Hewlett-Packard-41 CV calculator

4) The HP-41 CV calculator that functions as a data storage and processor unit as well as a communication link between the operator and the measuring coil

The SI-1 unit determines the magnetic susceptibility (MS) of a sample by performing two equally timed measurements of the inductance of the measuring coil. The first, L_s, is measured with the sample inside the coil and the second, L_a, with the sample removed from the coil so that inductance of the air and background is measured. Thus the samples susceptibility, K_s, is determined by;

$$K_s = L_s - L_a$$

A Saphire Instrument program determines the orientation of the principal susceptibility axes and the magnitude of the anisotropy of magnetic susceptibility of magnetic specimens from MS measurements for either 6, 12 or 24 specified orientations inside the measuring coil. The number of orientations and the measuring time required for meaningful reproducible AMS results depends on the magnitude of the specimen's magnetic susceptibility and on the degree of anisotropy (See Appendix B).

Materials

The requirements for a suitable material for this study are many:

(i) Specimens used in the experiments have to be of relatively small size, to fit into the pressure vessel. Consequently, the bulk susceptibility has to be high so that the anisotropy of susceptibility can be determined precisely.

(ii) The initial anisotropy of susceptibility of the specimens has to be low so that the difference in shapes of the specimen before and after strain does not produce a shape effect which adversely affects the determination of the susceptibility ellipsoid.

(iii) The experimental demands on the material are such that it has to be suitably strong so that it permits the pistons of the triaxial rig to be precisely seated against the specimen at the start of the test; suitably ductile at the range of confining pressures and strain rates permissible and of a suitable grain size to favour homogeneous deformation.

With the success of similar experimentation utilizing synthetic materials prior to this investigation (Borradaile and Alford 1987) and being unable to find a natural material which met these requirements, an artificially cemented 'sandstone' was synthesized.

In order to facilitate a comparison of changes in the AMS with strain, under differing deformation mechanisms, two compositionally different 'sandstones' will be used.

The chief component of the first cemented 'sandstone' block is a glacio-lacustrine beach sand. Presumably, this composition would illustrate deformation by cataclasis when subjected to experimental strain rates (i.e. Donath and Fruth 1971).

The sand originated from the northern coast of Black Sturgeon Lake, Northern Ontario (Figure 3-6). It was chosen for its reportedly high content of magnetite (Coates 1972). The sand was then sieved to retain an aggregate in the grain size range of 2.0 - 2.5 Ø (0.25-0.176 mm). The sieved sand had at this stage a mineralogy dominated by pyroxene, quartz and feldspar with an enhanced magnetite content of about 15 wt. %.

Calcite was chosen to be the chief component of the second block as it has proven to be a fairly 'soft' material under experimental conditions (Donath & Wood 1976) and has been reported to accommodate strain by plastic grain deformation (i.e. Friedman et al., 1976).

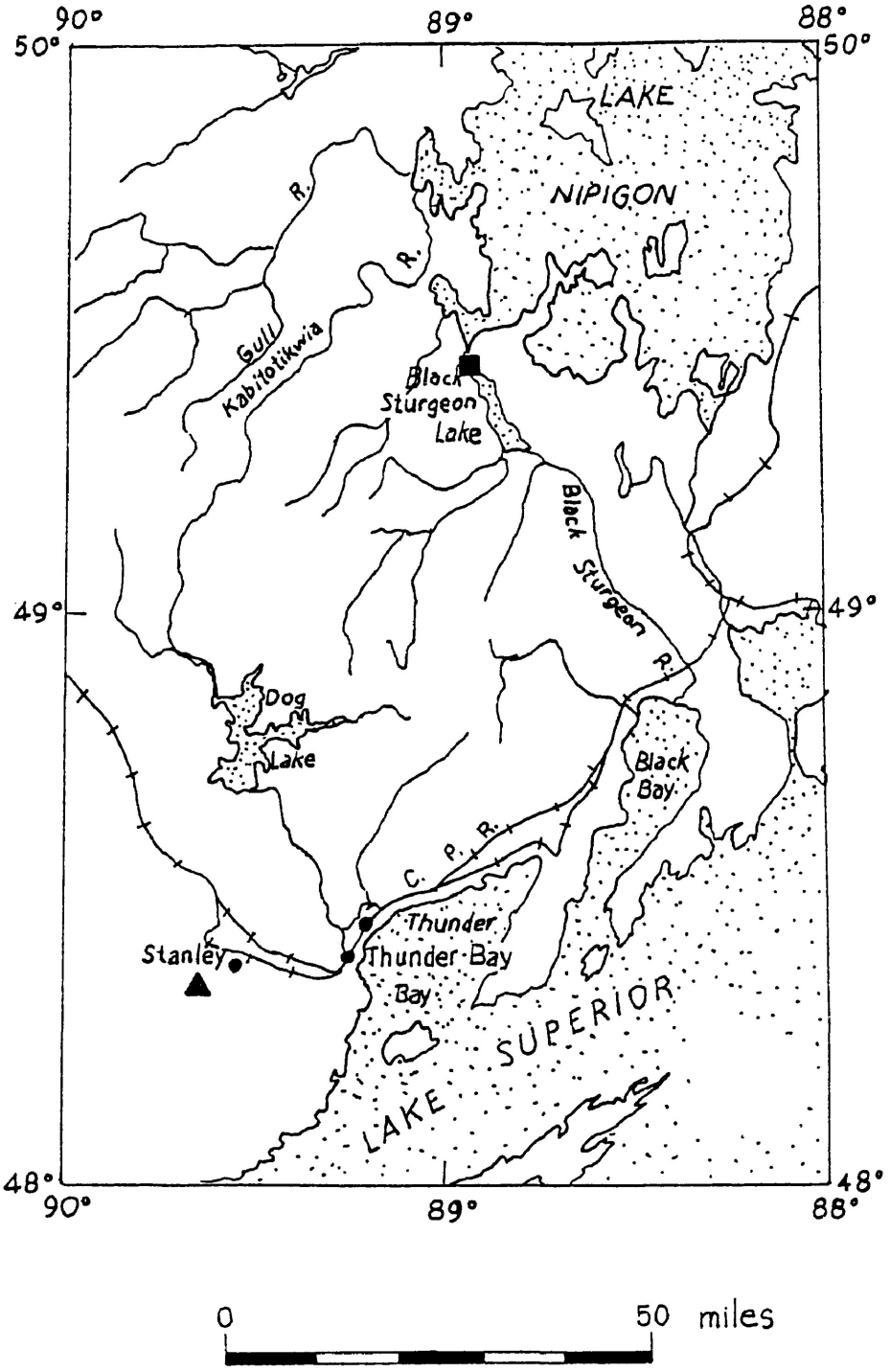

Figure 3-6. Location map of materials used for this study. The magnetite rich sand (indicated by a ■) originated from the north shore of Black Sturgeon Lake and the calcite (indicated by a ▲) from a vein approximately 4 miles west of Stanley, Ont.

The calcite was sampled from a vein near Stanley, Northern Ontario (Figure 3-6). It was later crushed and sieved to a grain size of 2.0 - 2.5 Ø (0.25-0.176 mm). Magnetite, crushed and sieved to the same grain size, in non-ferrous sieves, was added to the sieved calcite.

Both aggregates were cemented with 30% (dry volume proportion) Portland cement, which was evenly distributed through the sieved material before the addition of warm water which facilitated rapid setting. 'Flow fabrics' of the fluid mixture were prevented by setting the aggregate in a large shallow tray. The tray was rotated during setting to minimize the aligning effect of the Earth's magnetic field on the magnetite.

Both blocks were left to set for approximately one month before cylindrical specimens, 0.75 inches in diameter, were core-drilled from the blocks.

The materials have approximately 10% magnetite by weight. This produces a bulk susceptibility of $4.79 \times 10^{-3} \pm 6.892 \times 10^{-7}$ c.g.s./cm^3 in the sand-cement mixture and $7.114 \times 10^{-3} \pm 2.236 \times 10^{-7}$ c.g.s./cm^3 in the calcite-cement mixture, which is sufficient for precise determination of the MSA (See Appendix B).

The specimens were then angle-cut with a slow speed rock saw such that the cut from the cylindrical specimen makes an angle of 55^{o} with its long axis. Rough edges on the elliptical disk pieces were then ground down by hand so that the sides were parallel to

within 0.002 inches.

To create a shear zone environment, the elliptical angled disks were placed between two equal diameter cylindrical end-pieces of cut to a similar angle (Plate 3-2). Berea sandstone was chosen as the material for the end pieces because of its strength, low bulk susceptibility ($1.47x10^{-6} \pm 2.43x10^{-7}$ c.g.s./cm^3) and ease of handling.

In order to record displacements parallel to the shear zone, two reference makers were drawn on the elliptical inclined disk, such that when the assembly is viewed from the side, the markers would be on either side of the shear zone at the end-piece contact.

Several of the cylindrical specimens were retained as cylinders for pure shear tests and bulk susceptibility measurements . In this case, care was taken to ensure that the ends of the specimens were ground flat such that they were parallel to within 0.002 inches and that the specimens were of an appropriate length for both deformation and AMS measurement.

Plate 3-2. Shear zone specimens. From left to right, the upper and lower pistons, the composnents of the shear zone assembly: an angle cut disk of the sand-cement material between two angle cut pieces of Berea sandstone and to the right a complete shear zone assembly.

Determination of Magnetic Susceptibility

The anisotropy of magnetic susceptibility of the cylindrical cores and shear zone specimens were determined before and after deformation in the SI-1 MSA unit, described previously.

The AMS measurement may be influenced by the shape of the specimen, especially in the case of materials with a low bulk susceptibility that are very weakly anisotropic. In this case, the maximum susceptibility will appear to be parallel the specimen's long axis and the minimum susceptibility will appear to be parallel to the short axis. This effect is simply the result of the difference in the amount of material, due to the geometry of the specimen, interacting with the lines of magnetic force induced in the sensing coil during a measurement.

For right-circular cylindrical specimens, the length/diameter ratio can be critical to the outcome of the determination of the MSA. A length/diameter ratio of 0.85 has been found to produce the minimum shape response with right cylinders (Porath et. al. 1966). Previous tests, however, on a high bulk susceptibility material very similar to those used in this investigation, have shown no significant change in the orientations of the principal susceptibility directions and the degree of anisotropy, P', when the length/diameter ratio differs slightly from 0.85 (Borradaile and Alford 1987).

Thus, any shape effect caused by the length/diameter ratios of the cylindrical specimens employed is considered to be negligible.

To test if the shape of the angled disk pieces in the shear zone assembly would cause any shape effect problems, two experiments were conducted.

First, a cylindrical specimen was cut and ground down such that its length/diameter ratio was 0.85. Its AMS was then measured, the degree (P') and shape (T) of the anisotropy of magnetic susceptibility calculated and the principal orientations of susceptibility plotted on a lower hemisphere equal area stereonet.

Next, two cuts were made at an angle of 55^{o} from the cylinder axis such that an inclined disk of maximum possible width was generated from the specimen. Again, the specimen's AMS was measured, the P' and T parameters calculated and the orientations of the principal susceptibility directions plotted on the same stereonet (Figure 3-7).

The P' and T parameters calculated from the cylindrical specimen and the resultant inclined disk are plotted on a Hrouda-Jelinek diagram (Figure 3-8).

Since it is desirable to have the least degree of heterogeneous shear strain within the shear zone, the width of the inclined disks should be as narrow as possible. To test this effect of narrowing the shear zone on any possible shape effect, a second experiment

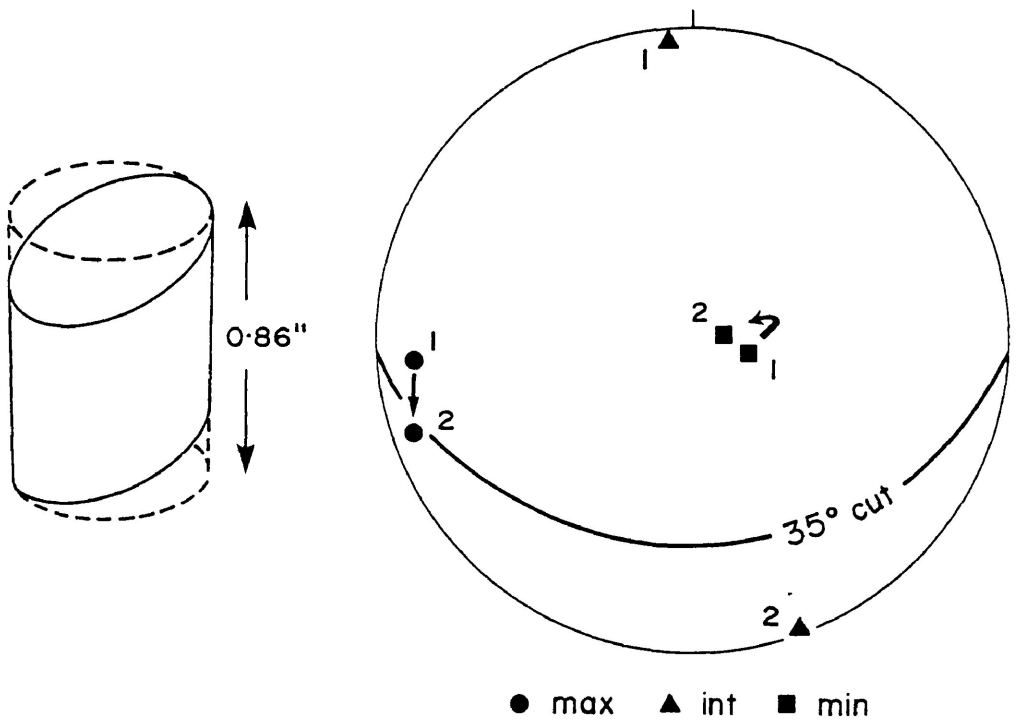

Figure 3-7. The directions of the principal susceptibilities plotted on a lower hemisphere equal area stereonet for 1, the cylindrical specimen and 2, for the inclined elliptical disk cut from the cylindrical specimen. Note how the orientation of the susceptibility directions do not change significantly.

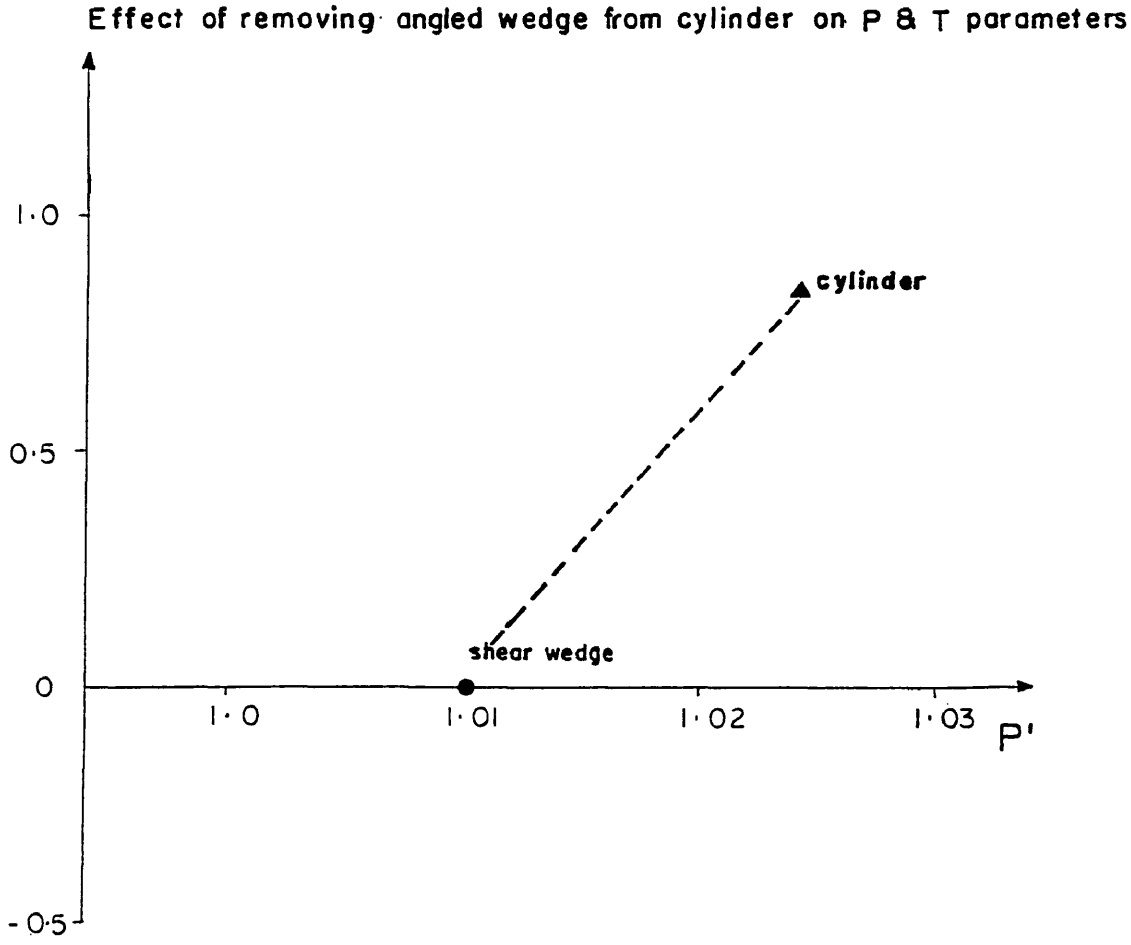

Figure 3-8. Illustrating the change in the shape (T) and the degree of anisotropy (P') of the magnetic susceptibility's magnitude ellipsoid as the inclined elliptical disk is removed from the cylindrical specimen.

was conducted.

For this test, an inclined elliptical disk of some thickness was incrementally ground down to the narrowest possible width allowing for material constraints. At each step the AMS was measured before the shear zones' width was further reduced.

Figure 3-9 displays the orientations of the principal susceptibility directions for the experiments.

The degree of anisotropy (P') and shape (T) parameters are plotted separately against the changing width of the disk as described by the width/diameter ratio (Figures 3-10 & 3-11).

Since the 95% cone of confidence about a determined principal direction can be as much as 3^{o} (See Appendix B) and since the process of grinding down the sample removes much magnetic material, the true change in the principal susceptibility directions of the previous experiments (see Figures 3-7 & 3-9) can be considered negligible.

Therefore, with respect to the principal susceptibility directions, any change in shape from a cylinder to an inclined elliptical disk, or a moderate decrease in the width of the disk, does not induce any significant changes in MSA orientations. Similarily, no significant change occurred in the value of the degree of anisotropy, P' (see Figures 3-8 & 3-10). However, the shape ellipsoid parameter, T, was slightly reduced in value in both experiments (see Figures 3-8 & 3-11). While such a change appears

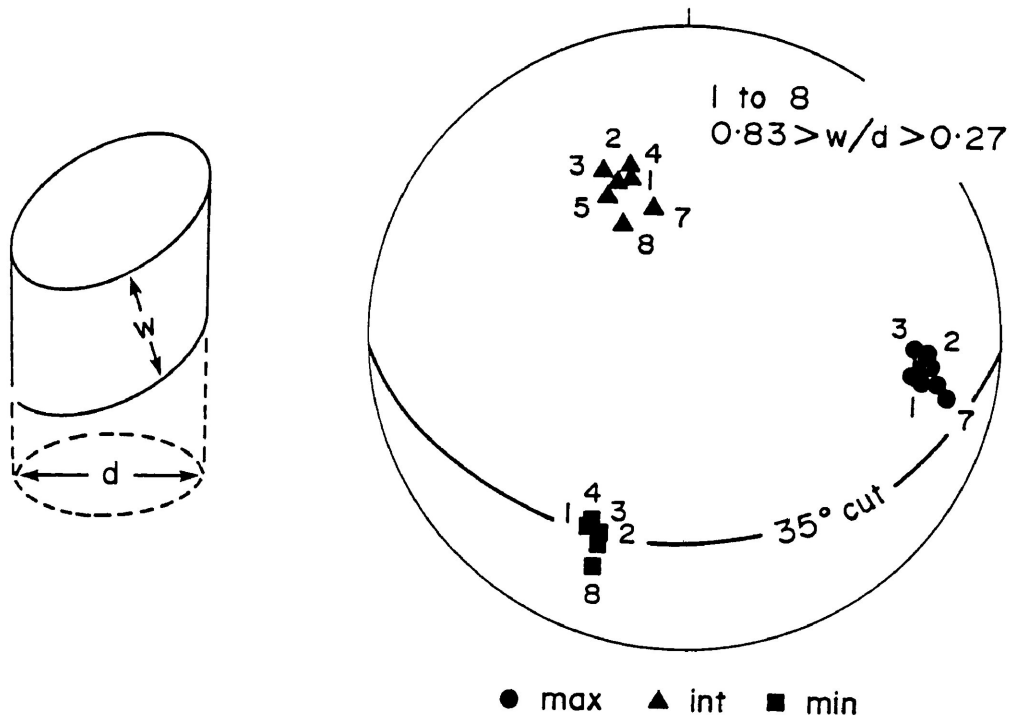

Figure 3-9. A lower hemisphere equal area stereonet displaying the orientations of the principal susceptibility directions for each inclined elliptical disk (1 to 8) as the width is being reduced.

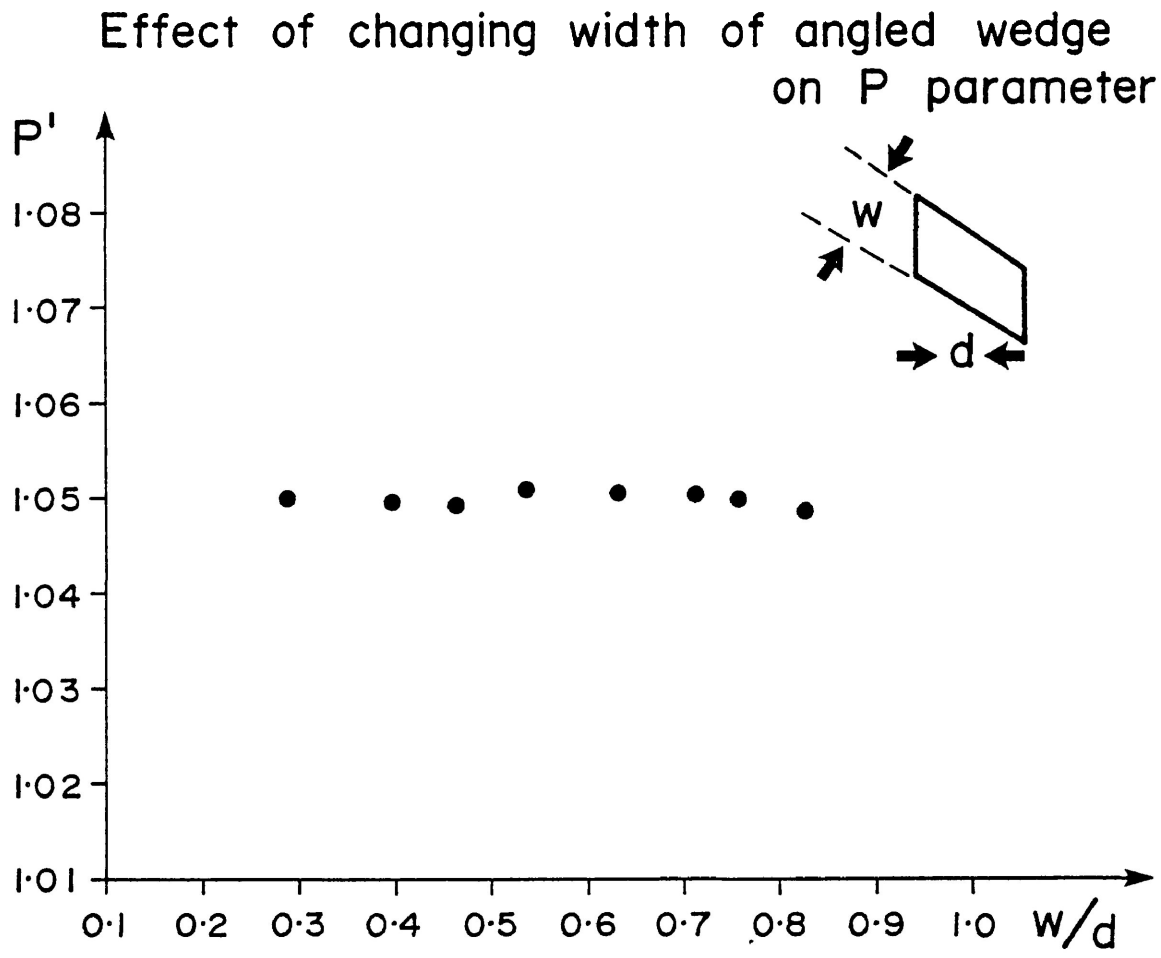

Figure 3-10. Illustrating the degree of anisotropy (P') of the magnetic susceptibility ellipsoid from each inclined elliptical disk as the width/diameter ratio is being incrementally reduced. Note that the reduction of width has little effect on the degree of anisotropy.

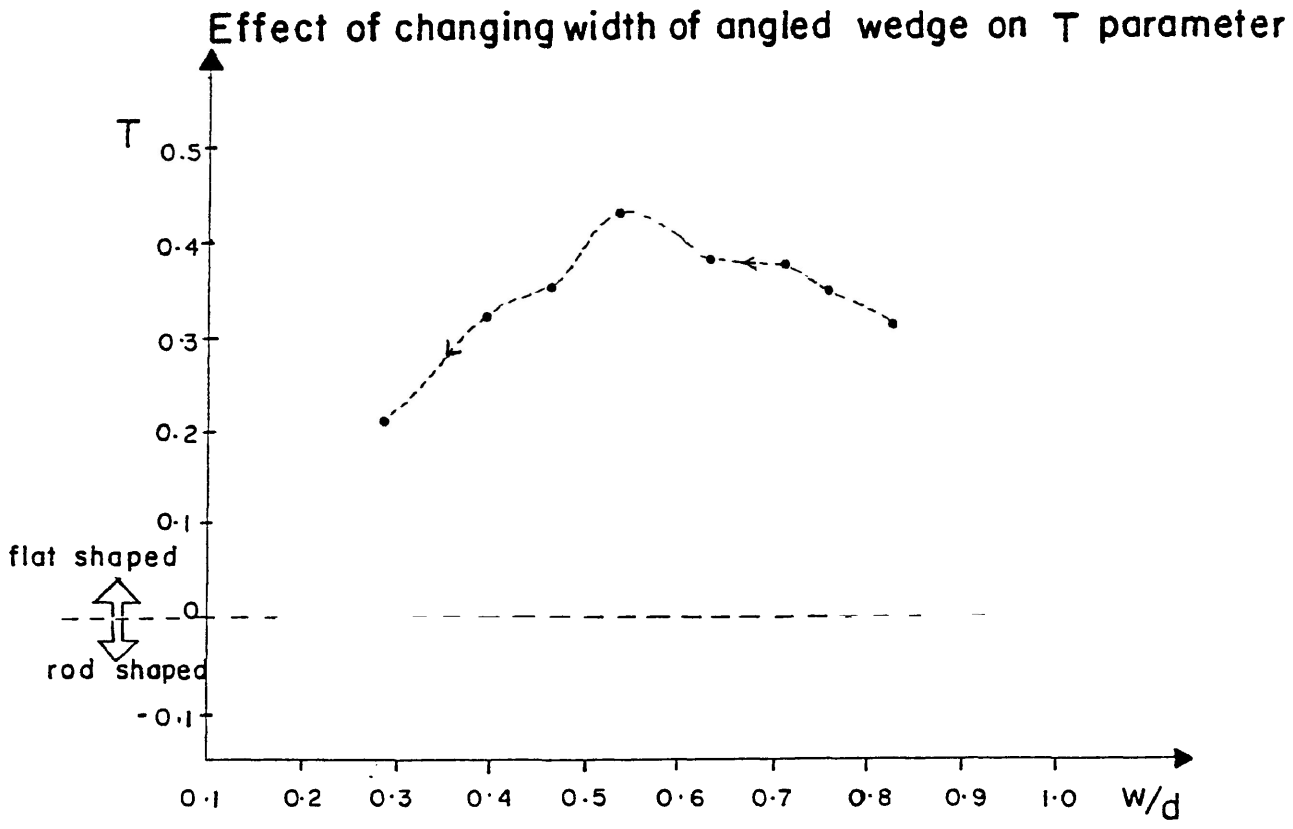

Figure 3-11. Illustrating the shape (T) of the magnetic susceptibility ellipsoid from each inclined elliptical disk as the width diameter ratio is being incrementally reduced. Note that the flattened shape of the susceptibility ellipsoid is generally being reduced along with the width of the disk.

substantial it should be realized that the ellipsoids described are very nearly spherical and plot near the origin on a graph of K_{max}/K_{int} versus K_{int}/K_{min}, since their P' values are so low.

Thus any substantial changes in P', T and orientation of the susceptibility ellipsoid, after an experiment, can be attributed to deformation.

Previous experimental shear zones (Friedman and Higgs 1981, Rutter et al., 1985, Knapp et al., 1987) have used an angle of 35^{o} between the shear zone and the maximum shortening direction (the Z-axis) for the entire shear zone assembly. This smaller angle ensures that, during deformation, most of the displacement of the end pieces will be along the shear zone boundaries. However, for AMS work, problems arise with this experimental set up. Since the angle between the shear zone and the Z-axis is fairly small the shear zone assembly must be relatively longer than the 55^{o} shear zone assembly in order to accompany this angle (Figure 3-12). Such a lengthy shear zone would be difficult to produce due to material strength considerations and although not tested, a disk of such shape would be more likely to cause a shape effect when measuring the AMS of the specimen. Thus the 55^{o} shear zone orientation was necessesarily used.

In terms of shear strain, the 55^{o} orientation will experience an equal amount of shear stress as will the 35^{o} shear zone orientation.

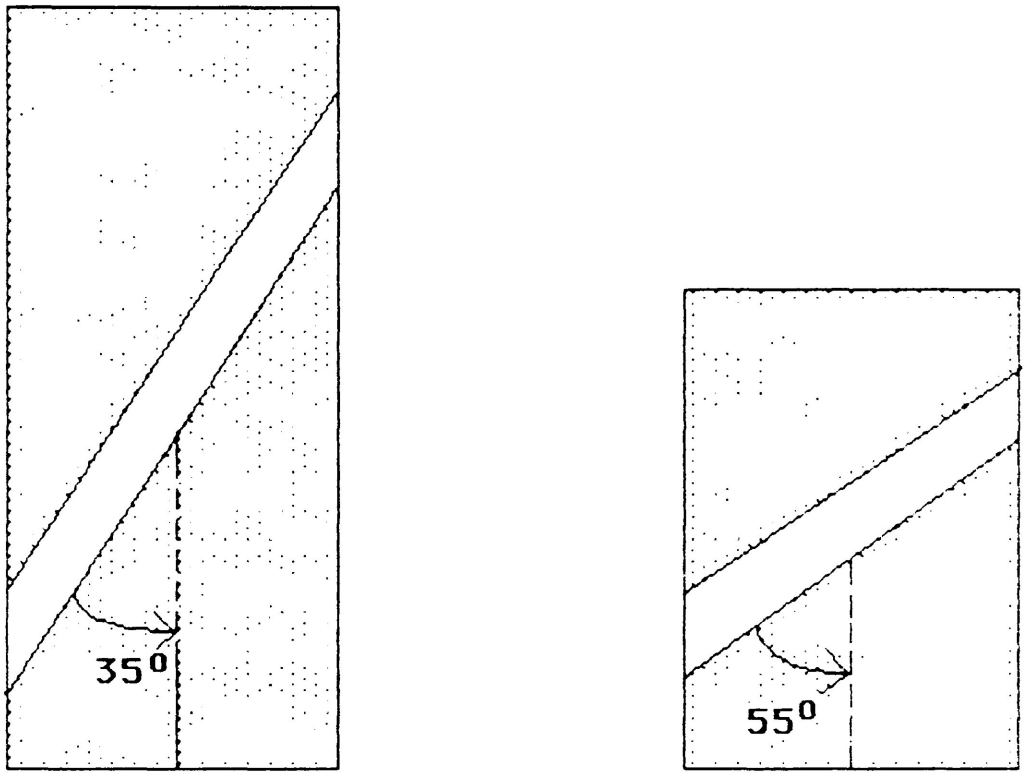

Figure 3-12. Illustrating the relative lengths of two experimental shear zone assemblies, to the left the commonly used shear zone orientation of 35^0, and the other, the 55^0 orientation, which is used in this study.

The MSA measurements of the experimentally deformed samples were conducted using the 12-orientation method. A reference arrow was placed on one end of the shear zone assembly and on one end of the cylindrical specimens to permit changes in the susceptibility orientations to be detected relative to that marker.

Experimental Deformation

Dry specimens (atmospheric pore fluid pressure) of known magnetic susceptibility were deformed at room temperature in the triaxial rig described earlier.

The specimens were double jacketed in Teflon tubing prior to deformation. Teflon, having a negligible susceptibility, allows the samples to be left in their jackets for the MSA measurement after the sample has been shortened. The use of the teflon jackets are particularly useful for the shear zone tests, as the assembly must be reasonably cohesive even before deformation, as well as for tests involving multiple episodes of experimental deformation on single specimens, since materials would likely crumble if removed from their jackets after some amount of strain.

Several series of tests were initiated for the sand-cement and the calcite-cement shear zones. At first, single step-deformation experiments were conducted (i.e. Sand-cement Series A), however, as it will later become apparent, this type of test was found to be less informative than the multiple-step deformation test.

For a single step deformation test, the specimen is seated against the upper and lower pistons of the triaxial rig, subjected to some desired confining pressure, then reseated against the pistons and deformed to a certain axial strain. At the end of the test, the differential stress is removed by slowly reducing the

ram pressure, eventually unseating the specimen. The confining pressure is then reduced to zero and the specimen removed from the pressure vessel.

For the multiple-step deformation test the single step procedure is repeated several times on one sample, usually in 2-4% increments of axial strain. Figure 3-13 illustrates how the multiple-step test would appear on the X-Y chart recorder.

In each case, the MSA is measured before and after deformation.

Three separate series of experiments, each at a different confining pressure (P_C), were conducted for the sand-cement shear zones.

Series A at a P_C of 10,000 p.s.i. (0.689 kbar)

Series B at a P_C of 14,500 p.s.i. (1.0 kbar)

Series C at a P_C of 21,750 p.s.i. (1.5 kbar)

The calcite-cement shear zones were deformed in two separate series.

Series 1 at a P_C of 14,500 p.s.i. (1.0 kbar)

Series 2 at a P_C of 21,750 p.s.i. (1.5 kbar)

Before deformation, each of the shear zone assemblies were

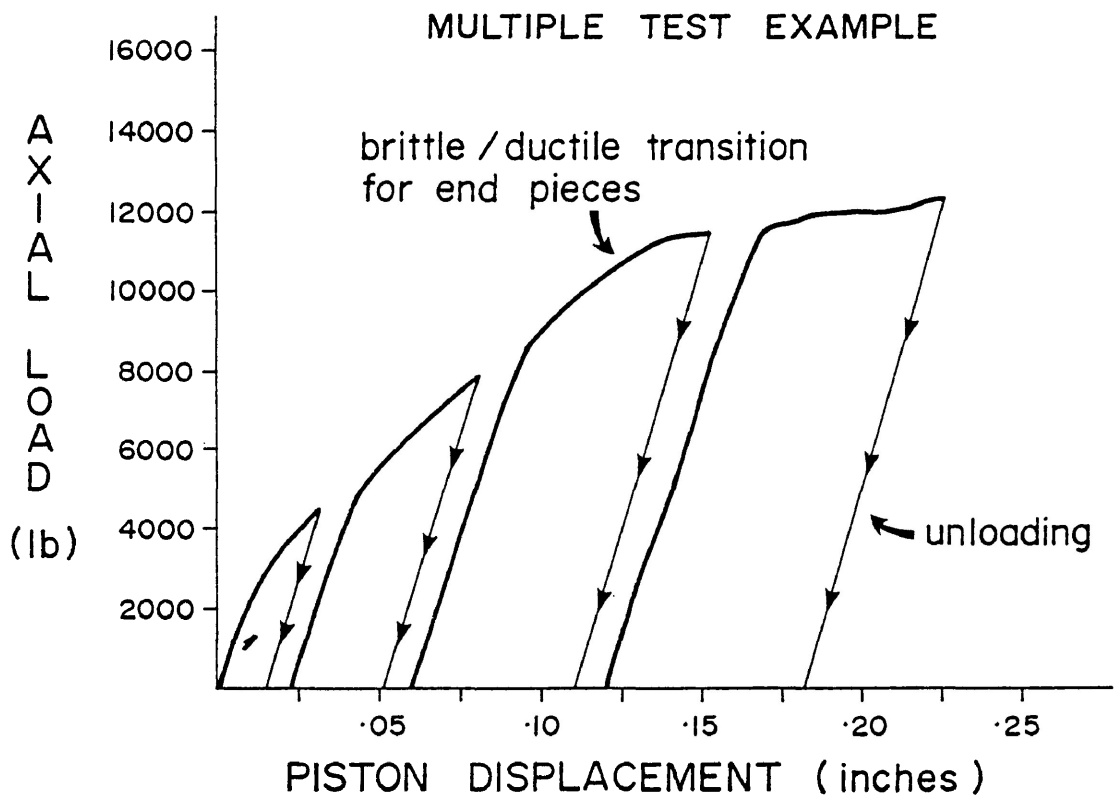

Figure 3-13. The multiple-step deformation method. After an increment of deformation the sample is removed from the pressure vessel and its magnetic susceptibility anisotropy recorded. The sample is deformed in as many increments as is possible within the limitations of the apparatus, usually in 2-4% increments of axial strain.

pre-compacted, for 12 hours, under a slightly higher confining pressure than that required for the experiment. This ensured a proper seating of all the components of the assemlby.

All the shear zone experiments were deformed at a constant displacement-rate of 5.0×10^{-6} inches. s^{-1} (whole sample shortening). Shear strain measurements were calculated from the shear zone width and displacements parallel to the shear zone by:

$$\gamma = \text{shear displacement/width}$$

See Figure 3-14 for reference.

In total 90 shear zone experiments were conducted.

Only one series of pure shear experiments were conducted. The material used for the tests was the calcite-cement 'sandstone'. A specimen shape was selected which would suppress faulting as a mode of failure and encourage failure by a macroscopically ductile fashion. The initial length/diameter (l/d) ratio was in the range $1.29 > l/d > 0.95$. This was varied so that the final l/d ratio expected after a certain amount of shortening would produce the minimum shape effect upon the determination of the MSA. The samples were all deformed at a constant strain-rate of 5.0×10^{-6} sec^{-1} under a confining pressure of 21,750 p.s.i. (1.5 kbar). In total, 9 single-step and 14 multiple-step deformation experiments were conducted in pure shear.

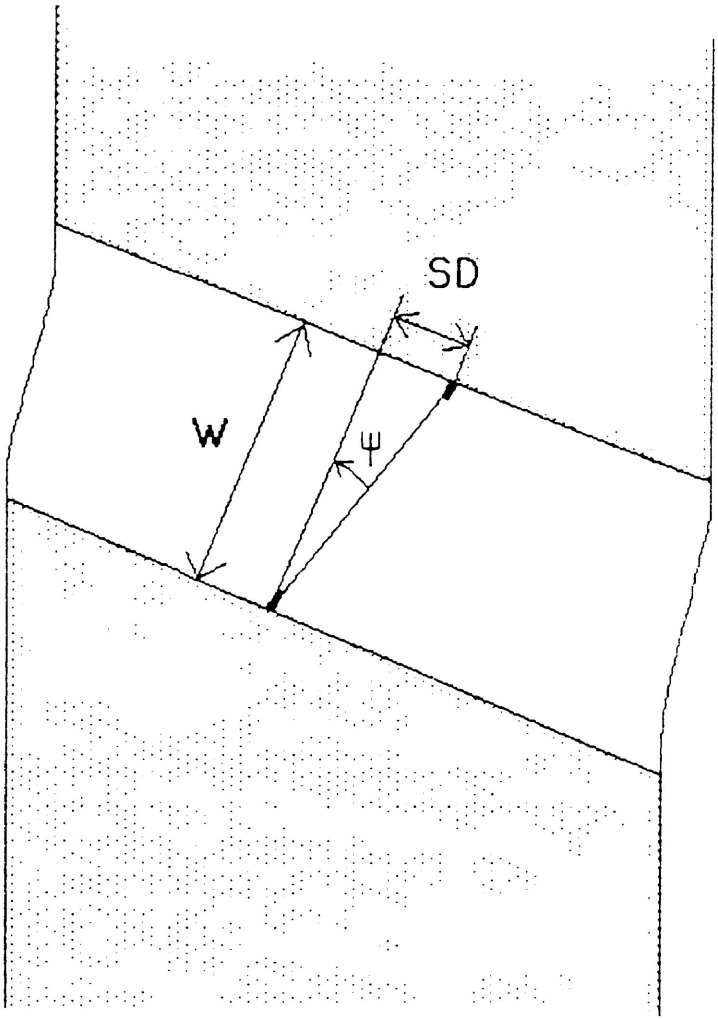

$$\gamma = \tan \Psi = \frac{SD(\text{shear displacement})}{W(\text{width})}$$

Figure 3-14. Schematic diagram of the shear deformation of the inclined elliptical disk. The width of the shear zone is measured directly and two originally diametrically opposed markers record the amount of displacement parallel to the shear zone walls (SD). The amount of shear strain (γ) occuring within the shear zone is then calculated.

Stress Relaxation

After the accumulation of approximately 5% axial strain a computer subroutine is invoked (See Appendix A) which first stops any further advance of the pistons in contact with the specimen.

The pistons are then 'locked' into place by manually closing a valve which isolates and contains the pressure in the hydraulic fluid supporting differential load. The lower piston cannot then back away from the specimen, as the hydraulic fluid is essentially incompressible.

The currently stored elastic strain in the specimen-piston assembly is then dissipated into permanent strain within the specimen, over a period of time. During this time, the computer monitors the length of the specimen and the reduction in differential load and then determines the rate of accumulation of permanent strain in the specimen.

During stress relaxation, the first or fastest strain-rate that would be recorded is commonly slower than the strain-rate which was employed throughout the loading procedure. In order to attain strain-rates which are faster, the strain-rate is increased by an order of magnitude just prior to invoking the stress relaxation sub-routine.

The stress relaxation procedure was performed on 0.75 inch diameter cylindrical specimens of both the sand-cement and

calcite-cement material at each of the confining pressures utilized for the shear zone tests.

Stress relaxation was also conducted on Berea sandstone, the material used for the end pieces of the shear zone specimen assembly. One test at a confining pressure of 21,750 p.s.i. was deemed sufficient to determine the flow law of the sandstone at the experimental strain-rates.

CHAPTER FOUR

Observations

Two types of tests were conducted such that changes in MSA with strain would be represented by experimental approximations to two distinct idealized strain histories, pure shear and simple shear. Although the criteria for the strain histories are not strictly met, experiments involving axial shortening of cylindrical specimens are considered to be analogous to deformation by pure shear. Deformation by simple shear with some transpressive compaction is considered to be represented by the shear zone experiments.

In describing the experimental results from the "simple shear" and "pure shear" tests, attention will be focussed on:

1) Changes in the orientation of the susceptibility ellipsoid with strain
2) Rate of Rotation of the susceptibility axes
3) Changes in the shape and anisotropy of the susceptibility ellipsoid with strain
4) Microscopic observations
5) Stress relaxation results

For the purpose of visually describing changes in the principal

susceptibility directions an equal area stereonet has been employed. For deformation in simple shear, the results have been rotated in a manner following Friedman and Higgs (1981). In this way, the top of the stereonet represents the top of the sample and the shear direction (55^{o} from the specimen axis) is the perpendicular to the viewer (Figure 4-1). Changes in orientation of the susceptibility ellipsoid can then be easily reconciled with the sense of movement within the shear zone, and compared to the finite and incremental strain ellipse appropriate for the shear strains.

For deformation in pure shear, the stereonet is simply a lower hemisphere view. The edge of the stereonet is in this way coplanar with the plane of flattening (the X-Y plane of the strain ellipsoid) and the center of the stereonet coaxial with the maximum shortening direction (the Z-axis) (Figure 4-2). Rotation of the principal susceptibility directions during shortening of the cylindrical specimens can be then easily interpreted in relation to the principal strain directions.

The rotation of the principal susceptibility axes are compared to the rotation of a theoretical linear line element undergoing similar amounts of simple and pure shear. In this manner, some estimate can be made of the rate of rotation of the susceptibility ellipsoid with strain.

The change in shape of the susceptibility ellipsoids are

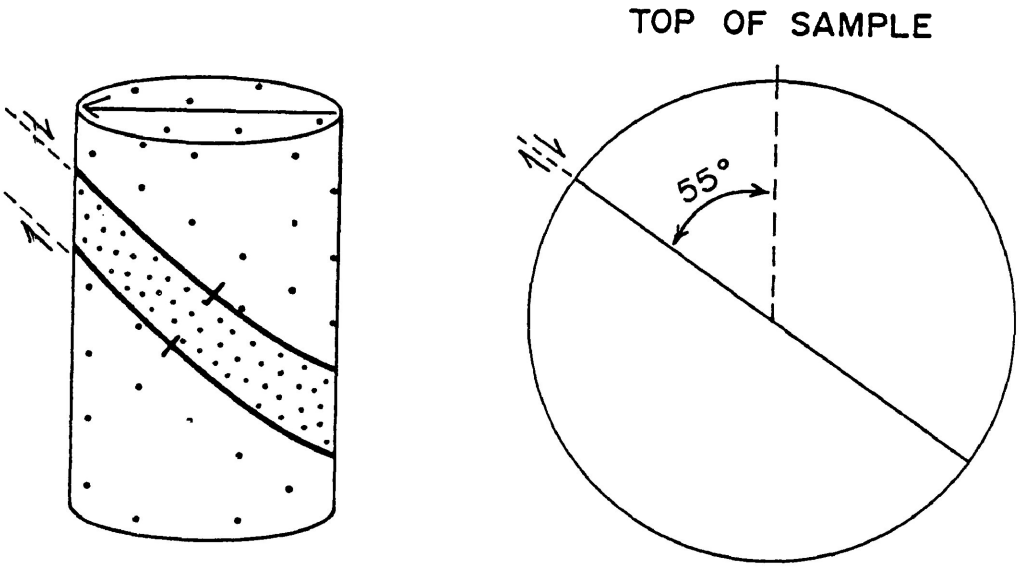

Figure 4-1 Orientation of the equal area stereonet with respect to the shear zone assembly used throughout this study to describe changes in the orientation of the principal susceptibility directions in experimental simple shear.

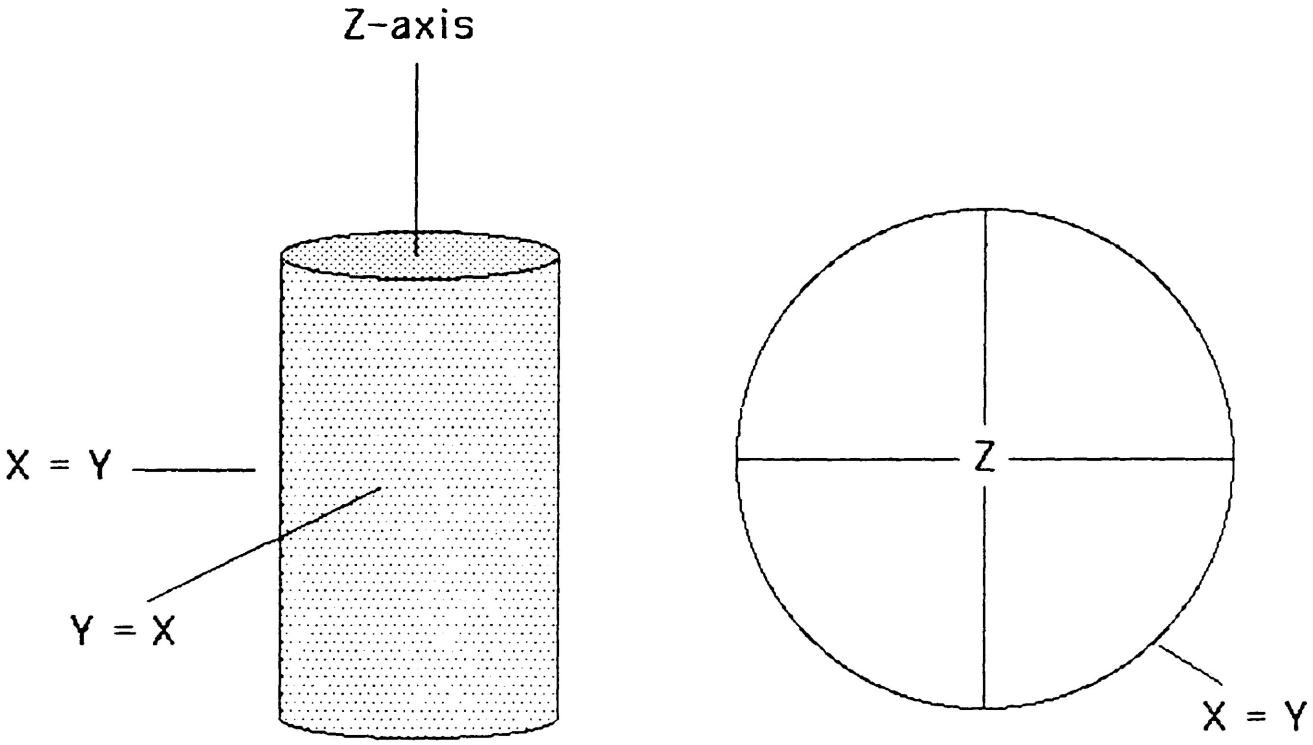

Figure 4-2. Orientation of the lower hemisphere equal area stereonet with respect to the direction of the maximum shortening (Z-axis) and the plane of flattening (X-Y plane) for the experimental pure shear tests.

illustrated by the use of natural log 'susceptibility plots' showing the changes in ratios of the principal susceptibilities. Jelineks' (1981) parameters P' and T are used to illustrate changes in both anisotropy and shape of the susceptibility ellipsoid.

In correlating the strain with the difference in total anisotropy, $\Delta P'$ is used, which is the difference between the anisotropy degree before deformation, P_o', and after any increment of deformation, P_n', so that:

$$\Delta P' = P_n' - P_o'$$

Strain in pure shear has been represented by ln(x/z) where:

$$z = 1 - e$$

$$x = z^{-1/2}$$

and

$$e = (l_o - l_n)/l_o$$

where l_o is the initial length of the specimen and l_n is the length after strain.

In simple shear strain is represented by ln(x/z) where:

$$x/z = (\lambda_1/\lambda_2)^{1/2}$$

and

$$\lambda_1 \text{ or } \lambda_2 = 1/2\,(\gamma^2 + 2 \pm \gamma\,(\gamma^2 + 4)^{1/2})$$

$$\lambda_1 = x^2$$

$$\lambda_2 = z^2$$

after Ramsay (1967)

Strain has been plotted in this fashion such that any power-law relationship of the sort;

$$\Delta P \propto \ln(x/z)$$

such as recognized in pure shear deformation by Borradaile and Alford (1987), will be apparent for both the current pure and simple shear experiments.

Thin sections were prepared for the pure and simple shear specimens such that both the undeformed materials and at least one deformed specimen from each series of tests would be represented.

Stress relaxation results are plotted on log stress versus -log(strain-rate) graphs such that the relationship;

$$\text{strain rate} \propto (\text{stress})^n$$

may be illustrated. As discussed earlier, the slope of the line fitting the data presented on the stress relaxation plot is equivalent to the stress exponent, n. Thus;

$$n = (\log \dot{e}_a - \log \dot{e}_b)/(\log \sigma_a - \log \sigma_b)$$

where $\dot{e}$ is the rate of permanent strain accumulation, in s^{-1}, and σ is in bars.

Relaxation of materials in a shear zone assembly have been previously recorded (Rutter et. al. 1985). However, the materials used in the shear zone assemblies of this investigation are noteably different from those of Rutter et. al. (1985). Also, the effect of relaxing two rheologically different materials at the same time is not yet understood, thus an initial series of relaxation tests were conducted on the materials that would be used to form the shear zone disks.

Three tests were conducted:

1) Relaxation of a 0.75 inch diameter cylindrical specimen of the end piece material for the shear zone assemblies (Berea sandstone) at a confining pressure of 21,750 p.s.i (1.5 kbars)

2) Relaxation of a 0.75 inch diameter cylindrical specimen of the Sand-cement material at a confining pressure of 10,000 p.s.i. (0.689 kbars)

3) Relaxation of the Berea sandstone/Sand-cement shear zone assembly at a confining pressure of 10,000 p.s.i. (0.689 kbars)

The results of the relaxation of Berea sandstone are illustrated in Figure 4-3. The slope of the data (n) is approximately 40 over the range of strain-rates permitted during the relaxation.

The confining pressure chosen for the relaxation of the Sand-cement and shear zone assembly are less than that for the Berea sandstone test, as caution was taken regarding any possible leaks due to jacket failure. However, since the rheological behaviour of the Berea sandstone is indicative of deformation by cataclasis, it would indicate that at lower confining pressures the result would be the same.

Figure 4-4 displays the result of the relaxation of the Sand-cement material. The behaviour of the material varies markedly from the Berea sandstone, as there is a noticeable change in slope at a strain-rate of approximately 7.0x10-7 s^{-1} (on graph $10^{-6.15}$).

Two relaxation tests on one shear zone assembly were conducted, the first test during the elastic field of deformation for the assembly (noted in the normal testing of the specimens)

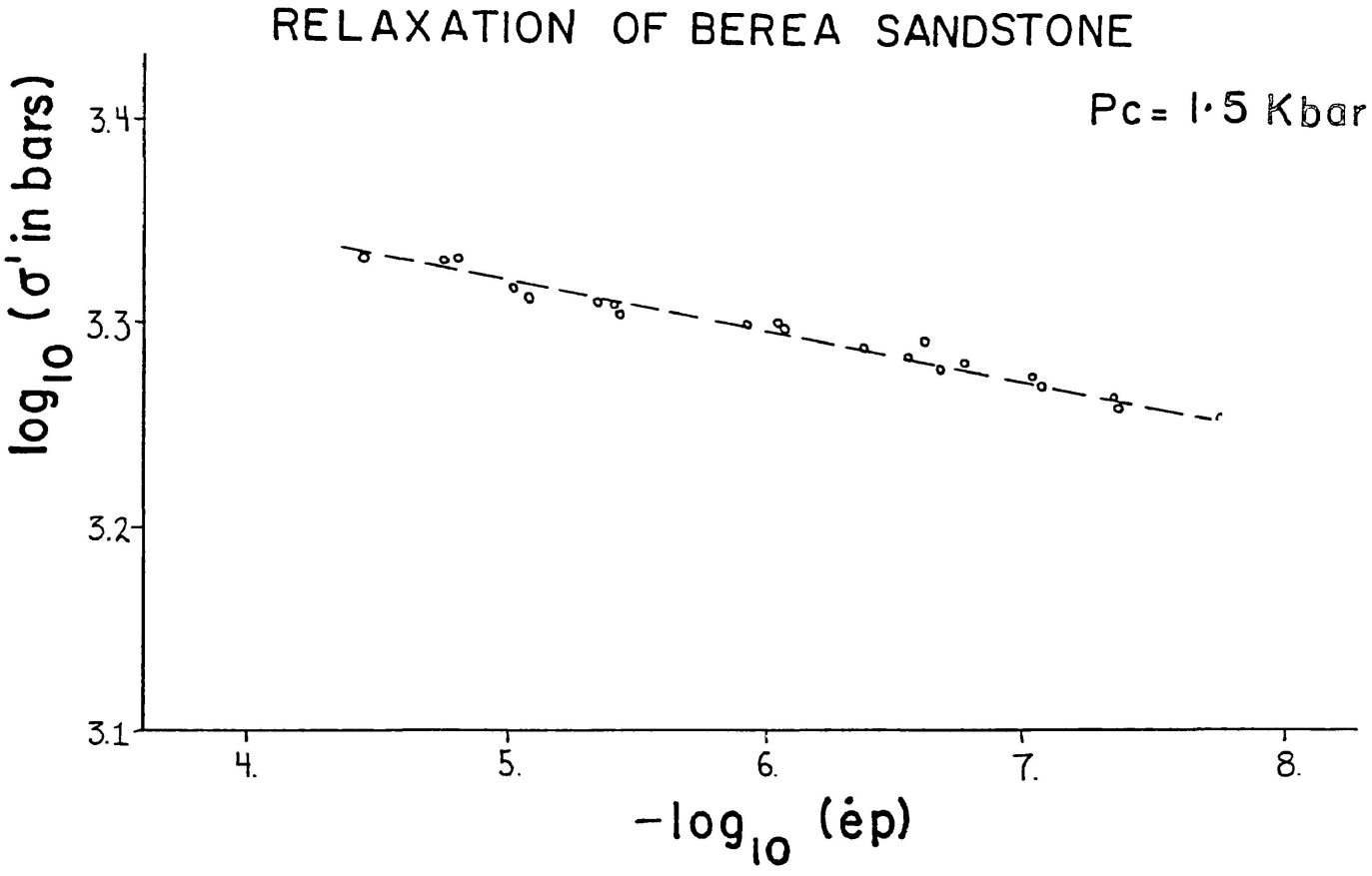

Figure 4-3. Stress relaxation results for 0.75 inch diameter cylindrical specimen of medium grained Berea sandstone at 1.5 Kbars confining pressure (σ = differential stress in bars, $\dot{e}p$ = the rate of accumulation of permanent strain).

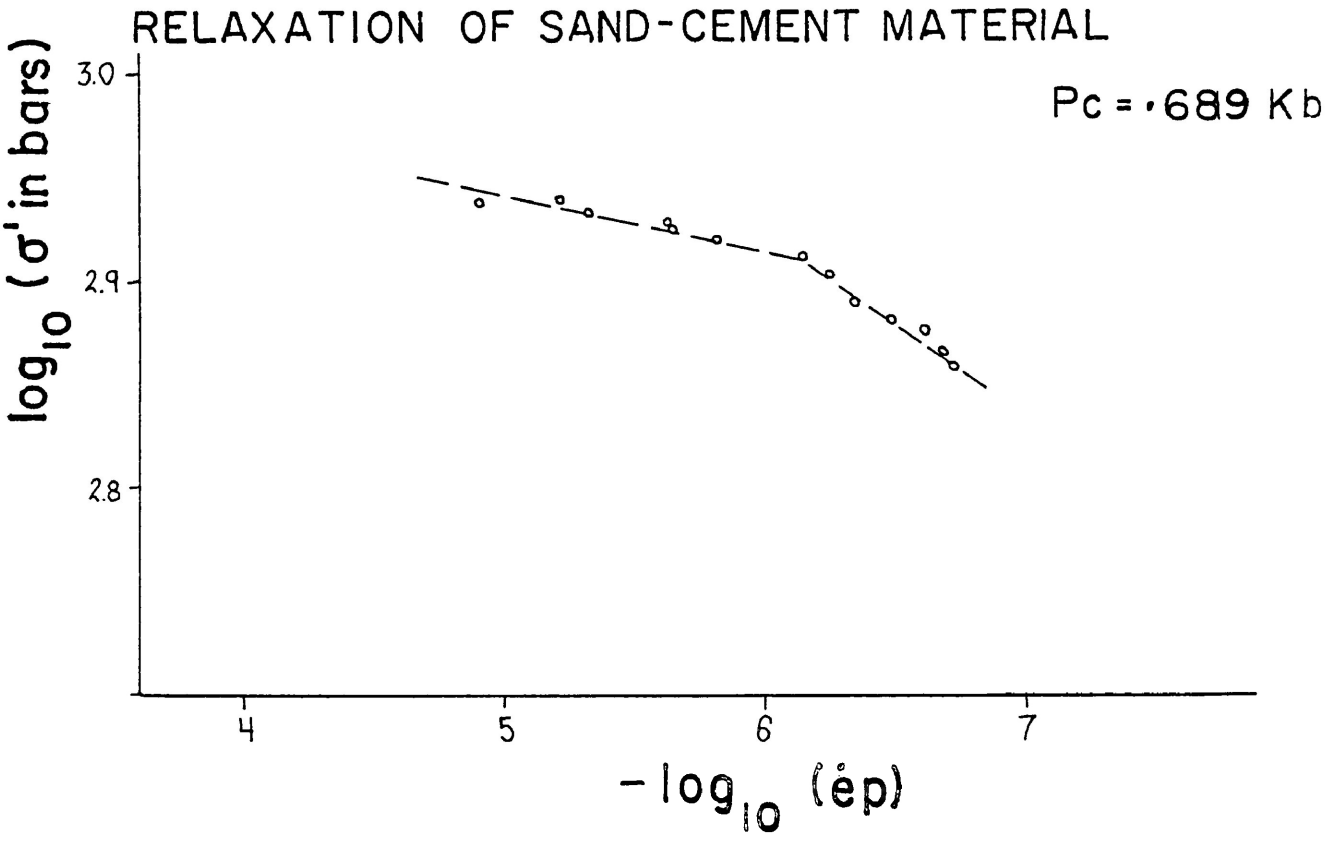

Figure 4-4. Stress relaxation resuts for 0.75 inch diameter cylindrical specimen of the sand-cement material at 0.689 Kbars or 10,000 p.s.i. confining pressure.

and the second within the field of non-recoverable deformation. For both tests, the value for the rock constant normally entered into the calculation of stress relaxation (See Appendix A) was arbitrarliy set to zero. This was done because the contributions of each of the angled-cut materials to the elastic constant for the entire shear zone assembly are unknown. Thus if any differences existed between these two tests, they would be detected.

The data from the two tests display very little difference in slope on the log stress versus -log (strain-rate) graph (Figure 4-5). Thus there would appear to be no rheological significance in relaxing the shear zone assembly at either amounts of strain used. The behaviour of the assembly as a whole is remarkably similar to the behaviour of the Berea sandstone, indeed the shear zone assembly consists mostly of the sandstone end pieces with only a small amount of the artificial material (approximately 23% of the volume in a typical one inch specimen) set between them.

Thus it is concluded that the resultant relaxation of the shear zone assembly is principally due to the Berea sandstone, the result lacking any similarity to the behaviour of the Sand-cement material (See Figure 4-4). Of the two materials, Berea sandstone also possesses the greater elastic rock constant value, the greater value tending to mask the lesser when two materials are relaxed together.

Therefore, at this time, precise stress relaxation results of the

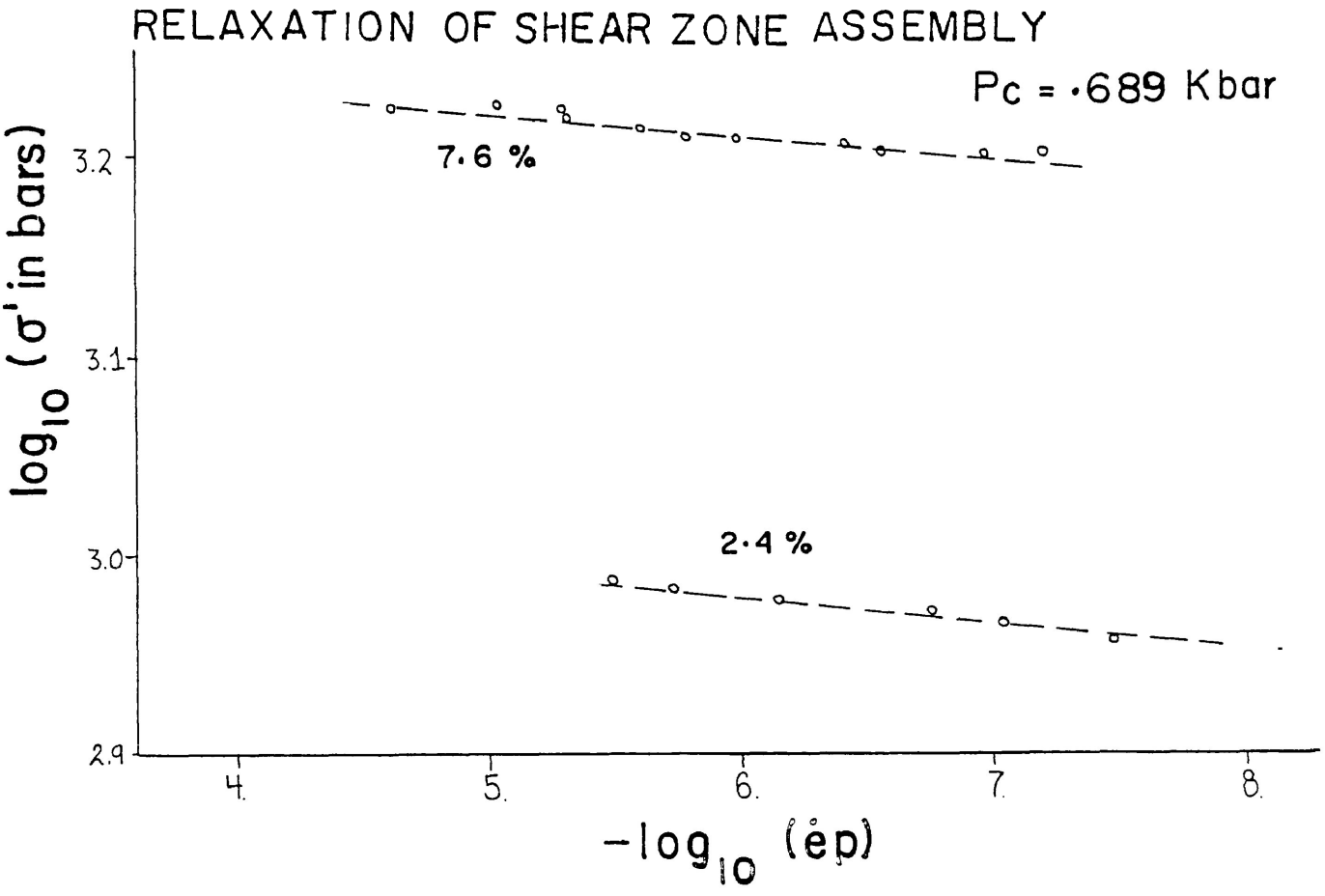

Figure 4-5. The results of two stress relaxation test of a sand-cement shear zone assembly at 0.689 Kbars or 10,000 p.s.i. confining pressure. The 2.4% deformation result represents relaxation within the elastic range for the material and the 7.6% deformation represents relaxation within the range of plastic deformation.

sandwiched materials cannot be obtained due to the complex specimen geometry. Therefore, only cylindrical specimens of each individual material will be investigated.

Subsequently, the relaxation of the shear zone materials, at the various confining pressures used, will be conducted in a pure shear geometry. At each confining pressure, at least two relaxation tests were attempted. The first, after approximately 5% axial strain and the second relaxation result was obtained by relaxing the same specimen by reloading it after its initial relaxation. The data from the tests, which run for a period of up to 48 hours, will be dismissed in part or in whole if an inordinate amount of confining pressure was lost or significant line voltage fluctuations occurred (See Appendix B).

Sand-Cement Shear Zones

For the sand-cement material three separate series (A, B and C) of tests were conducted, each at a different confining pressure.

Changes in the anisotropy, shape and orientation of the susceptibility ellipsoid:

For the first series, A at 0.689 kbars confining pressure, eleven shear zone specimens (A to K) were deformed using the single-step method. Shear strain (γ) values ranging from 0.02 to 0.4 were produced.

The rotations of the principal susceptibility directions from the experiments do not display any consistency in the direction of their displacement. Although the principal susceptibility directions can be significantly rotated (i.e. Figure 4-6), it is not known whether the alterations in the susceptibility ellipsoid correspond to the finite or incremental strains within the shear zone.

The susceptibility ellipsoids for most of the undeformed specimens lie in the field of flat-shaped ellipsoids (Figure 4-7). In nearly all cases, the effect of the experimental simple shear type of deformation is to move the susceptibilty ellipsoid away from the origin and further toward or into the field of flattening. A reasonably consistent pattern is displayed on the T versus P' plot (Figure 4-8). The susceptibility ellipsoids (except for shear

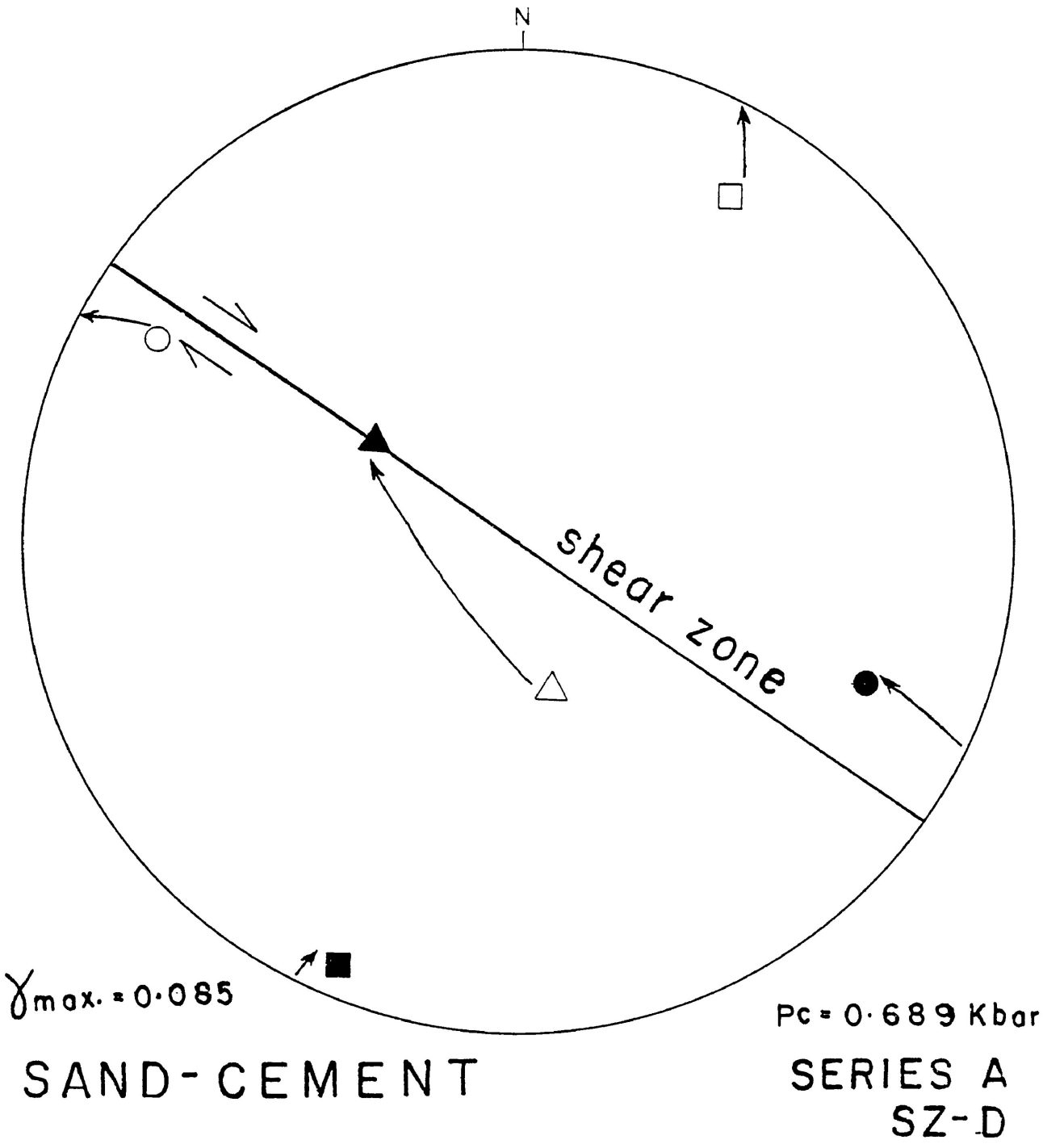

Figure 4-6. Stereonet illustrating the changes in orientation of the principal susceptibility directions for sand-cement SZ-D of Series A.

Note that throughtout this study K_{max} will be represented by a circle (O), K_{int} by a triangle (△) and K_{min} by a square (□). Those susceptibility directions relating to the undeformed specimens are unshaded while those relating to the specimen in the deformed state are filled.

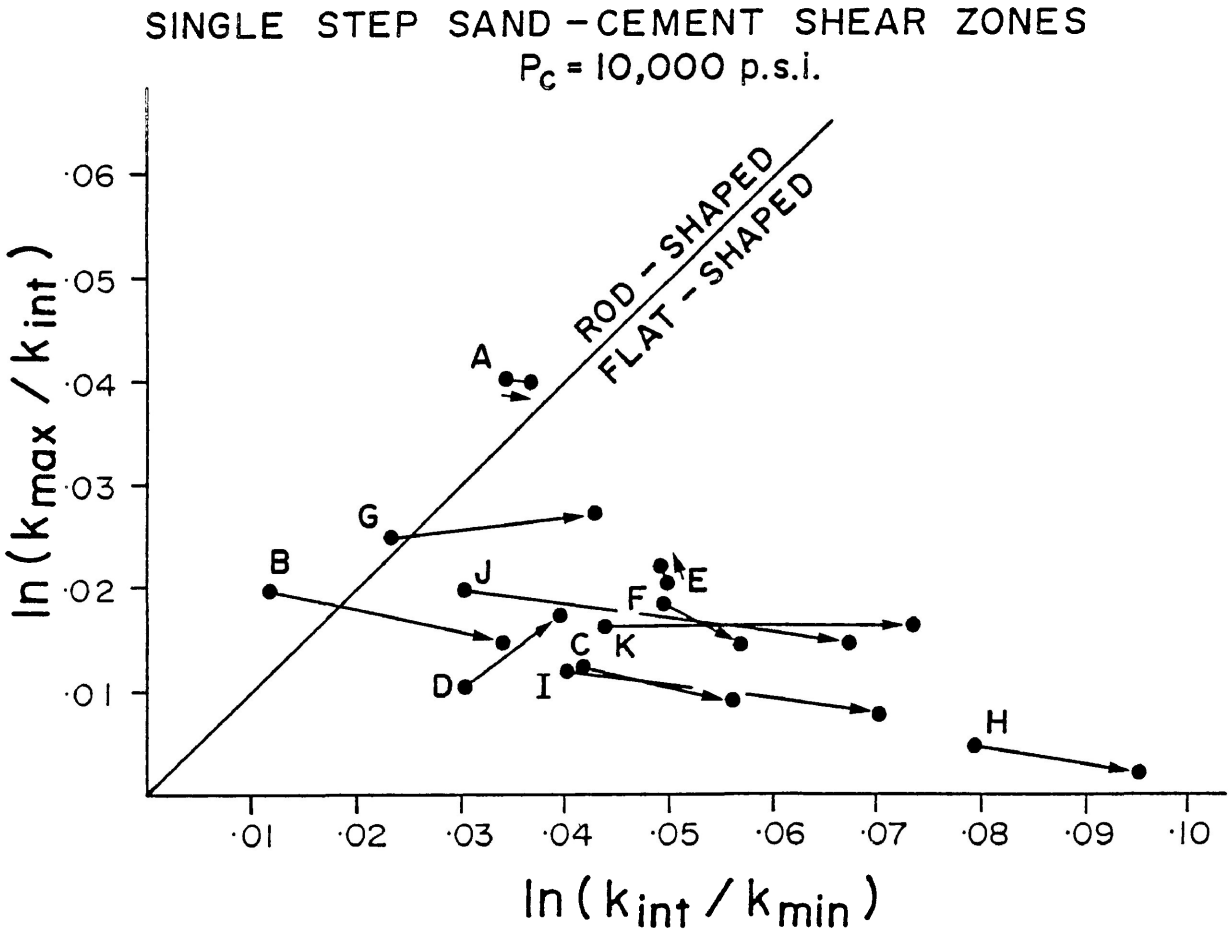

Figure 4-7. Changes in ratios of the principal susceptibilities, equivalent to changes in the shape of the susceptibility ellipsoids for the sand-cement single step deformation experiments. Most of the undeformed susceptibility ellipsoids lie in the field of flat-shaped ellipsoids and with shear strain the ellipsoids move into or further into the field of flattened shapes.

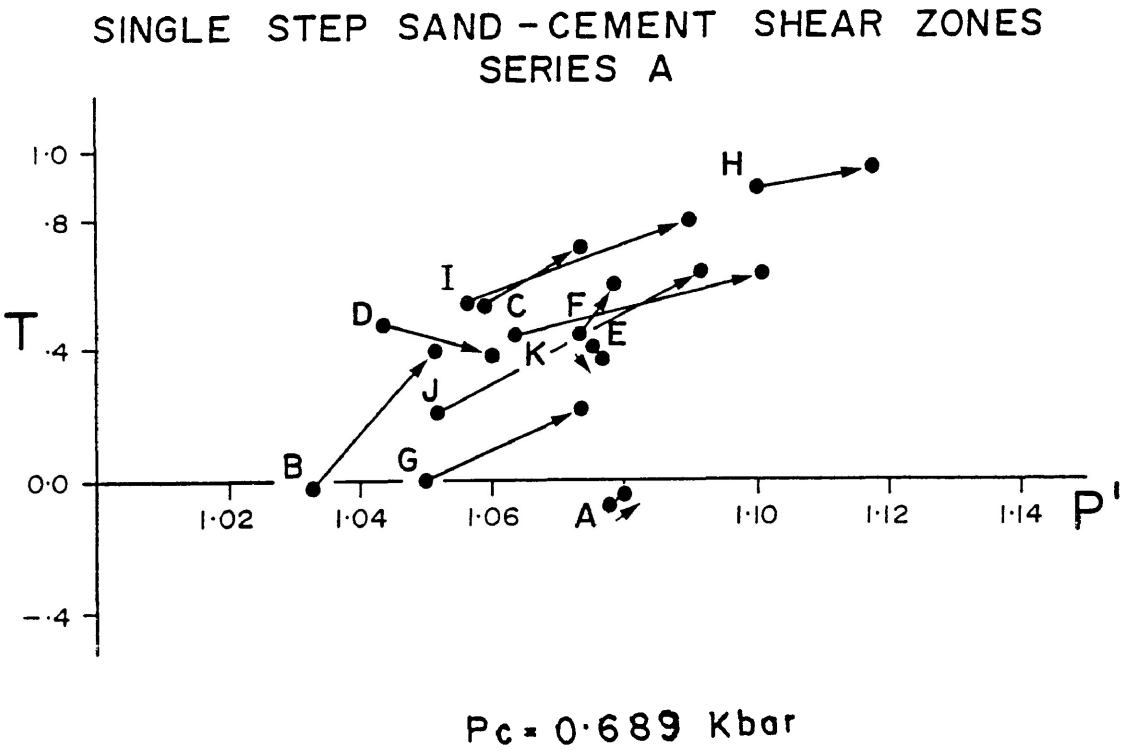

Figure 4-8. Illustrating the effect of the single-step experimental simple shear deformation on the susceptibility ellipsoids shape (T) and degree of anisotropy (P'). Generally the ellipsoids become more anisotropic and flattened with shear strain.

zone specimens D and E) have become flattened and in all cases the ellipsoids have suffered a general increase in their degree of anisotropy with shear strain.

However, when the change in the degree of anisotropy for each of the susceptibility ellipsoids are plotted against their respective shear strain values, a scattering of data occurs (Figure 4-9).

From the pure shear experiments of Borradaile and Alford (1987), it was surmized that even a linear relationship between $\Delta P'$ and ln(X/Z) only partly illustrated the dependence of the changes in anisotropy on strain. The susceptibility ellipsoid, in this manner behaves somewhat like a passive physical ellipsoid object, in that besides its shape, its initial orientation is critical to the change in the MSA with strain.

A wide degree of variability is found in the initial orientations of the principal susceptibility directions for experiments A to K. However, a close comparison of the initial susceptibilty directions in the series yields reasonably similar initial orientations in specimens A,G and J; and in B and E. Isolating the results from the experiments A,G and J (Figure 4-10), indicates that some linear correlation may exist between them. Therefore, the initial orientation of the susceptibility ellipsoid is perhaps significant in controlling the final ellipsoids' shape and anisotropy within the shear zone specimens.

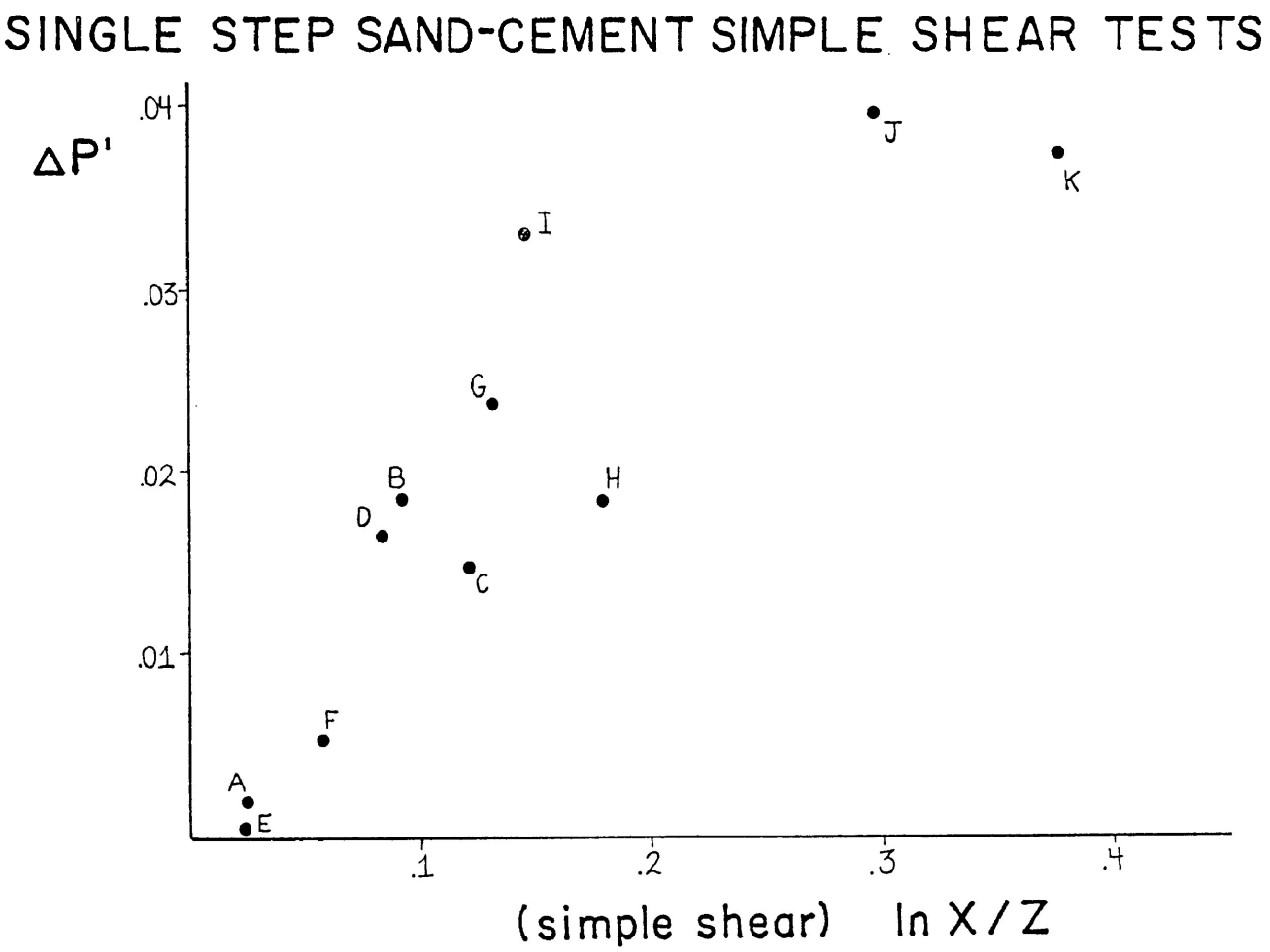

Figure 4-9. Illustrating the change in the degree of anisotropy before and after shear strain ($\Delta P'$), against the natural logarithm of the shear strain ratio (X/Z) for all the sand-cement single step experiments. Note that no significant correlation is observed from the data from the individual shear zones.

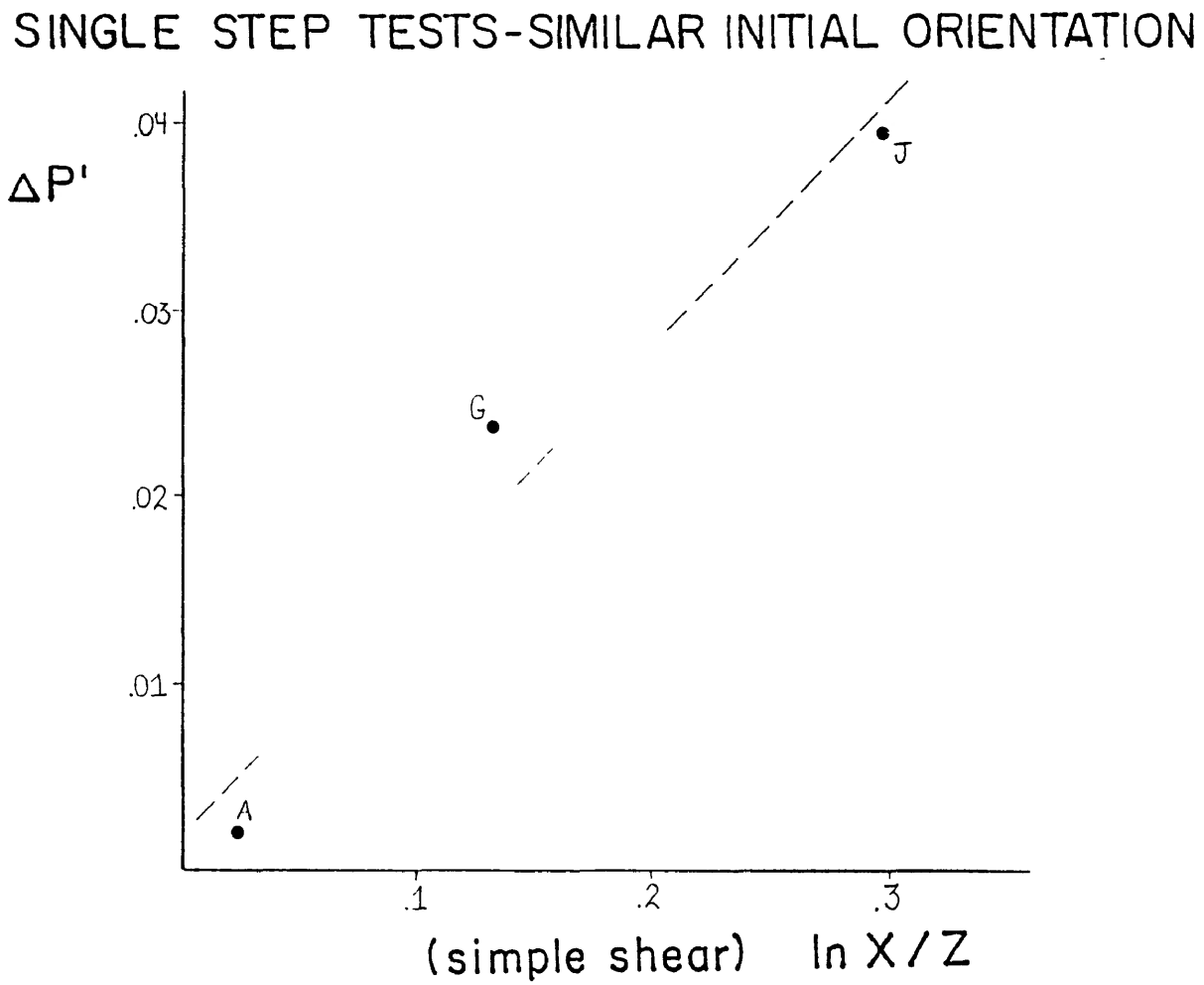

Figure 4-10. Correlation of ΔP' and the shear strain ratio (ln (X/Z)) for experiments SZ--A, SZ-G and SZ-J of Series A. These experiments are isolated from the others due to their common initial orientation. The correlation coefficient is 0.977.

Subsequently, all further shear zone specimens were deformed several times in small axial strain increments (the multiple-step method). In this way, progressive changes in the magnitude and orientation of the susceptibility ellipsoid could be observed for each individual shear zone.

Two individual multiple-step deformation tests were conducted for series A, totalling 16 experiments.

The principal susceptibility directions for the two progressive tests are similar (Figures 4-11 & 4-12) and during the experiments, do not display any significant change in orientation.

The angle between any principal susceptibility direction and the shear zone (α') can be measured directly on the primitive plane of the stereonet for each increment of shear strain. Using a diagram of the angular position, α, versus shear strain, γ, it is possible to compare the rotation (the change in angular position) of the principal susceptibility directions to the rotation of a hypothetical line undergoing simple shear, as given by:

$$\cot\alpha' = \cot\alpha + \gamma$$

Where any line starting with an initial orientation, α, is rotated to a new position, α', after an amount of shear strain, (Figure 4-13). Thus every line of different initial orientation

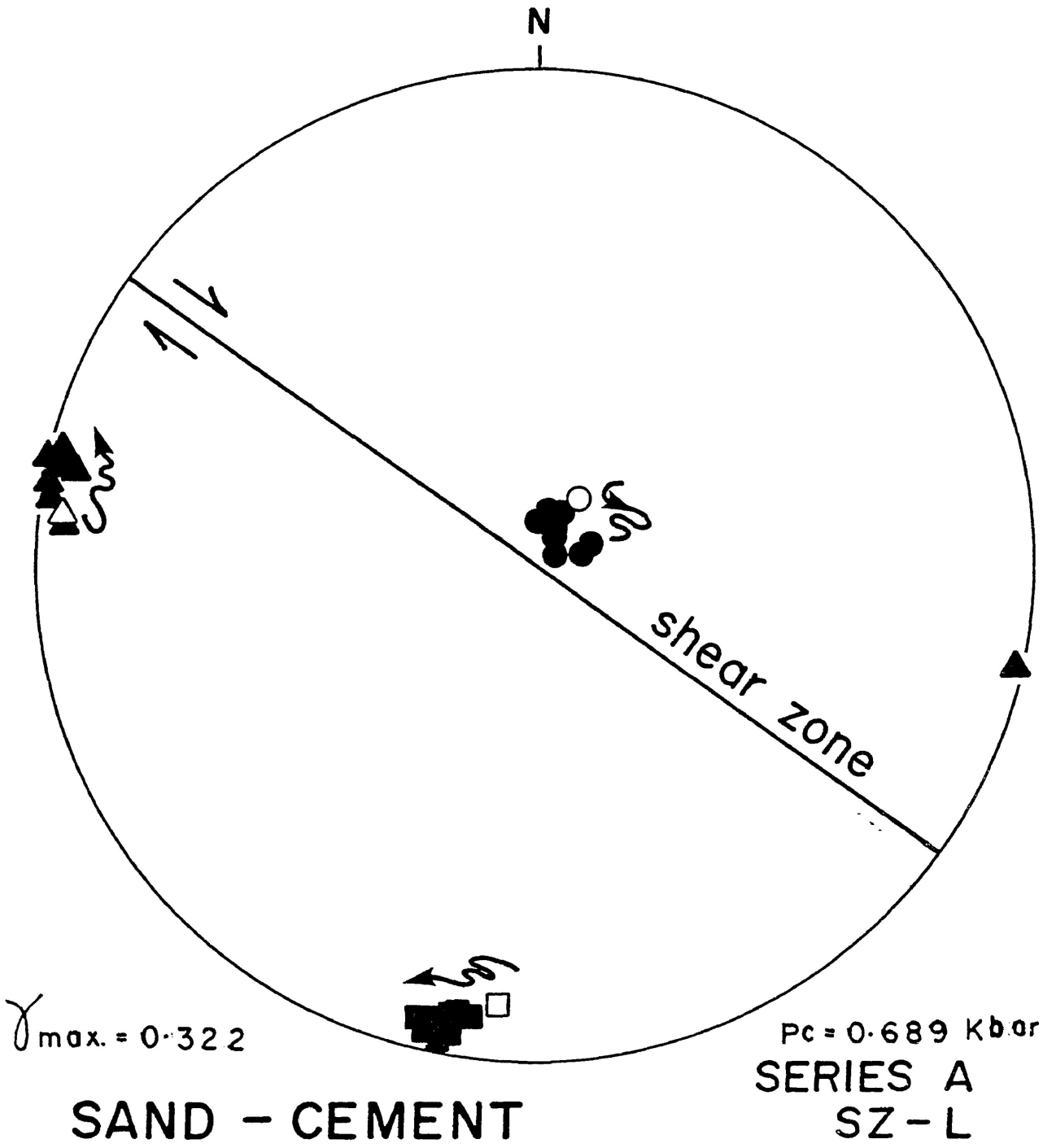

Figure 4-11. The changes in orientation of the principal susceptibility directions for the multiply deformed sand-cement SZ-L of Series A.

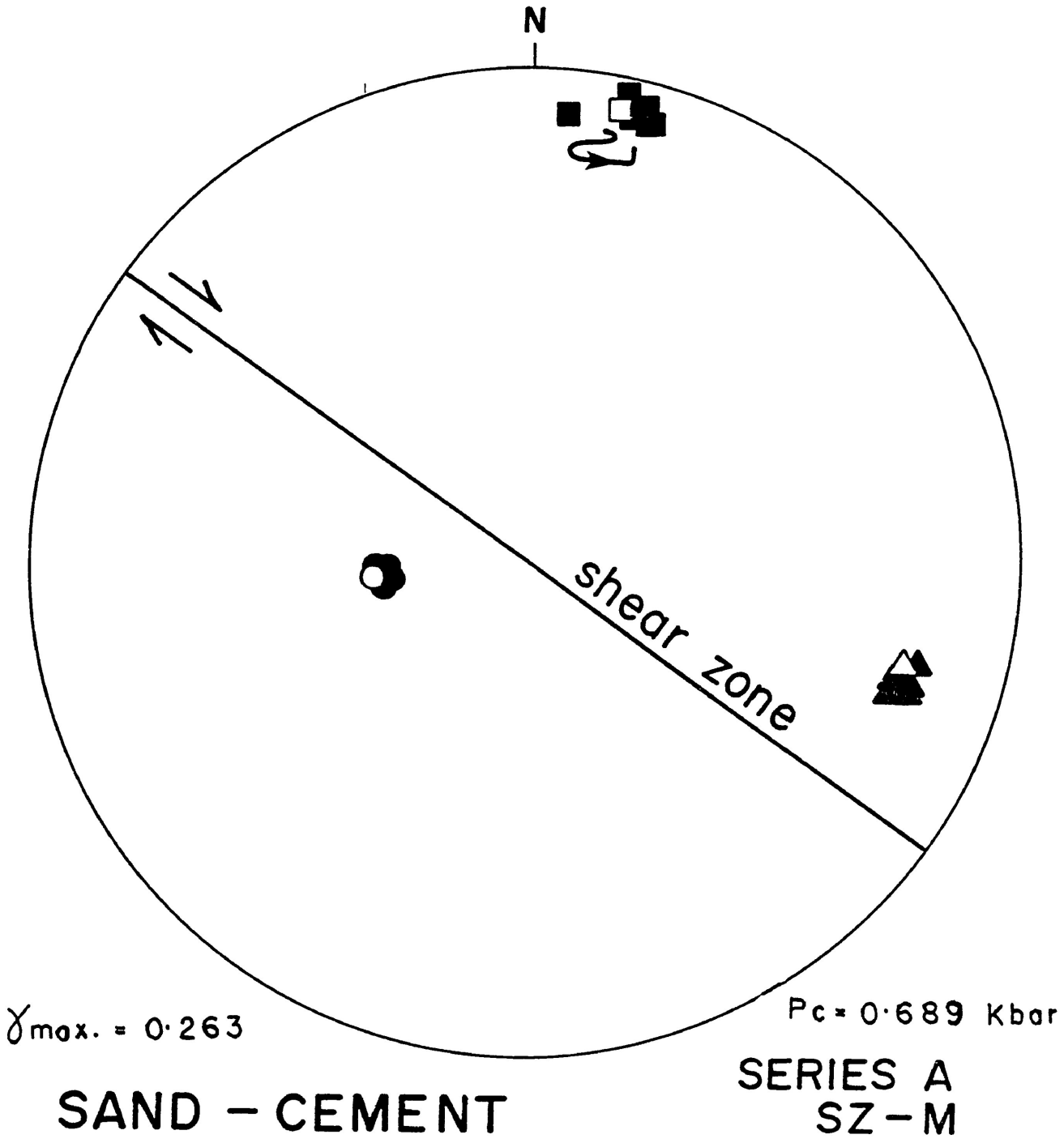

Figure 4-12. The change in orientation of the principal susceptibility directions for the sand-cement SZ-M of Series A.

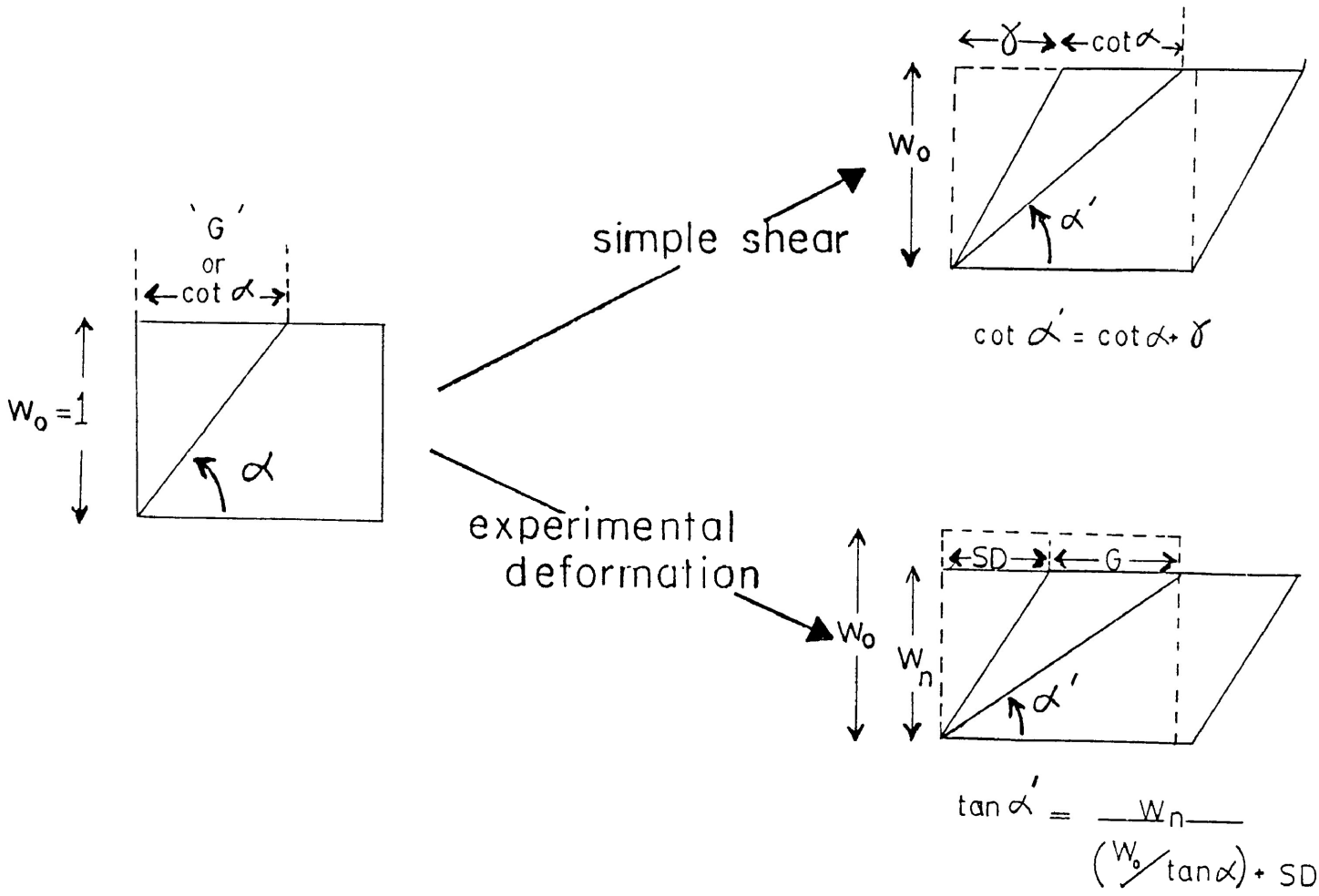

Figure 4-13. The equations describing the change in angular position of a material line within a block deforming by simple shear and the experimental deformation.

undergoes a different line rotation for a given shear strain value (after Ramsay and Huber 1983).

Figure 4-14 displays the rotation of the principal susceptibility directions for experiment SZ-L (dashed lines) against those expected from variously orientated hypothetical lines undergoing simple shear (solid lines). Each of the three principal susceptibility directions displays a different behaviour: K_{min} initially rotates faster than would be expected from a hypothetical line of the same initial orientation and with further shear strain continues to rotate toward the direction of shear but in a manner that is slower than that of the line. K_{int} intially rotates slower than would the line, and with further shear strain rotates toward the direction of shear in a manner that is faster than the similarly orientated line element. Throughout deformation K_{max} assumes orientations that show it to be rotating in a manner that is sometimes slower and sometimes faster than the hypothetical line. The probable reason for this rather eccentric behaviour is its orientation; K_{max}, in this shear zone, is nearly perpendicular to the plane which 1) contains the shear direction and is 2) perpendicular to the shear zone (e.g. the primitive plane of the stereonet). Subsequently, only those susceptibility directions that exist in or near ($\pm 20^{o}$) this plane will be considered.

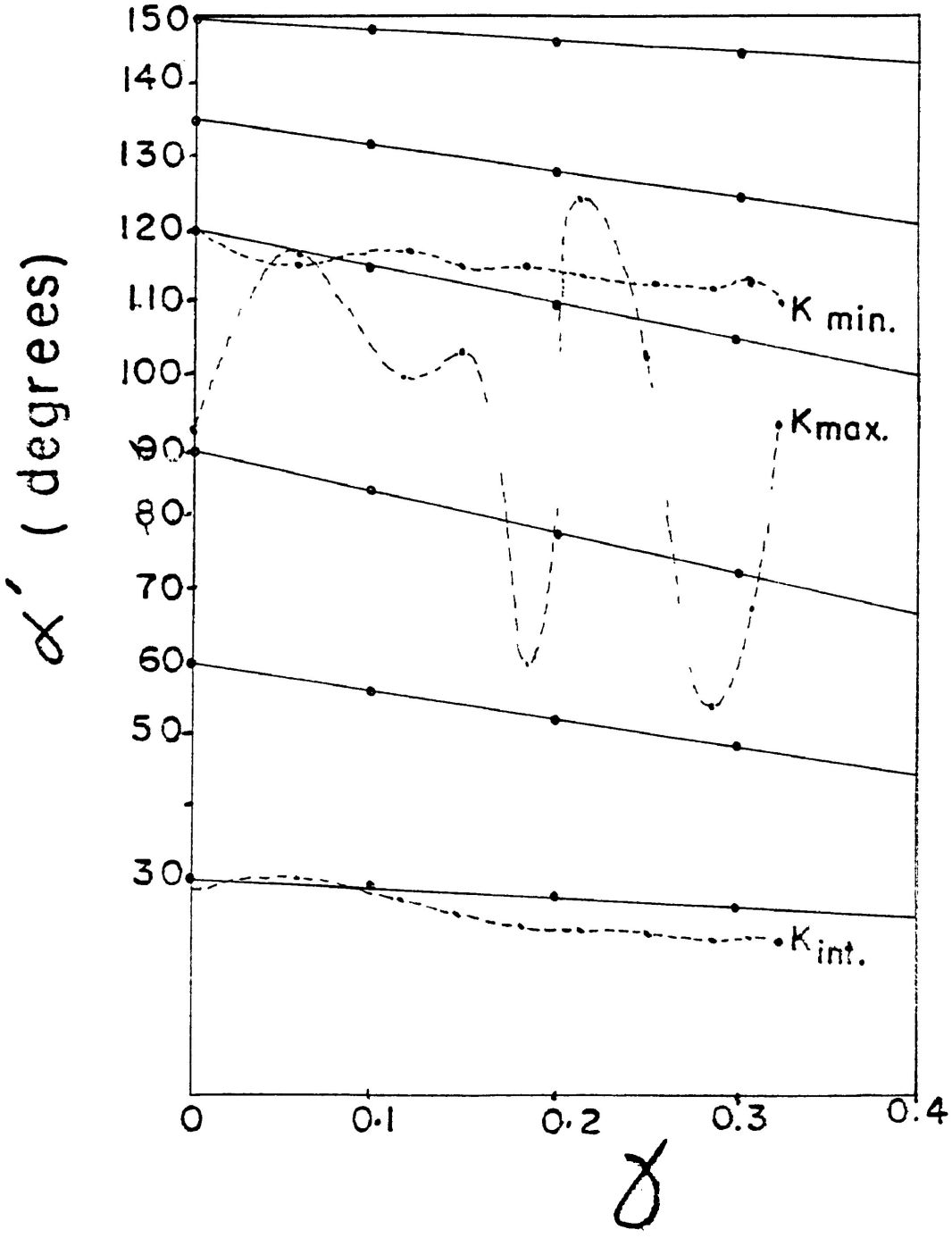

Figure 4-14. Comparison of the change in angular position, measured within the primitive plane of the stereonet, of the three principal susceptibility directions with respect to the shear zone (dashed lines) against the changes in angular orientation expected from variously orientated material lines (solid lines).

The change in angular position experienced by the hypothetical material lines are calculated assuming simple shear, where no change occurs in the width of the shear zone. However, in experimental conditions an appreciable change in the width of the shear zone may occur (up to 10%). Therefore, to accurately calculate the change in angular position of a hypothetical line undergoing deformation similar to that which is experimentally produced, it is necessary to take into account the width change within the shear zone (see Figure 4-13). Thus the new orientation, α', is a function of the amount of shear displacement, SD, the original width, W_o, the new width, W_n, and the old orientation, α, by:

$$\tan\alpha' = \frac{W_n}{(W_o/\tan\alpha) + SD}$$

If no change in width occurs, the equation reduces to that describing the case of simple shear.

The change in angular position can in this way be determined for any initially oriented line from the marks on the deformed specimens. So although no lines were actually drawn onto the shear zone the rotation described can be said to be equivalent to that of a 'real' line element.

Figure 4-15 dispays the rotation of those principal susceptibilty directions (dashed lines) within or near the plane containing the shear direction (the edge of the stereonet) from SZ-L in relation to a 'real' line of exactly the same initial orientation (solid lines) which is experiencing the same deformation. K_{min} and K_{int} still display an initial rotation differing from those of the line elements. On the whole however, the rotations of K_{min} and K_{int} match those of the 'real' line elements much more closely than the rotations predicted using the previous method which did not account for compression of the shear zone (see Figure 4-14).

The rotation of the K_{min} principal susceptibility direction in SZ-M is somewhat different from that of the 'real' line of the same initial orientation (Figure 4-16). K_{min} initially rotates toward the direction of shear at a rate much faster than the 'real' line element. However, with further shear strain Kmin rotates slightly away from the shear direction and then back toward it at a rate very close to the 'real' line.

Both of the susceptibility ellipsoids of SZ-L and SZ-M initially began their deformation history as slightly flat-shaped ellipsoids (Figure 4-17). The ellipsoid for SZ-L takes on shapes during the first several increments of deformation that are sometimes less anisotropic and less flat before becoming progressively flatter

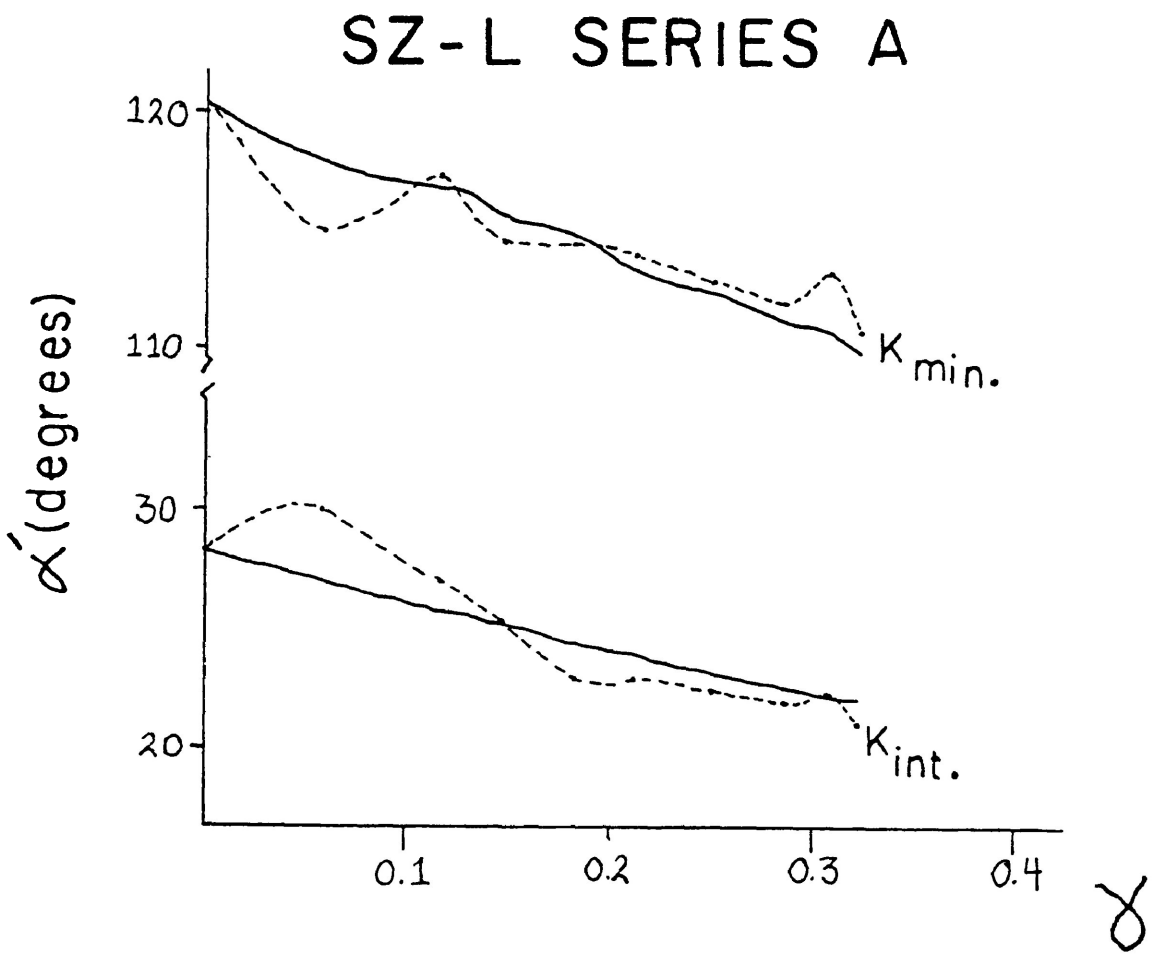

Figure 4-15. The change in angular position with respect to the shear zone, α', of the K_{min} and K_{int} susceptibility axes, measured from the stereonet, for SZ-L of Series A (dashed lines) against those expected from real material lines of similar initial orientation (solid lines).

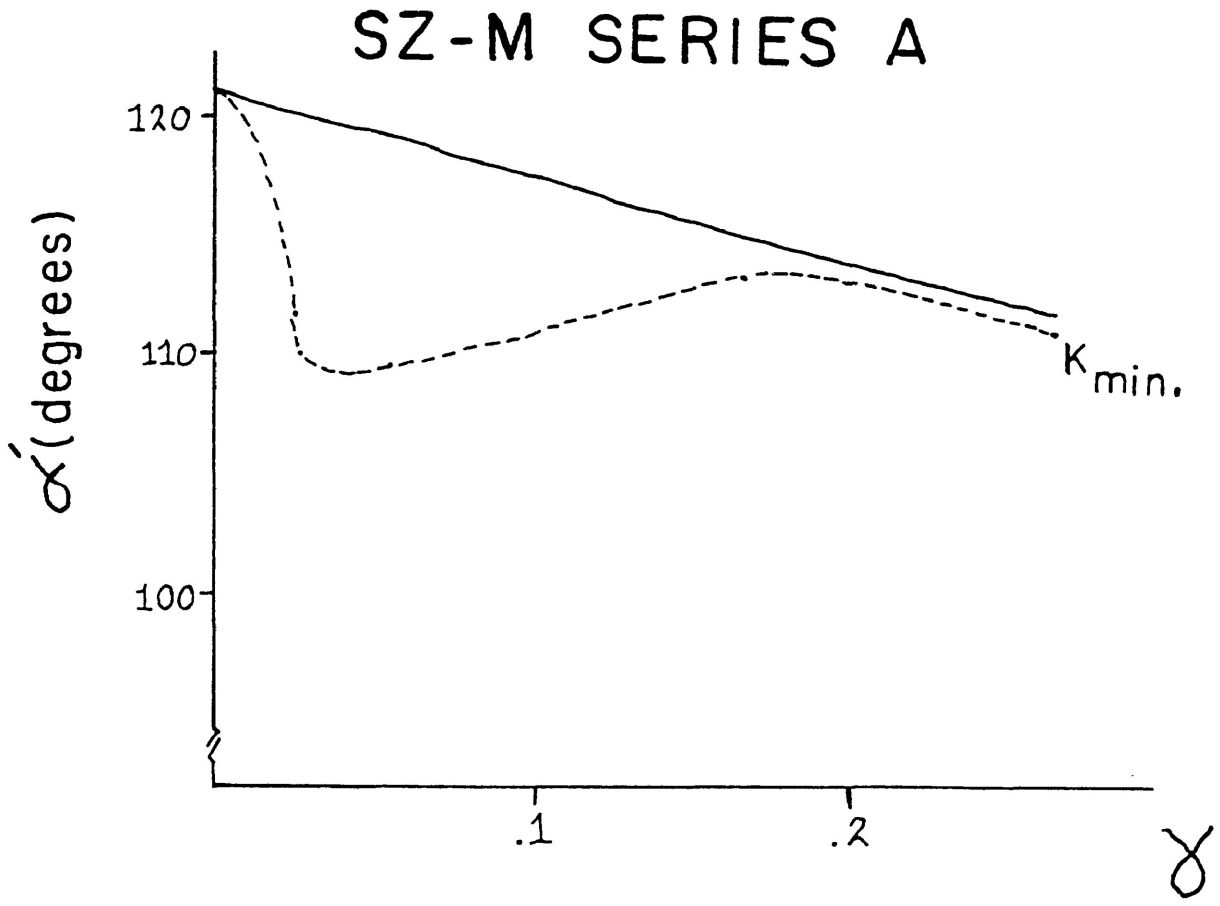

Figure 4-16. The change in angular position measured for the Kmin susceptibility axis (dashed line) against that expected for a similarily oriented real material line (solid line).

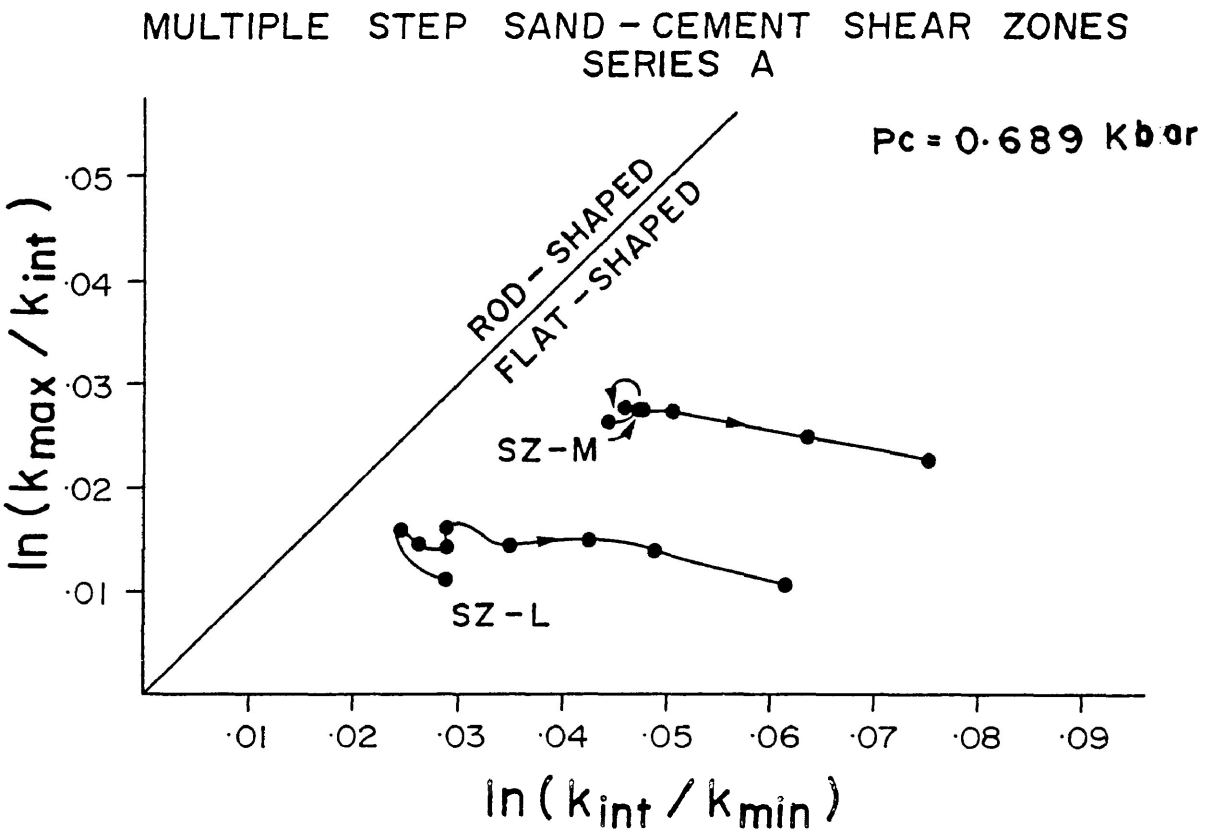

Figure 4-17. Illustrating the progressive change in shape of the susceptibility ellipsoids for the two multiply deformed sand-cement shear zones, SZ-L and SZ-M of Series A.

and more anisotropic with increased shear strain (Figure 4-18). The susceptibility ellipsoid of SZ-M, except for one minor step, becomes increasingly flatter and more anisotropic throughout the test.

The correlations between the degree of anisotropy and shear strain, for the two experiments are illustrated in Figures 4-19 & 4-20. The data from experiment L display an upward curve, whereas the data from experiment M display a linear power-law correlation.

Three individual specimens were deformed in Series B, totalling 15 experiments. A confining pressure of 1.0 kbar was employed throughout the series.

In shear zone one (SZ-1) the principal susceptibility directions remained in a relatively stable or 'fixed' orientation throughout the test (Figure 4-21). Thus, SZ-1 displayed a very similar behaviour to the previous multiple-step experiments SZ-L and SZ-M in Series A.

In order to aid in differentiating effects associated with the finite strain, the incremental shear strain and any compaction of the shear zone on changes in the principal susceptibility directions it is necessary to:

(a) Identify specialized orientations of the principal susceptibility directions before strain that will yield decisive information about the strain history; and

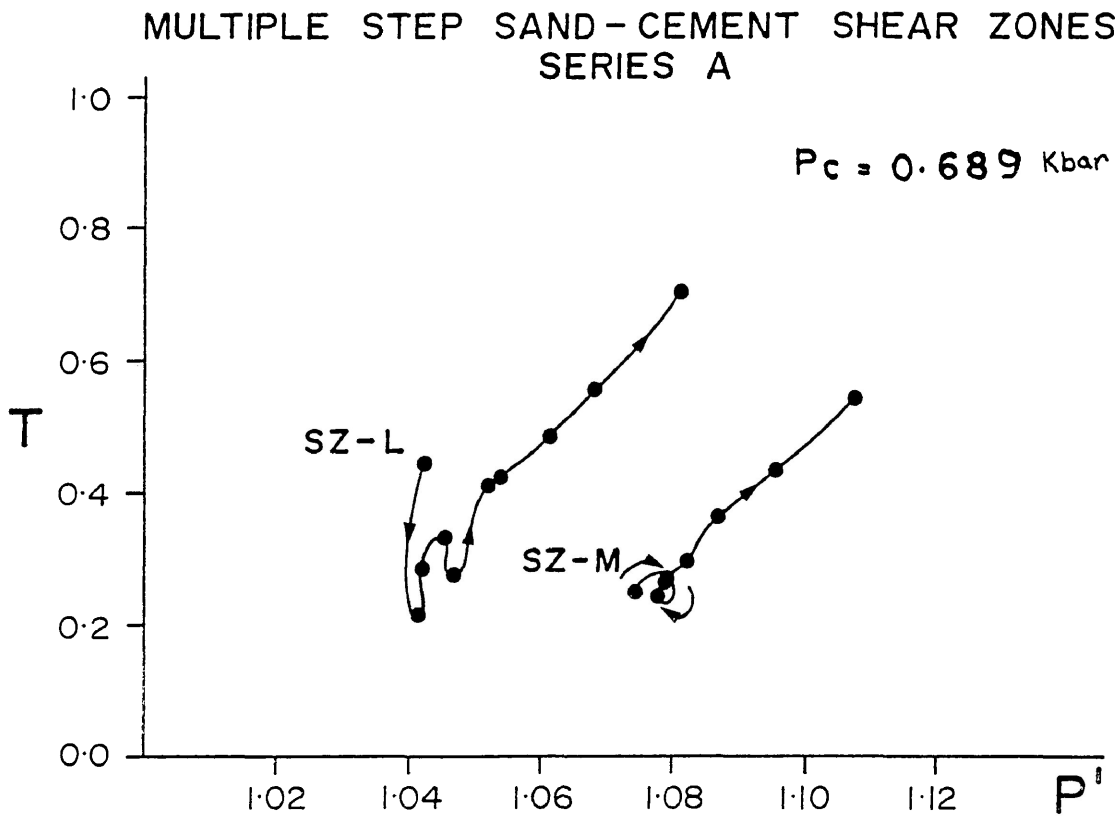

Figure 4-18. Illustrating the progressive changes in shape and anisotropy for the multiply deformed shear zones of Series A.

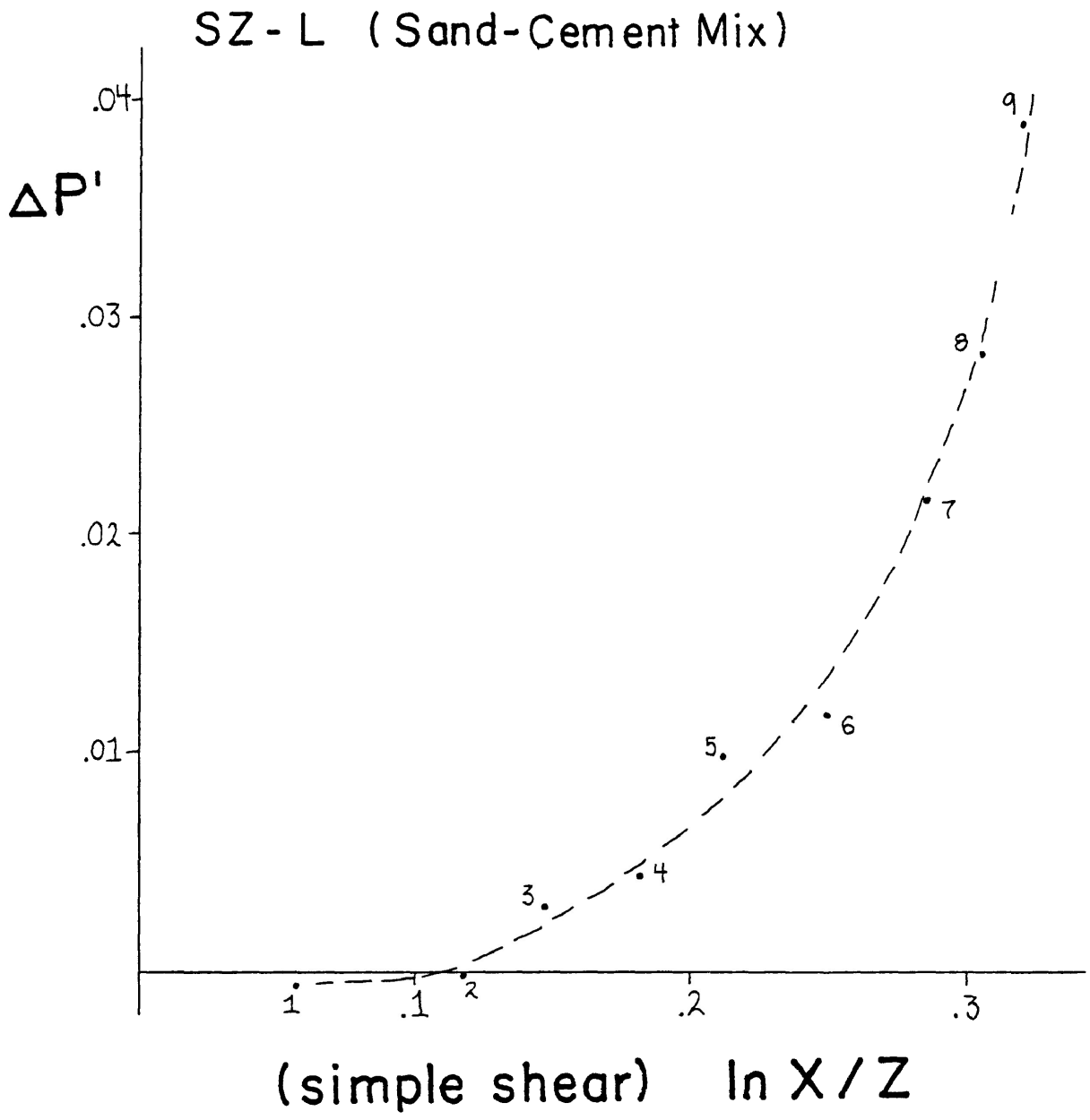

Figure 4-19. Correlation of the change in the degree of anisotropy with the shear strain ratio for SZ-L of Series A.

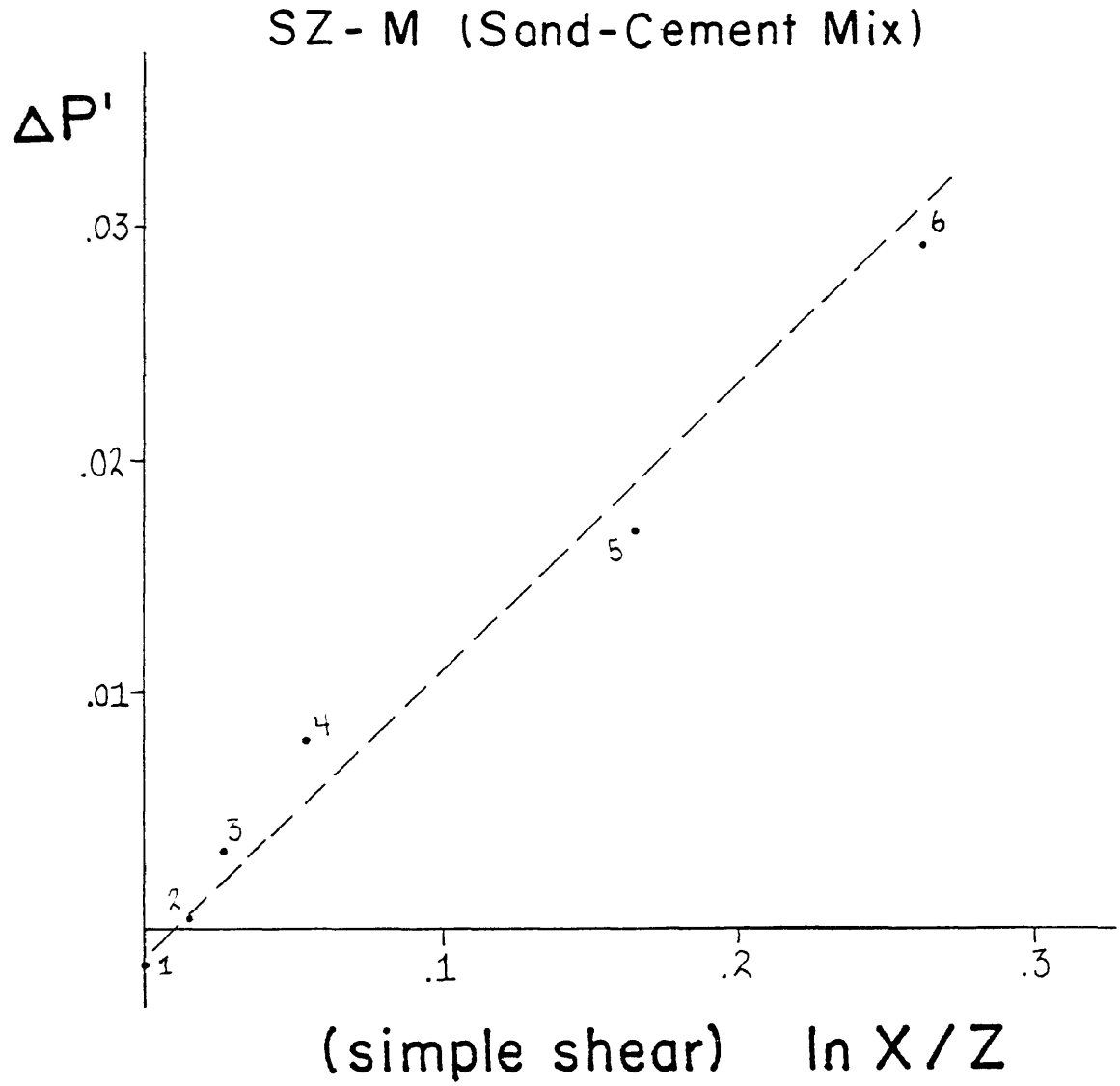

Figure 4-20. Correlation of the change in the degree of anisotropy with the shear strain ratio for SZ-M of Series A. The correlation is significant at the 95% level with a coefficient of 0.993.

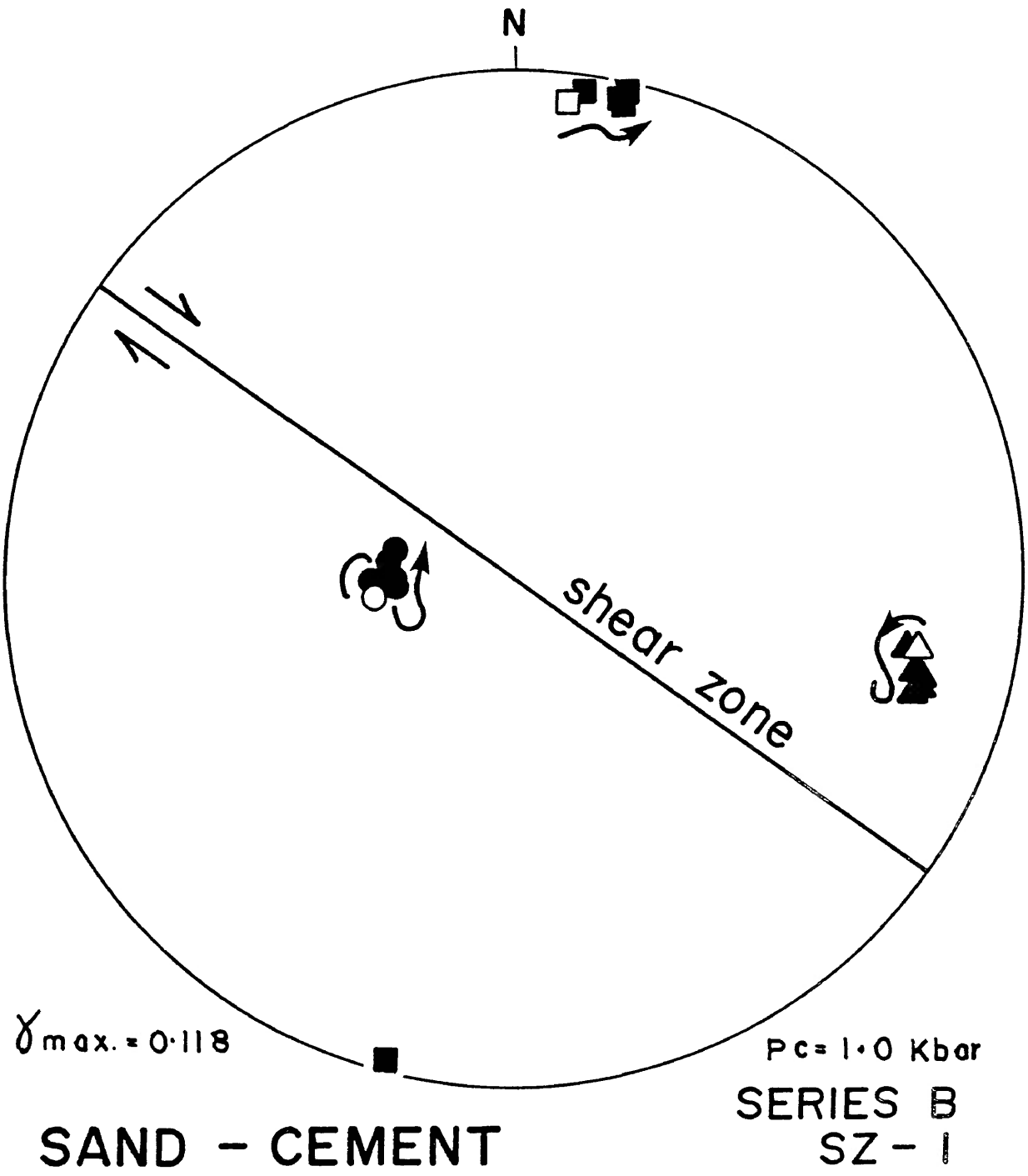

Figure 4-21. Illustrating the progressive changes in the orientation of the principal susceptibility ellipsoids for SZ-1 of Series B.

(b) Deform the specimen by an amount of strain necessary to observe significant changes in the susceptibility orientation.

An orientation that might satisfy the above mentioned criteria is illustrated in Figure 4-22. Note that the maximum and minimum principal susceptibilities lie between the direction of the earliest 'schistosity' (representing the maximum principal axis of the incremental strain ellipse) and the direction of the plane of flattening that could exist due to axial compaction of the shear zone. In this orientation, rotation due to compaction would be clockwise, towards the plane of flattening, whereas a counterclockwise rotation would correspond to an initial movement towards the direction of the embryonic schistosity.

In order to detect this effect it would be necessary to stop the test at this point because any further amount of shear strain would rotate the finite strain ellipse in a clockwise manner. The net motion would then be indistinguishable from an early rotation due to compaction.

Fortunately, SZ-2 began with an initial susceptibility orientation very near to the previously mentioned 'special' orientation. The initial and subsequent rotation of the principal susceptibilities (steps 0 to 1 through 4) is towards the direction of shear (Figure 4-23). The rotation is in a clockwise sense, but

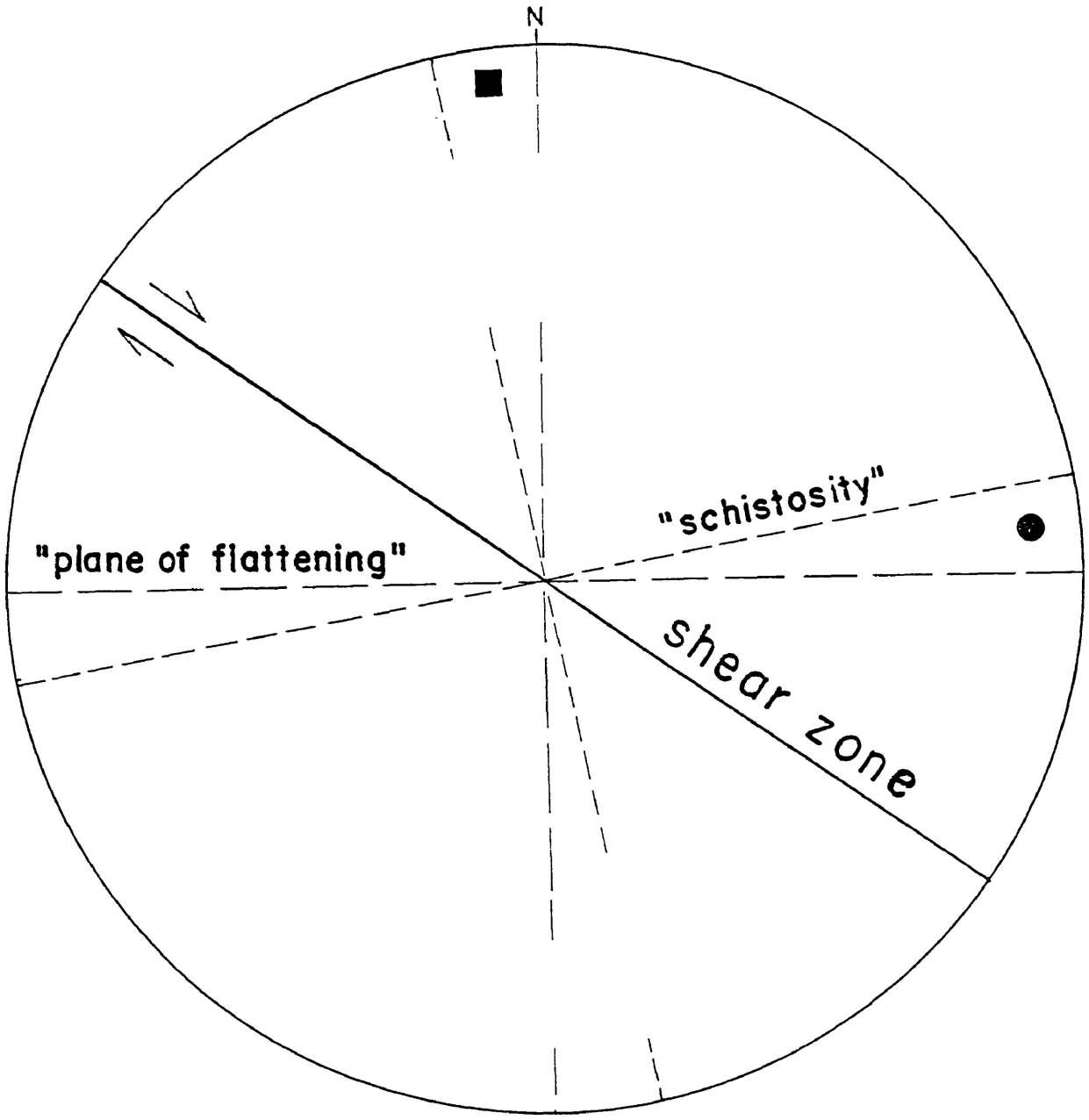

Figure 4-22. One possible orientation of the K_{max} and K_{min} susceptibility axes that, during the initial increment of experimental simple shear deformation, may differentiate the rotation of the suscpetibility axes as to whether the simple shear or compaction component of deformation is primarily responsible for re-orientating the susceptibility ellipsoid. In this orientation the initial increment of strain may rotate the susceptibility directions toward the initial schistosity if the susceptibilities correspond to the finited strain ellipse within the zone or toward the plane of flattening if they correspond to the flattening of the shear zone.

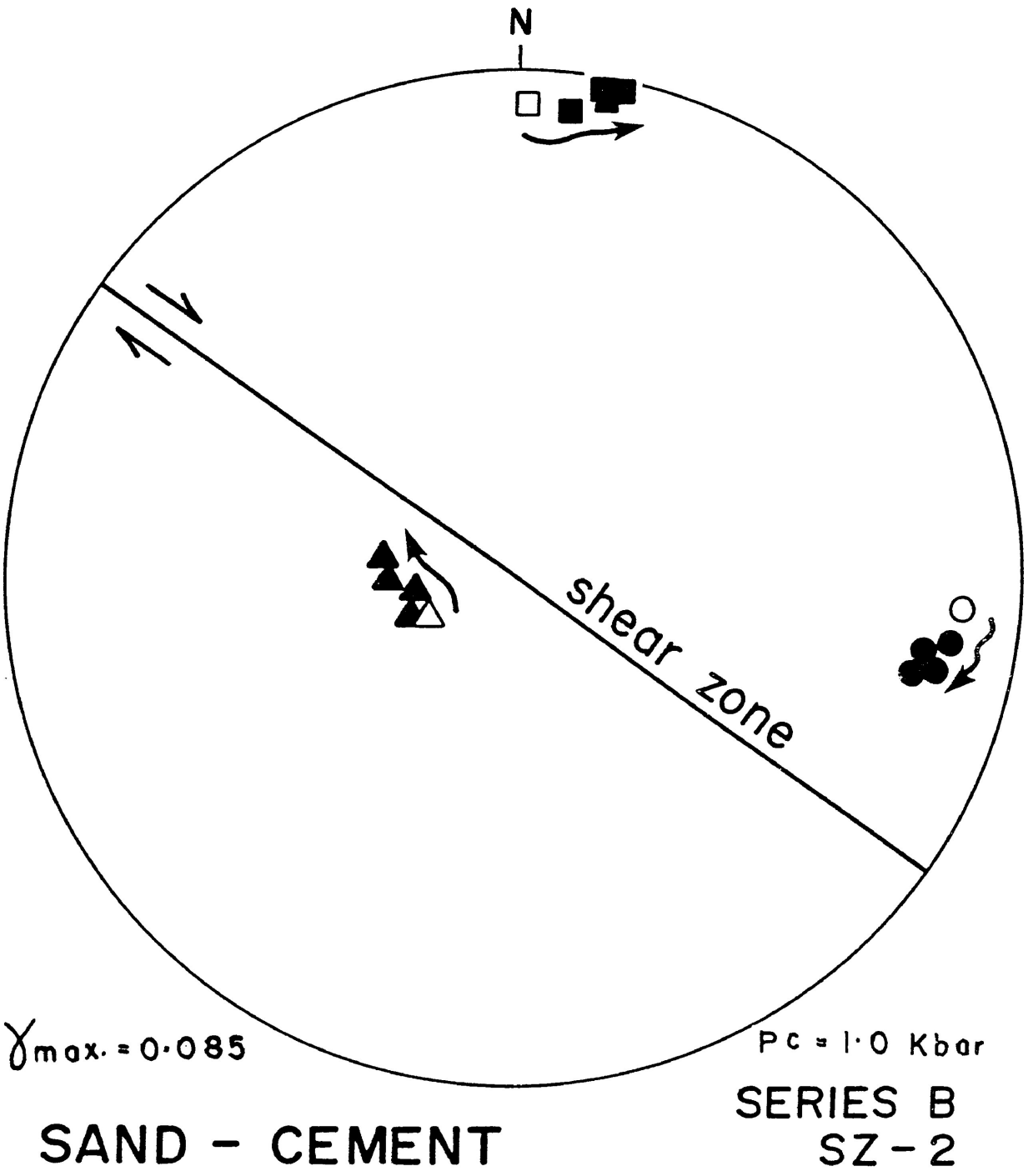

Figure 4-23. Illustating the progressive changes in orientation of the principal susceptibility directions for SZ-2 of Series B.

the susceptibility axes rotate beyond the trace of the plane of flattening. Thus, for this test the susceptibility directions appear to be behaving in a manner similar to the finite strain ellipse in that the maximum elongation direction continually rotates toward the shear direction, however no initial movement toward the embryonic 'schistosity' direction was recorded.

All the susceptibility directions of SZ-3, in this series, displayed an initial counter-clockwise rotation and importantly the maximum susceptibility rotates towards the trace of the initial 'schistosity' (Figure 4-24). With further shear strain, the susceptibility directions (especially K_{int}) rotated in a clockwise manner and eventually rotated into an orientation similar to SZ-2.

Each of the prinicipal susceptibility axes within or near the plane described by the primitive plane of the stereonet, illustrates differing degrees of conformability to their respective 'real' line elements. Within SZ-1 the susceptibilty axes K_{min} and K_{int} initially rotate faster than the calculated rotations for the 'real' lines of similar initial orientation (Figure 4-25). With increasing shear strain, the rotation of Kmin and Kint both slow and their angular position become near to that of the 'real' line elements. The principal susceptibility directions K_{max} and K_{min} in SZ-2 (Figure 4-26) rotate in manner that is slightly faster but very similar to that of the 'real' lines.

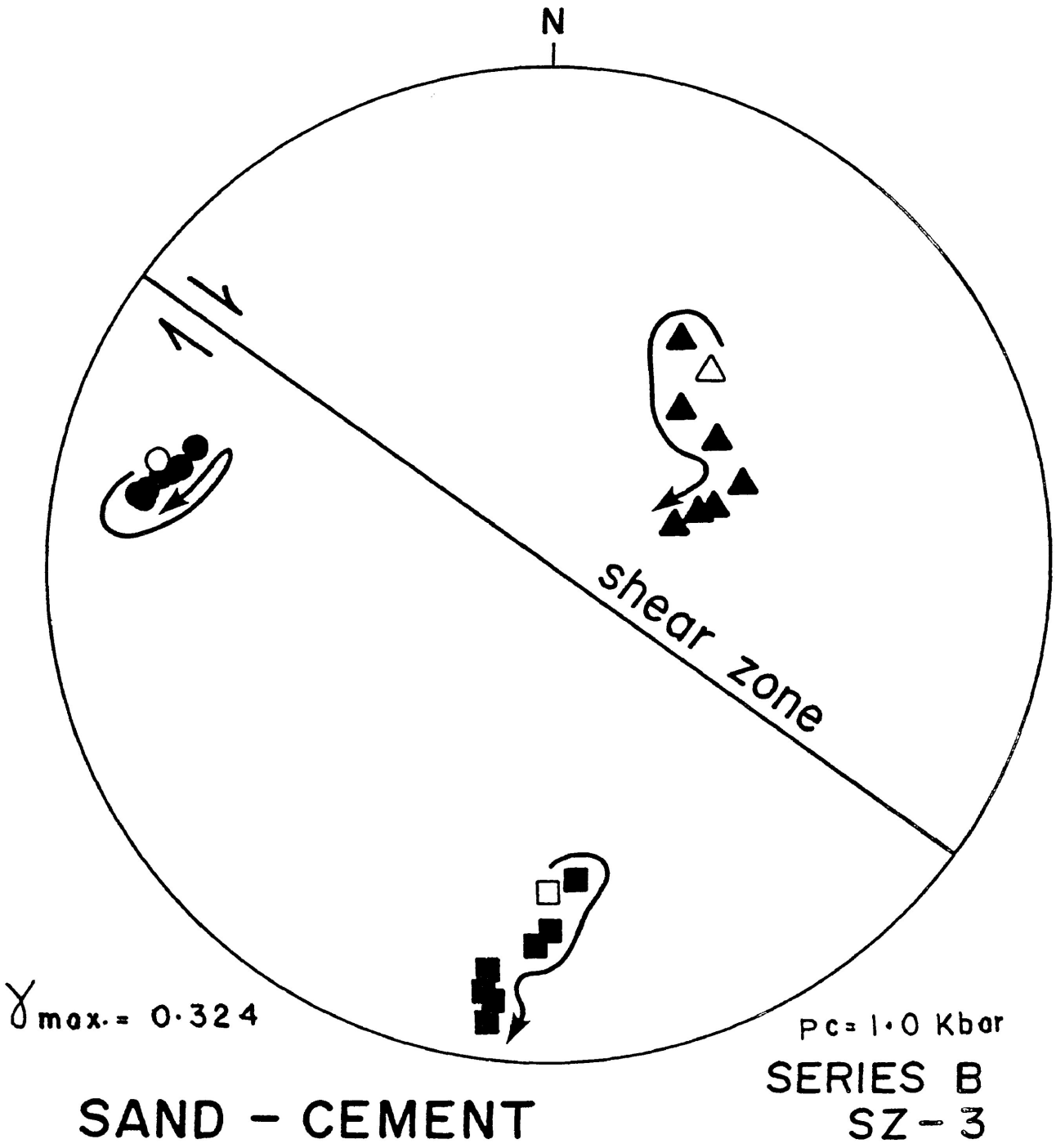

Figure 4-24. Illustrating the progressive changes in orientation of the pricipal susceptibility directions for SZ-3 of Series B.

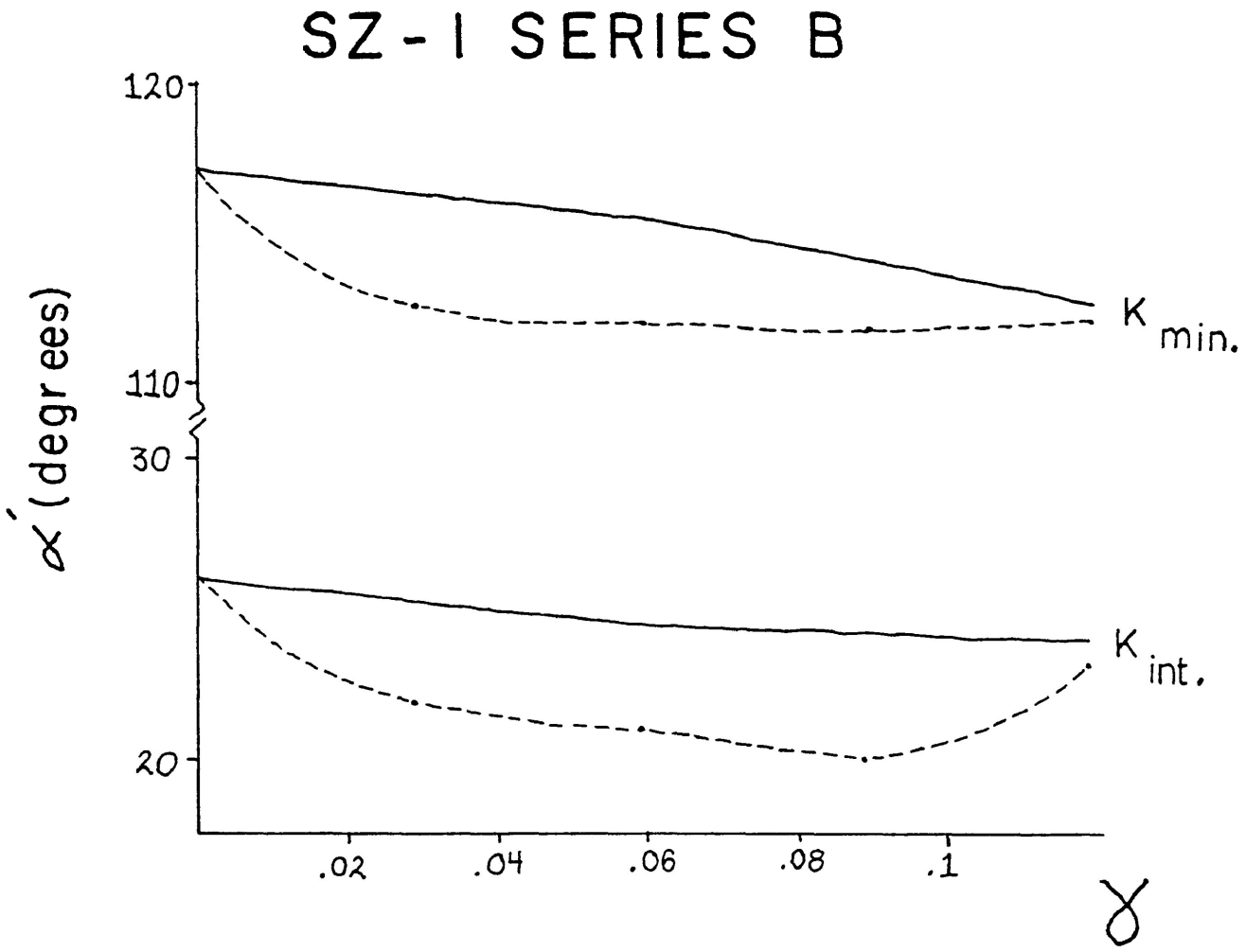

Figure 4-25. The measured change in angular position of the K_{min} and K_{int} susceptibility directions (dashed lines) for SZ-1 of Series B against those calculated for similarily orientated real material lines (solid lines) experiencing the same shear strain.

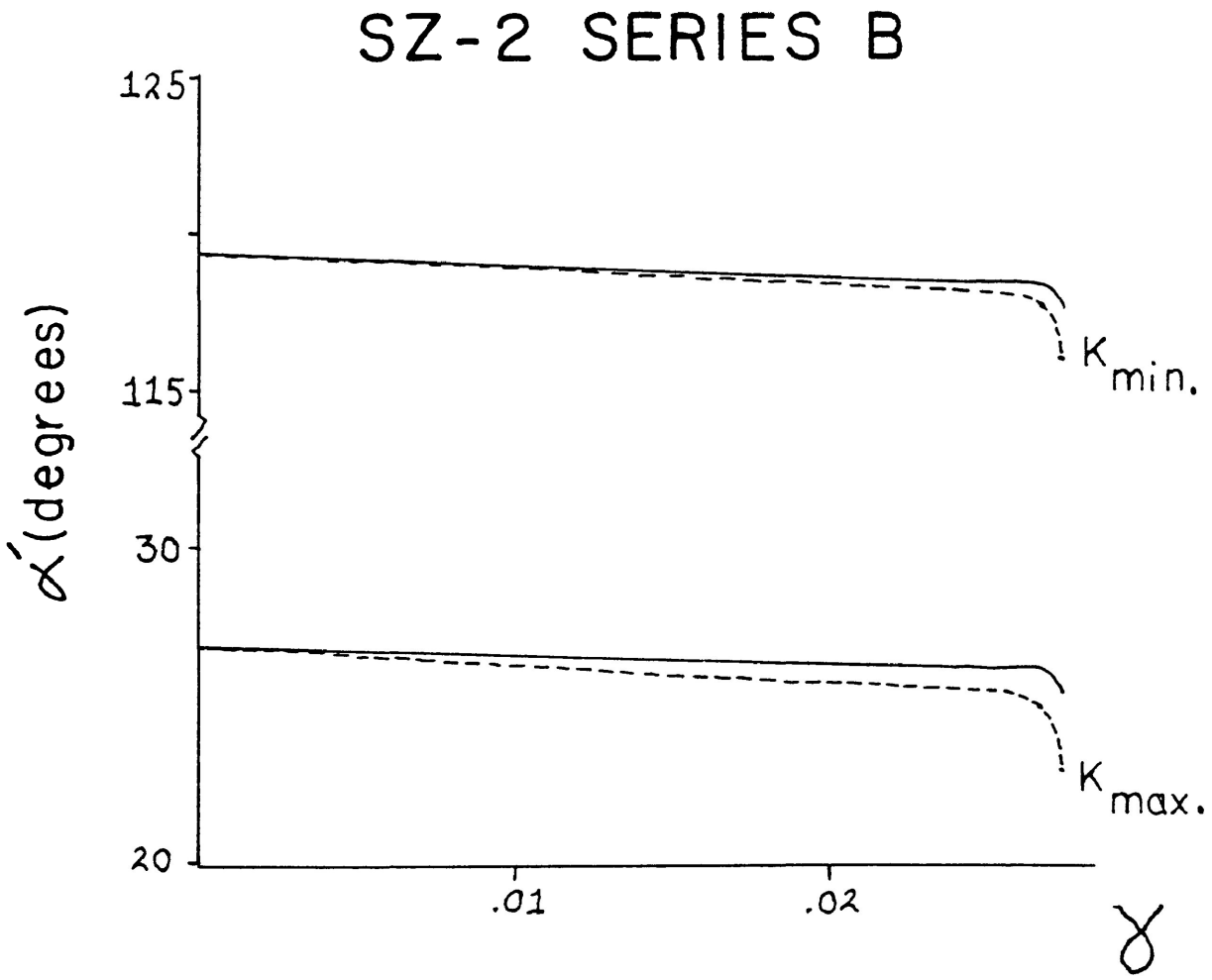

Figure 4-26. The measured change in angular position of the K_{min} and K_{max} susceptibility direction (dashed lines) for SZ-2 of Series B compared with the change in angular orientaion experienced by similarily oriented material lines.

Within the susceptibility ellipsoid obtained from SZ-3, none of the principal susceptibility axes were near enough to the plane perpendicular to the shear zone and parallel to the direction of shear, and thus were not plotted.

Each of the susceptibility ellipsoids progressed into or further into the field of flat-shaped ellipsoids but displayed a slightly different initial shape change (Figures 4-27 and 4-28). The susceptibility ellipsoid of SZ-1 in the series simply became progressively flatter and more anisotropic with shear strain. SZ-2 becomes progressively flatter with deformation, however in the initial increment of shear strain the ellipsoid became slightly less anisotropic. SZ-3, unlike the previous two shear zones, began in the field of rod-shaped ellipsoids. The first increments of deformation caused the susceptibility ellipsoid to become less anisotropic and assume a slightly more rod-shaped configuration. Further shear strain deformed the ellipsoid in a manner similar to the previous shear zones, with the exception of one increment where the ellipsoids shape (T) did not change but its degree of anisotropy did.

For each shear zone, a linear correlation of $\Delta P'$ versus $\ln(X/Z)$ could be determined (Figures 4-29 to 4-31).

Three individual tests were conducted for Series C, totalling 16 experiments. A confining pressure of 1.5 kbars was employed throughout Series C.

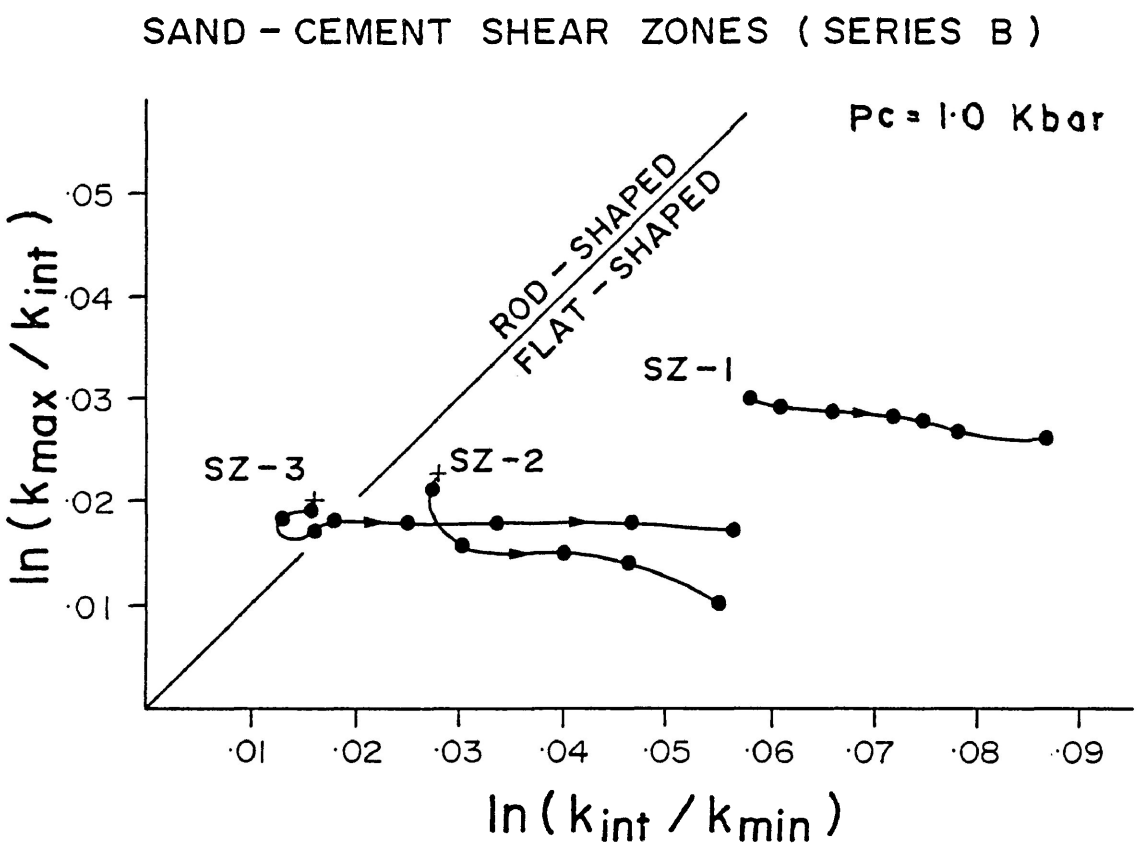

Figure 4-27. Illustrating the progressive changes in shape of the magetic susceptibility ellipsoids of the experimental sand-cement shear zones of Series B.

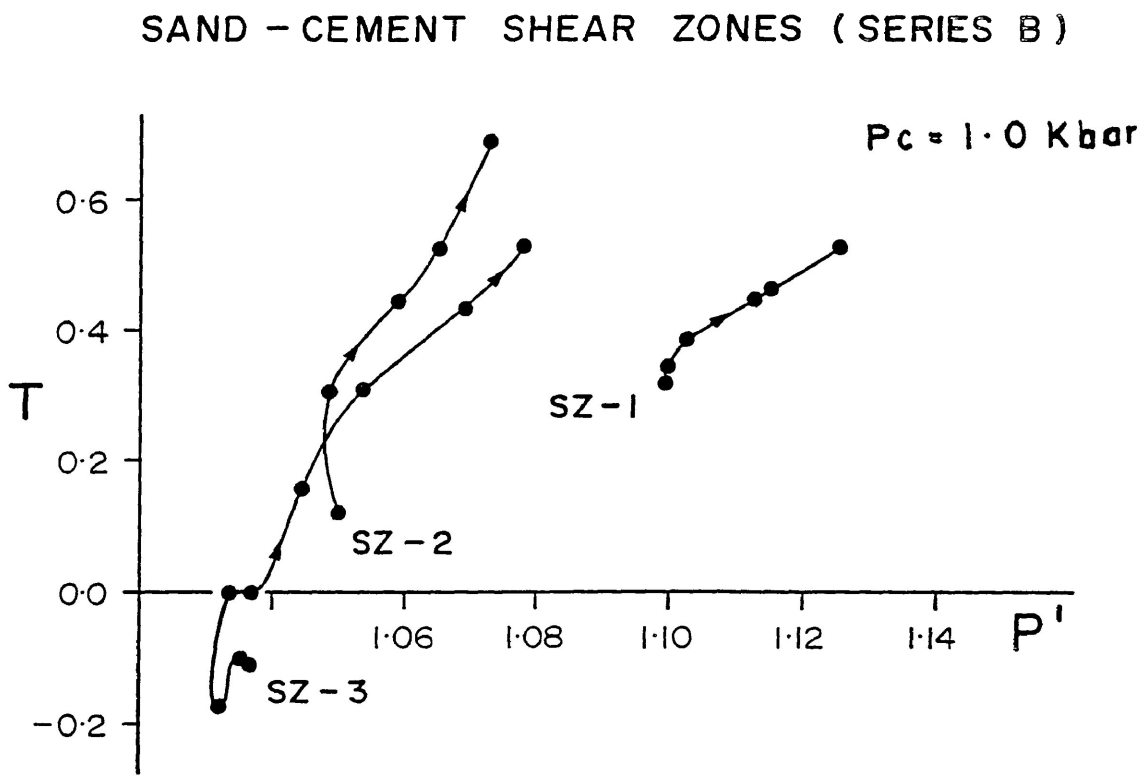

Figure 4-28. Illustrating the progressive changes in shape and anisotropy of the susceptibility ellipsoids of Series B.

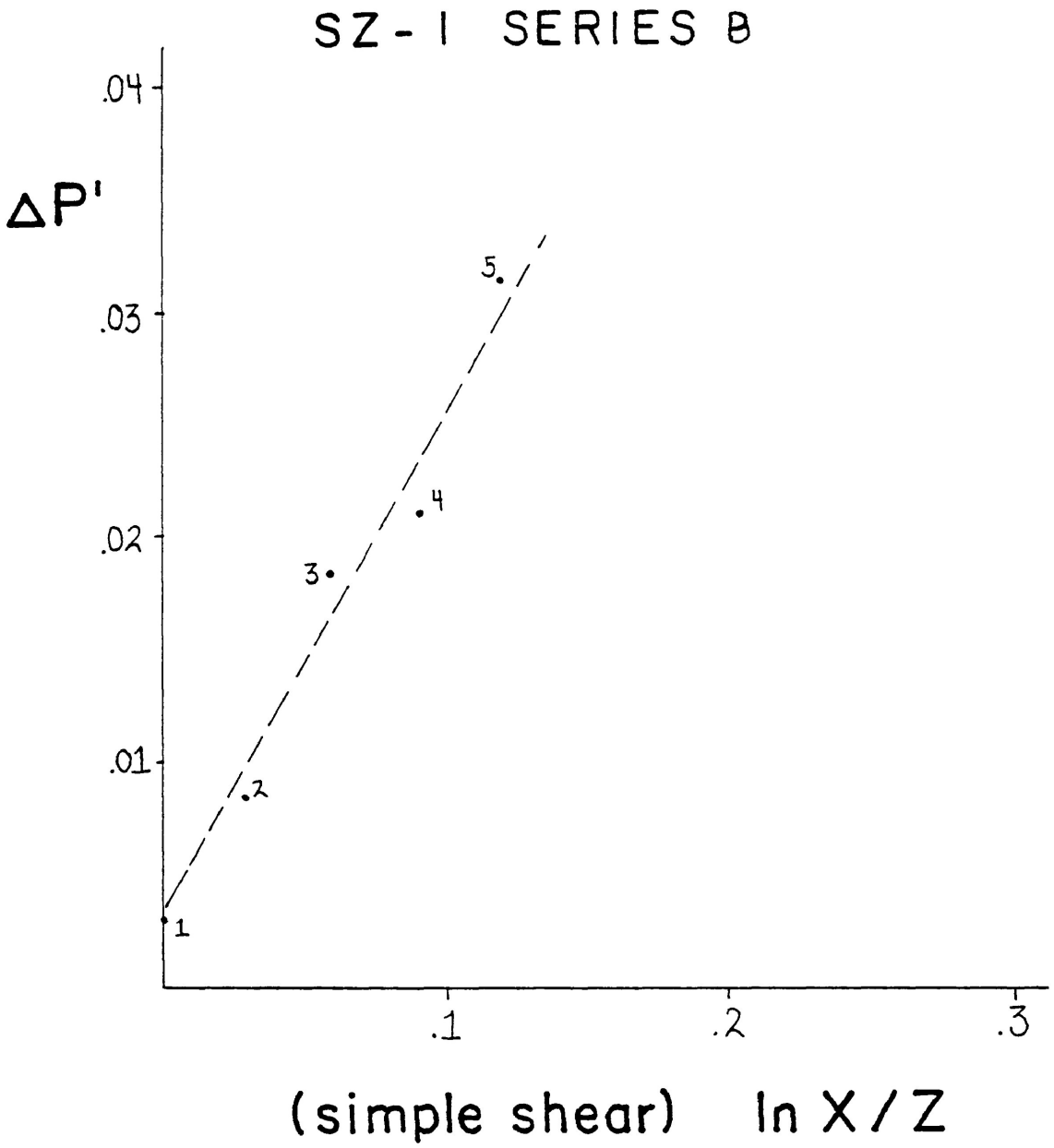

Figure 4-29. The correlation between the change in the degree of anisotropy (ΔP') and the shear strain ratio (ln (X/Z)) for SZ-1 of Series B. The correlation coefficient is 0.989.

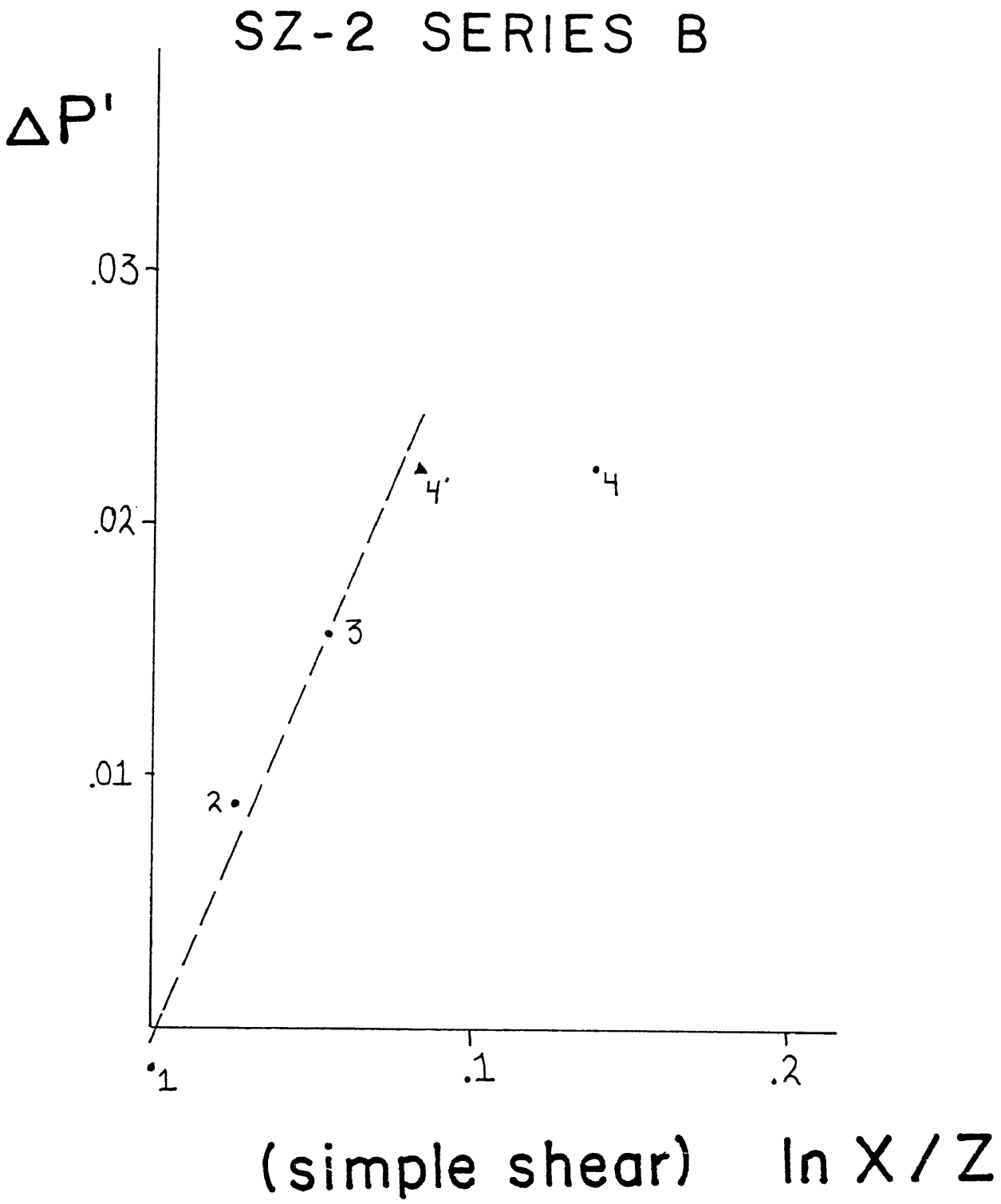

Figure 4-30. Illustrating the correlation between the change in the degree of anisotropy and the shear strain ratio for SZ-2 of Series B. The correlation coefficient is 0.993. Note that the fourth data from the fourth experiment is corrected for bulk simple shear, this is due to the faulting of the shear zone assembly.

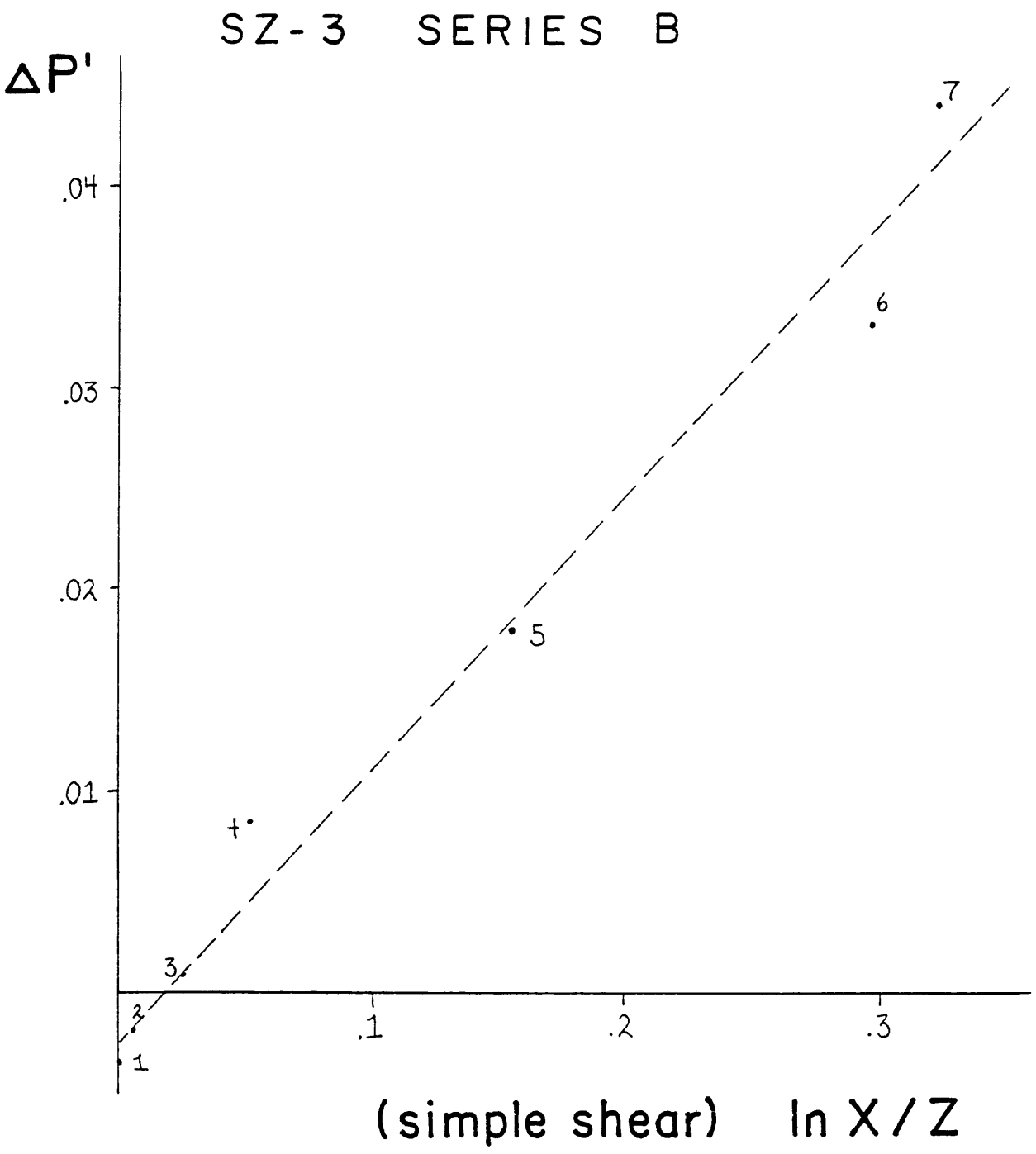

Figure 4-31. Illustrating the correlation between the change in the degree of anisotropy and the shear strain ratio for SZ-3 of Series B. The correlation coefficient is 0.989.

For each of the tests in Series C, there was an attempt to position the initial susceptibilities in the 'special' orientation discussed earlier. For SZ-1 and SZ-2 in Series C the orientation of the principal susceptibility directions (Figures 4-32 & 4-33) corresponded to the 'fixed' position noted in many of the previous sand-cement shear zone experiments. In SZ-3 the initial susceptibility directions were initially very similar to those of SZ-2 in Series B (Figure 4-34), but due to an initial increment of strain that was either too small or too large, a rotation towards the initial schistosity was not observed. Eventually the principal susceptibility directions became 'fixed' in an orientation, except for the reversal in the positions of K_{max} and K_{int} (as noted in SZ-2 Series B), similar to all of the sand-cement shear zone experiments.

The rotations of the susceptibility axes for the shear zones of Series C display a varied behaviour with respect to their respective 'real' line elements. Within SZ-1 the principal susceptibility axis K_{min} rotates at a rate very nearly equal to that expected for the 'real' line (Figure 4-35). K_{min} in SZ-2 of the series displays a markedly different rate of rotation from that expected from a similarily orientated 'real' line element (Figure 4-36). Within SZ-2, K_{min} rotates much faster toward the direction of shear than does the 'real' line. Within SZ-3, the principal

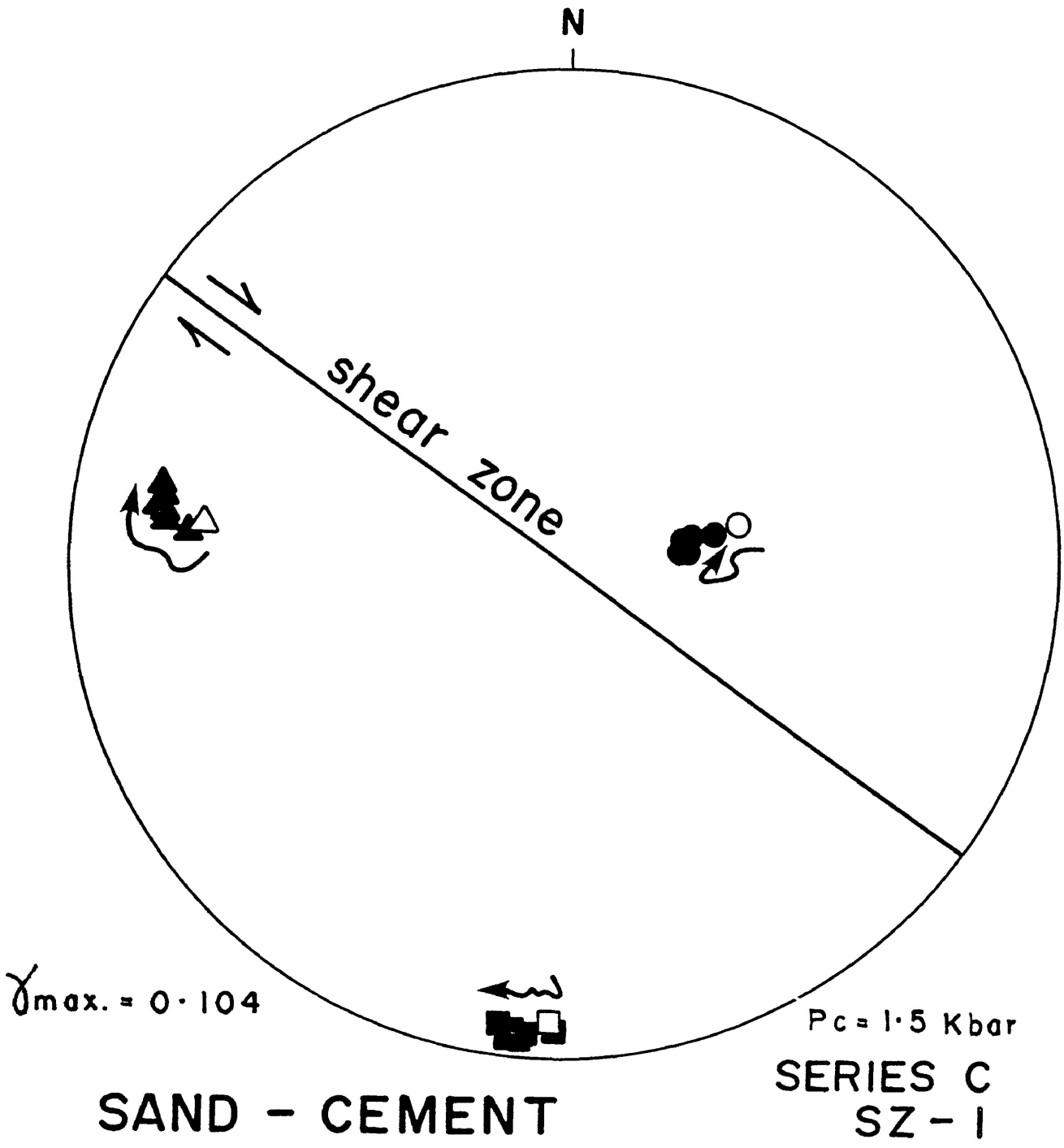

Figure 4-32. Illustrating the progressive changes in orientation of the principal susceptibility directions for SZ-1 of Series C.

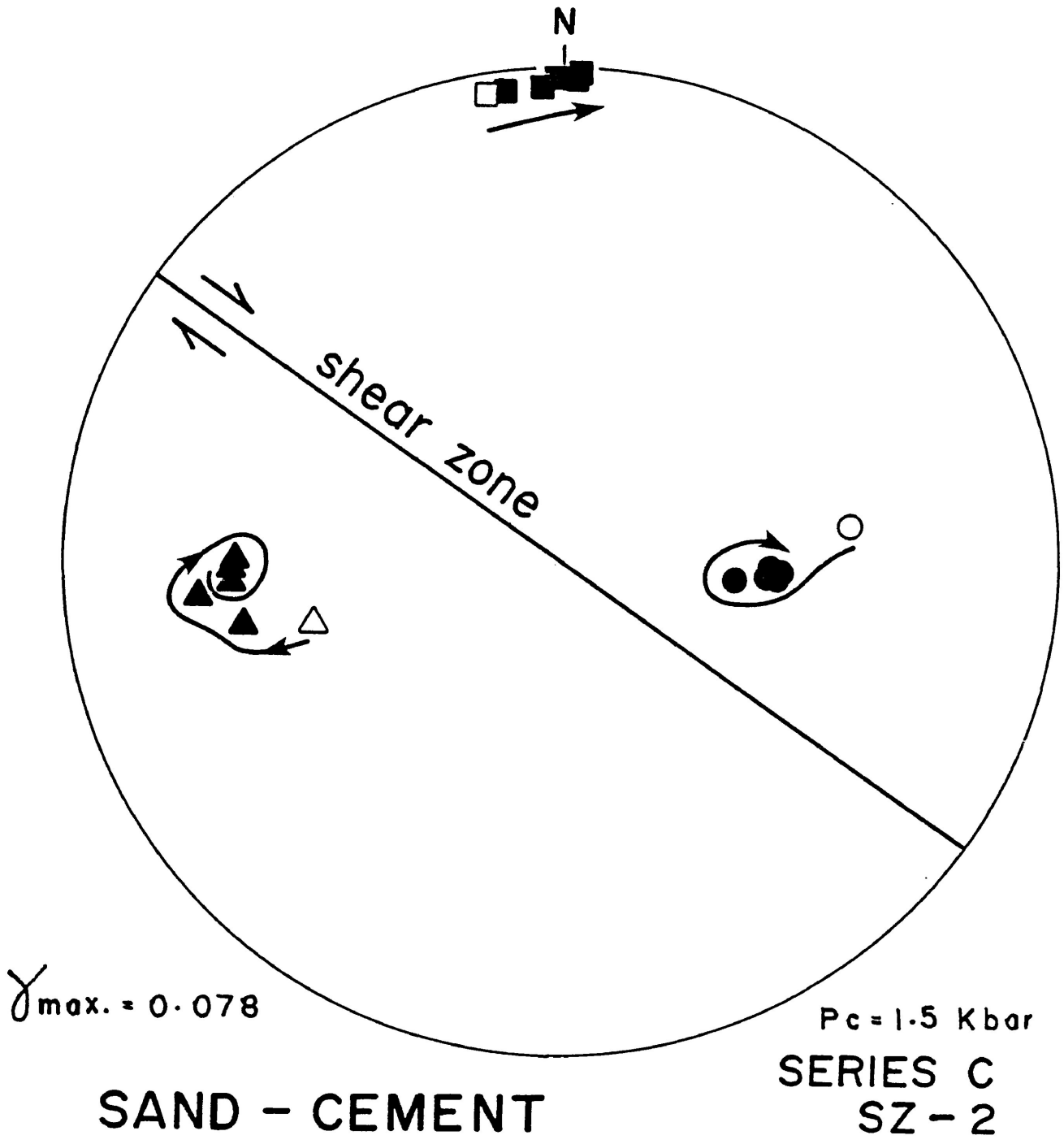

Figure 4-33. The progressive changes in orientation of the principal susceptibility directions of SZ-2 Series C.

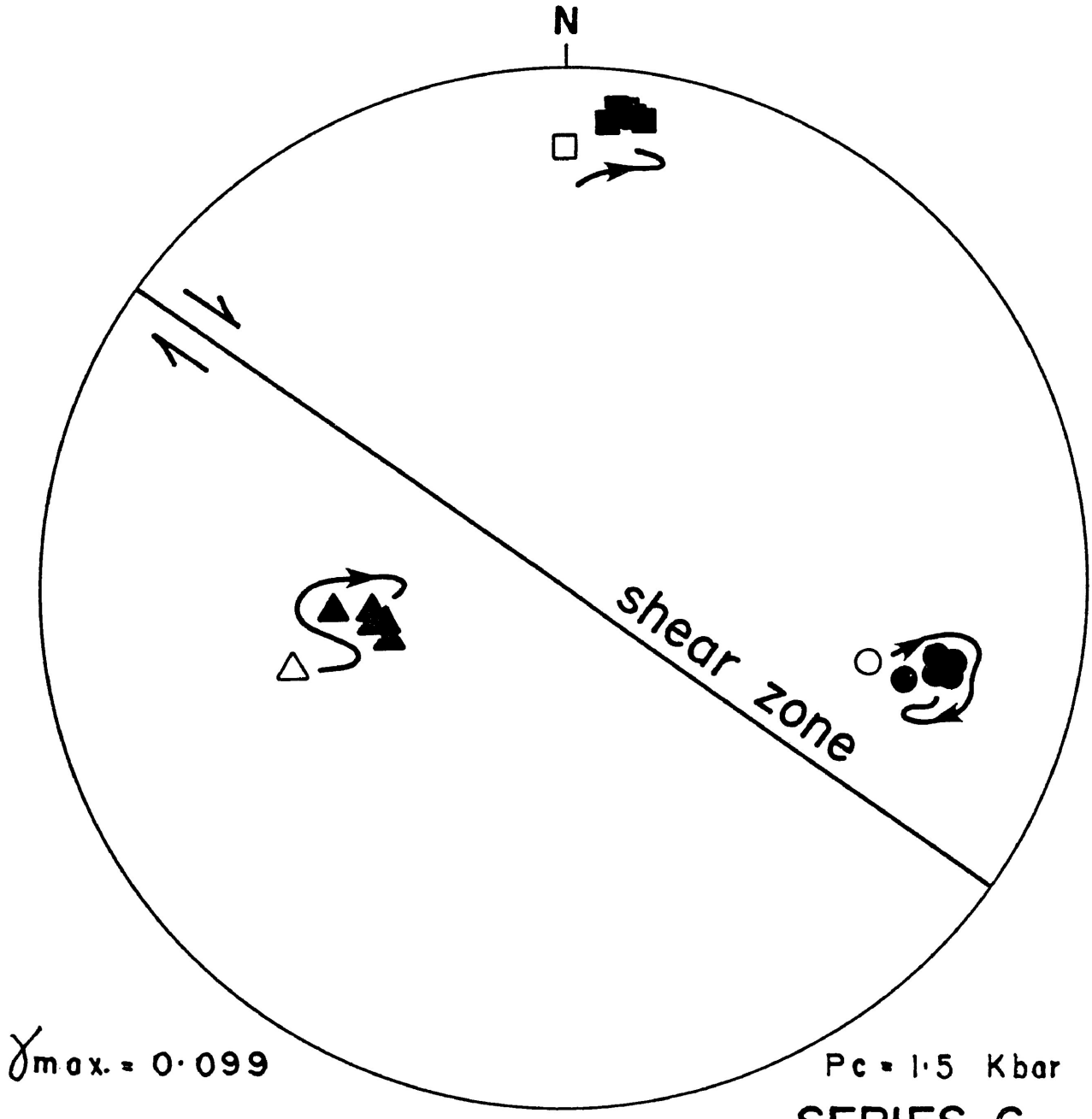

Figure 4-34. The progressive changes in orientation of the principal susceptibility directions of SZ-3 Series C.

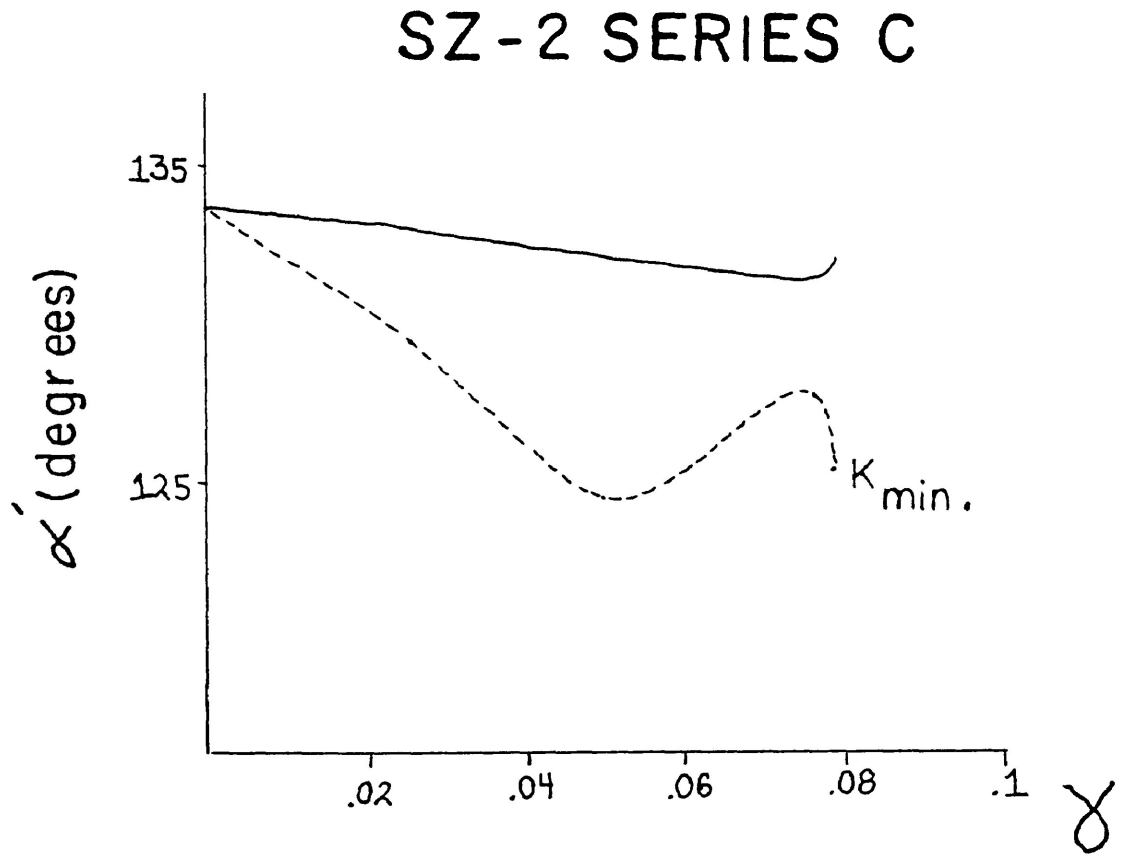

Figure 4-36. Illustrating the measured change in angular position of the K_{min} susceptibility axes (dashed line) of SZ-2 Series C against that of a real material line of a similar initial orientation experiencing an equivalent shear strain.

susceptibility axis K_{min} initially rotates much faster than the 'real' line, however with further shear strain K_{min} begins to rotate in a manner which is similar to that of its equivalent 'real' line element (Figure 4-37).

All of the undeformed susceptibility ellipsoids in series C lie in the field of the flat-shaped ellipsoids (Figures 4-38 & 4-39). The initial increment of shear causes the susceptibility ellipsoids to become slightly less flat-shaped. Further experimental shear strain deforms the ellipsoids such that their degree of anisotropy progressively increases and the ellipsoids become increasingly flatter. (Note the initial data point of SZ-3 may be in error).

Again, there was a reasonably good linear correlation of the data for these sand-cement shear zones for the change in anisotropy with shear strain (Figures 4-40 to 4-42).

Microscopic Observations

The undeformed sand-cement material is superfically like a matrix-supported sandstone in thin section (Plate 4-1). The material consists of randomly oriented, round to sub-angular grains supported in a fine grained matrix of Portland cement. Grain to grain contacts are few (0 to 2 per grain) and because the sand was sieved prior to cementation the grain size variation is minimal.

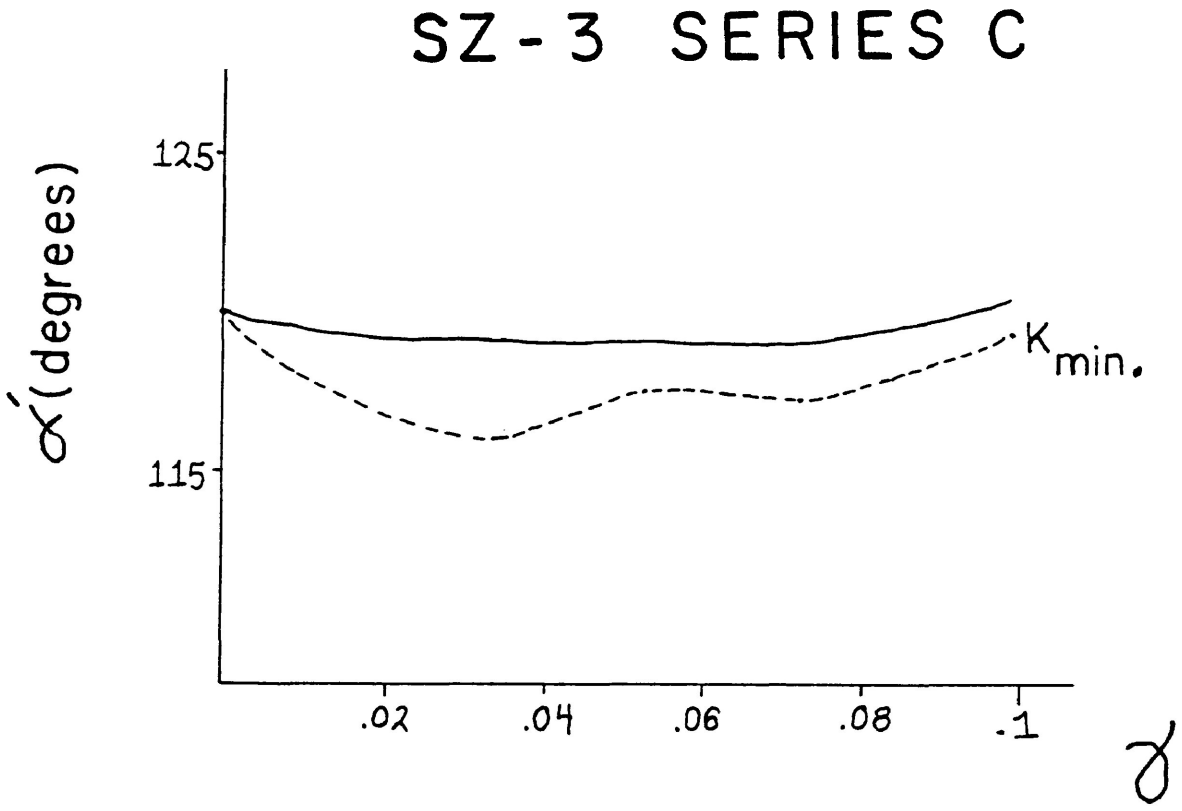

Figure 4-37. The change in angular position of the Kmin principal susceptibility direction of SZ-3 Series C (dashed line) plotted against that of a real material line of similar initial orientation experiencing an equivalent amount of shear strain.

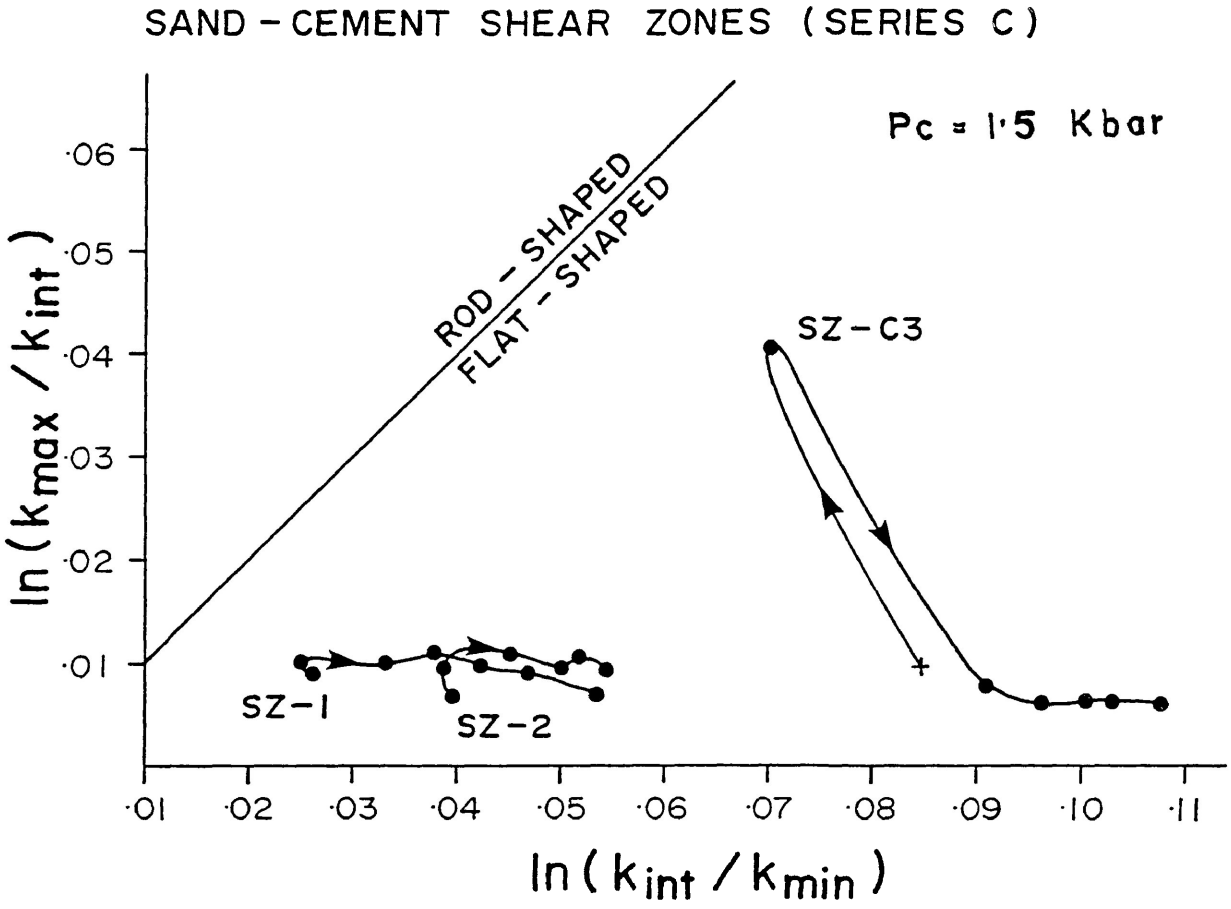

Figure 4-38. Illustrating the progressive changes in shape of the susceptibility ellipsoids of Series C as expressed by the ratios of the principal susceptibilities.

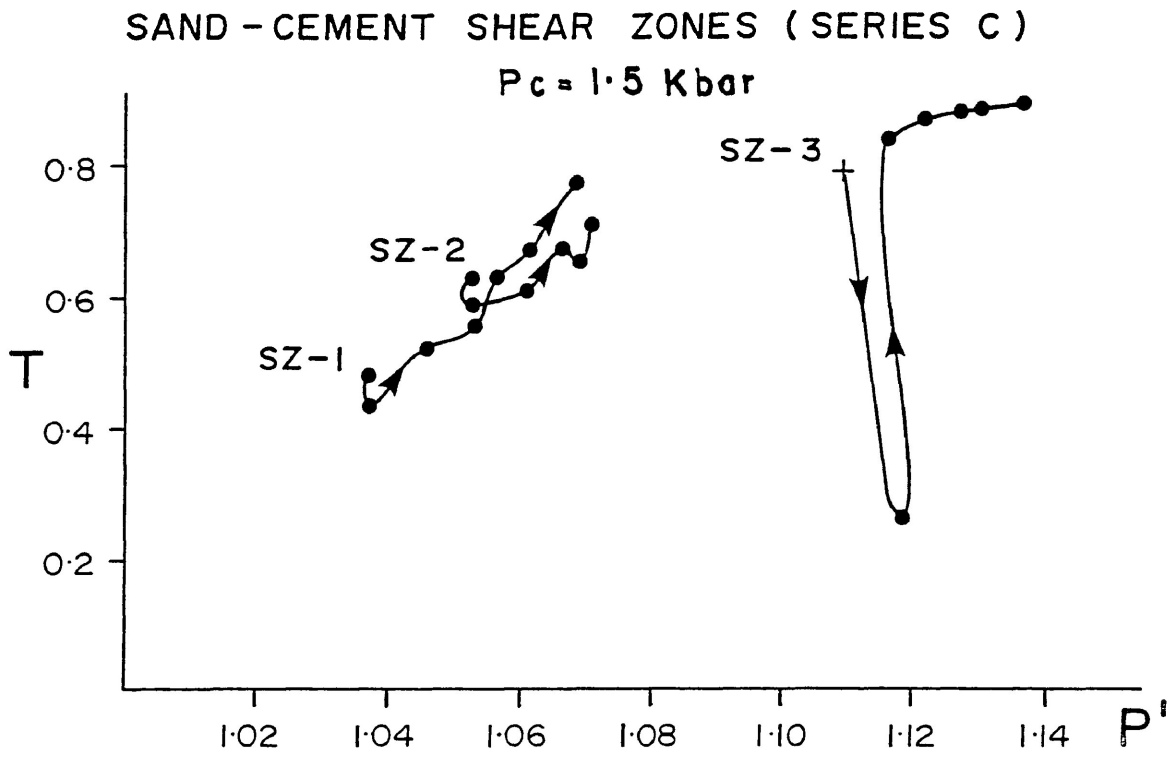

Figure 4-39. Illustrating the progressive changes in shape (T) and degree of anisotropy (P') of the susceptibility ellipsoids of Series C.

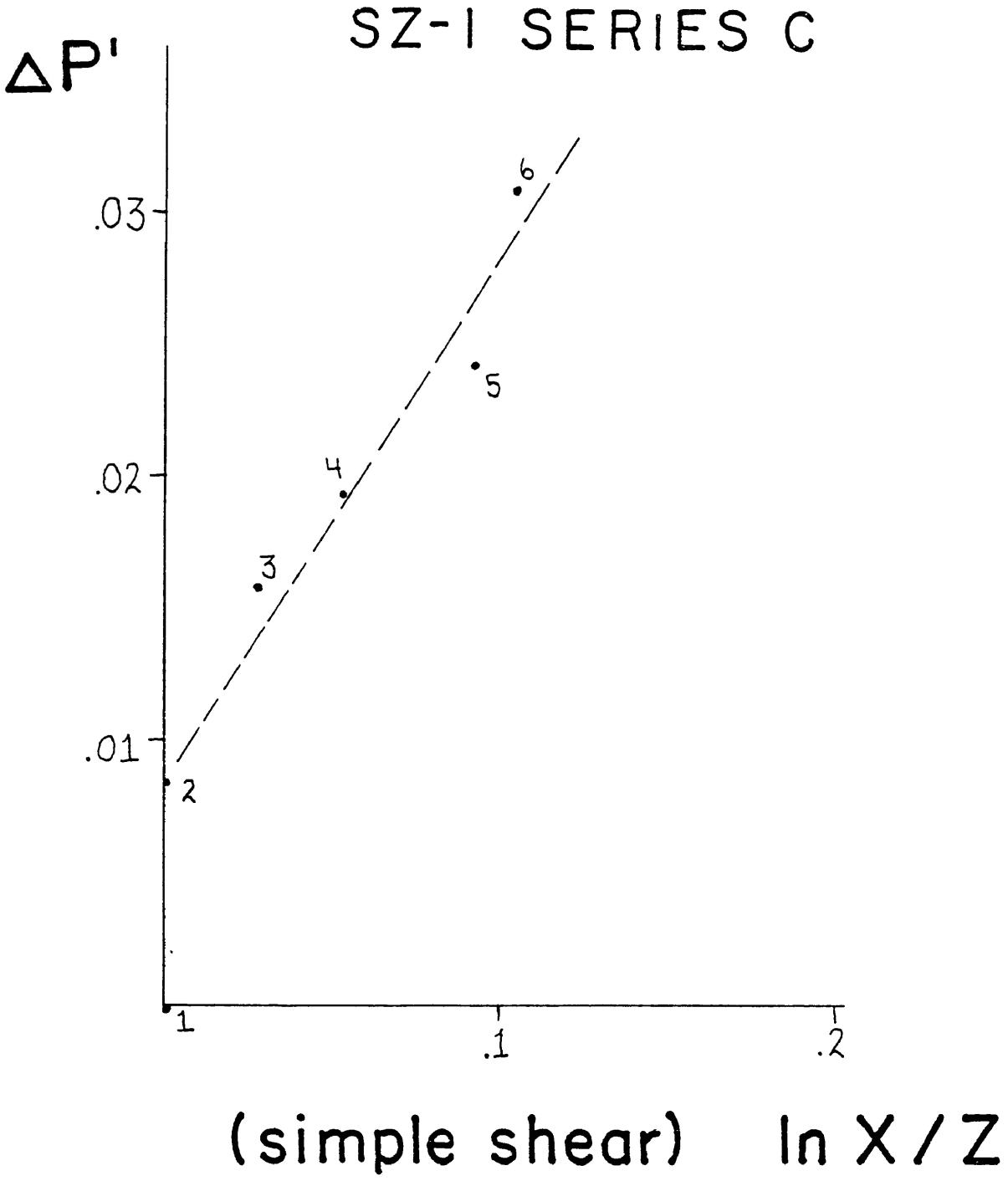

Figure 4-40. The correlation between the change in the degree of anisotropy before and after successive increments of experimental simple shear deformation (ΔP') and the shear strain ratio (ln (X/Z) for SZ-1 of Series C. The correlation coefficient is 0.979.

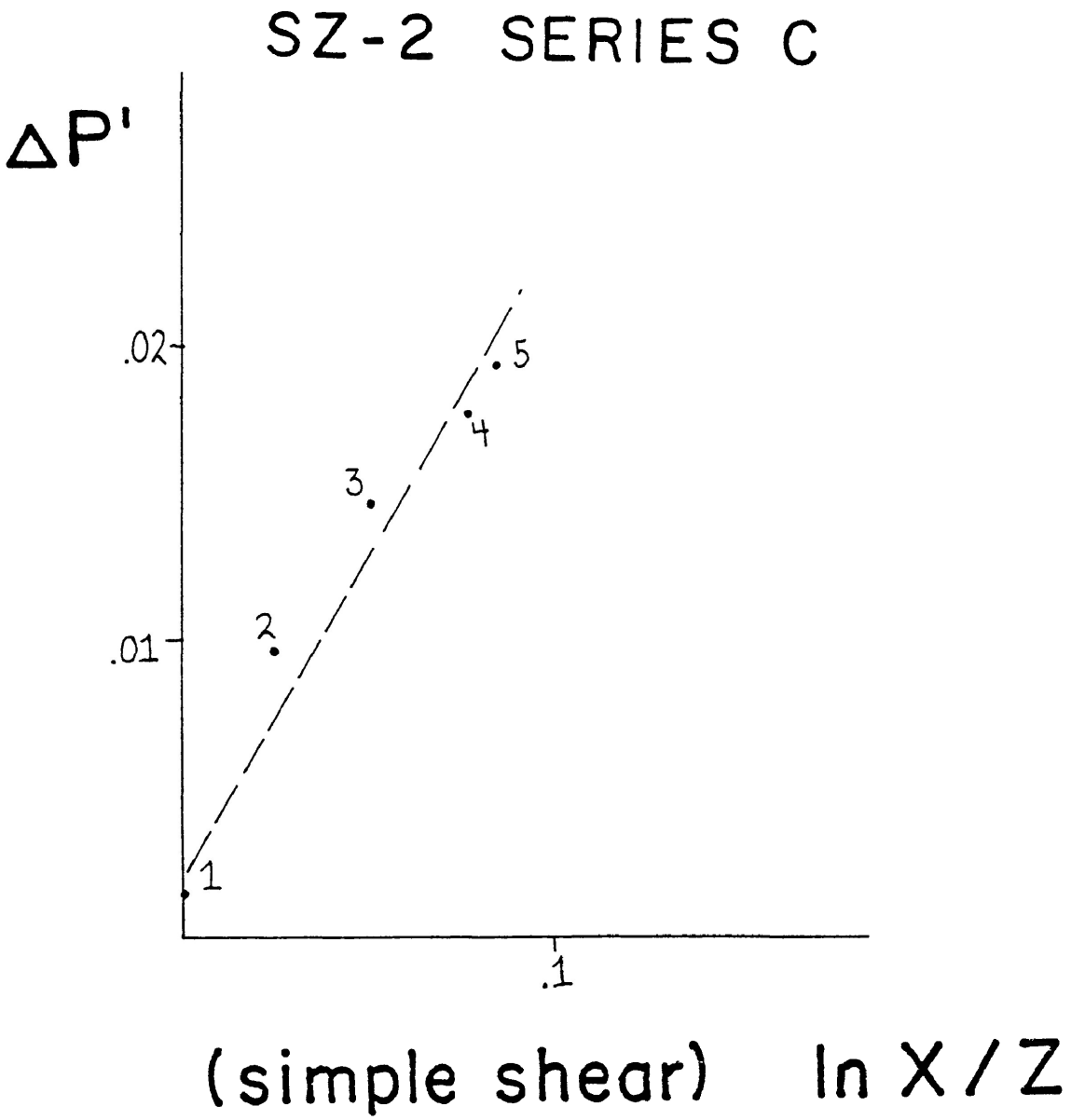

Figure 4-41. The correlation between the change in the degree of anisotropy and the shear strain ratio for SZ-2 of Series C. The correlation coefficient is 0.982.

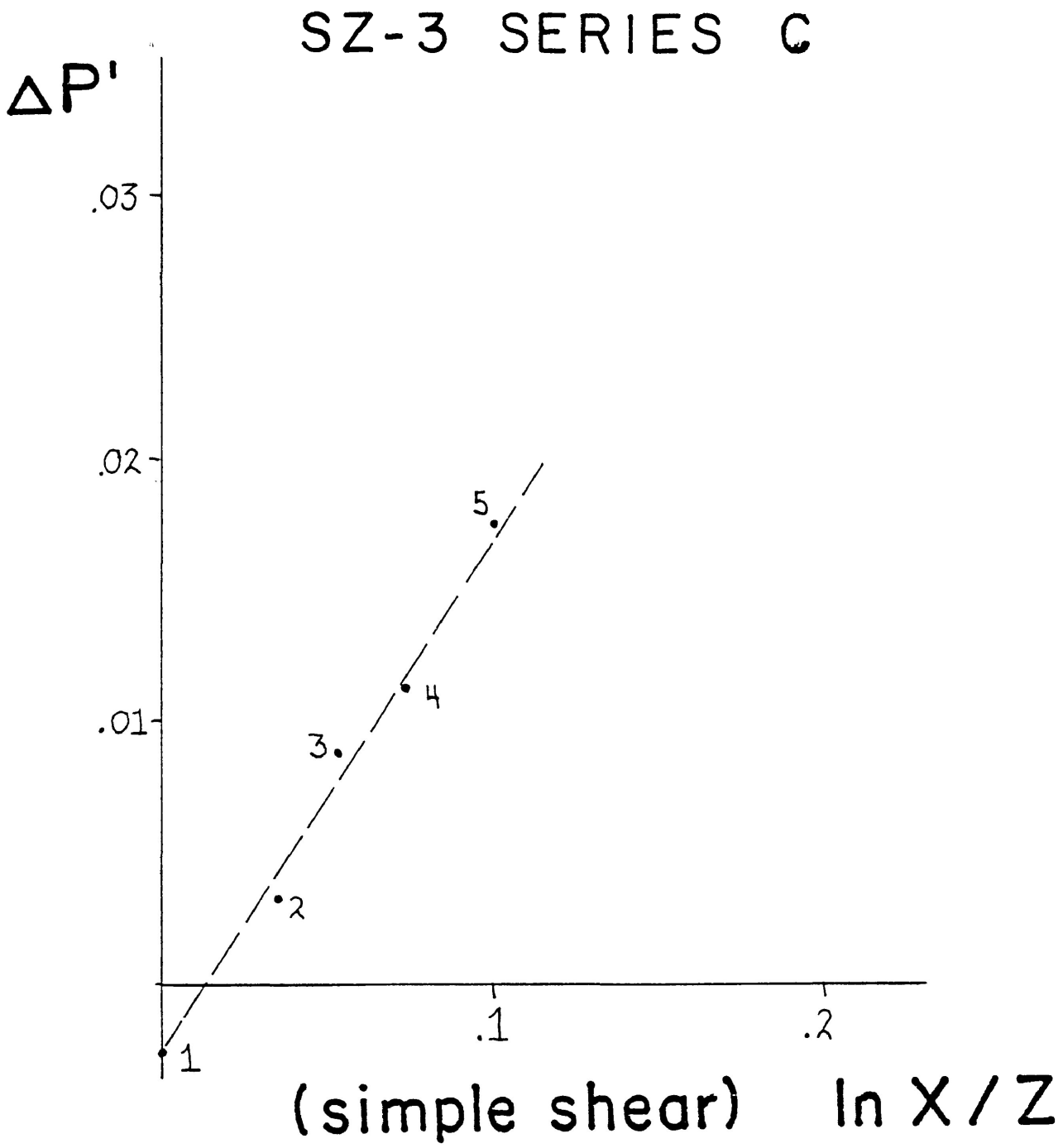

Figure 4-42. The correlation between the change in the degree of anisotropy and the shear strain ratio for SZ-3 of Series C. The correlation coefficient is 0.997.

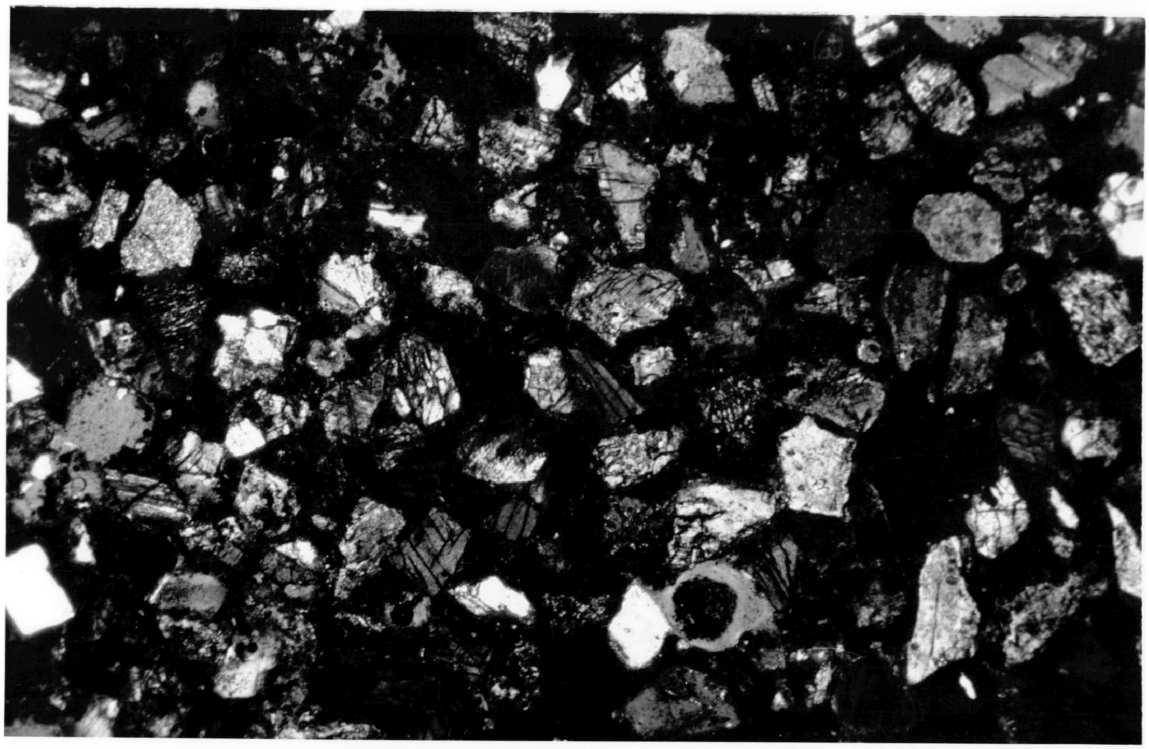

Plate 4-1. Photograph of the undeformed sand-cement material.

The grains within the material are essentially monomineralic. The predominant grain minerals ,in order of abundance, are pyroxene, magnetite, feldspar and quartz.

The pyroxenes are predominantly of a clinopyroxene composition displaying well a developed cleavage. Orthopyroxene exsolution lamellae are found in a number of the pyroxene grains. Neither the cleavage planes nor the exsolution lamellae within the pyroxene grains exhibit any preferred orientation in the undeformed material.

The magnetite grains are opaque in thin section. Approximately 10% of the grains contain inclusions of quartz.

Individual feldspar grains are twinned according to either simple or polysynthetic twin laws. The twin planes of the feldspars display no preferred orientation within the undeformed material.

From Series A, two samples, representing a relatively small (γ =0.025 in SZ-A) and large (γ=0.378 in SZ-K) amount of shear strain were chosen for microscopic analysis.

Within SZ-A there is little evidence of deformation except along the boundary of the shear zone where it meets the end pieces. In this region there appears have been some compaction, as evidenced by the cracking of grains and a greater number of grain to grain contacts. Within the centre of the shear zone the fabric could be representative of the undeformed material. This suggests

that shearing starts at the edges of the zone and progresses into the central portion.

The material, in SZ-K, is more intensely compacted, evidenced by a greater number of grain to grain contacts and cracked grains appearing throughout the whole of the shear zone (Plate 4-2). Undulose extinction is noted in the quartz grains. Twin lamellae within the feldspars are thinner and more numerous. A weak preferred dimensional orientation of magnetite appears to have formed at an angle of approximately 40^{o} to the shear zone. Grains along the boundary of the shear zone are reduced in size and pervasively cracked.

SZ-1 and SZ-3 of Series B were sectioned. Both shear zones displayed a fabric similar to the highly deformed SZ-K of Series A. The number of grain contacts had inreased and many grains were cracked and some fragmented. One important feature noted in SZ-3 of Series B was the inclusion of magnetite grains within several microfaults. The magnetite appears to have 'flowed' in a quasi-plastic sense rather than broken and rolled into the faults, as it remains visually cohesive (Plate 4-3).

Only SZ-1 from Series C was sectioned. The fabric of the shear zone appears largely similar to the previous multiply deformed specimens of Series B. The grains display a pervasive cracking, twins within the feldspars are thinner and more numerous, undulose exinction is common in quartz grains and there appears to

Plate 4-2. Composite photograph of SZ-K of Series A (P_c=0.689 kbars) illustrating the deformed texture of the sand-cement shear zones. γ = 0.378.

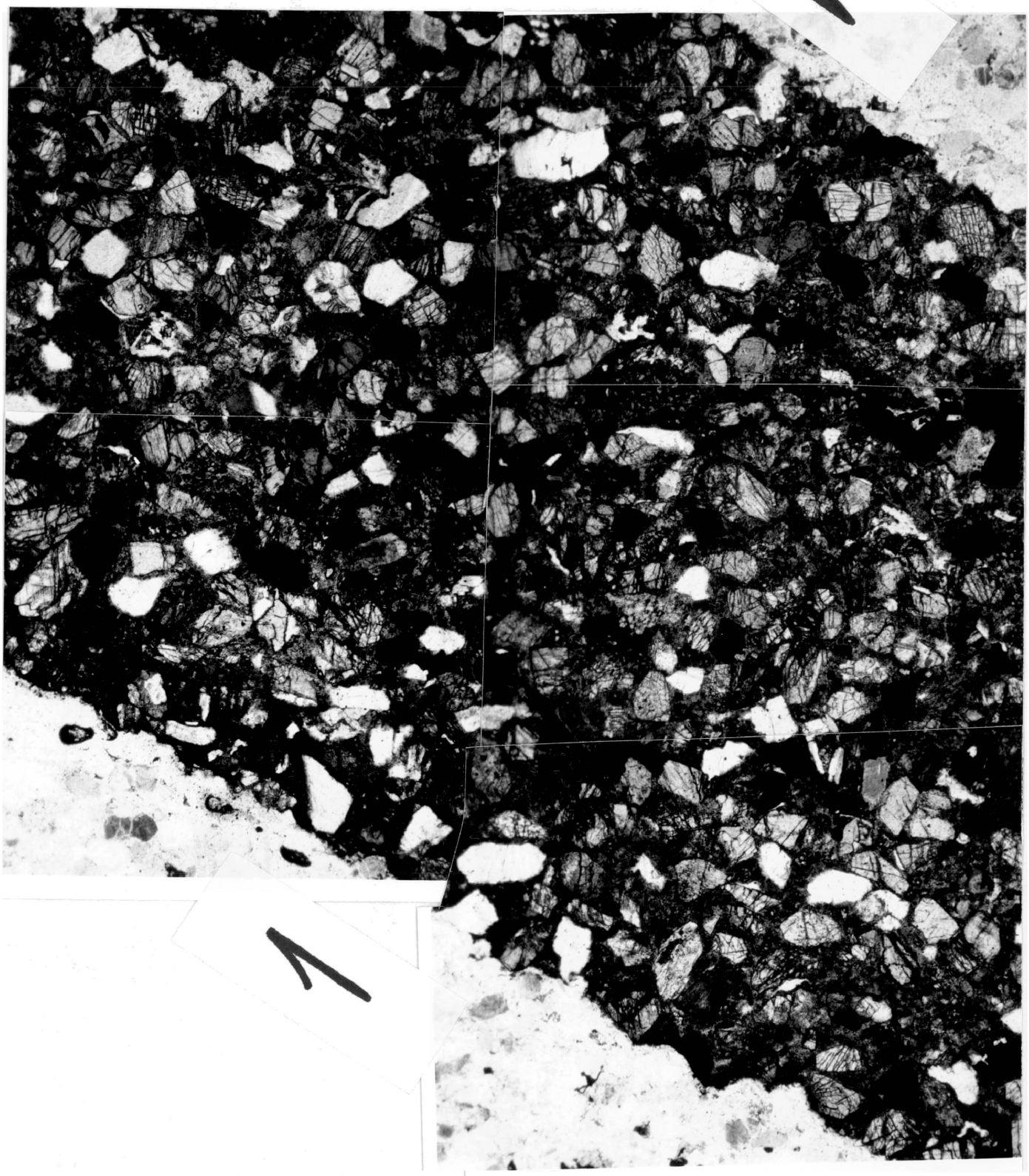

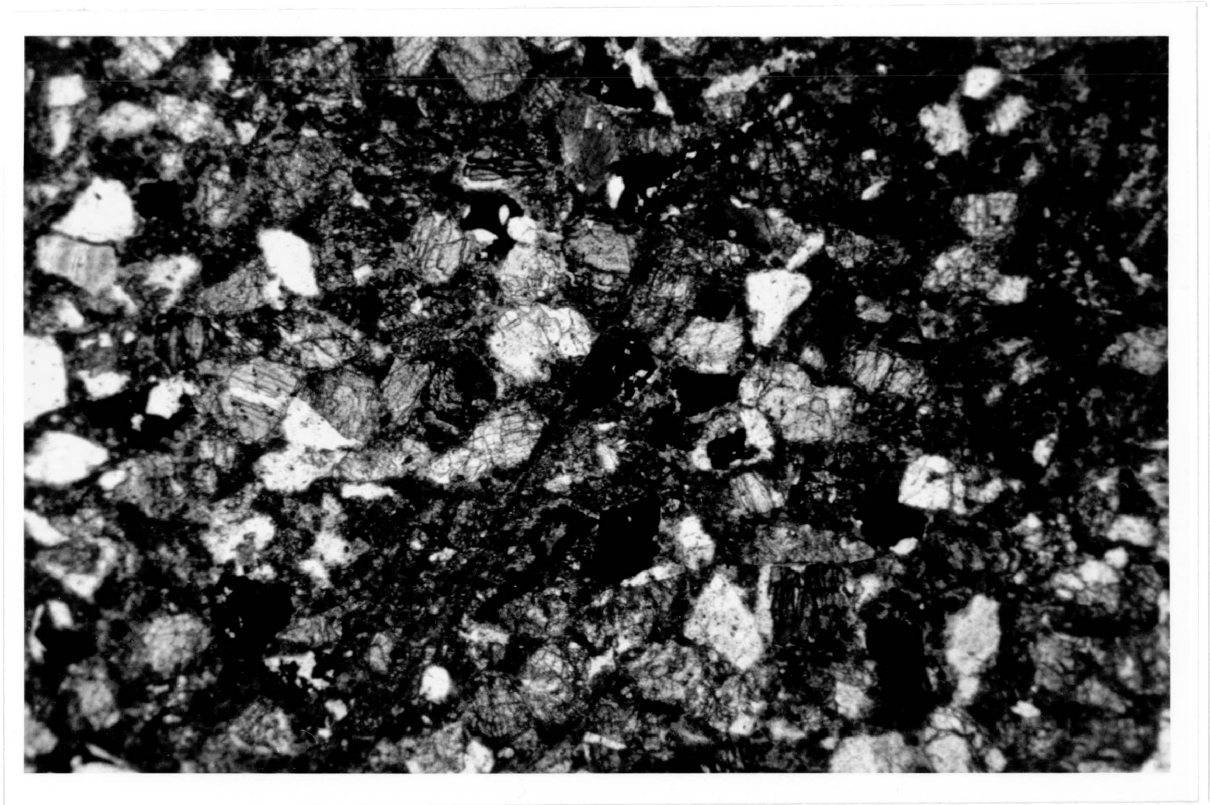

Plate 4-3. Optically continuos magnetite within a microfault (centre of photograph) from experiment SZ-3 of Series B.

be a moderate to weak preferred dimensional orientation of the magnetite grains.

Stress Relaxation

Stress relaxation tests on three 0.75 inch diameter cylindrical specimens of sand-cement material were conducted at the confining pressures utilized in the shear zone series. At the time of the stress relaxation tests the material had been set for 8 months, which is ample time for the cement to cure. (Neville 1981)

Figure 4-43 displays the result of stress relaxation of the sand-cement material at a confining pressure of 10,000 p.s.i. For strain-rates between 2.0×10^{-7} and 3.98×10^{-5} s^{-1} (on graph the range would be from $10^{-4.4}$ to$10^{-6.7}$) the data from the two tests yielded slopes (n values) of 48 and 54. Due to a slow confining pressure leak in the first test data pertaining to strain-rates less than 2.0×10^{-7} s^{-1} were dismissed, however, the second test was quite successful and a slope of 25 was determined for strain-rates from 2.5×10^{-8} to $2.0 \times 10^{-7} s^{-1}$ (on graph range is from $10^{-6.7}$ to $10^{-7.6}$).

Figure 4-44 displays the results of relaxation at 14,500 p.s.i. (1.0 kbar). Significant fluctuations of the line voltage occurred during the second test, thus the results are probably invalid, however the results of the first test indicate that a slope of 42

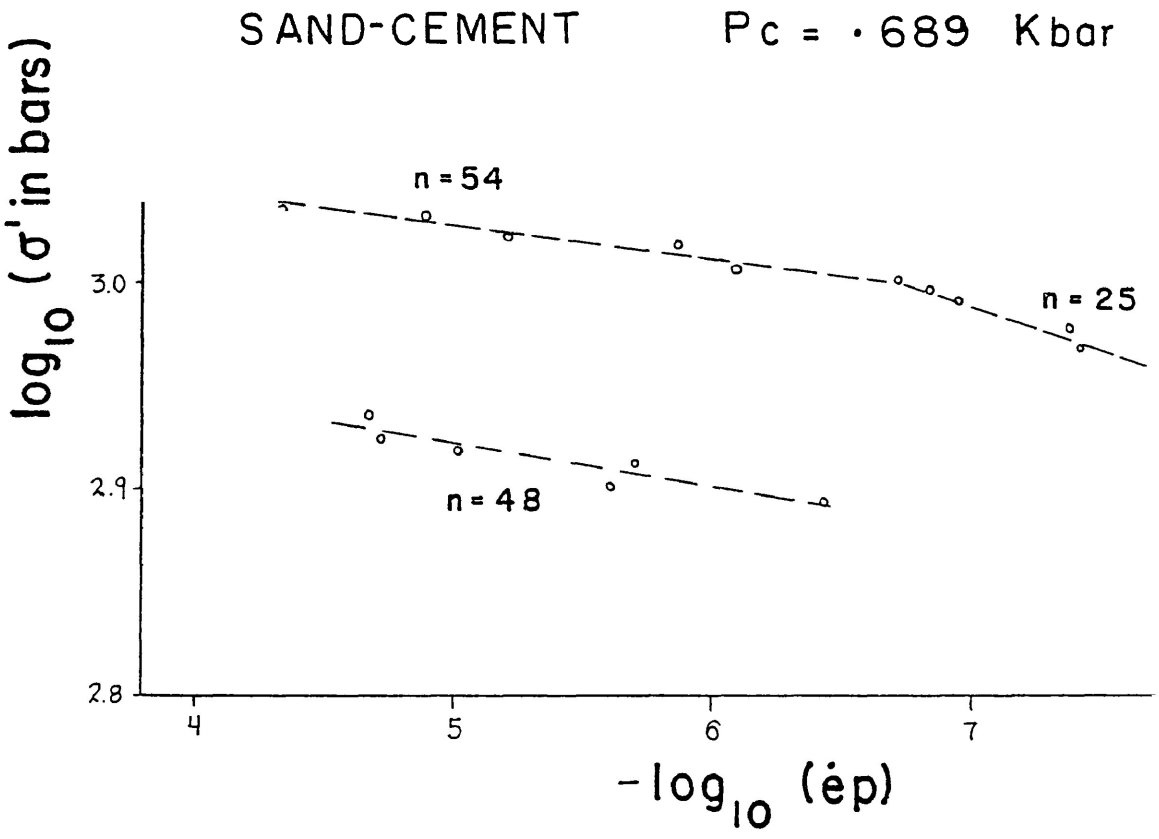

Figure 4-43. The results of two stress relaxation tests of a 0.75 inch diameter cylindrical specimen of the sand-cement material at 0.689 Kbar or 10,000 p.s.i. confining pressure (σ = differential stress in bars and $\dot{e}p$ = the rate of permanent strain accumulation).

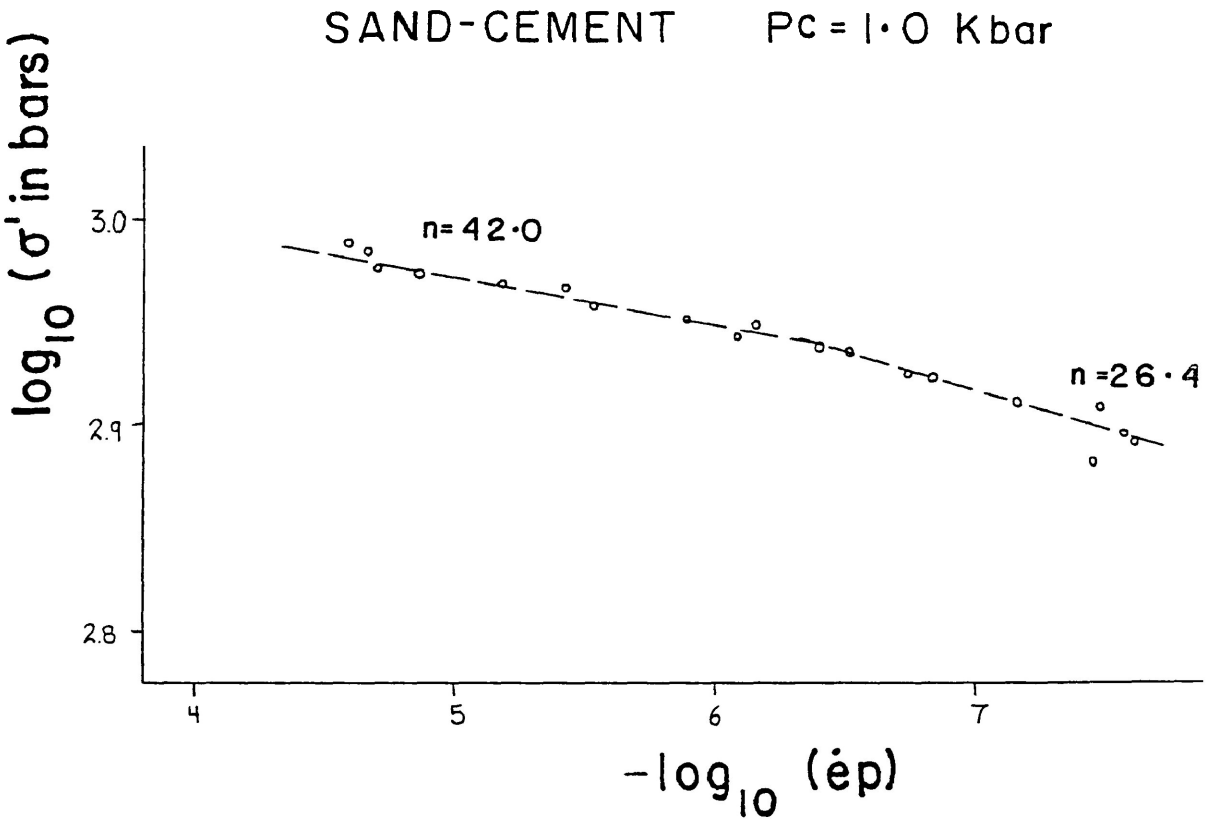

Figure 4-44. The results of stress relaxation of a 0.75 inch diameter cylindrical specimen of the sand-cement material at 1.0 Kbar confining pressure.

fits the data from strain-rates between $3.16x10^{-7}$ and $6.31x10^{-5}$ s^{-1} (on graph range is $10^{-4.2}$ to $10^{-6.5}$) and for strain-rates in the range between $2.51x10^{-8}$ and $3.16x10^{-7}$ s^{-1} ($10^{-6.5}$ to $10^{-7.6}$) a slope of 26 fits the data.

Both stress relaxation tests were good for the 1.5 kbar confining pressure experiment (Figure 4-45). For strain-rates between $2.0x10^{-7}$ and $3.16x10^{-5}$ s^{-1} (on graph the range would be $10^{-4.5}$ to $10^{-6.7}$) a line with a slope of 49 to 50 fits the data. At lower strain-rates, between $1.0x10^{-8}$ and $2.0x10^{-7}$ s^{-1} ($10^{-6.7}$ to $10^{-8.0}$) a slope of 21 to 22 occurs.

The relaxation results are all similar in their overall form. Although there is an increase in the amount of load supported at 5% axial strain with confining pressure, the fact that the data have similar slopes and a common inflection point indicates that there is no significant effect, on the stress-strain behaviour, caused by altering the confining pressure over the range employed by the experiments.

In each graph two distinct slopes (n values) are present. At relatively 'fast' strain-rates, between $3.0x10^{-7}$ and $6.31x10^{-5}$ s^{-1}, the value of n ranges from 42 to 54 and decreases to a n value between 21 and 26 at strain-rates slower than $2.5x10^{-7}$ s^{-1}. This distinct slope break is thought to mark a change in the dominance of one deformation mechanism to another.

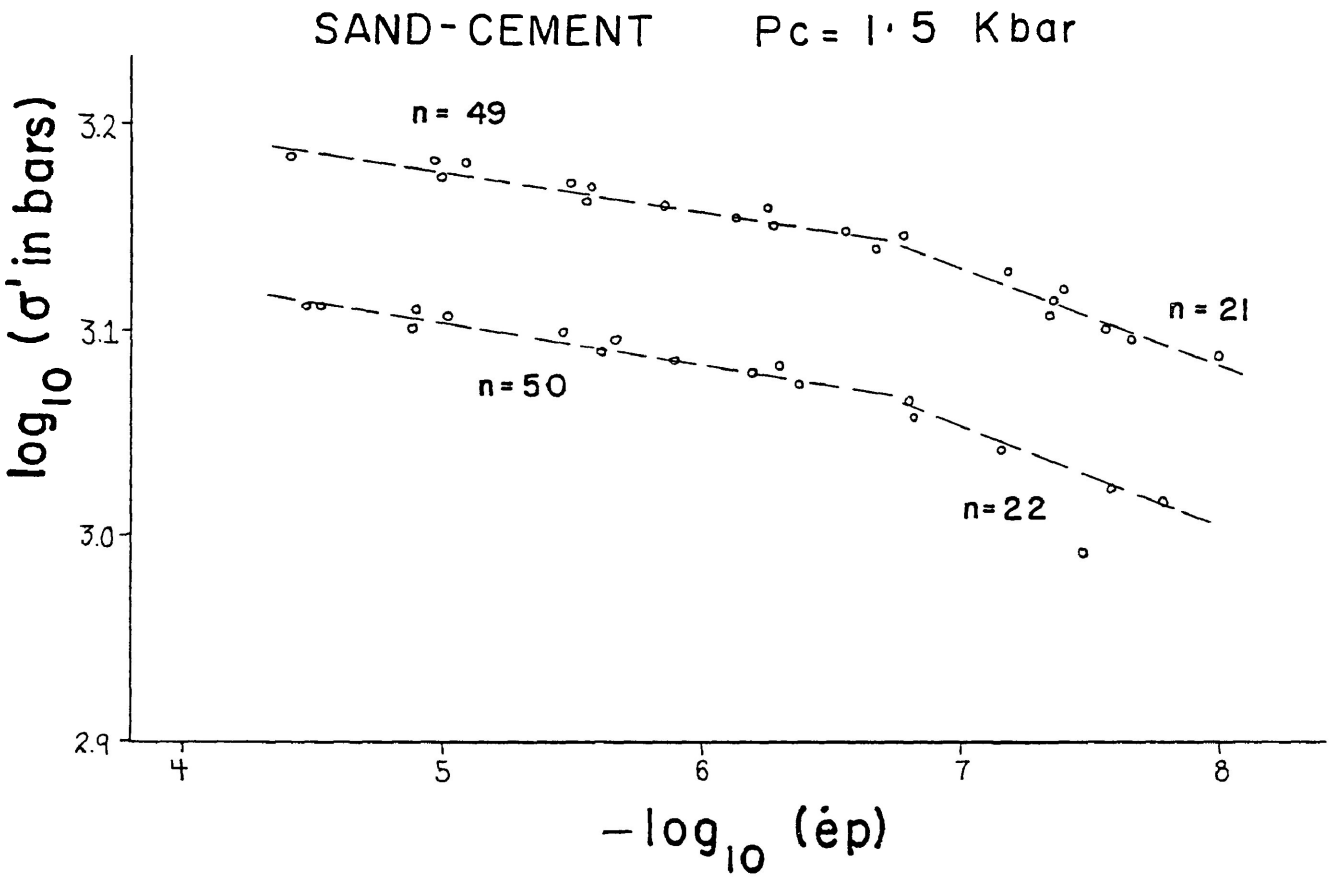

Figure 4-45. The results of two stress relaxation tests of a 0.75 inch diameter cylindrical specimen of the sand-cement material at 1.5 Kbars confining pressure.

Calcite-Cement Shear Zones

For the calcite-cement shear zones two separate series (1 and 2) of tests, each at a particular confining pressure, were conducted.

Changes in anisotropy, shape and orientation of the susceptibility ellipsoid:

For the first series, Series 1 at 1.0 kbar confining pressure, three individual specimens were deformed, totalling 12 experiments.

The changes in the orientation of the principal susceptibility directions of SZ-C1 and SZ-C2 in Series 1 (Figures 4-46 & 4-47) are somewhat reminiscent of the previous sand-cement shear zones as movements are not great. However, with increasing shear strain, there appears to be a continuous movement of K_{min} towards the edge of the stereonet, subtending an angle of 70^{o} to the shear zone. Unlike the sand-cement material, the principal susceptibility directions K_{max} and K_{int} are typically in the same hemisphere with respect to the shear direction, thus lying in a plane at a small angle to the shear plane.

In SZ-C3 of Series 1 the principal susceptibility directions, K_{max} and K_{int}, appear to be continually rotating about a fixed K_{min} (Figure 4-48). Within this shear zone the trend of K_{min} is

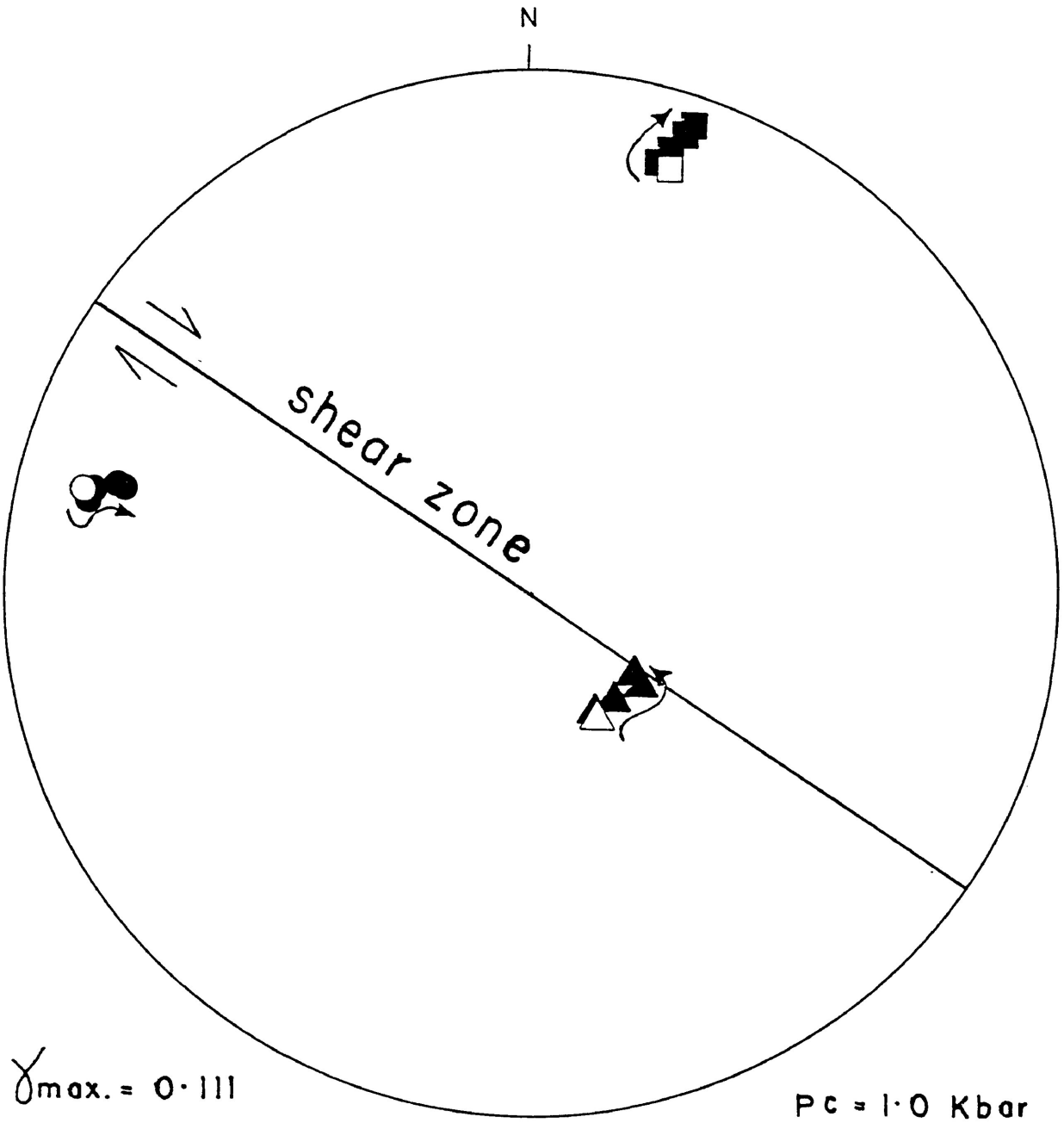

Figure 4-46. The progressive changes in orientation of the principal susceptibility directions for the calcite-cement SZ-C1 of Series 1.

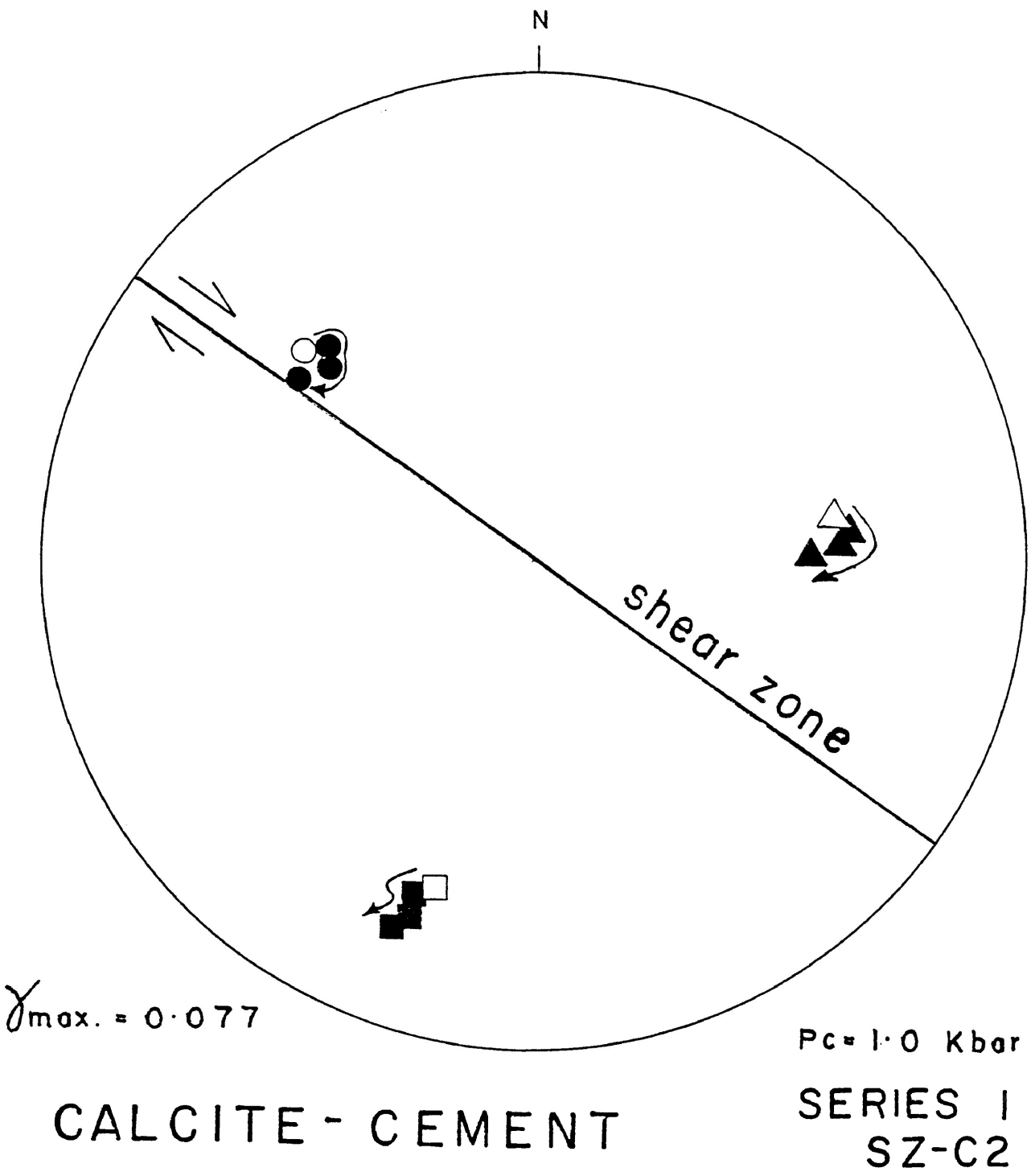

Figure 4-47. The progressive changes in orientation of the principal susceptibility directions for the calcite-cement SZ-C2 of Series 1.

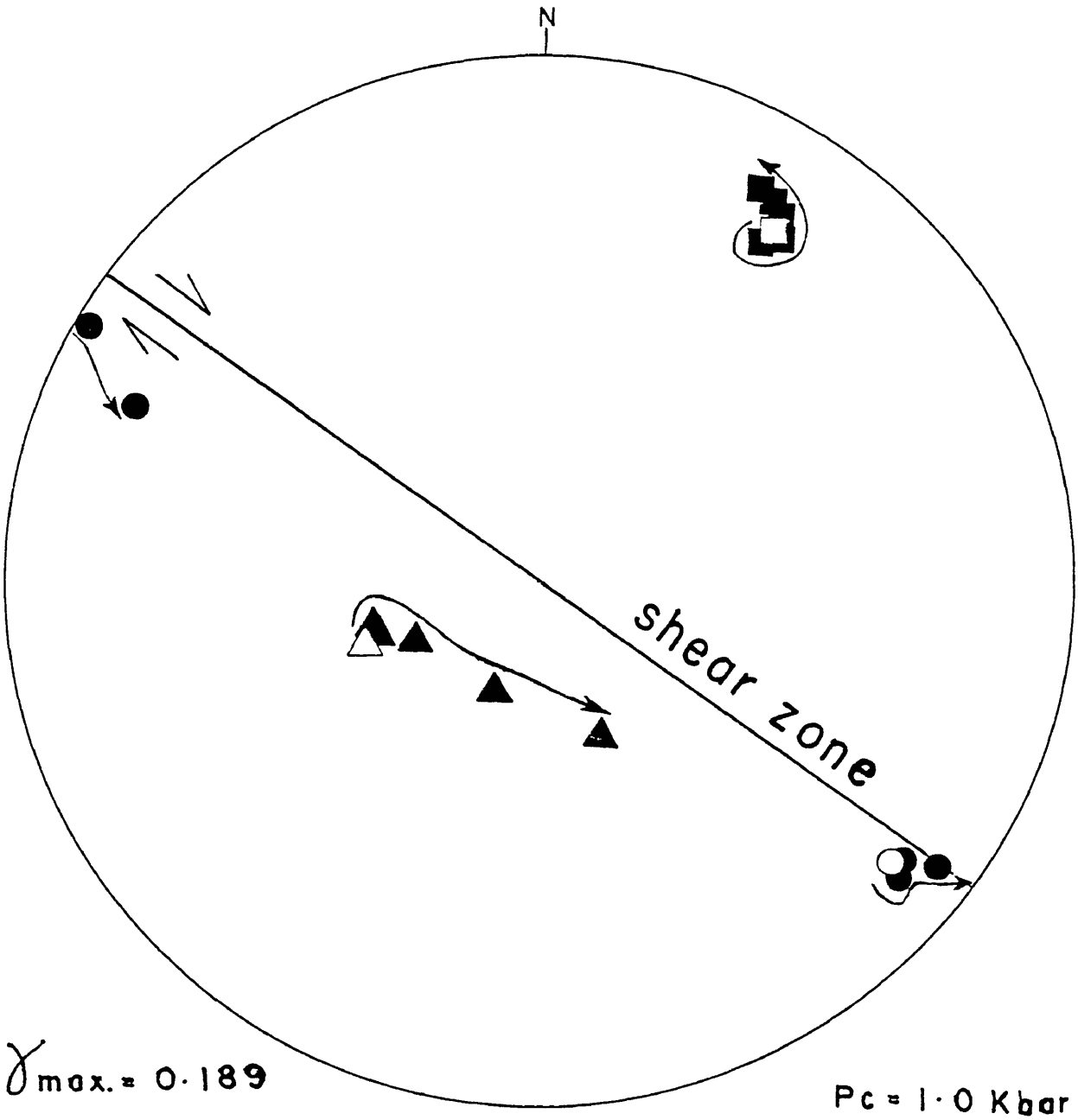

Figure 4-48. The progressive changes in orientation of the principal susceptibility directions for the calcite-cement SZ-C3 of Series 1.

nearly perpendicular to the direction of shear, and the rotation of K_{max} and K_{int} are within a plane that is parallel to the shear direction. Although K_{max} and K_{int} had experienced a rotation of 40^{o} by the end of testing, there is no indication where or if the rotation would stop, as the condition of the sample would not allow further testing.

The rotations of the principal susceptibility axes, K_{min} and K_{max}, in SZ-C1 are slower but very close to that expected of 'real' line elements of the same initial angular position (Figure 4-49). In SZ-C2, all three principal susceptibility directions are beyond the 20^{o} limit from the plane parallel to the shear direction and perpendicular to the shear zone, and thus their rotations cannot be compared to those of 'real' lines rotating within this plane. In SZ-C3 of the series, the rotation of K_{max} susceptibility direction diverges considerably from its respective 'real' line (Figure 4-50). K_{max} displays an initial rotation away from the direction of shear, and with further shear strain rotates toward the shear direction at a much faster rate than the 'real' line element and eventually rotates considerably beyond the shear direction.

All of the susceptibility ellipsoids in Series 1 of the calcite-cement material originated in the field of flat-shaped ellipsoids (Figures 4-51 & 4-52). The effect of experimental shear

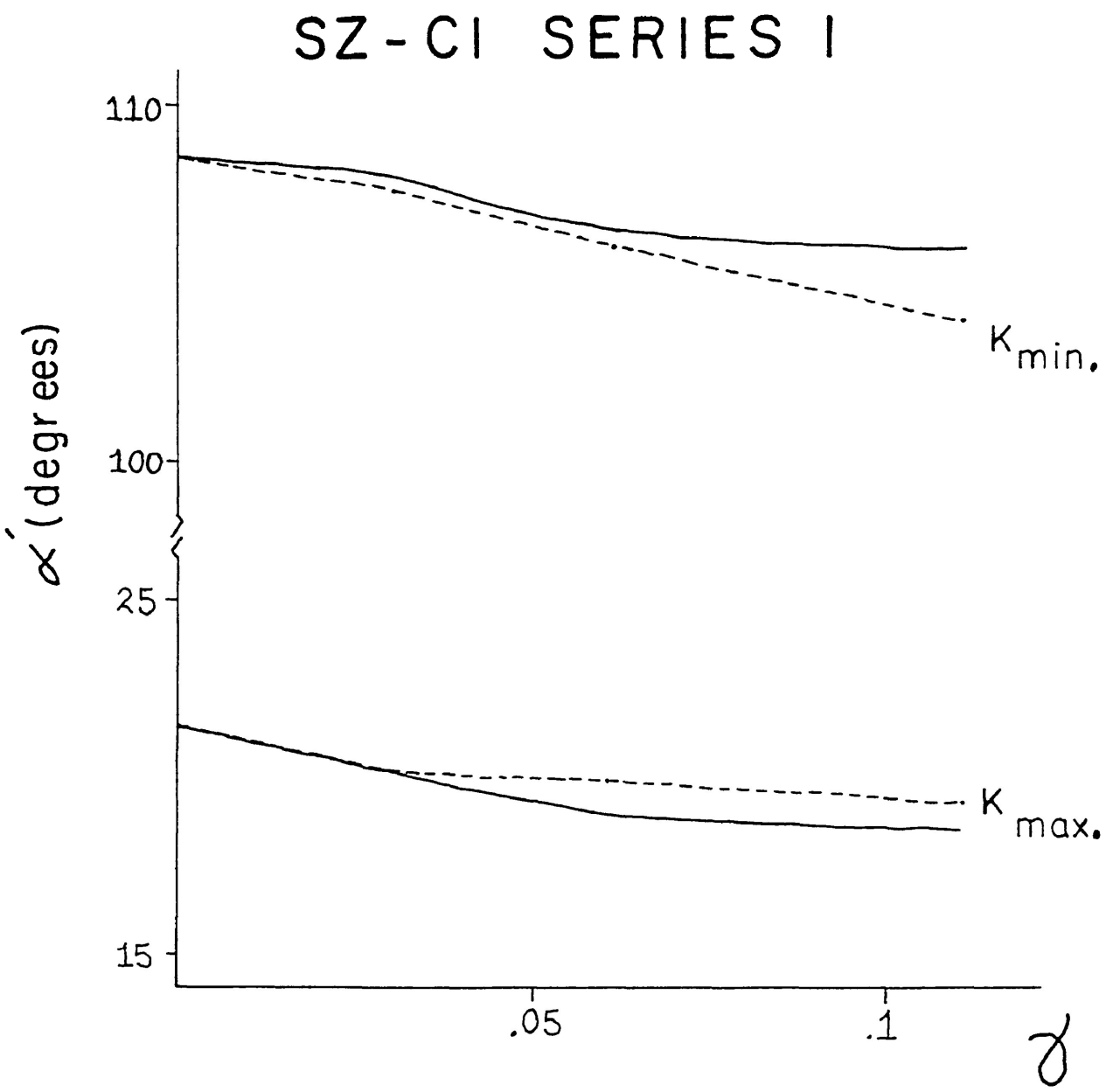

Figure 4-49. Illustrating the measured changes in angular position with respect to the shear zone (α') of the K_{min} and K_{max} principal susceptibility directions of SZ-C1 of Series 1 (dashed lines) against those calculated for real material lines (solid lines) of a similar initial orientation experiencing a equivalent shear strain.

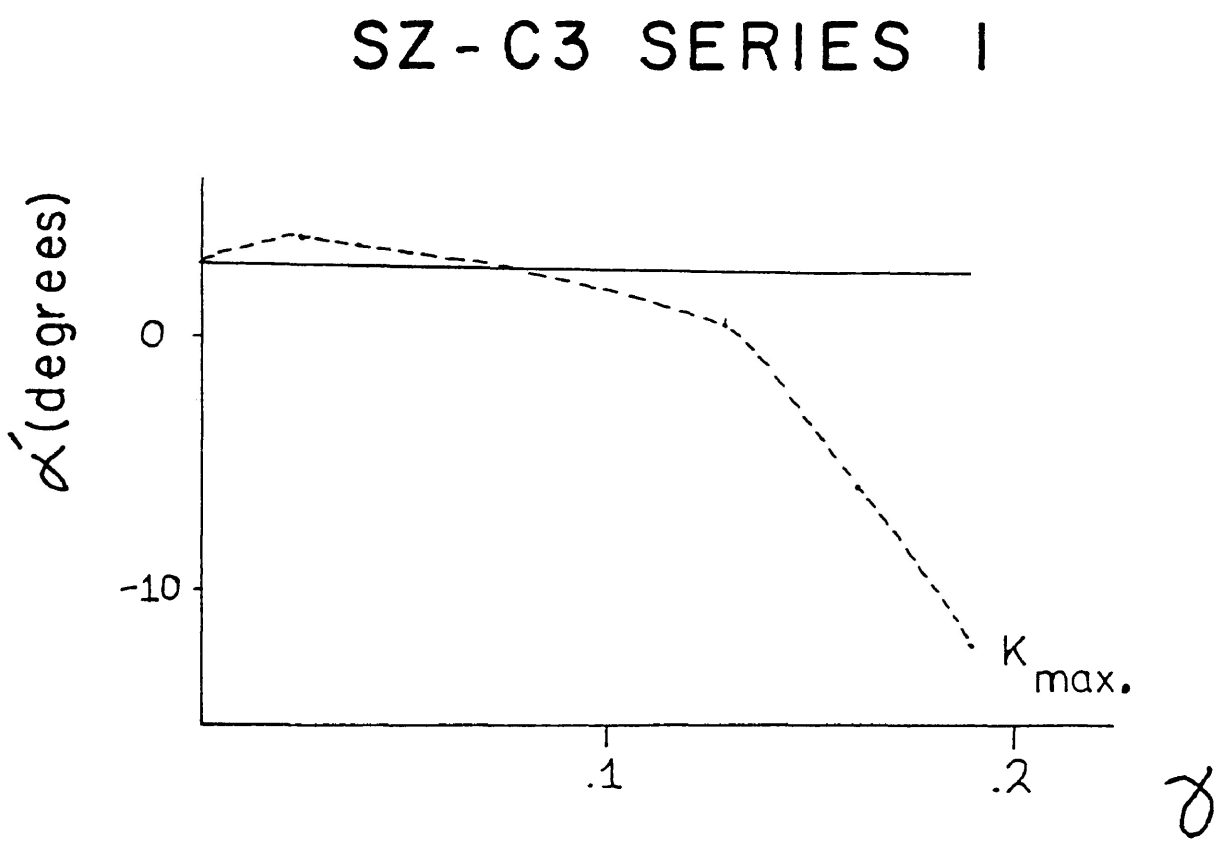

Figure 4-50. Illustrating the measured changes in angular position of the Kmax susceptibility direction of SZ-C3 of Series 1 (dashed line) against that calculated for a similarily orientated material line.

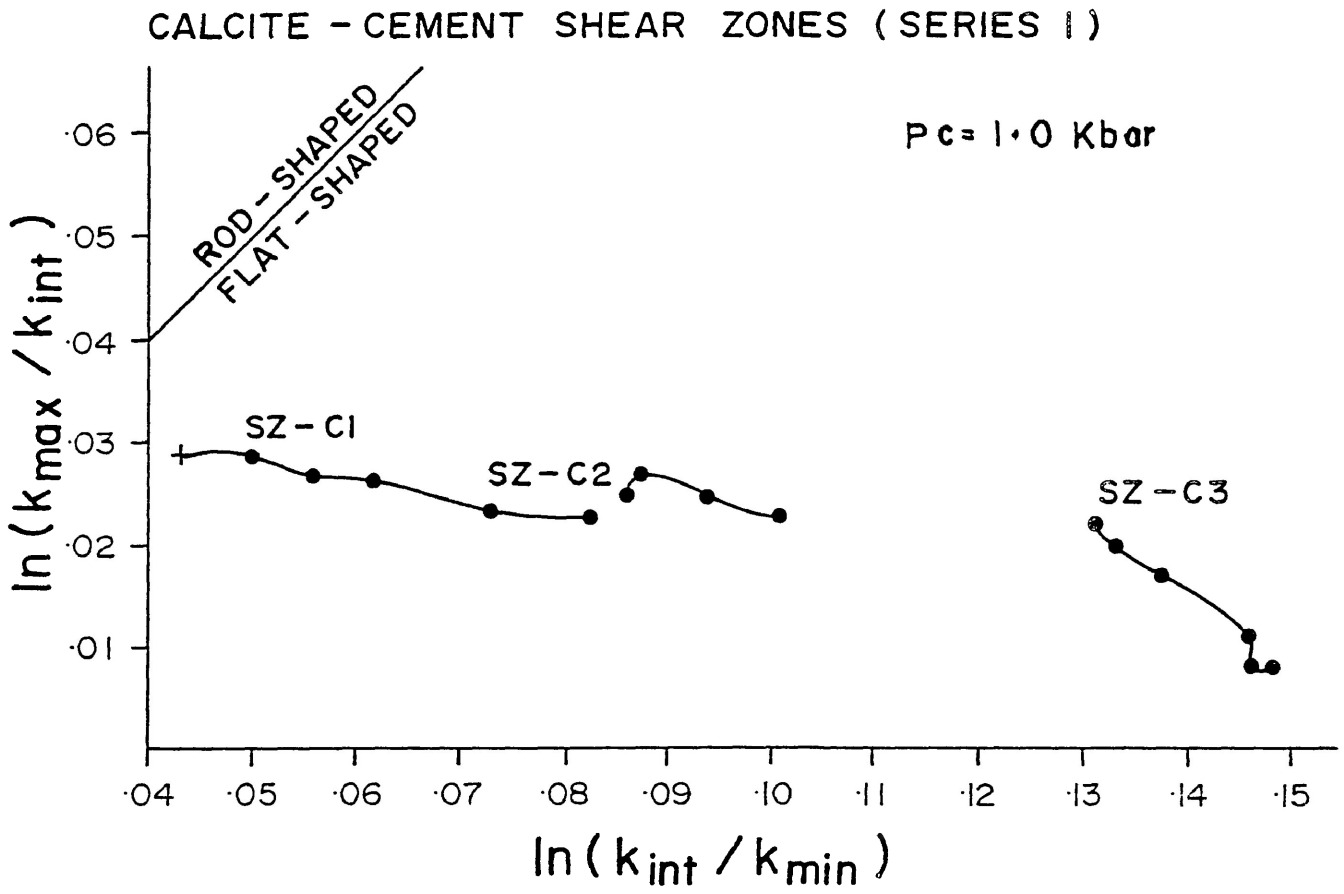

Figure 4-51. *Illustating the progressive change of shape of the* magnetic susceptibility's magnitude ellipsoids for Series 1 of the calcite-cement shear zones.

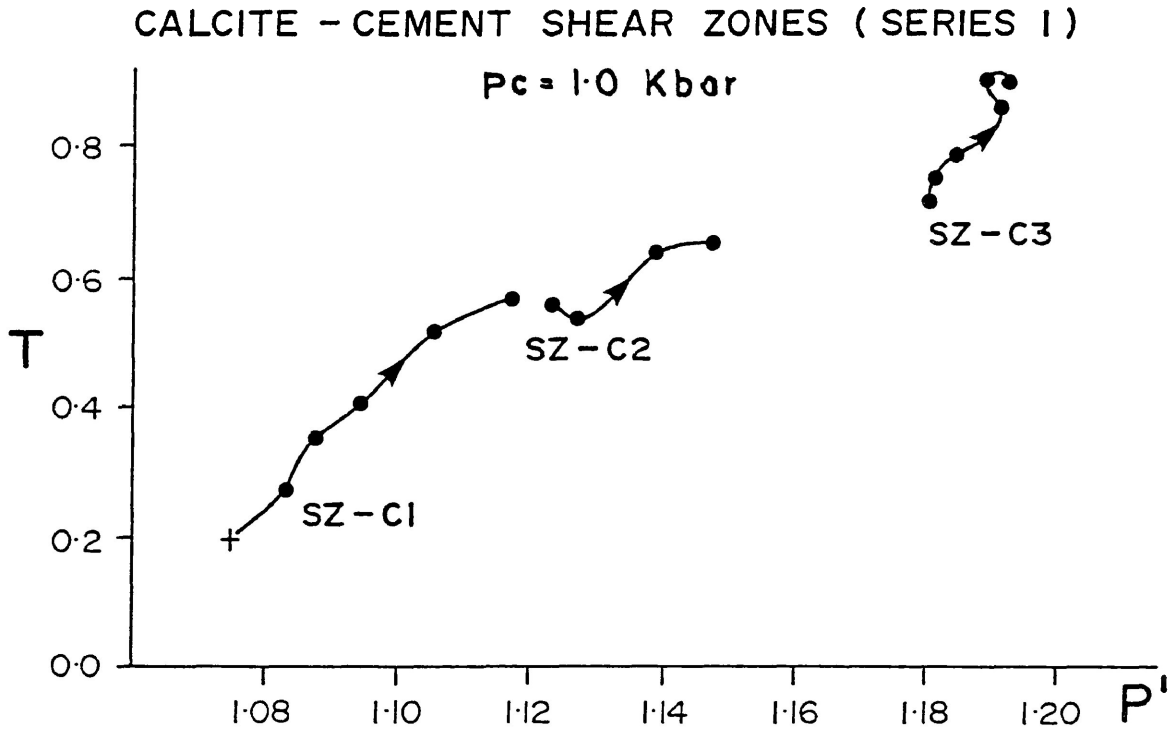

Figure 4-52. Illustating the progressive changes in the shape (T) and degree of anisotrotpy (P') of the susceptibility ellipsoid of Series 1.

strain on the susceptibility ellipsoids in each of the specimens, except for the initial increment, in SZ-C2 and second to last increment of shear strain in SZ-C3, caused the ellipsoids to become incresingly flatter and more anisotropic.

Reasonably good to very good linear correlations could be discerned between the change in anisotropy ($\Delta P'$) and the shear strain (ln (X/Z)) (Figures 4-53 to 4-55).

Three individual specimens were deformed in Series 2, totalling 20 experiments. A confining pressure of 1.5 kbars was employed throughout this series.

Figure 4-56 displays the changes in orientation of the susceptibility ellipsoid for SZ-2 of the series. The principal susceptibility directions demonstrate consistently directed progressive movements during shear strain. K_{max} is observed to rotate into the plane of shear however, the final orientation of the plane containing both K_{max} and K_{int} cannot be easily related to the shear sense. K_{min} is observed to rotate towards the edge of the stereonet.

The initial susceptibiltiy orientation of SZ-3 of Series 2 (Figure 4-57) was very near to the 'fixed' orientation described in the sand-cement shear zone experiments. K_{min} is noted to move towards the plane perpendicular to the shear zone and parallel to the shear direction (the edge of the stereonet) at an angle of

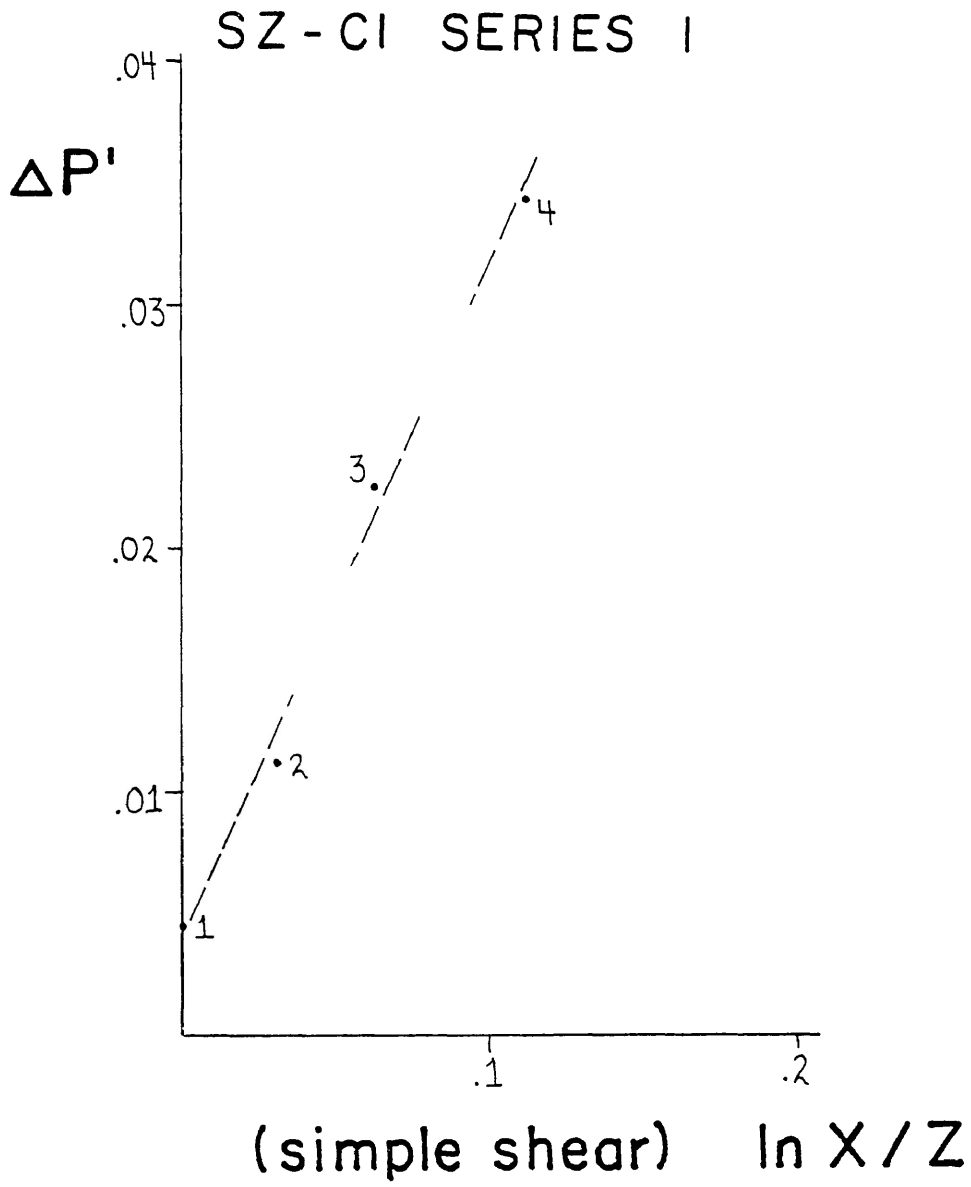

Figure 4-53. The correlation between the change in the degree of anisotropy before and after each increment of deformation (ΔP') and the shear strain ratio (ln (X/Z)) for SZ-C1 of the calcite-cement Series 1. The correlation is significant at the 95% level with a coefficient of 0.996.

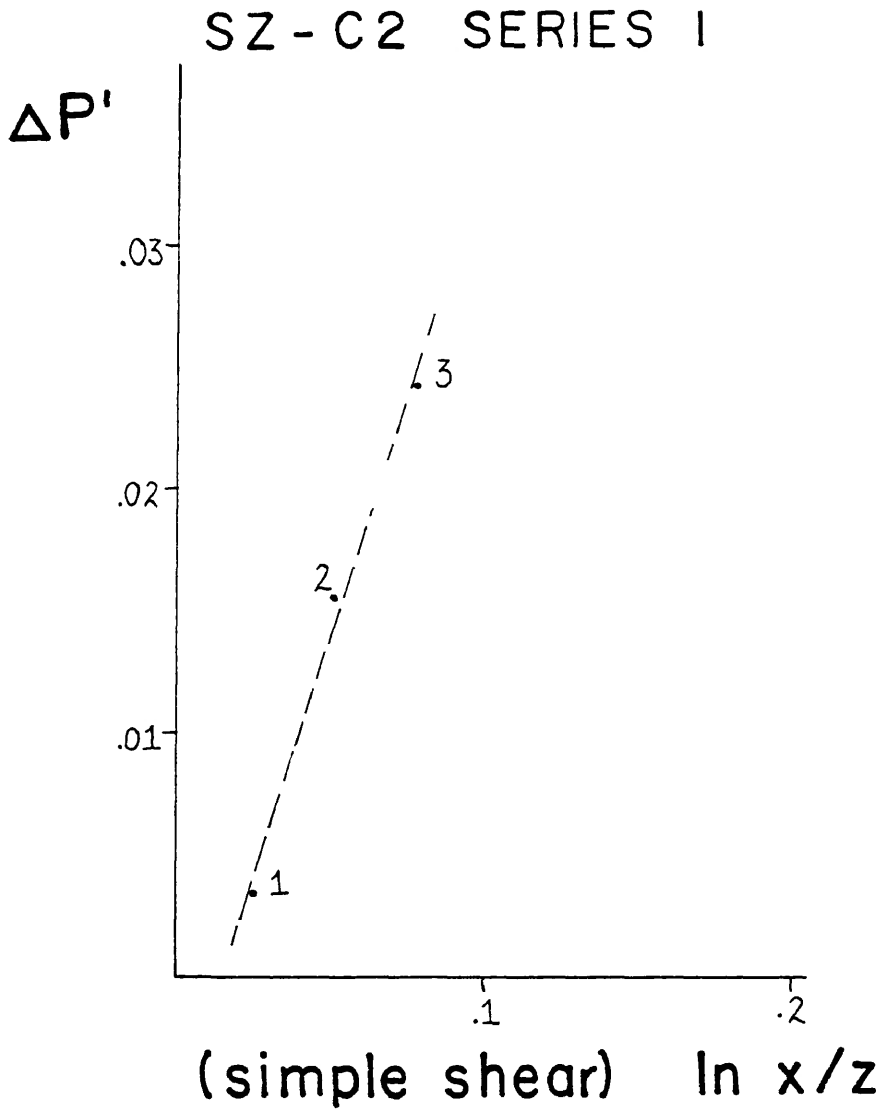

Figure 4-54. The correlation between the change in the degree of anisotropy and the shear strain ratio for SZ-C2 of Series 1. The correlation coefficient is 0.995.

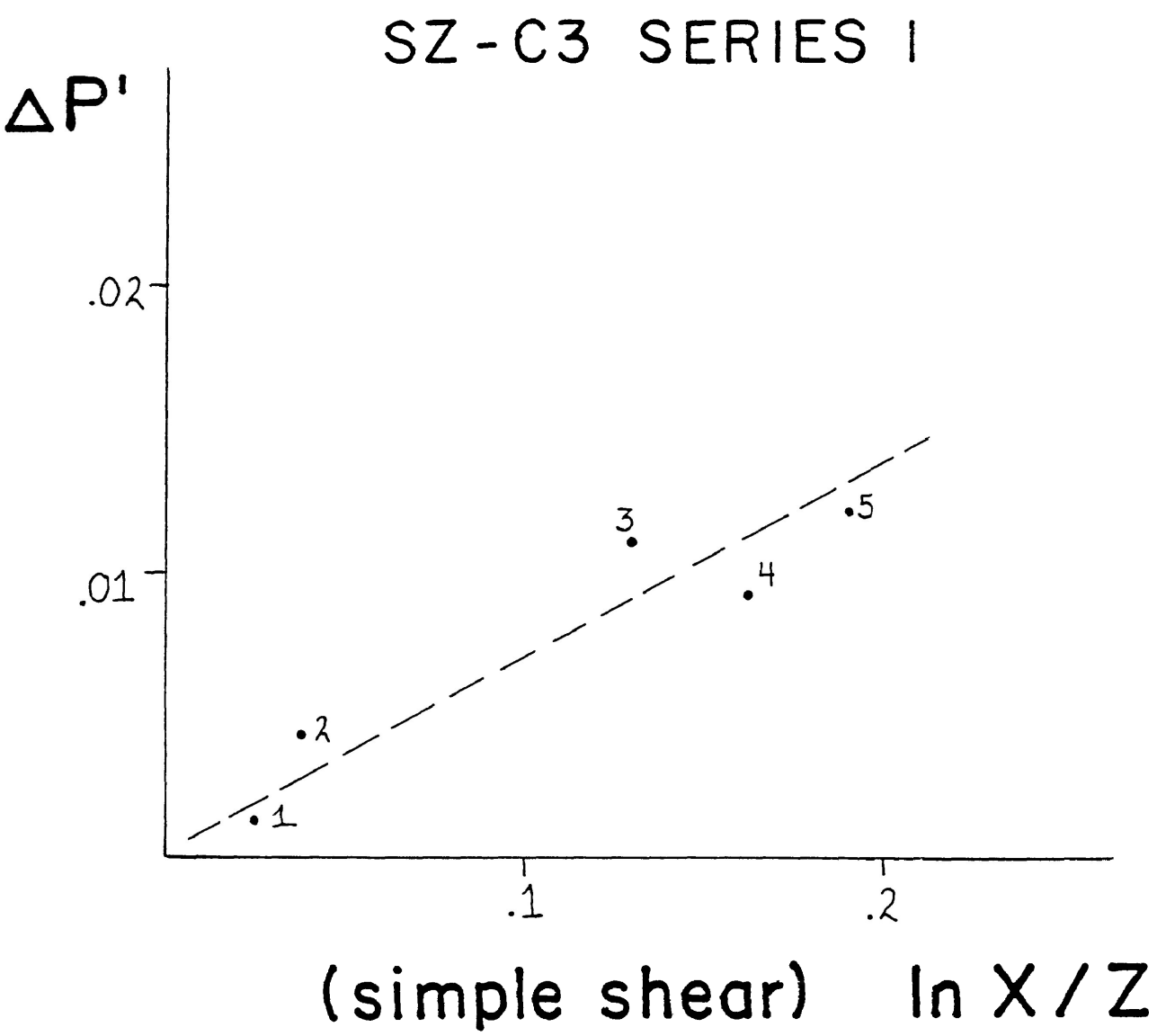

Figure 4-55. The correlation between the change in the degree of anisotropy and the shear strain ratio for SZ-C3 of Series 1. The correlation coefficient is 0.936.

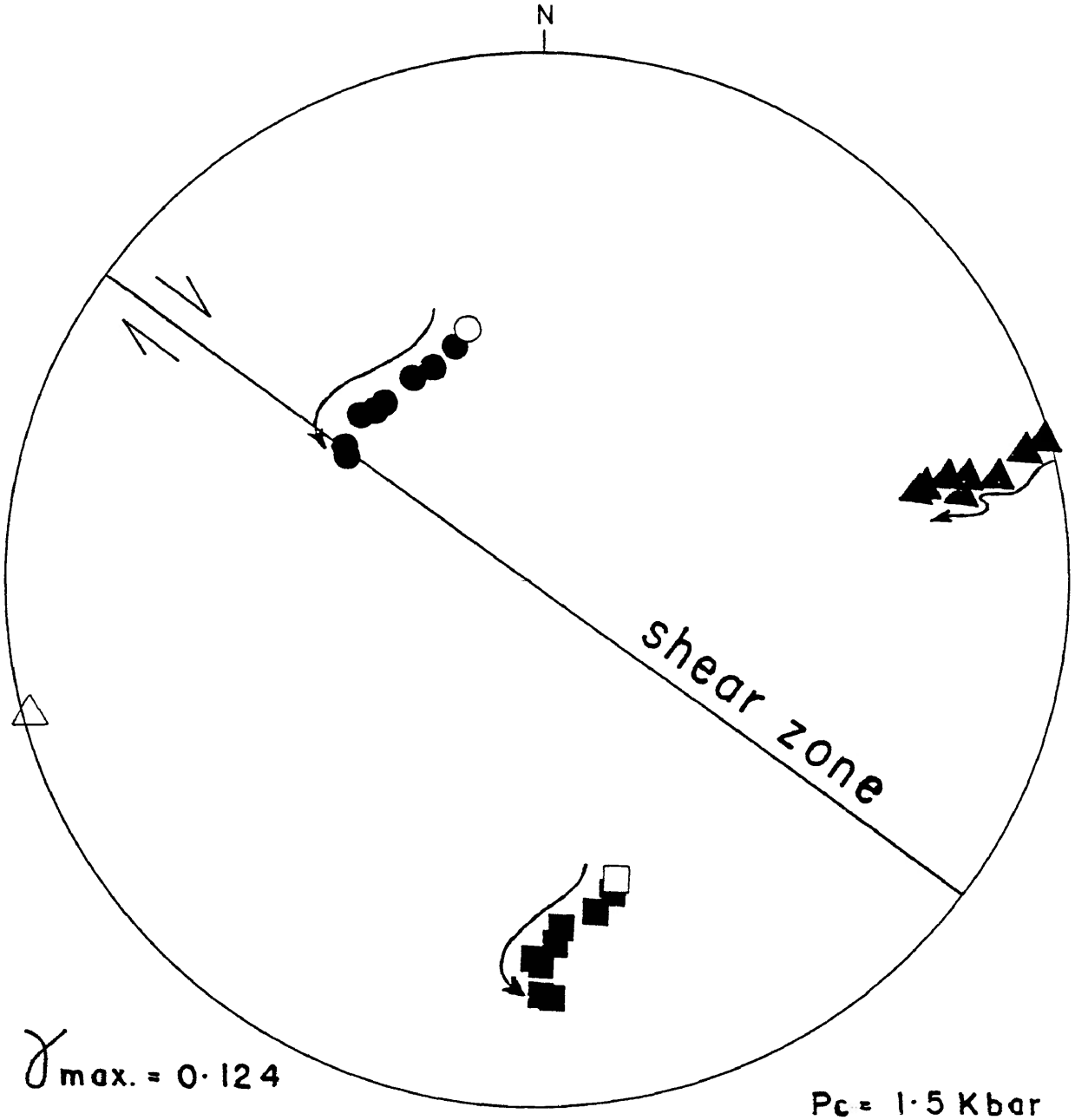

Figure 4-56. The progressive changes in orientation of the principal susceptibility directions for SZ-C2 of the calcite-cement Series 2.

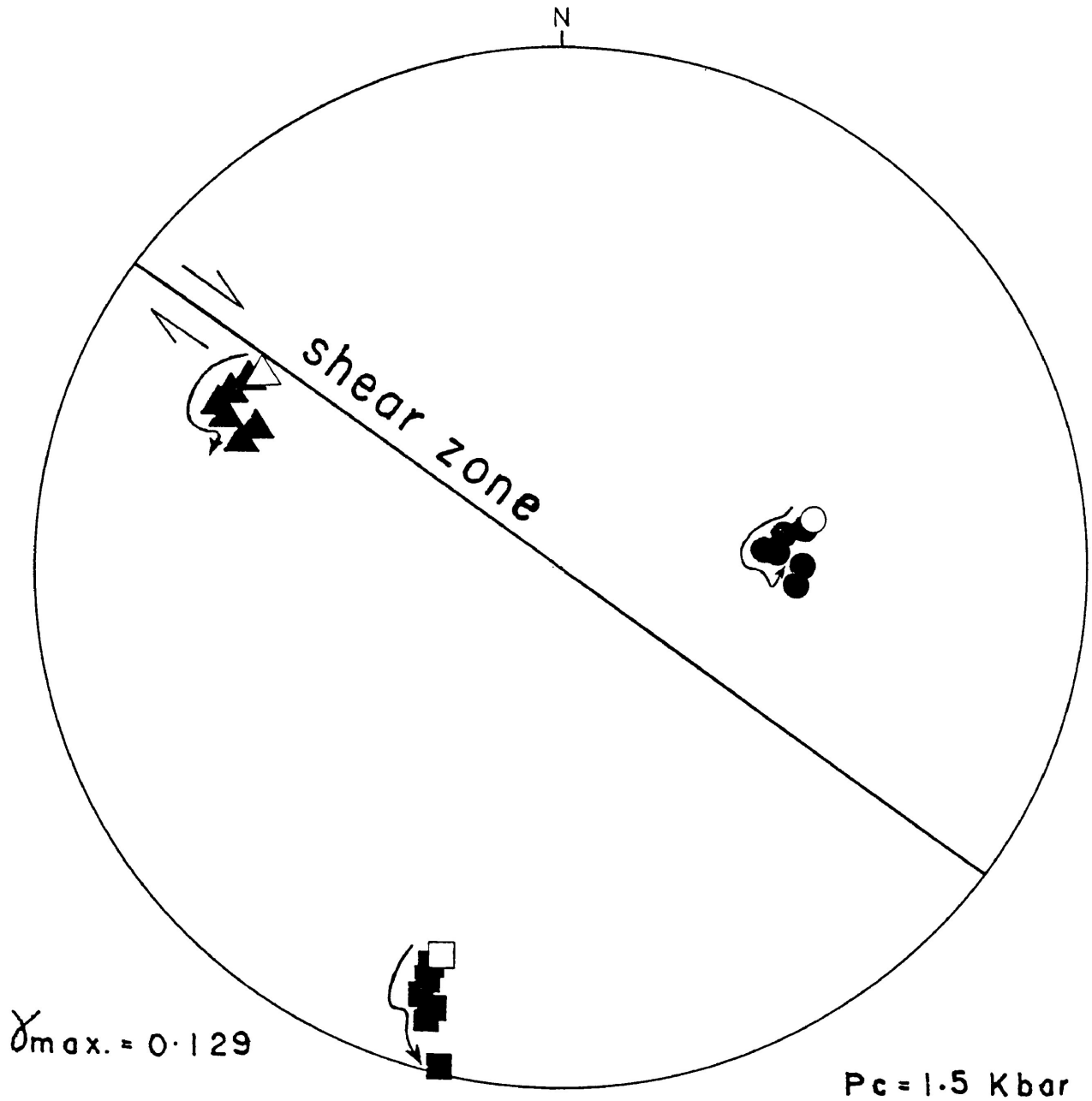

Figure 4-57 The progressive changes in orientation of the principal susceptibility directions for SZ-C3 of Series 2.

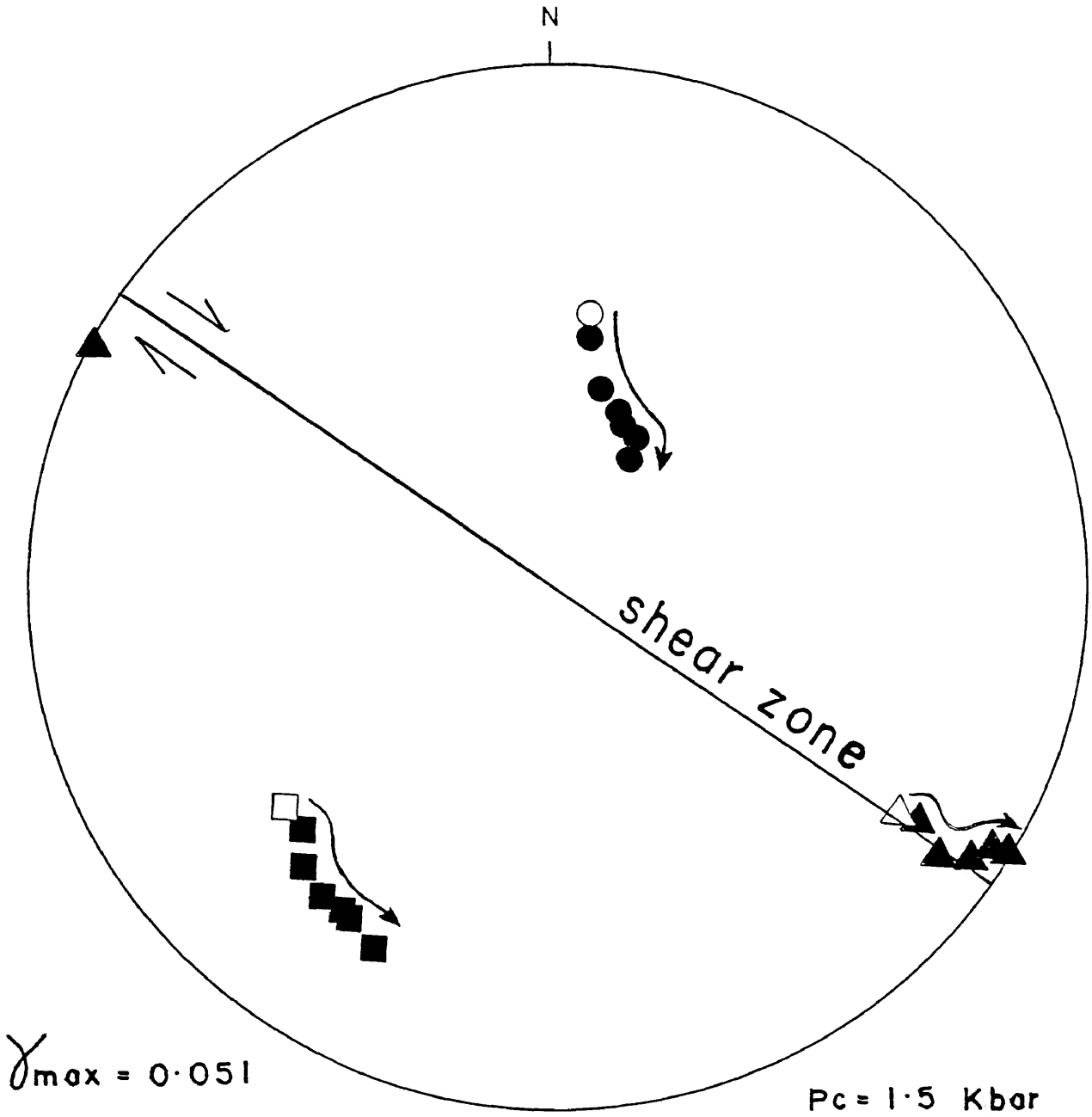

Figure 4-58. The progressive changes in orientation of the principal susceptibility directions for SZ-C4 of Series 2.

approximately 70^{o} to the shear direction. The initial rotations of K_{max} and K_{int} do not show any simple relationship to the direction of the initial 'schistosity'. Further rotations of K_{max} and K_{int} are toward a plane that makes a small angle with the shear plane.

Figure 4-58 displays the rotations of the principal susceptibility directions for SZ-4. K_{max} and K_{int} rotate in a sense towards the direction of shear to a plane nearly parallel to the shear plane. K_{min} rotates towards the plane which is perpendicular to the shear zone and parallel to the shear direction (the edge of the stereonet) to a position approximately 70^{o} to the shear direction.

All of the rotations of the significant principal susceptibility directions for Series 2 display non-conformable behaviour to their respective 'real' line elements. In SZ-C2, K_{int} initally rotates away from the shear direction and with further shear strain rotates in a mildly erratic manner toward the shear direction (Figure 4-59). In SZ-C3 the susceptibility axis, K_{min}, rotates away from the direction of shear (Figure 4-60). The K_{int} susceptibility axis also rotates away from the direction of shear during the deformation of SZ-C4 (Figure 4-61). In all the experiments of this series the movement of the susceptibility axes are not wholely contained within the plane which is perpendicular to the shear

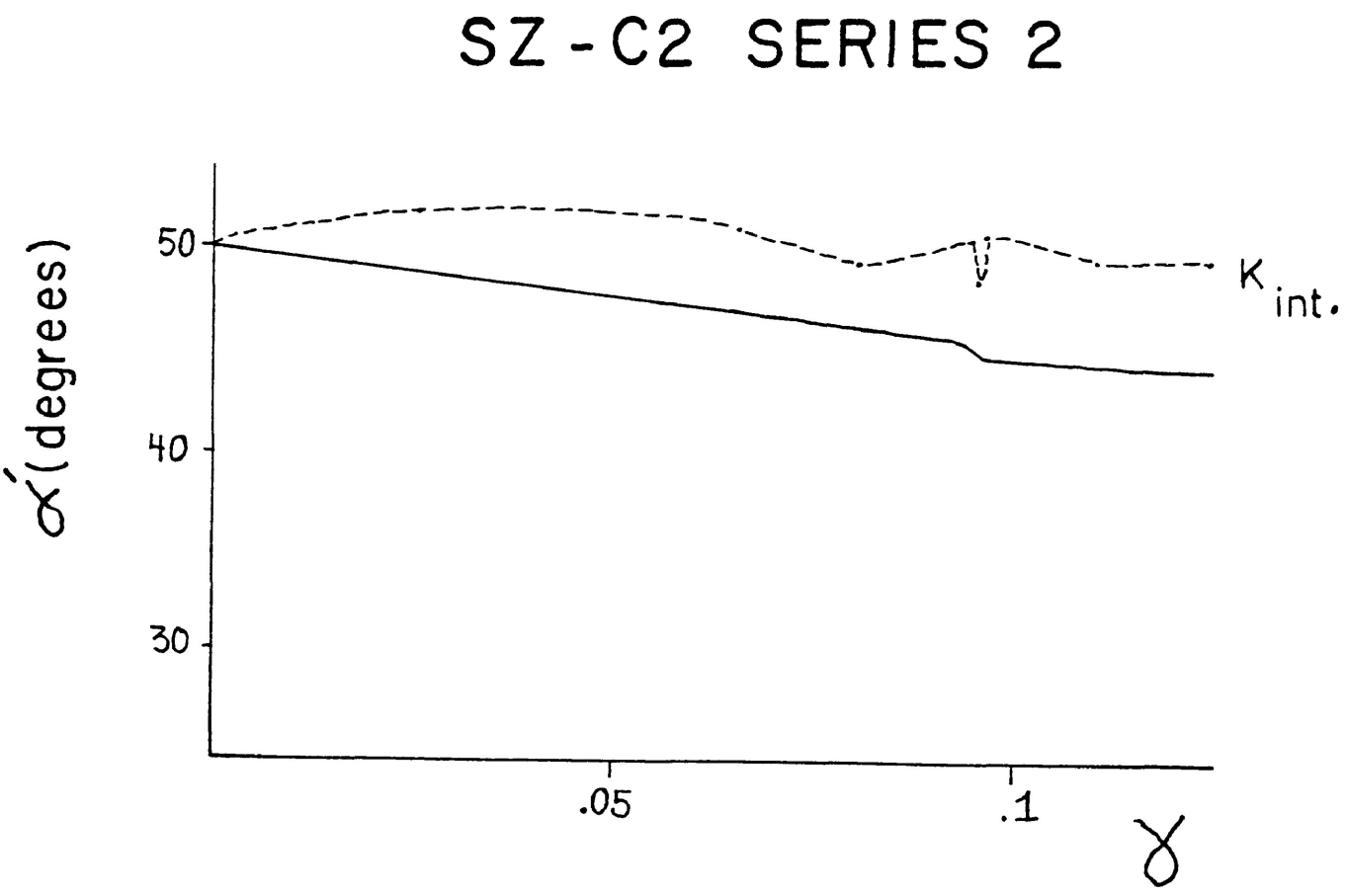

Figure 4-59. Illustrating the measured change in angular position with respect to the shear zone (α') of the K_{int} susceptibility axis of SZ-C2 of Series 2 (dashed line) against that calculated for a real material line of similar initial orientation experiencing the equivalent shear strain (solid line).

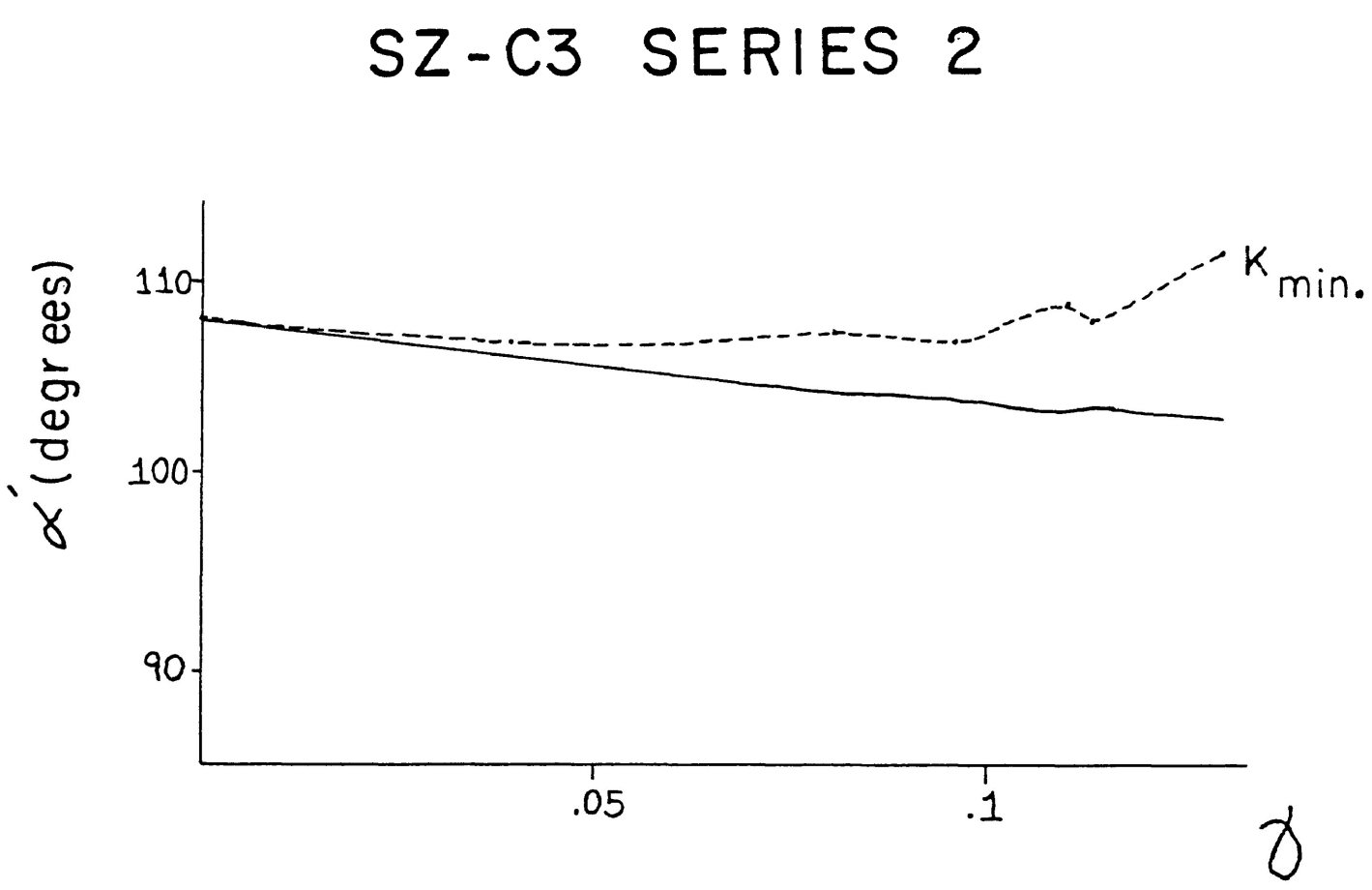

Figure 4-60. Illustrating the measured change in angular position of the K_{min} susceptibility axis of SZ-C3 of Series 2 (dashed line) against that calculated for a similarily oriented material line.

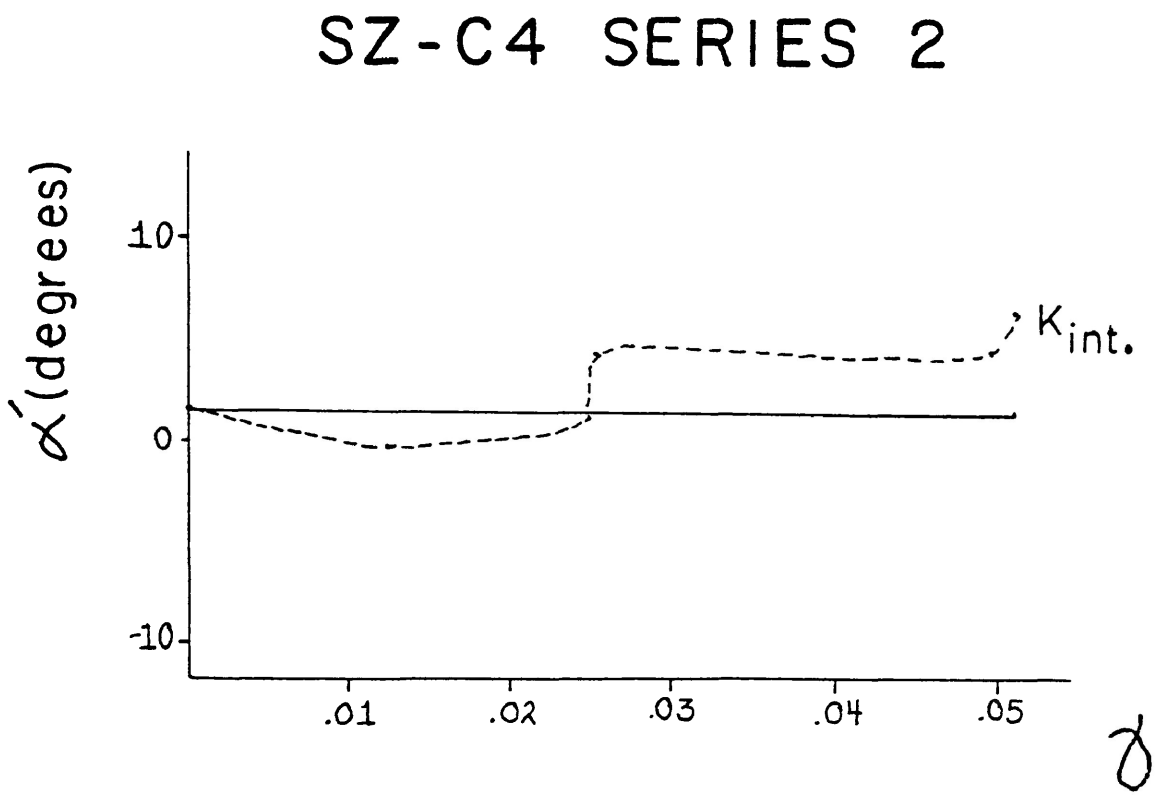

Figure 4-61. Illustating the measured change in angular position of the Kint susceptibility axis of SZ-C4 of Series 2 (dashed line) against that calculated for a similarily oriented material line.

zone and contains the direction of shear.

The undeformed susceptibility ellipsoids of SZ-C2 and SZ-C3 originated as within the field of flat-shaped ellipsoids, while SZ-C4 originated within the field of rod-shaped ellipsoids (Figures 4-62 & 4-63). The effect of experimental shear strain caused in each case a general flattening of the ellipsoids and an increase in the ellipsoids' degree of anisotropy. SZ-C2, however, displayed an initial decrease in its flat shape and anisotropy before becoming progressively flatter and more anisotropic. It is interesting to note that as the susceptibility ellipsoid of SZ-C4 was incrementally deformed from a rod-shaped ellipoid to a flat-shaped ellipsoid it experienced a couple of increments where the shape parameter T did not change while the anisotropy still increased (See Figure 4-63). This was also observed in the deformation of the sand-cement specimen SZ-3 of Series B as the susceptibility ellipsoid changed shape from rod-shaped to flat-shaped.

Each of the $\Delta P'$ versus natural log (shear strain) plots displays a different relationship between the anisotropy changes during the first and later increments of shear strain (Figures 4-64 to 4-66). Initially, the data fits a line that curves upward and, after some amount of shear strain, specific to each specimen, becomes linear in a power-law correlation similar to previous experiments.

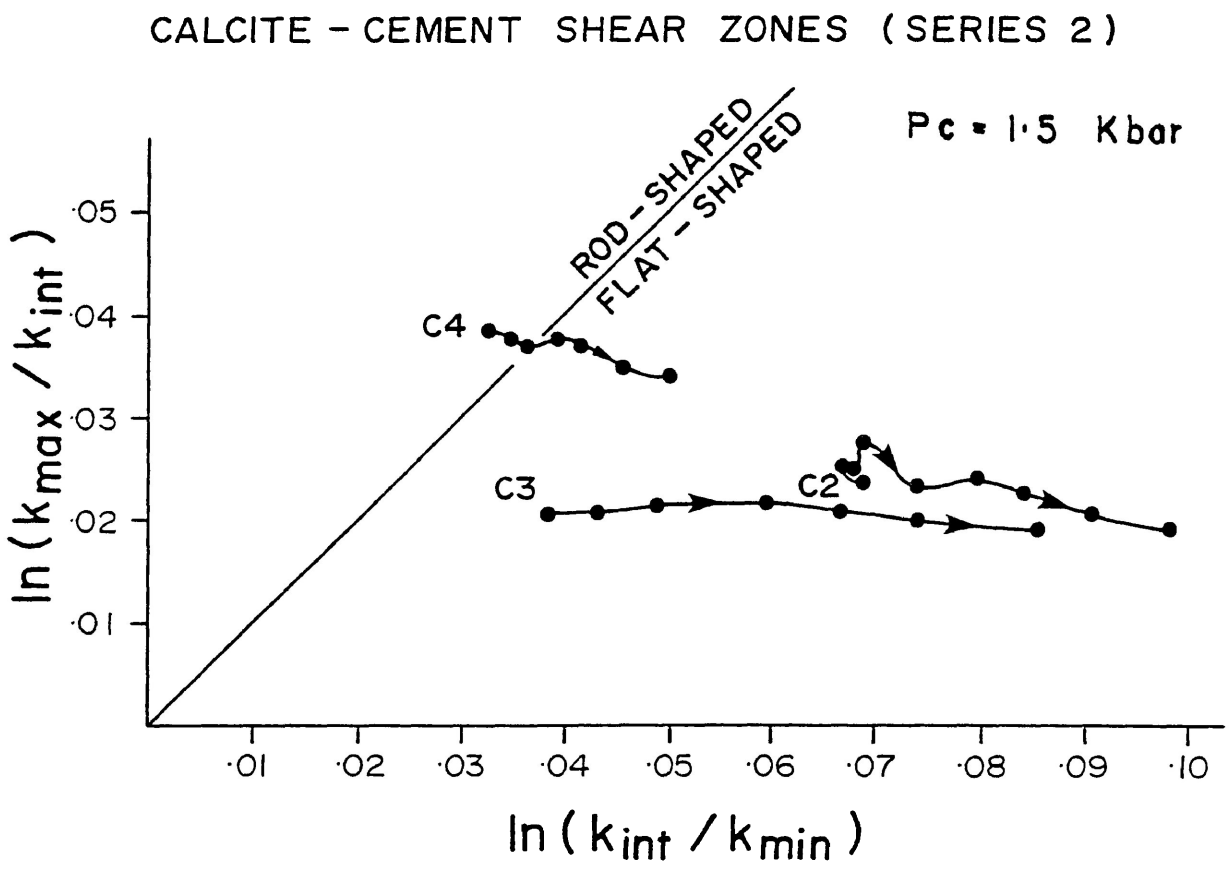

Figure 4-62 Illustrating the change in shape of the susceptibility ellipsoids of the calcite-cement Series 2.

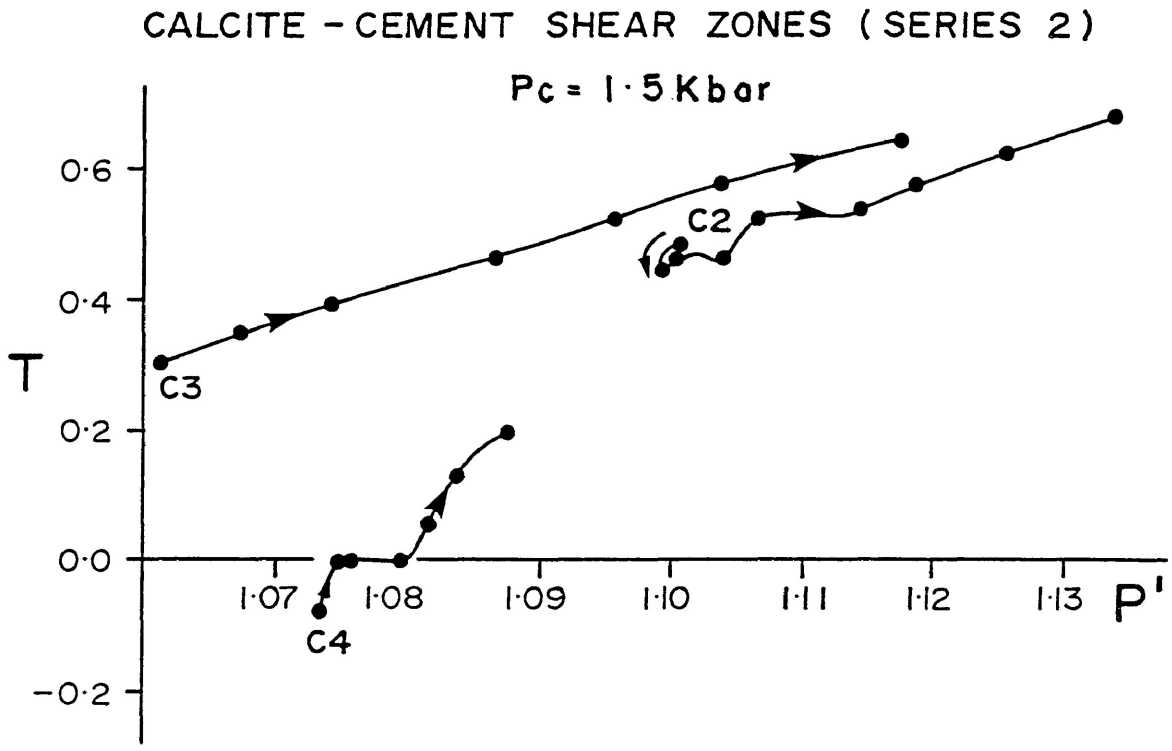

Figure 4-63 Illustrating the change in shape and degree of anisotropy of the susceptibility ellipsoids of Series 2.

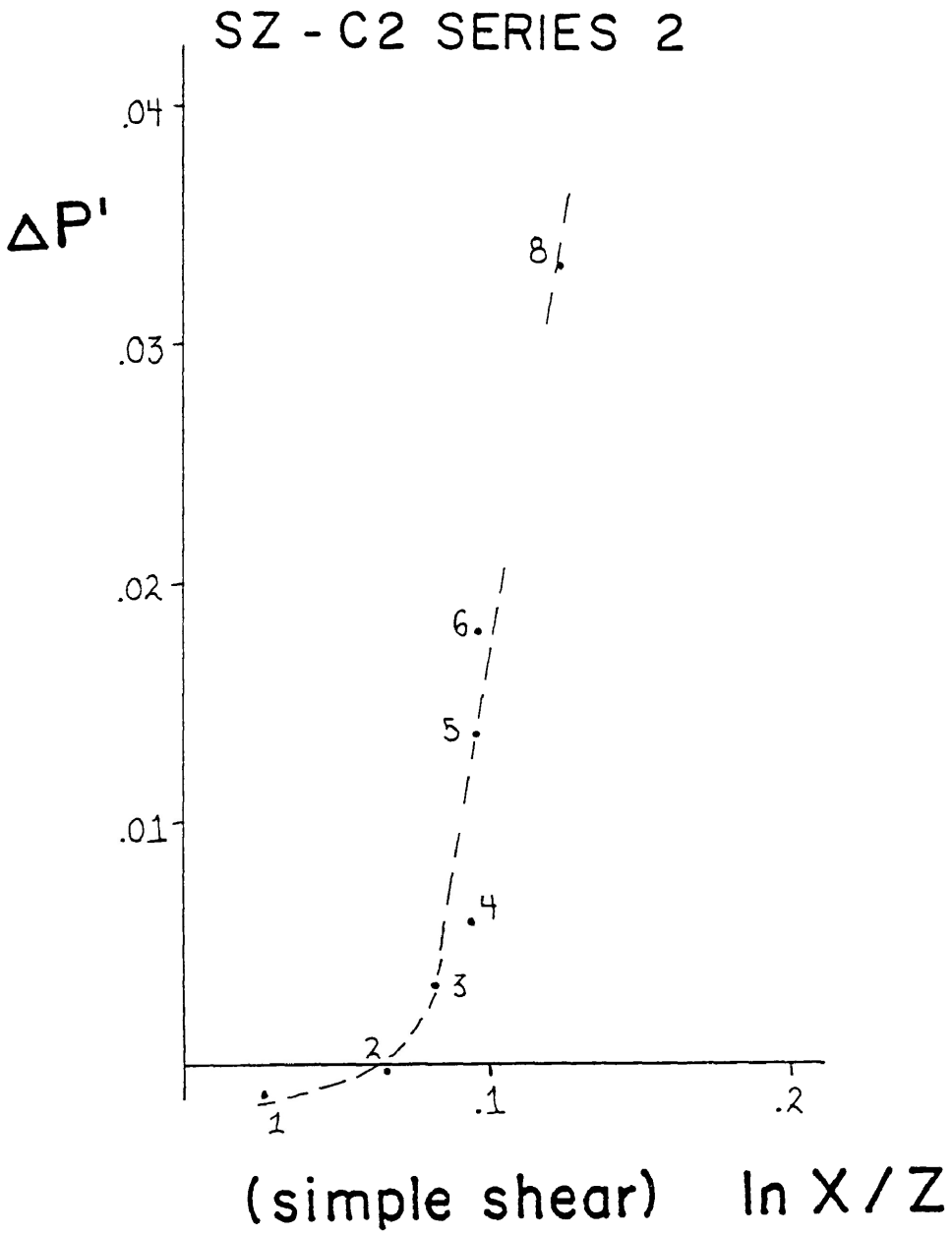

Figure 4-64. The correlation between the change in the degree of anisotropy and the shear strain ratio for SZ-C2 of Series 2. The correlation coefficient for the linear section (experiments 3 to 8) is 0.949.

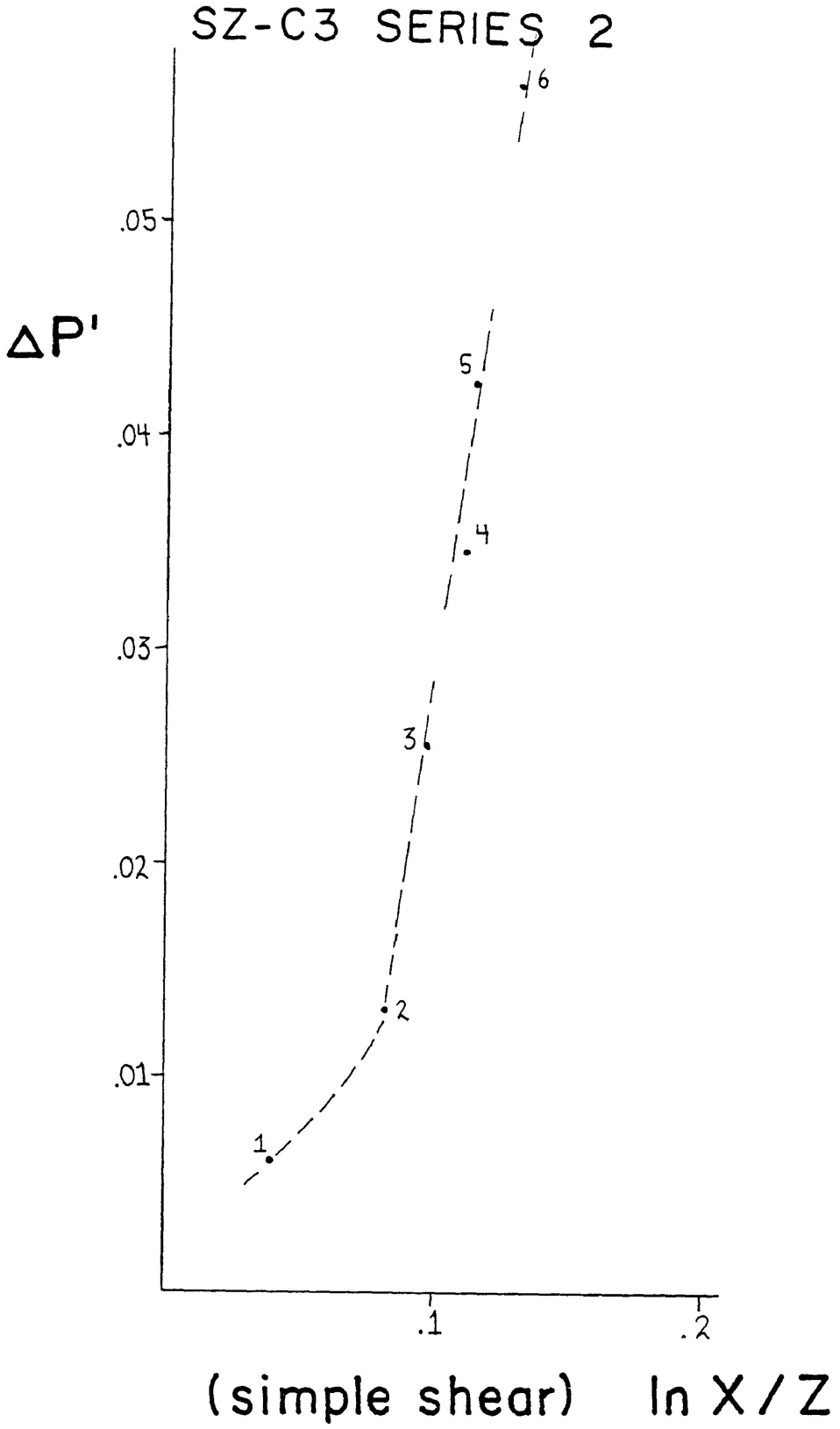

Figure 4-65. The correlation between the change in the degree of anisotropy and the shear strain ratio for SZ-C3 of Series 2. The correlation coefficient for the linear section is 0.994.

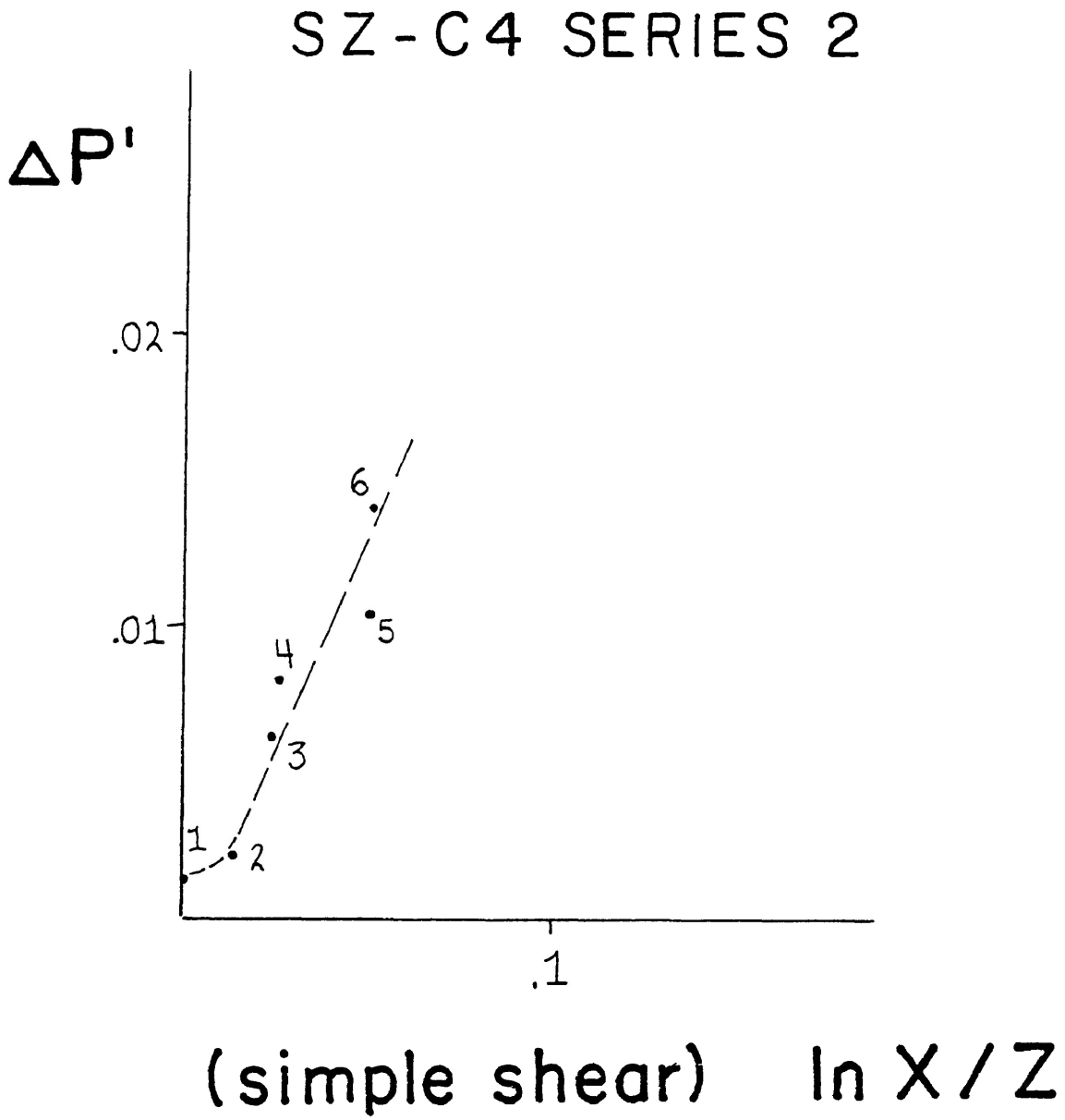

Figure 4-66. The correlation between the change in the degree of anisotropy and the shear strain ration for SZ-C4 of Series 2. The correlation coefficient for the linear section is 0.935.

Microscopic Observations

The undeformed calcite-cement material consists primarily of variously shaped angular to rhomboid calcite and sub-angular to rounded magnetite fragments supported in a fine grained matrix of Portland cement (Plate 4-4). Approximately 70% of the calcite fragments are twinned (predominantly by one law), the twin planes are straight and are commonly wide, such that there are few twins per grain. Grain to grain contacts are few (0 to 2 per grain). There is no preferred dimensional orientation of either the grains within the aggregate, or of the twin lamellae within the grains.

At least two samples in each of the deformed series were thin sectioned. The features of the deformed specimens from Series 1 were very similar; grain to grain contacts have incresed in number (1 to 3 per grain), each calcite grain now possesed new twin planes that are thinner and more numerous than the original twin lamellae. The new twin planes display a weak preferred dimensional orientation (Plate 4-5)and in some grains the planes are kinked or slightly bent (Plate 4-6). A moderate preferred dimensional orientation of the calcite fragments has developed, while the magnetite grains display no preferred dimensional orientation (Plate 4-7).

The deformed specimens of Series 2 display a similar deformation fabric to those of Series 1. Magnetite is randomly

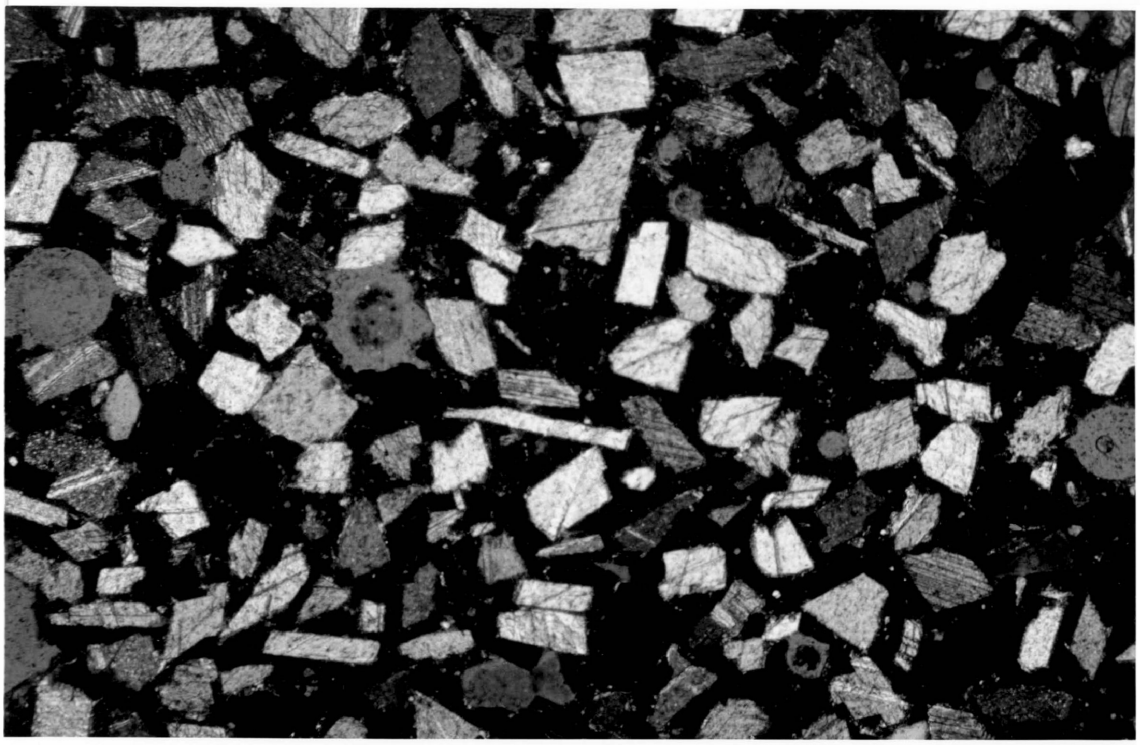

Plate 4-4. Photograph of the undeformed calcite-cement material.

Plate 4-5 Photograph of the weak to moderate preferred orientation of new twin lamellae relative to the shear zone boundary from SZ-C3 of Series 2 (Pc = 1.5 kbars). γ = 0.129.

Plate 4-6. SZ-C1 Series 1 (Pc = 1.0 kbar). Several calcite grains display bending and kinking of the new twin lamellae. γ = 0.111

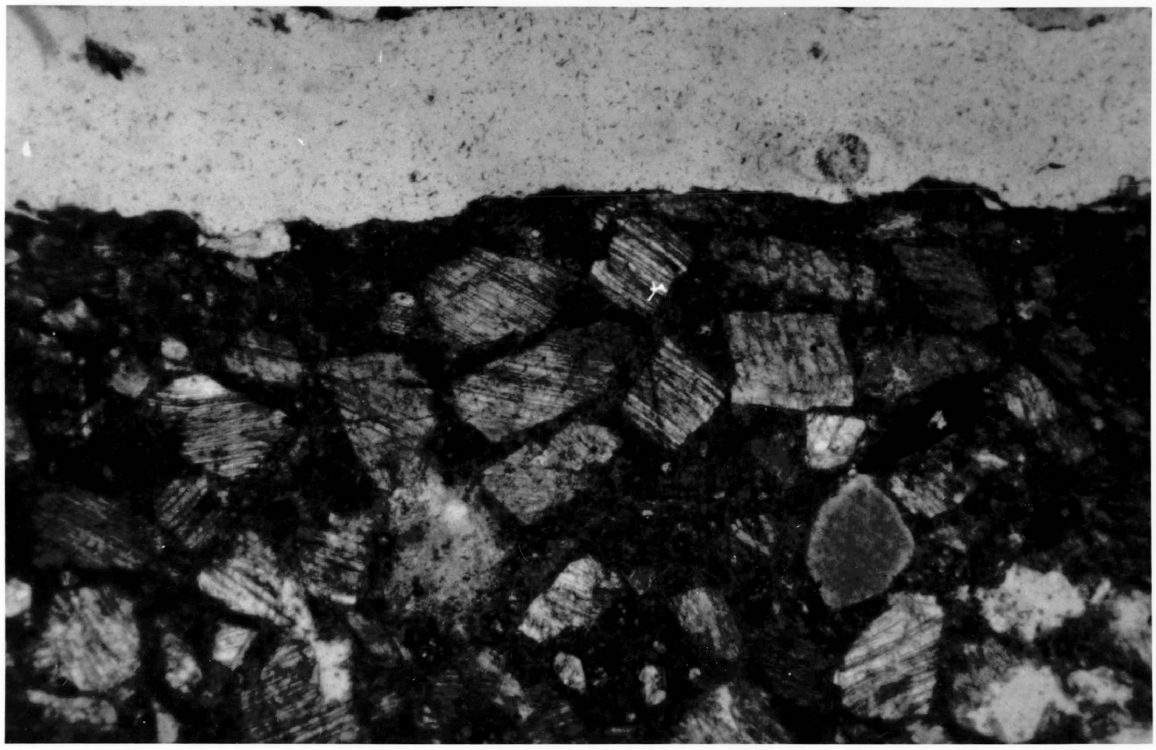

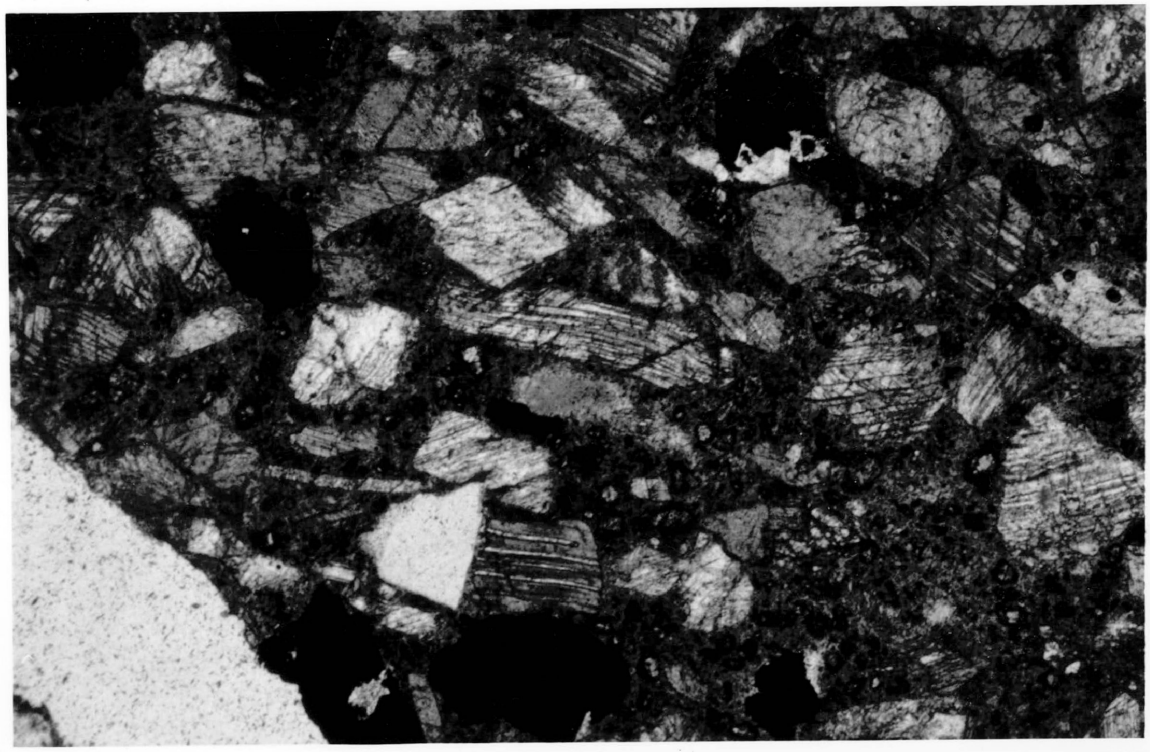

Plate 4-7. Composite photograph of SZ-C1 Series 1 (Pc = 1.0 kbar) illustrating the deformed fabric of the calcite-cement shear zones. $\gamma = 0.111$

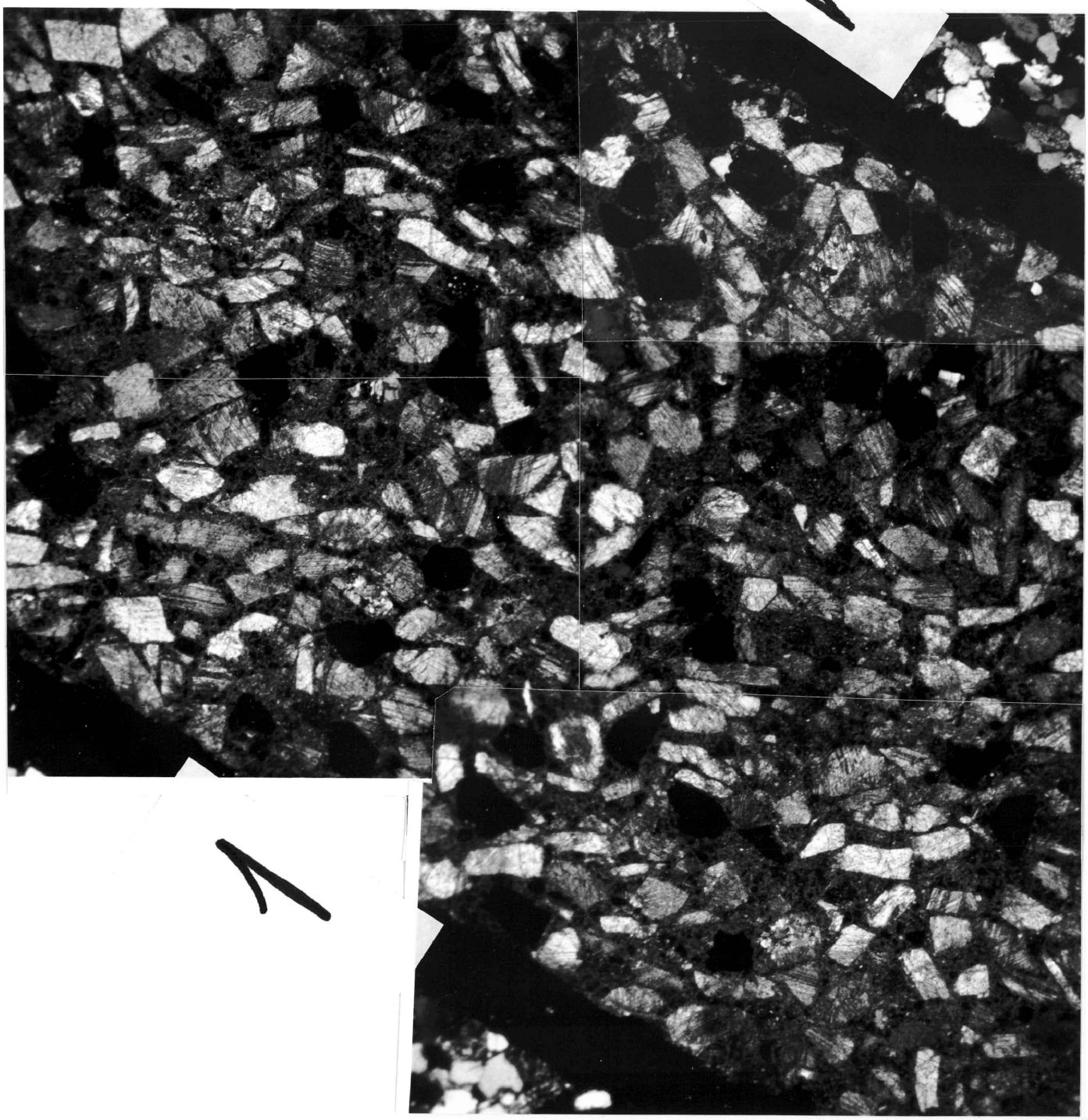

oriented throughout the shear zone. The calcite fragments no longer display their original rhomboid shapes and are now sub-rounded and display a moderate preferred dimensional orientation. The calcite fragments are now prevasively twinned with many fine twin planes that display a weak preferred dimensional orientation throughout the shear zone.

Stress Relaxation

The results of stress relaxation on two 0.75 inch diameter cylindrical specimens of the calcite-cement material conducted at the appropriate confining pressures are presented in Figures 4-67 & 4-68. At the time of the stress relaxation tests the calcite-cement material had been set for approximately 7 months.

The data from the two relaxation tests of the calcite-cement material at 1.0 kbar (Figure 4-67) produce a slope of 25 to 26 for strain-rates ranging between 2.0×10^{-7} and 5.0×10^{-5} s^{-1} (values range from $10^{-4.3}$ to $10^{-6.7}$ on the graph). Data from strain rates slower than 2.0×10^{-7} s^{-1} were dismissed due to the noise caused by voltage fluctuations, however, in the second run some of this data was acceptable, but was insufficient to define an accurate slope.

Figure 4-68 displays the results of relaxation at 1.5 kbar confining pressure. Both tests were successful, and a slope of 22 to 24 was determined for the data from strain-rates ranging

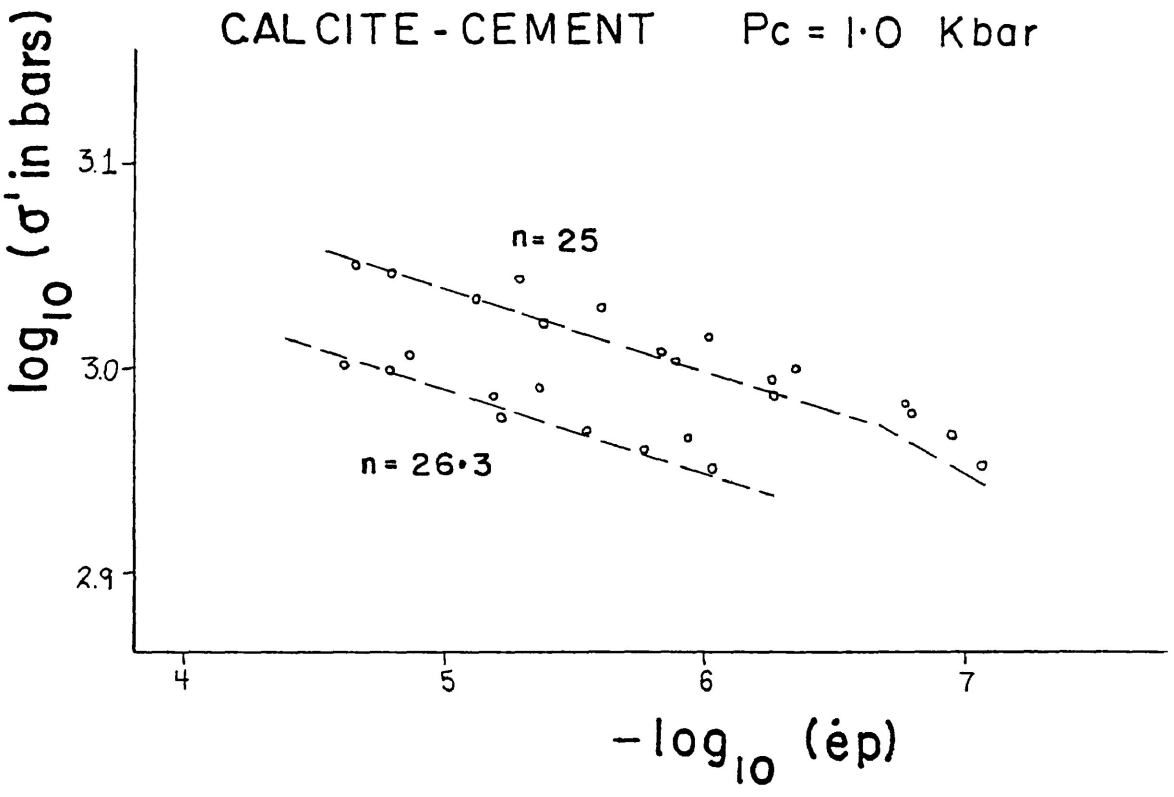

Figure 4-67. The results of two stress relaxation tests on a 0.75 inch diameter specimen of the calcite-cement material at 1.0 Kbar confining pressure.

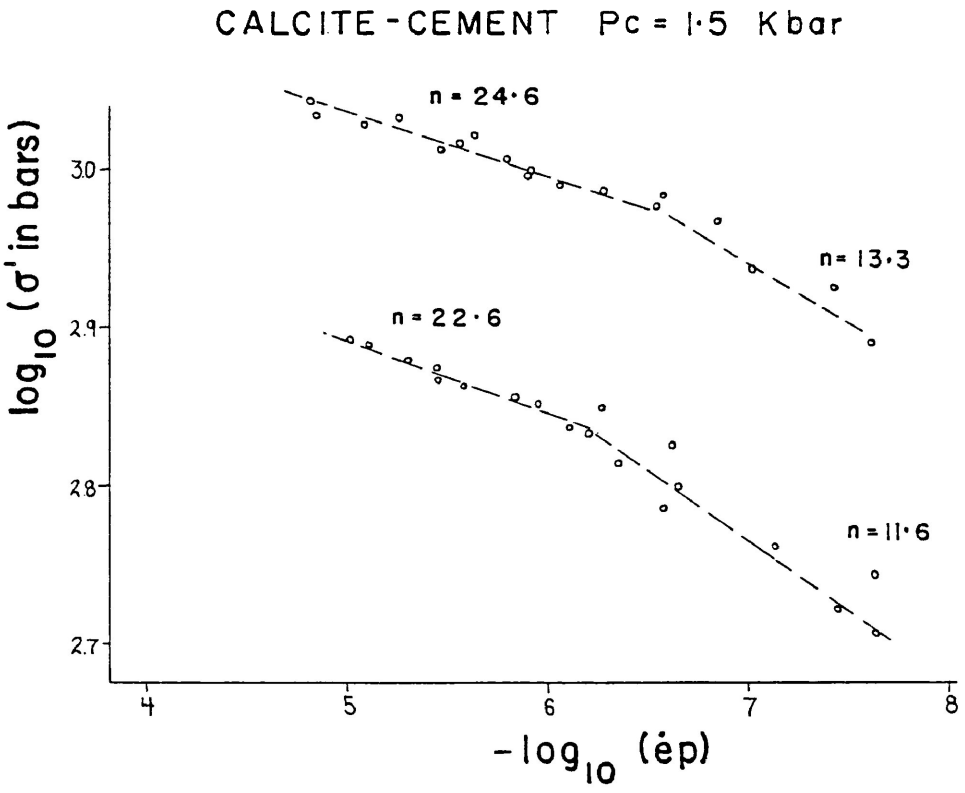

Figure 4-68. The results of two stress relaxation tests on a 0.75 inch diameter specimen of the calcite--cement material at 1.5 Kbars confining pressure.

between approximately 4.0×10^{-7} and 2.0×10^{-5} s^{-1} (between $10^{-4.7}$ and $10^{-6.4}$ on the graph). For strain-rates ranging between 2.0x10-8 and 4.0x10-7 s^{-1} ($10^{-6.4}$ to $10^{-7.7}$) a slope of 11 to 13 fits the data.

The increase in confining pressure between the two tests appears to have only a slight effect on the relaxation results. A definite change in slope, or value of n, occurs at a strain-rate of approximately 4.0×10^{-7} s^{-1} in the relaxation of the calcite material at 1.5 kbar confining pressure. A similar change in slope occurs at a slightly slower strain-rate in the results from relaxation of the material at 1.0 kbar. Thus the increase of confining pressure may cause this presumed change in deformation mechanism to occur at a slightly faster strain-rate. There also is a slight decrease in the load (or stress) supported at the beginning of the higher confining pressure relaxation.

Calcite-Cement Pure Shear Experiments

One series of pure shear tests were conducted on 0.75 inch diameter cylindrical specimens of the calcite-cement material at 1.5 kbars confining pressure.

Changes in the anisotropy, shape and orientation of the susceptibility ellipsoid :

Initially, nine specimens were deformed by the single-step deformation method. Thus, the magnetic susceptibility changes occurring with bulk pure shear of the calcite material could be compared with the results from the pure shear tests on the sand-cement material of Borradaile and Alford (1987).

Specimens were deformed by axial shortening of the cylindrical specimens. Ductile behaviour, in the macroscopic sense, was achieved within the range of the experimental deformation (4% to 18% shortening). However, even the best attempts at bulk homogeneous deformation of the calcite-cement material are merely approximations to that state. The typical sequence involving the change in the specimens' cylindrical shape with progressive shortening was; firstly, the specimen takes on a weak hourglass shape, after about 3.5% shortening this effect disappears and further strain causes the specimen to become progressively barrel-shaped. The initial compaction of the specimen under confining pressure, coupled with the frictional

resistance at the specimen-piston contacts inhibiting the compaction of the ends of the specimen is thought to account for the initial 'hourglass' shape (Borradaile and Alford 1987).

A general trend is observed in the changes of the principal susceptibility directions for the experiments. K_{min} is noted to rotate towards the Z-axis, and both K_{max} and K_{int} rotate towards the plane of flattening (i.e. Figure 4-69)

Similar rotations of the susceptibility axes were observed for the deformation of the sand-cement material of Borradaile and Alford (1987).

Using a diagram showing the change in angular position of K_{min} with respect to the Z-axis (θ_o changing to θ'), it is possible to compare the rotation of K_{min} with that of a hypothetical line element undergoing homogenous strain, as given by:

$$\frac{\tan \theta'}{\tan \theta_o} = \frac{Z}{X}$$

Figure 4-70 displays the changes in angular position of K_{min} with the strain expressed as the ratio Z/X.

In cases where the initial angle (θ_o) is 30^o or less, the line connecting the initial angle with the final angle (θ') after strain

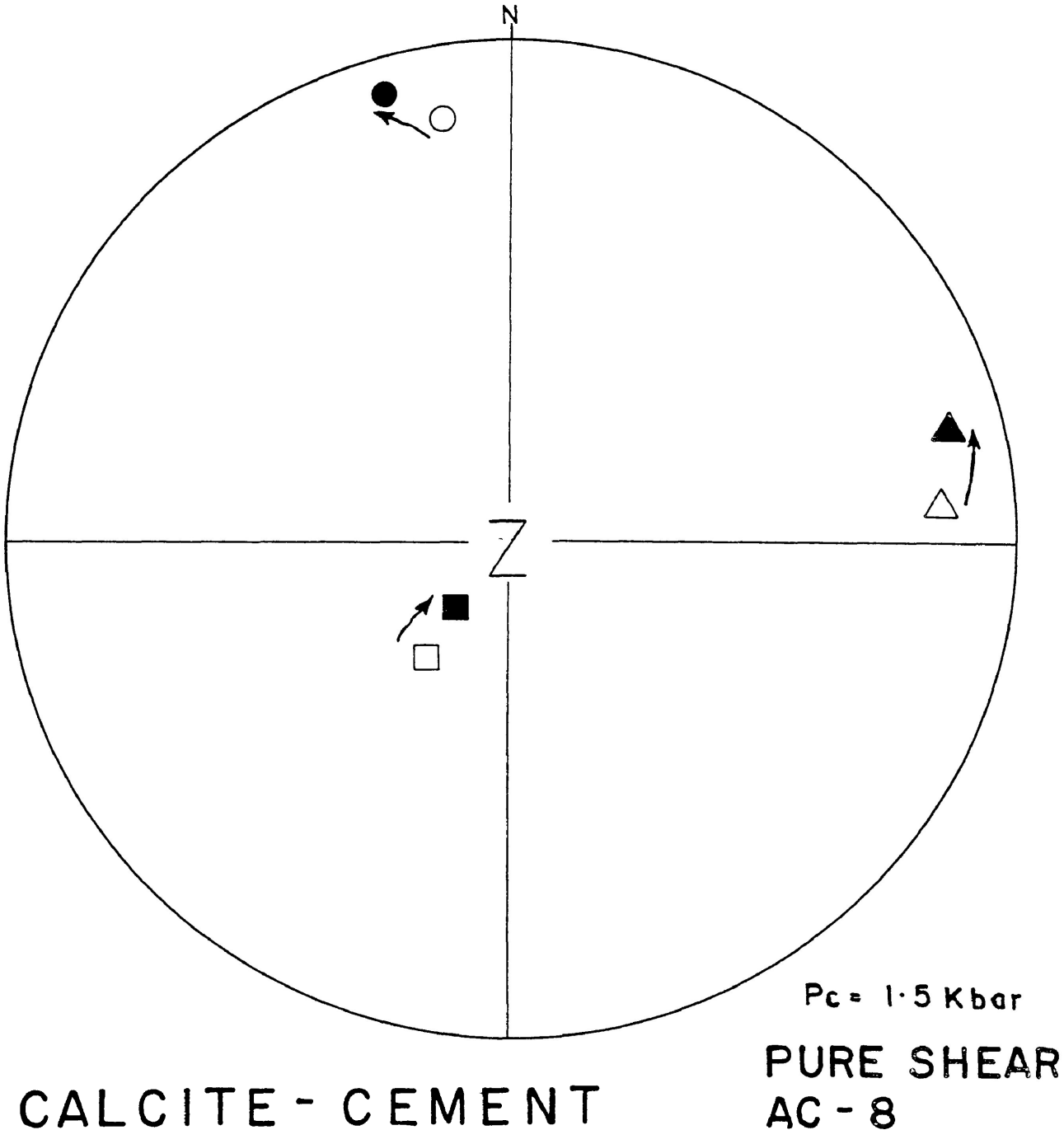

Figure 4-69. Lower hemisphere equal area stereonet illustrating the progressive changes of the principal susceptibility directions of the calcite-cement pure shear test AC-8.

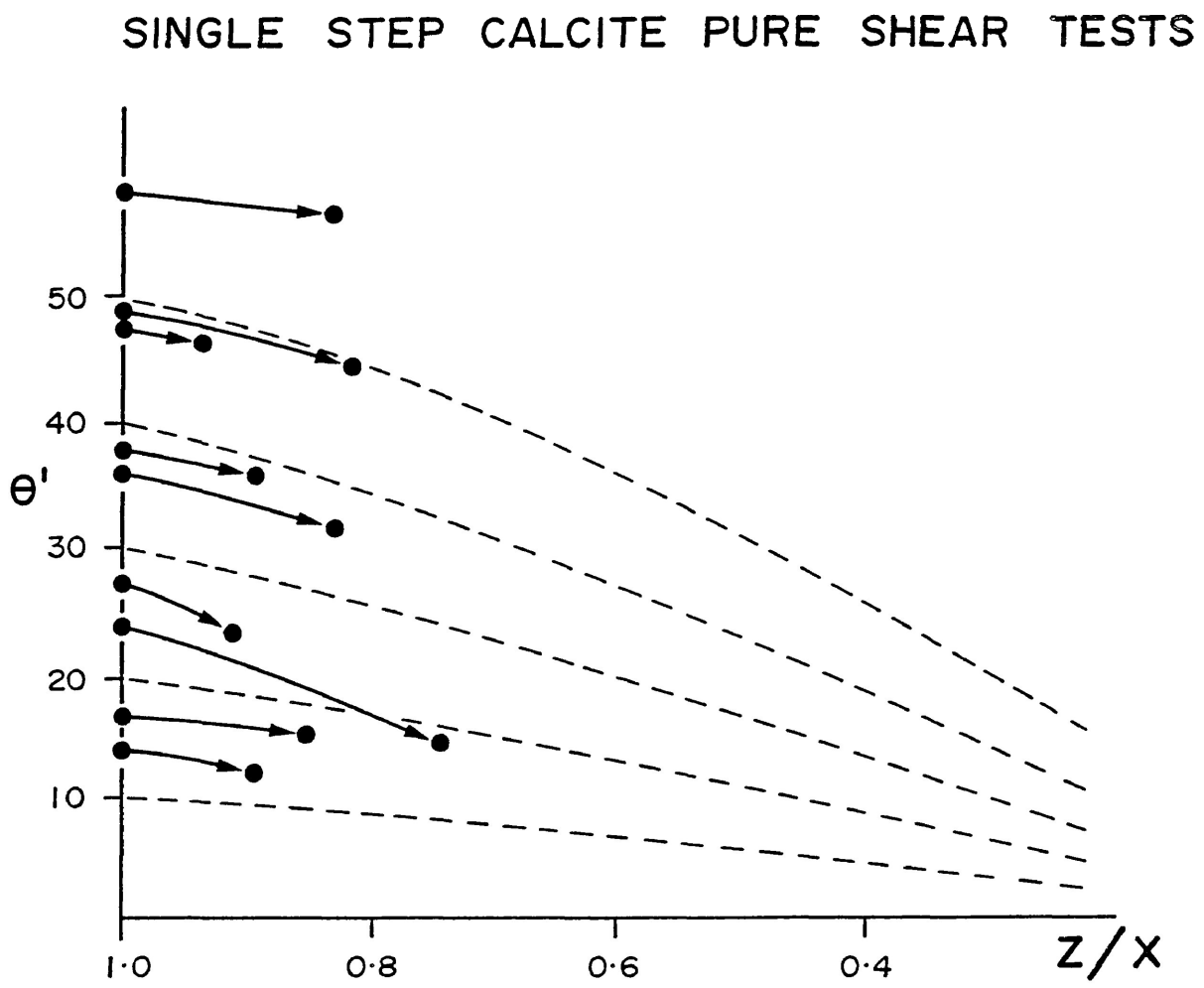

Figure 4-70. The dashed lines show the change in angle expected for a line rotating in homogenous strain with ratio Z/X. The solid lines connect the values of the angle between Kmin and the Z-axis before (left) and after (right) shortening.

(the actual path is not known) is usually steeper than the path which predicts the rotation of a line element. For susceptibility ellipsoids with an initial angle between K_{min} and the Z-axis greater than 30^{o}, the slope of the line connecting the initial angle and final angle after strain is usually gentler than that predicted for the rotation of the hypothetical line elements.

Thus it would appear that the original orientation of the principal susceptibility directions in the calcite-cement material has an influence on the rate of rotation of the susceptibiltiy axes. The susceptibility ellipsoids with their K_{min} axis within 30^{o} of the maximum shortening direction (the Z-axis), experience a rotation of the K_{min} axes which is faster than would be inferred from the effects of homogenous strain on a linear line element. Those susceptibility ellipsoids possessing a K_{min} axis subtending an angle greater than 30^{o} from Z, will experience a slower rotation.

For most of the undeformed specimens, the susceptibility ellipsoids lie in the field of flat (or pancake) shaped ellipsoids (Figure 4-71). In nearly all cases the effect of deformation, which is of a flattening character (X=Y>Z), due to the symmetry of the triaxial rig, is to move the susceptibility ellipsoid;

(i) away from the origin, and

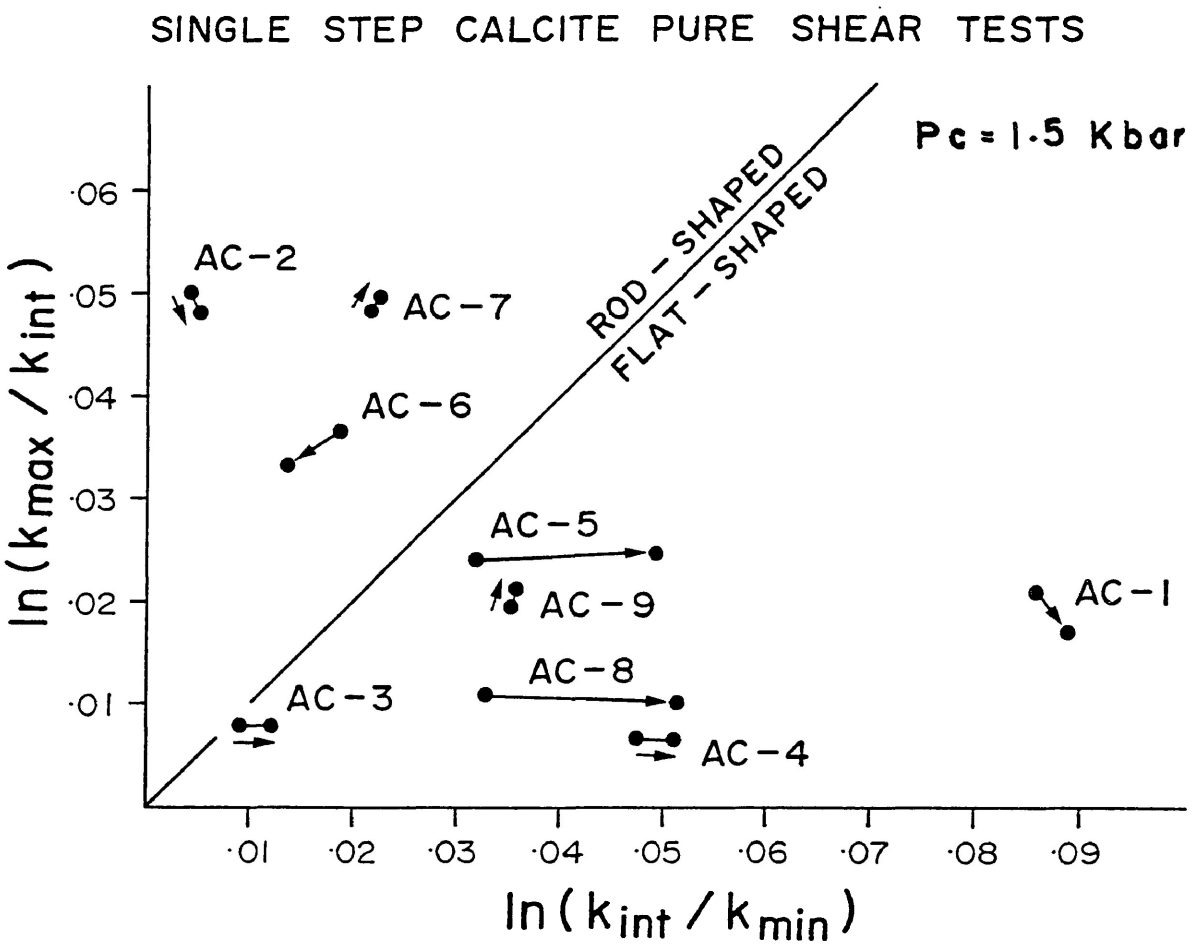

Figure 4-71. Illustrating the changes in shape of the susceptibility's magnitude ellipsoids (from the changes in the ratios of the principal susceptibilities) for the single-step calcite-cement pure shear tests.

(ii) further toward or into the field of flat-shaped ellipsoids

However, the susceptibility ellipsoid does not always adhere to the previous observations during the shortening history. After some amount of pure shear deformation, the susceptibility ellipsoid can be found to have become either less anisotropic (a decrease in the value of P', AC-6) or less eccentric (a decrease in the value of T, AC-7 and AC-9), or both (AC-2) (see Figure 4-72). This effect is most likely caused by an initial orientation such that the ellipsoid is elongate parallel or nearly parallel with the direction of maximum shortening. For the most part, however, the symmetry of the susceptibility ellipsoid tends to conform to that of the bulk strain ellipsoid for pure shear.

When the change in the degree of anisotropy ($\Delta P'$) is plotted against axial strain (ln X/Z) for the deformed specimens a scattering of the data is observed (Figure 4-73). This effect is thought to occur due to the variance in initial shape and orientation of the susceptibility ellipsoids.

To test for any possible power-law correlation between the change in the degree of anisotropy and axial strain for the calcite-cement pure shear experiments it was decided that multiple testing would be conducted. Two individual specimens were deformed by the multiple-step method, totalling 14 experiments.

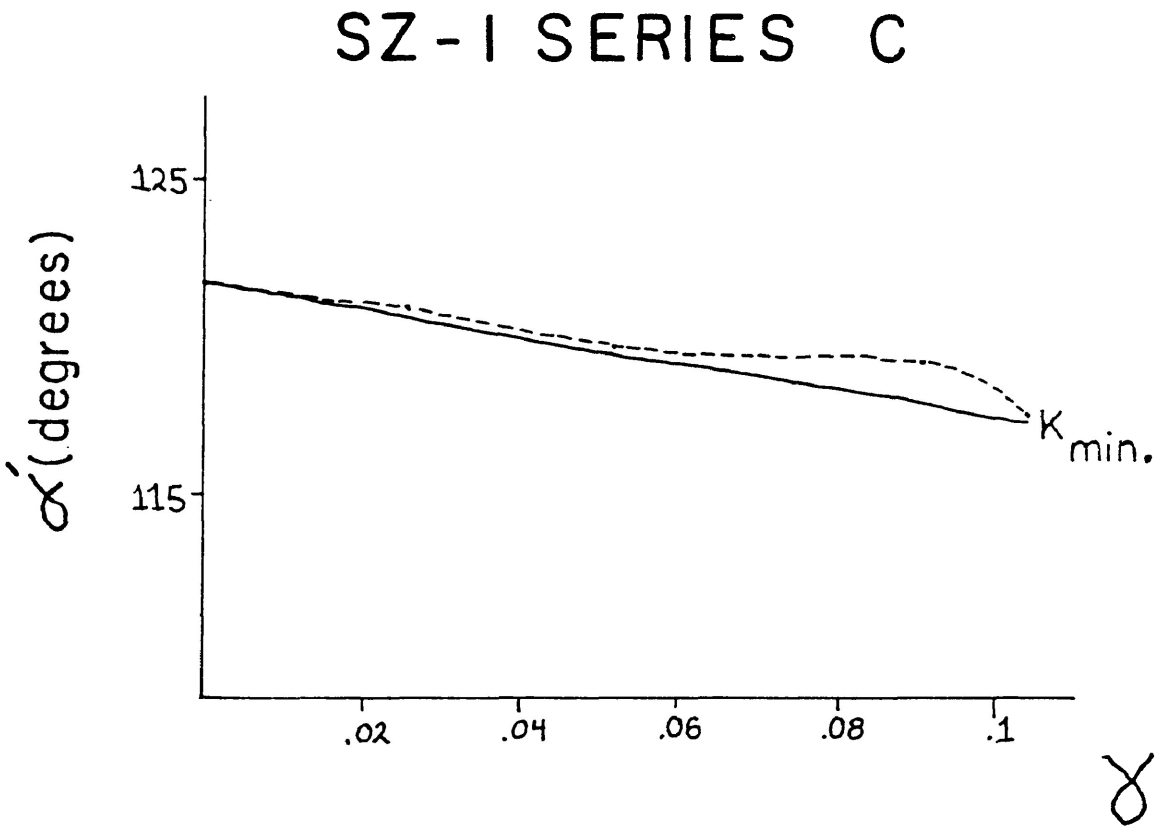

Figure 4-35. Illustrating the measured change in angular position of the K_{min} susceptibility axes (dashed line) of SZ-1 Series C against that of a real material line (solid line) of a similar initial orientation experiencing an equivalent shear strain.

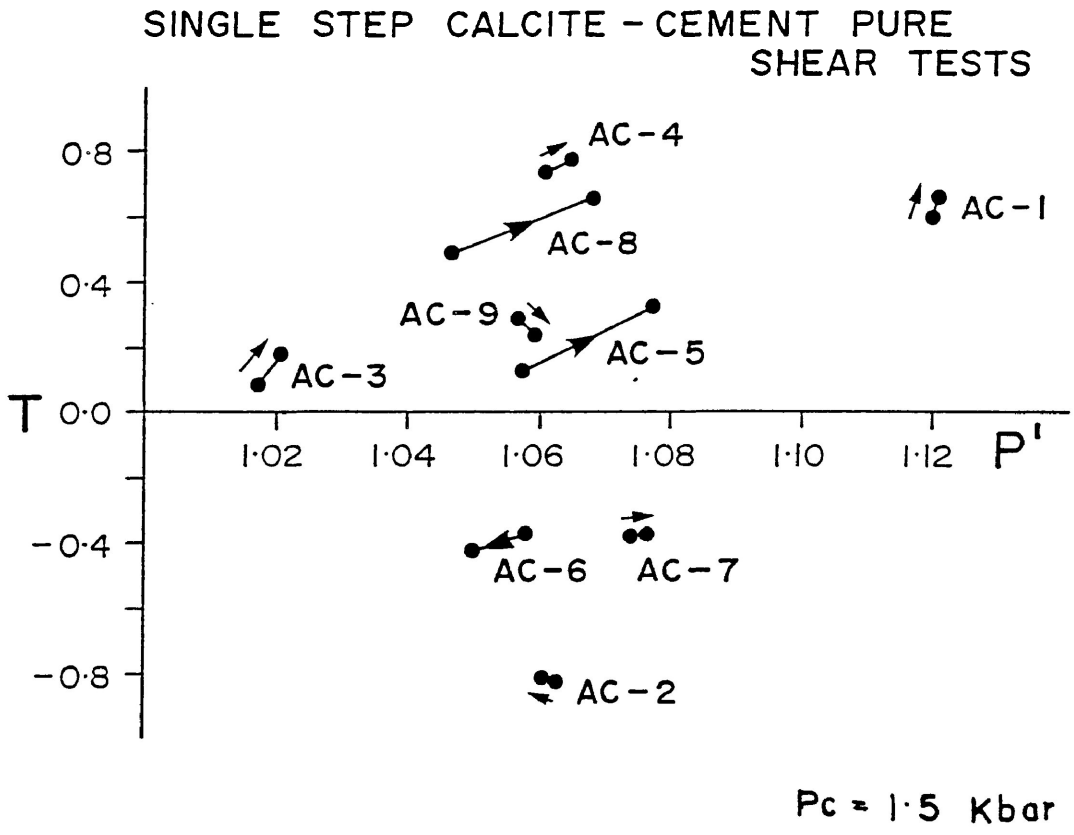

Figure 4-72. Illustating the changes in shape and degree of anisotropy (from Jelinek's T and P' parameters) for the susceptibility ellipsoids of the single-step calcite-cement pure shear tests.

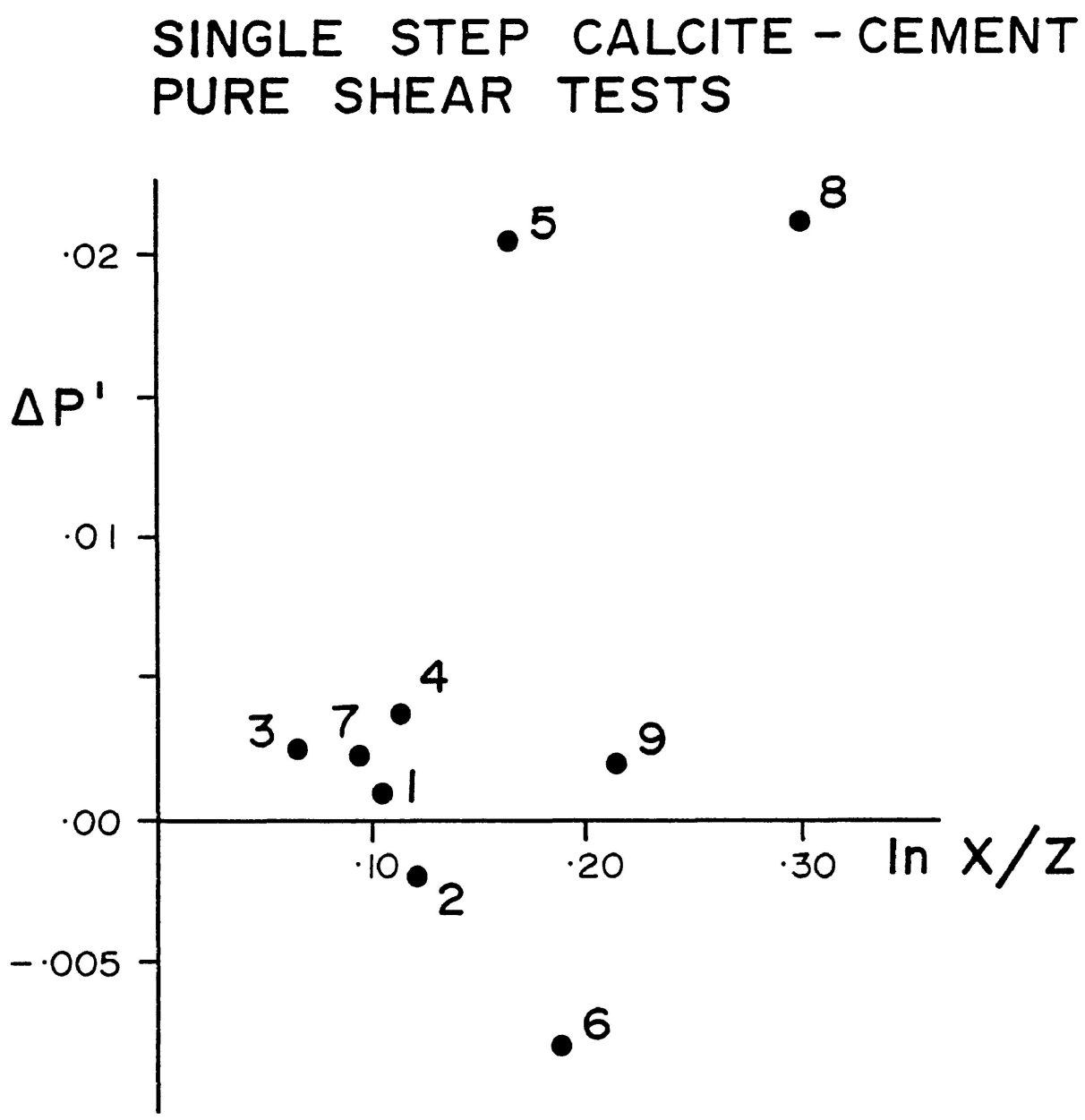

Figure 4-73. Illustrating the change in the degree of anisotropy before and after shear strain ($\Delta P'$), against the natural logarithm of the bulk strain ratio (X/Z) for all the calcite-cement single step experiments. Note that no significant correlation is observed from the data from the individual pure shear tests.

The progressive orientations of the principal susceptibility directions for the multiple-step pure shear tests are displayed in Figures 4-74 & 4-75. Both specimens dispay an initial rotation opposite to the latter and progressive movement of K_{max} and K_{int} towards the plane of flattening and K_{min} towards the Z-axis.

Figure 4-76 displays the strain (Z/X) versus changes in the angular position of K_{min} with respect to the Z-axis for AC-10 and AC-11. The lines connecting the data from the multiple-step tests illustrate the paths through which the K_{min} axes in the single-step tests may have taken during deformation.

In specimen AC-10, K_{min} begins at an angle of 28^{o} from Z and, during the first increments of deformation, swings further away from the shortening axis (as was noted on the stereonet). Further axial shortening, rotates K_{min} toward Z through a much steeper line than that predicted for a hypothetical line element. The net result for AC-10 is a rotation of K_{min} that is faster than would be inferred from the effects of strain on a line element.

K_{min} in specimen AC-11 begins at an angle of 30^{o} from the Z-axis. During specimen shortening, K_{min} initally rotates further away from Z and then towards the shortening axis at a rate approximately equal to that predicted for a similarly oriented line

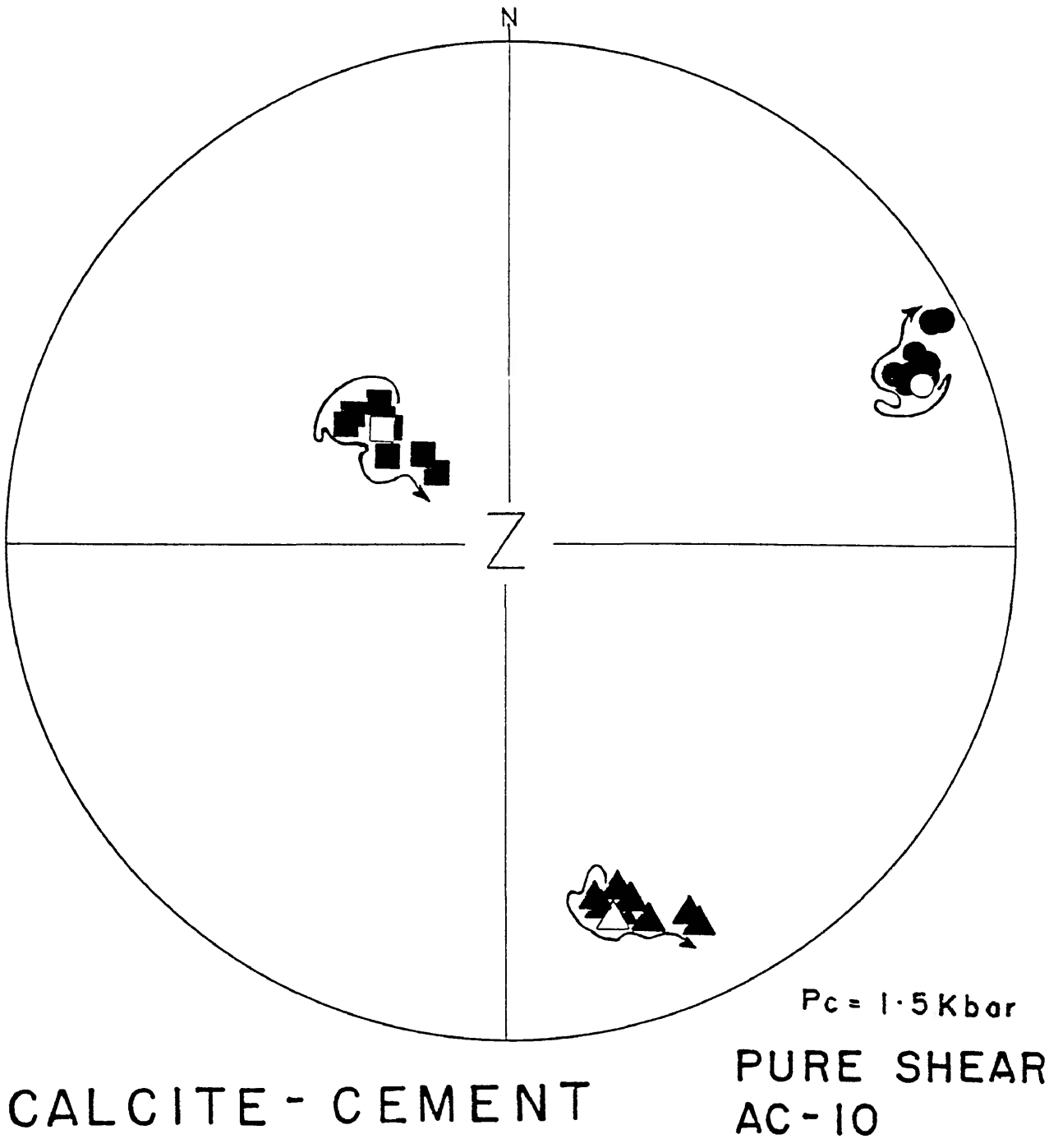

Figure 4-74. The progressive changes in orientation of the principal susceptibility directions for the multiply deformed pure shear specimen AC-10.

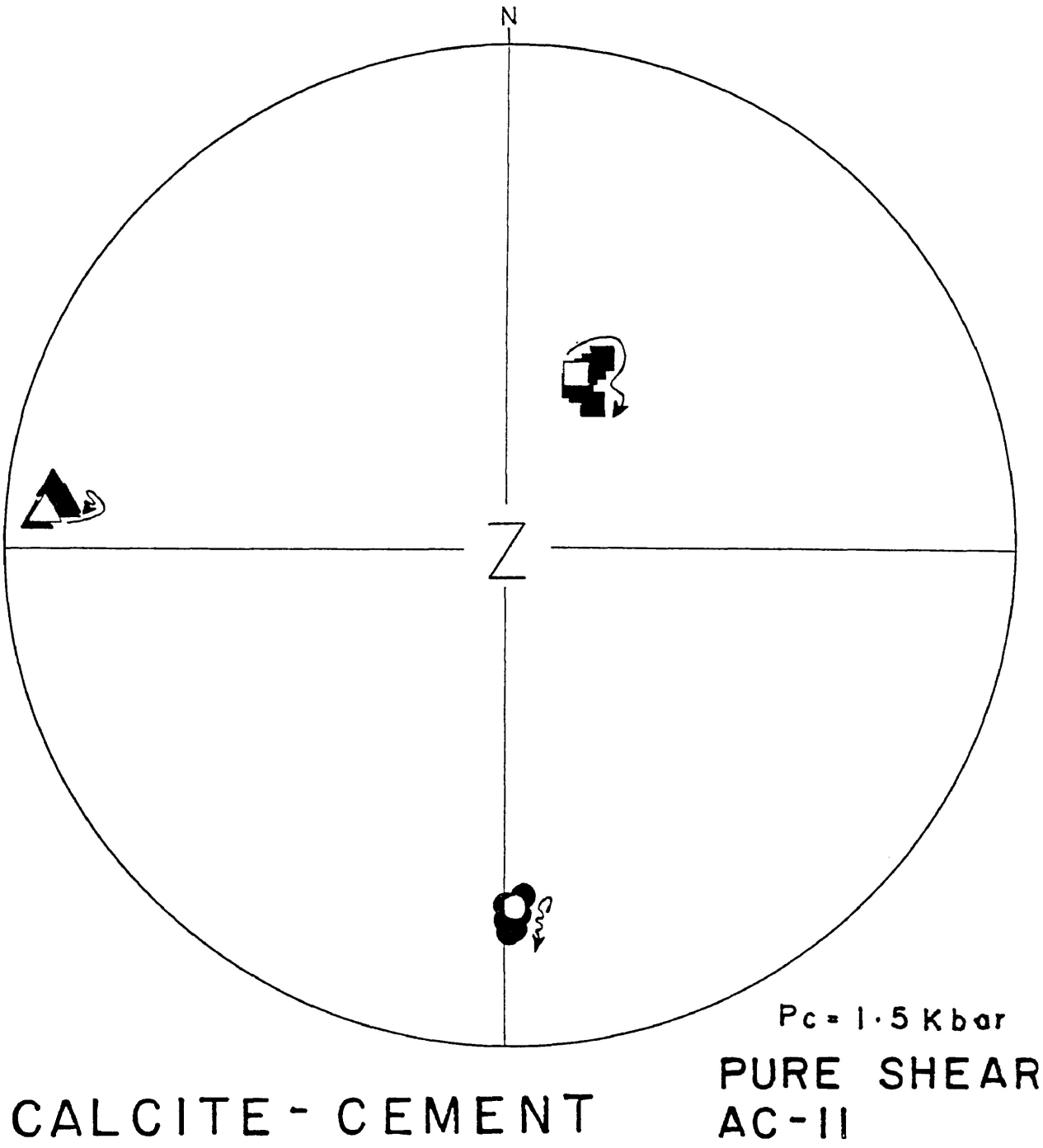

Figure 4-75. The progressive changes in orientation of the principal susceptibility directions for the multiply deformed pure shear specimen AC-11.

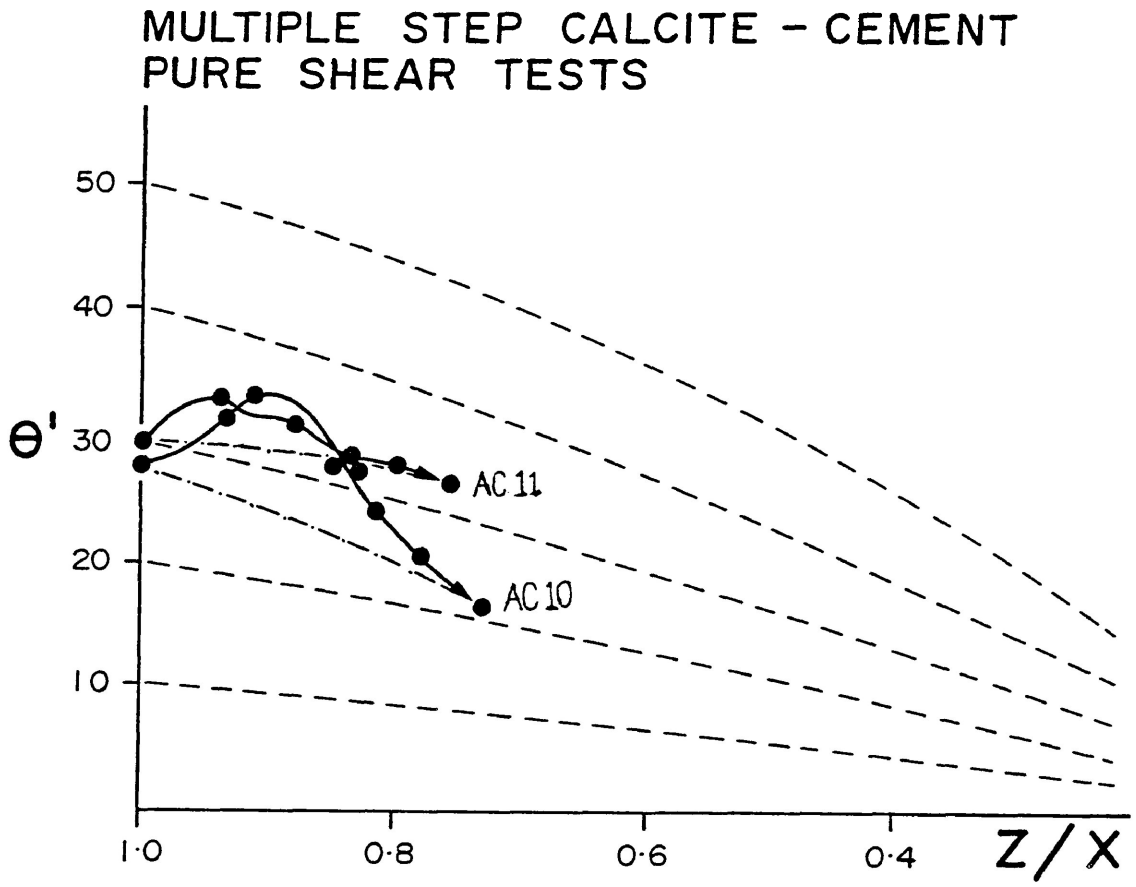

Figure 4-76. Comparison of the progressive changes in the angle between the K_{min} susceptibility direction for the two multiply deformed pure shear experiments and that expected for a line rotating in homogenous strain (dashed lines). The solid lines display the actual paths of the K_{min} principal susceptibility direction, while the dashed and dotted lines indicate the net rate of change in the angle from the original to the final susceptibility orientation.

element. The net result of deformation in AC-11 is a rotation of K_{min} that is slower than that which would occur if the susceptibility axis rotated as a line element.

The progressive shapes of the susceptibility ellipsoids for the two multiple-step experiments are illustrated in Figure 4-77. Both display a tendency to take on a slightly less flattened shape than the original during the initial increment of deformation and with further strain the ellipsoids become progressively flatter. In the P' vs T diagram (Figure 4-78) an initial decrease in both anisotropy (P') and shape (T) is observed. Further increments of deformation increase both P' and T in a manner similar to that noted in many of the simple shear experiments.

Changes in the degree of anisotropy with strain, for the two specimens, are illustrated in Figures 4-79 & 4-80. The data from specimen AC-10 displays an initial negative change in anisotropy ($\Delta P'$) that curves upward and becomes linear as progressive positive changes in $\Delta P'$ occur. Specimen AC-11 displays a fairly large initial negative change in the degree of anisotropy with further positive changes occurring in a linear fashion.

Microscopic Observations

The undeformed calcite-cement material has been previously described for the microscopic observations in the calcite-cement shear zones. The main features of the undeformed material

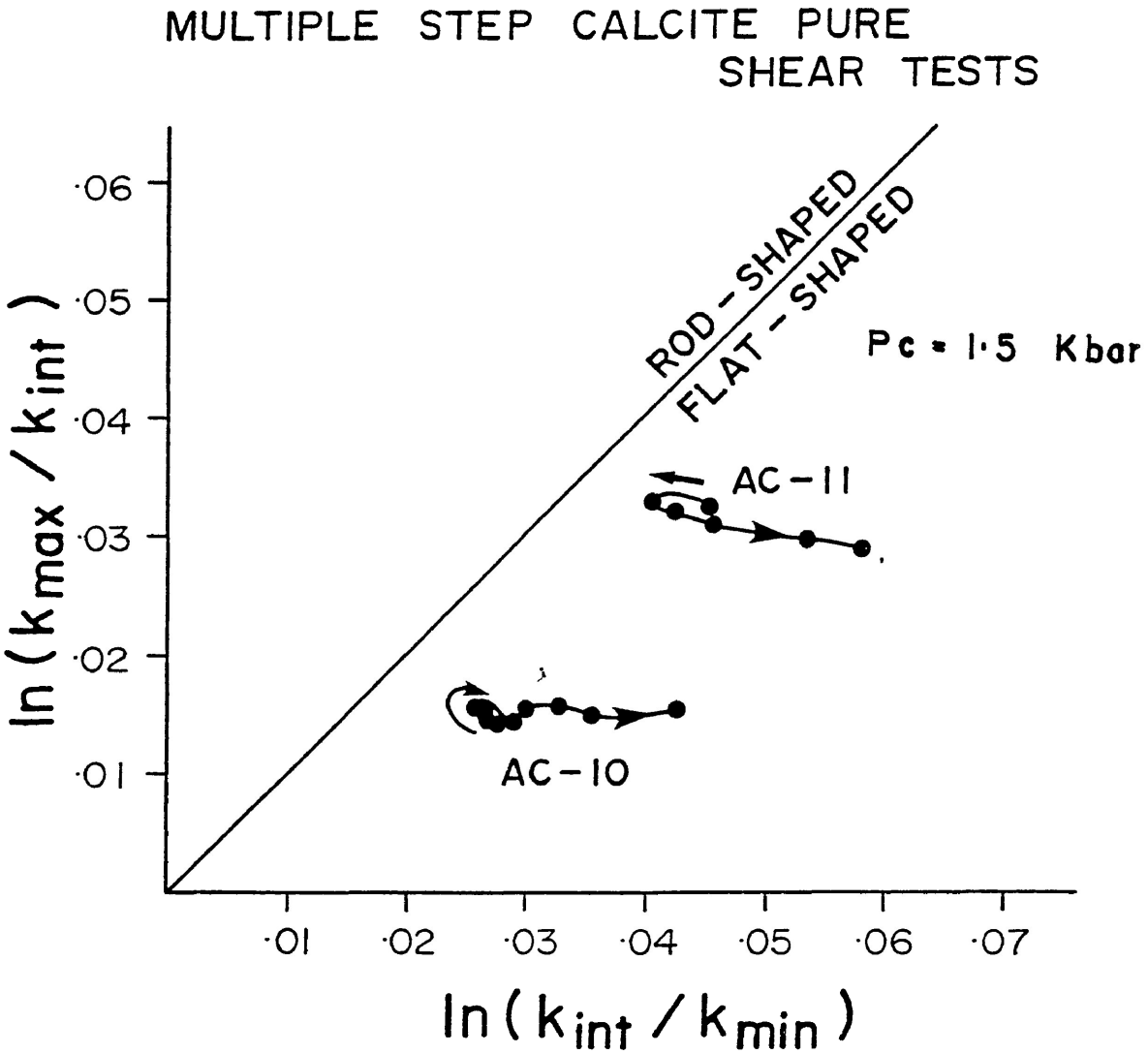

Figure 4-77. The progressive changes in shape of the susceptibility ellipsoids in pure shear as expressed by the ratios of the principal susceptibility directions.

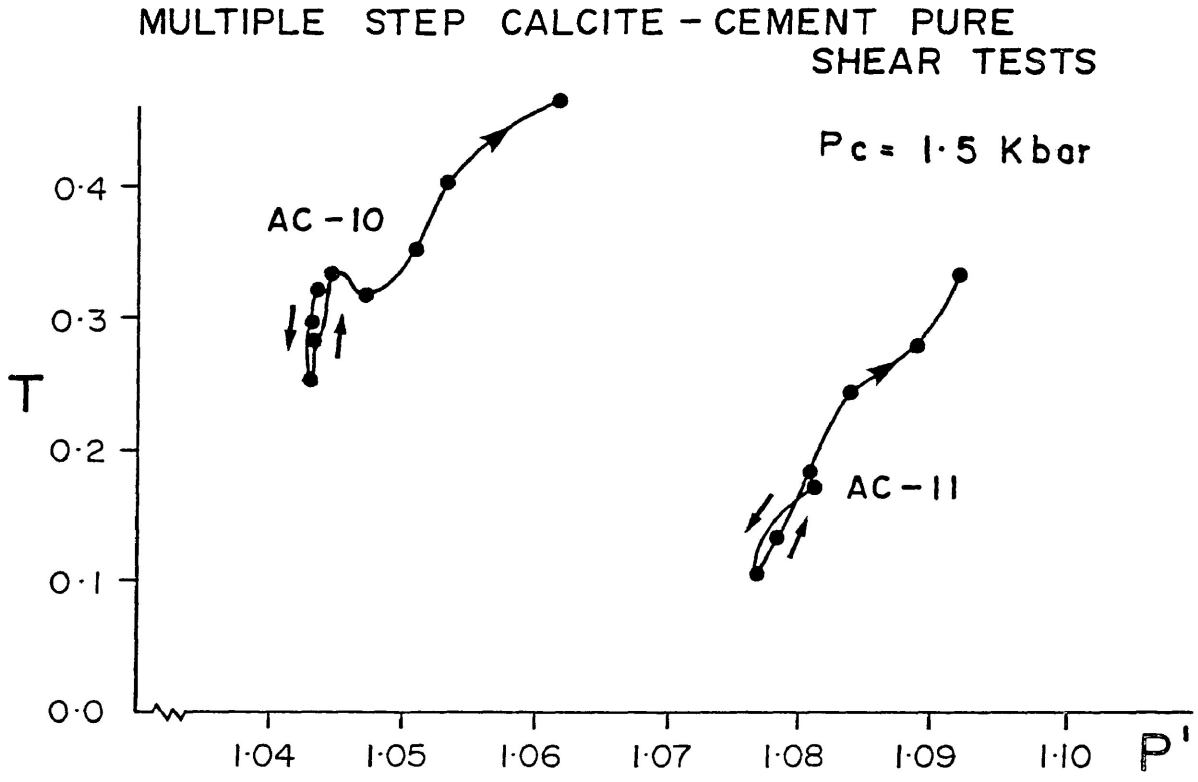

Figure 4-78. Illustrating the progressive changes in shape (T) and degree of anisotropy (P') for the two multiply deformed pure shear specimens.

Figure 4-79. The correlation between the change in the degree of anisotropy before and after each increment of strain ($\Delta P'$) and the bulk strain ratio (ln (X/Z)) for the calcite-cement pure shear specimen AC-10. The correlation coefficient for the linear section is 0.987.

Figure 4-80. The correlation between the change in the degree of anisotropy and the bulk strain ratio for specimen AC-11. The correlation coefficient is 0.994.

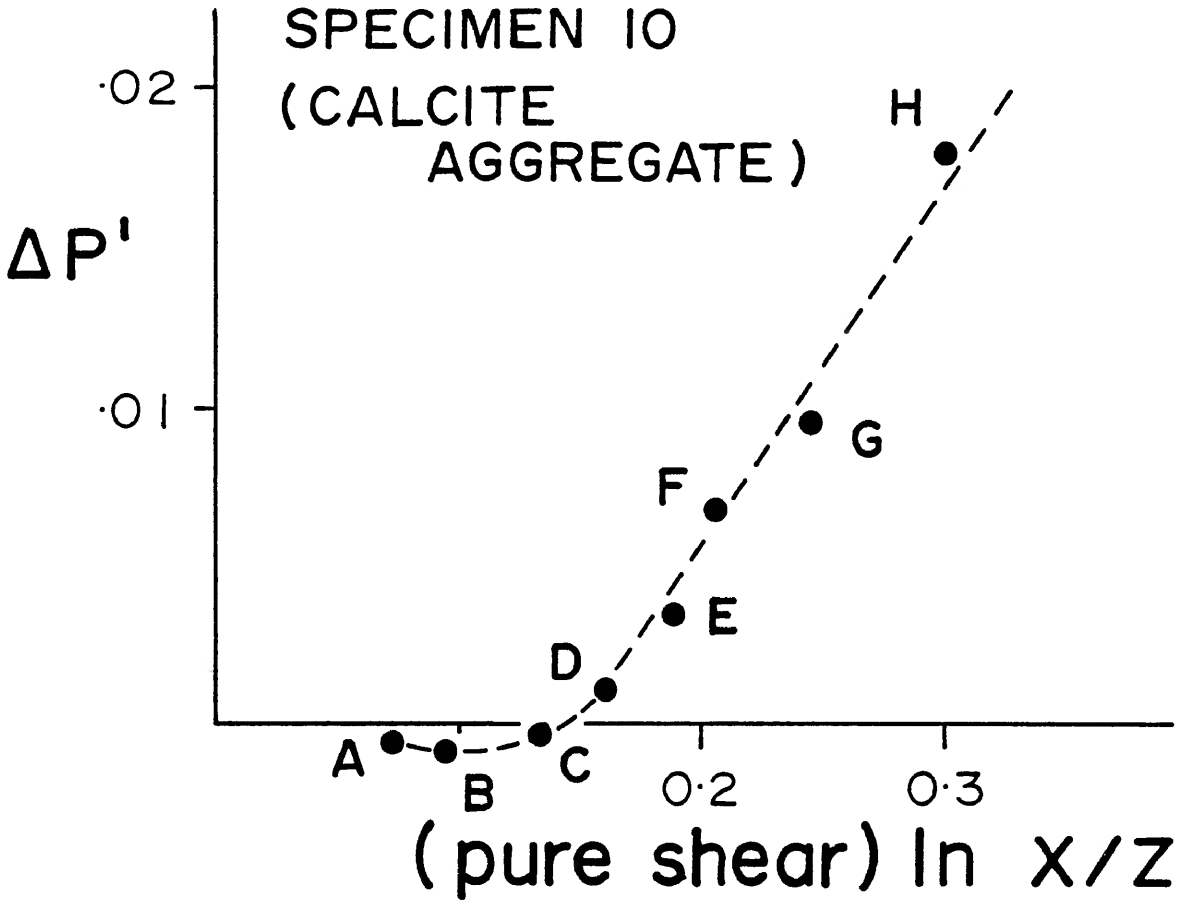
SPECIMEN 10
(CALCITE AGGREGATE)
·02
·01
ΔP'
H
G
F
E
D
A
B
C
0·2
0·3
(pure shear) ln X/Z

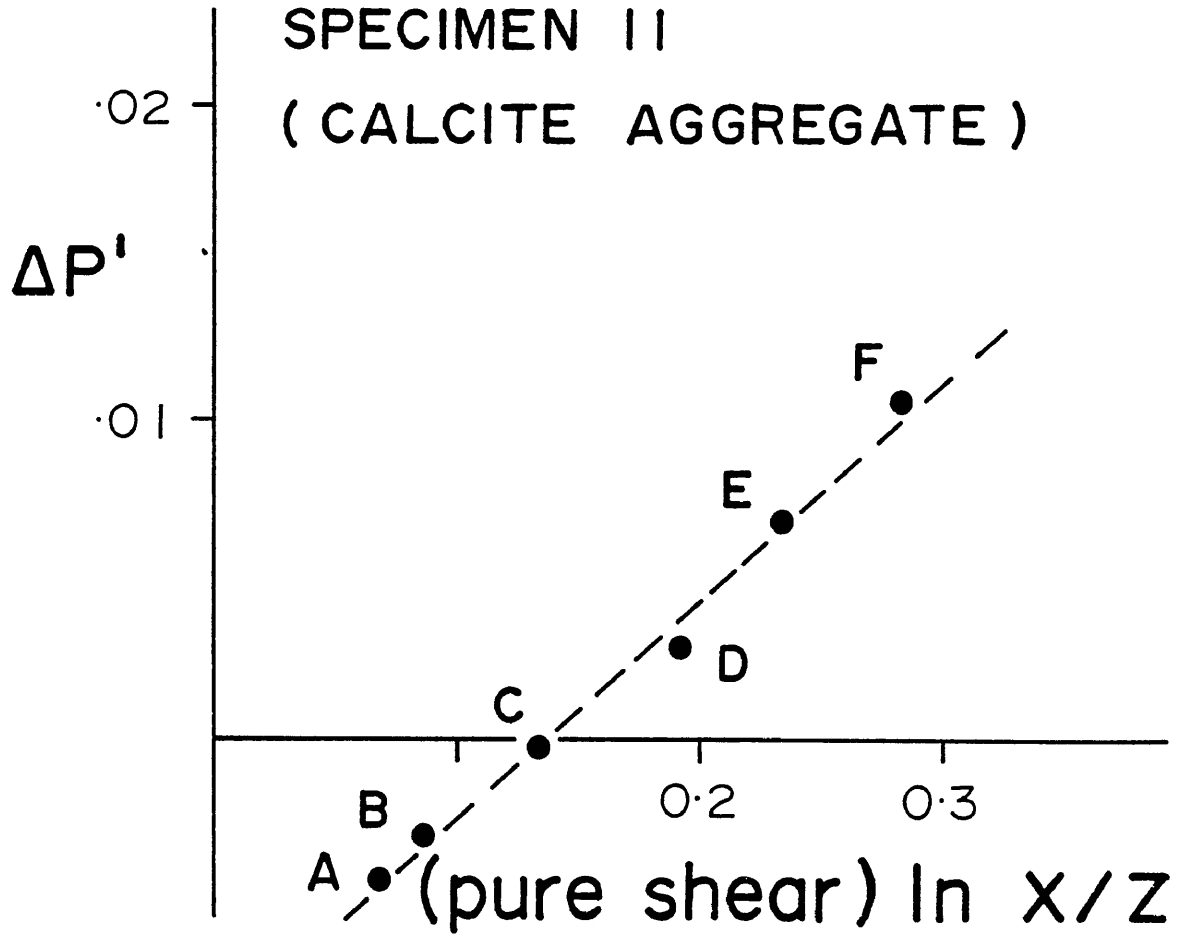
SPECIMEN 11
(CALCITE AGGREGATE)
·02
·01
ΔP'
F
E
D
C
B
A
0·2
0·3
(pure shear) ln X/Z

consisted of:

(i) few grain to grain contacts

(ii) the angular to rhomboid calcite and rounded to sub-angular magnetite grains displayed no preferred orientation within the aggregate

(iii) few twin lamellae per calcite grain were visible, within the material the twin lamellae displayed no preferred orientation

Three specimens from the deformed calcite-cement pure shear experiments were sectioned. These sections represent differing intensities of deformation; AC-3 (4.42% shortening), AC-9 (13.26% shortening), and AC-8 (18.03% shortening).

Microscopic investigation of AC-3 (4.42% shortening) revealed the development of new fabric features (Plate 4-8). The number of grain to grain contacts did not increase significantly, however, it is difficult to find a grain that was not in contact with another grain. No preferred dimensional orientation of the calcite or magnetite grains exists within the deformed aggregate. New twin planes are observed within the calcite fragments. These twin planes appear to be thinner and more numerous and often cut across or displace the existing twin lamellae (Plate 4-9). Within the aggregate, the new lamellae show no preferred dimensional orientation , however, when the twinned calcite grain was in

Plate 4-8. Composite photograph of AC-3 (4.42% shortening). The maximum compression axis is parallel to the length of the photograph, grain contacts have increased in number and calcite grains display new twin planes.

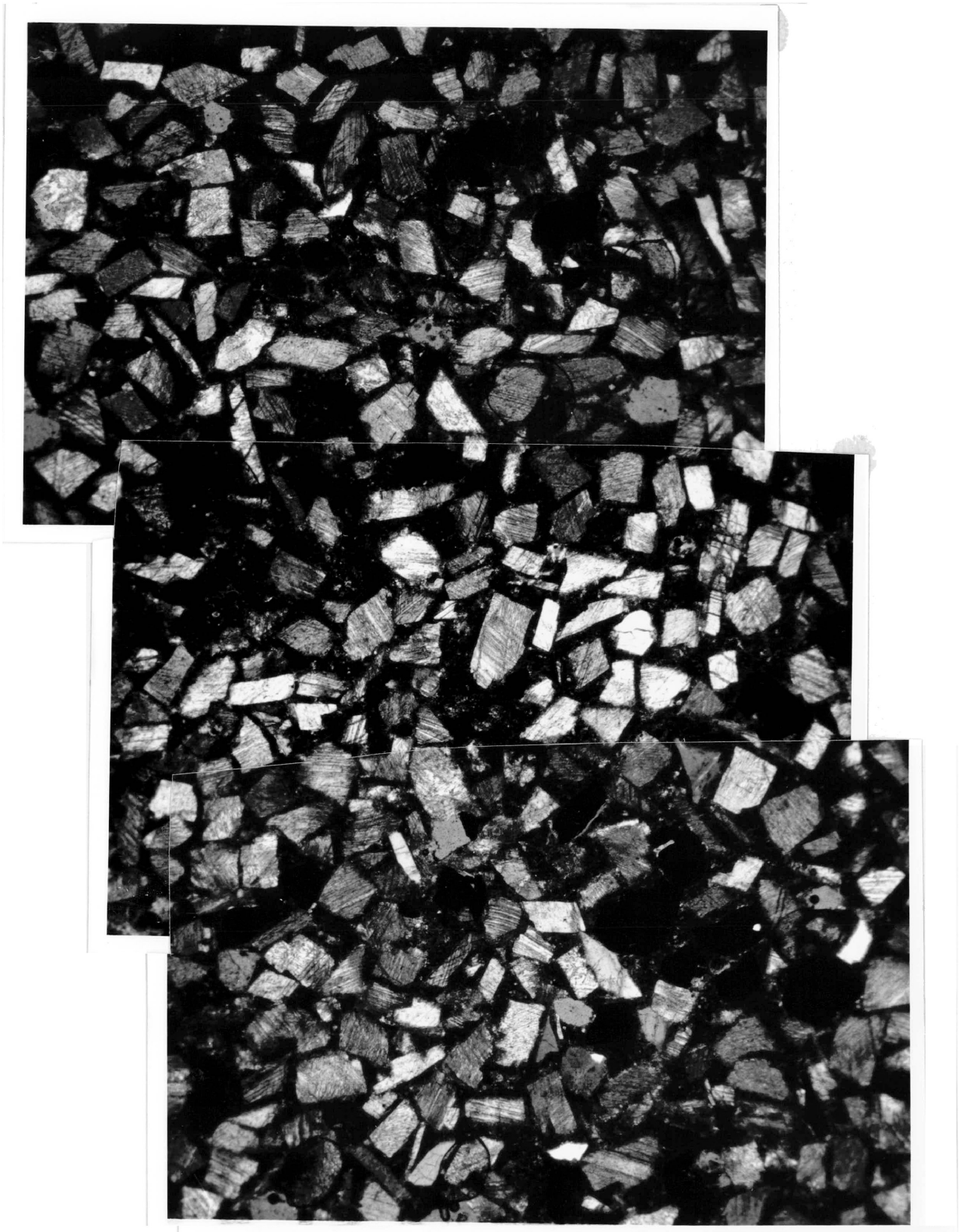

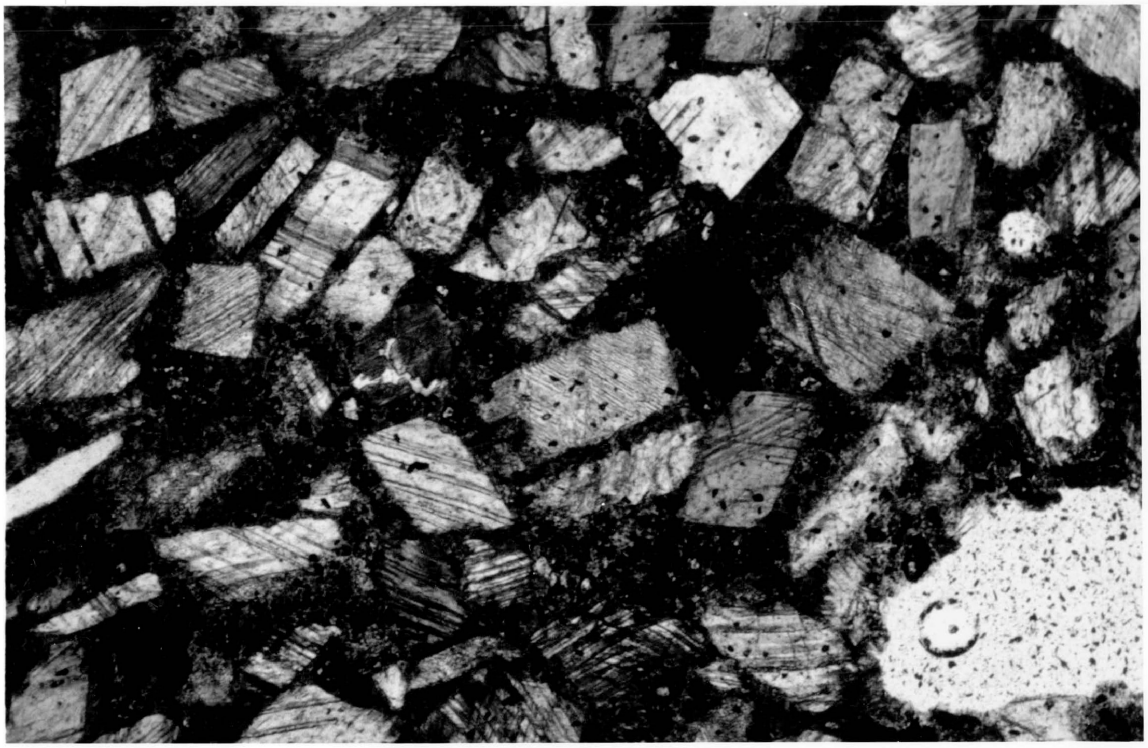

Plate 4-9. New, more closely spaced twin lamellae (centre calcite grain; twin planes oriented diagonal down from the left) cutting across older (oriented vertically) more widely spaced twin planes. From AC-3 (4.42% shortening).

contact with only one other grain, a consistent angle ($35^{o} \pm 5^{o}$) between the grain boundary and the twin lamellae was noted.

Within AC-9 (13.3% shortening), the number of grain to grain contacts have increased slightly (2 to 3 per grain). The calcite grains are less angular and display a weak preferred dimensional orientation perpendicular to the maximum shortening direction. A greater number of new twin lamellae are observed per grain of calcite, almost entirely obliterating the initial twin lamellae.

The fabric of AC-8 (Plate 4-10) depicts the most intense deformation (18.3% shortening). The calcite grains no longer possess the original rhomboidal shape. There is a moderate preferred dimensional orientation of the calcite grains within the aggregate and a weak preferred dimensional orientation of the twin lamellae, within the calcite, perpendicular to the maximum shortening direction. Within most of the calcite grains there is little to no evidence of the original twin lamellae and a greater density of the new twin lamellae are now observed (Plate 4-11). These twin lamellae show evidence of kinking and bending when the host calcite grain is in contact with a magnetite grain.

Plate 4-10. Composite photograph of AC-8 (18.03% shortening). The maximum compression axis is oriented parallel to the length of the photograph. Grain contacts have further increased in number and the calcite grains, as well as their twin lamellae, show a moderate preferred orientation.

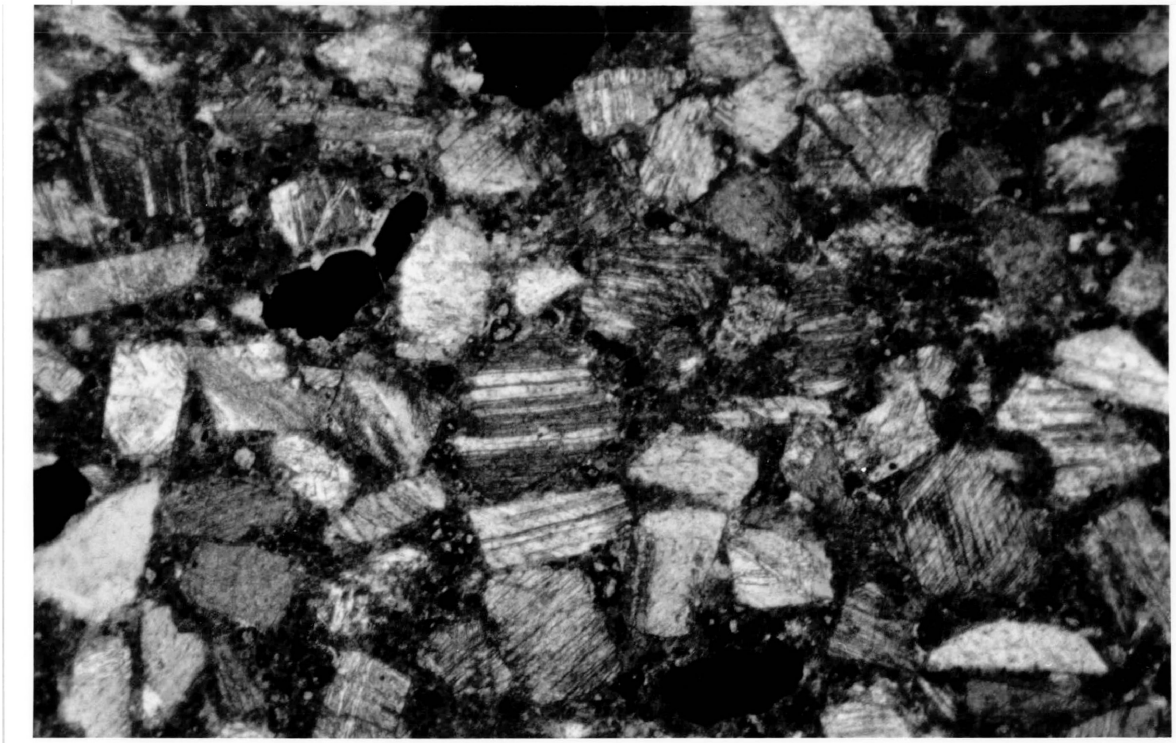

Plate 4-11. Photograph illustrating the very thin and numerous twin lamellae within the calcite grains of AC-8 (18.03% shortening).

CHAPTER FIVE

Discussion

How closely does the experimental deformation relate to natural deformation:

Simple Shear- During the experimental shear zone deformation it has been noted that, unlike true simple shear, some change in the width of the zone occurs along with the displacement parallel to the shear zone boundary. The shear zone makes a fairly large angle (55^{o}) with the maximum shortening direction for the shear zone assembly, thus during deformation some compaction of the shear zone is to be expected.

Within a shear zone of similar orientation to that used experimentally, displacement parallel to the shear zone could arise simply by a change in width, due to the orientation of the shear zone to the maximum compression axis.

In order to show that the displacement occurring parallel to the shear zones within the experimental procedure is not solely due to the change in width, a plot of the width versus the shear displacement was constructed for one arbitrarily chosen experiment for both types of shear zone material, SZ-3 of series B of the sand-cement material and SZ-C3 of series 1 from the calcite-cement material. The results (Figures 5-1 & 5-2) indicate that the displacement occurring parallel to the shear zone exceeds that which could occur by a change in width alone.

Figure 5-1. Comparison of the measured changes in width and shear displacement for SZ-3 of the sand-cement shear zone Series B (dashed line) against the shear displacement that would occur simply by a similar change in width of the shear zone (solid line).

Figure 5-2. Comparison of the measured changes in width and shear displacement for SZ-C3 of the calcite-cement shear zone Series 1 (dashed line) against the shear displacement that would occur simply by a similar change in width of the shear zone (solid line).

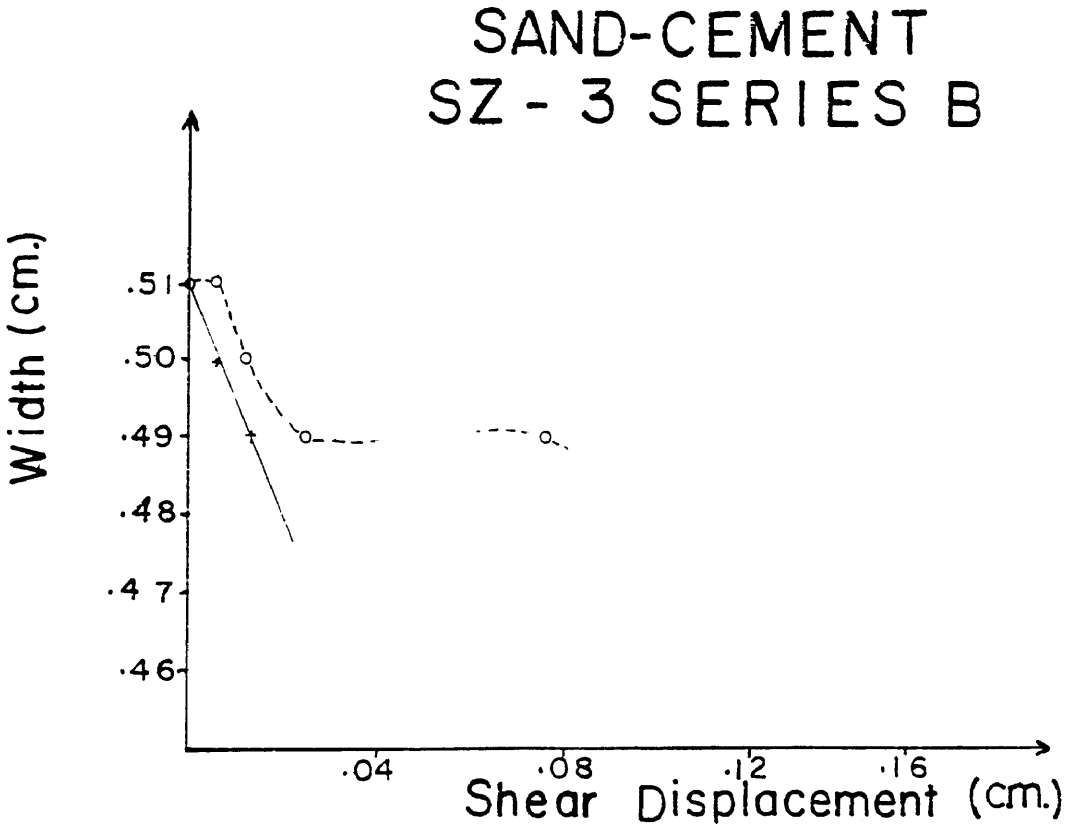
SAND-CEMENT
SZ - 3 SERIES B
Width (cm.)
.51
.50
.49
.48
.47
.46
.04
.08
.12
.16
Shear Displacement (cm.)

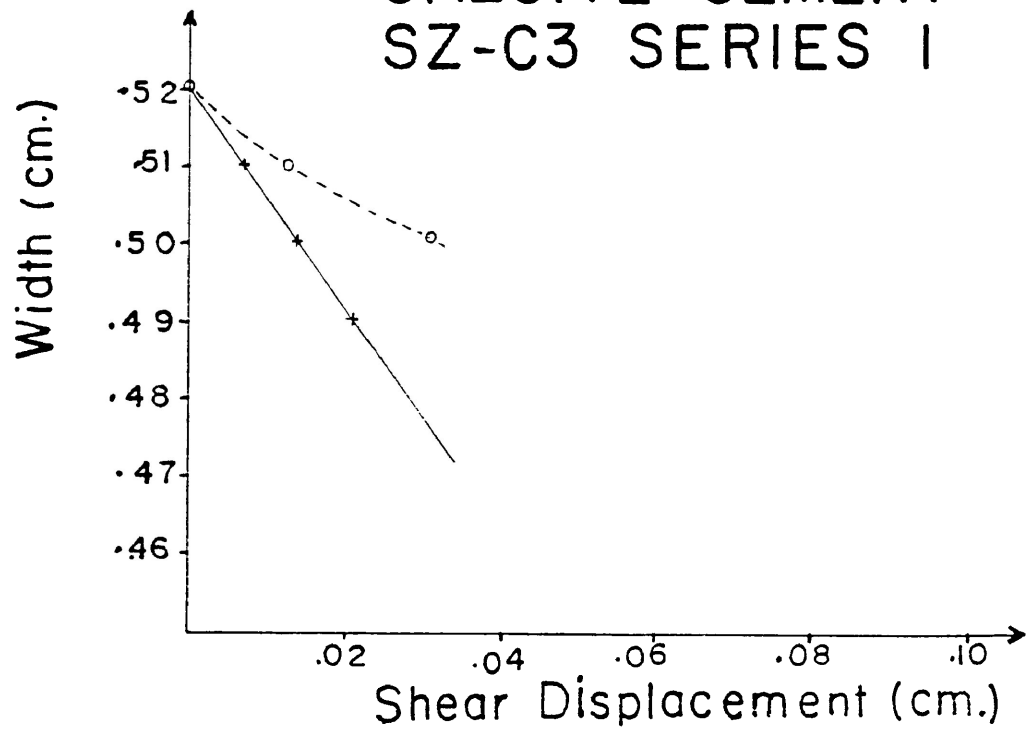
CALCITE-CEMENT
SZ-C3 SERIES I
Width (cm.)
.52
.51
.50
.49
.48
.47
.46
.02
.04
.06
.08
.10
Shear Displacement (cm.)

In terms of the deformation within the shear zone, what effect will the change in width of the zone have on the change of anisotropy and shape of the magnetic susceptibility ellipsoid? To test this effect, a comparison of the change in anisotropy between each increment of deformation ($\Delta P''$) and the change in width of the shear zone relative to the change in shear displacement ($[\Delta W+1]/[\Delta SD+1]$) was initiated for one randomly chosen shear zone experiment from each series of experiments (Figures 5-3 through 5-7). It was necessary to plot only the change in anisotropy of the susceptibility ellipsoid since the shape and anisotropy parameters both increase in a positive sense with shear strain. Each of the factors, $\Delta P''$ and $(\Delta W+1)/(\Delta SD+1)$ are plotted against the shear strain (γ) occurring within their related shear zone experiments.

The results from SZ-L of the Sand-cement series A, SZ-2 of the sand-cement series C and SZ-C3 of the calcite-cement series 1 all display an direct correlation between a decrease in the change of anisotropy between individual tests and a increase in the relative importance of the change in width in the deformation of the shear zone. However, both SZ-3 of the sand-cement series B and SZ-C2 of the calcite-cement series 2 show that a relative increase in the importance of the change of width in the shear zone deformation may correlate with an increase in the degree of anisotropy.

Thus it is to be expected that changes in the orientation, shape and degree of anisotropy of the magnetic susceptibility ellipsoids,

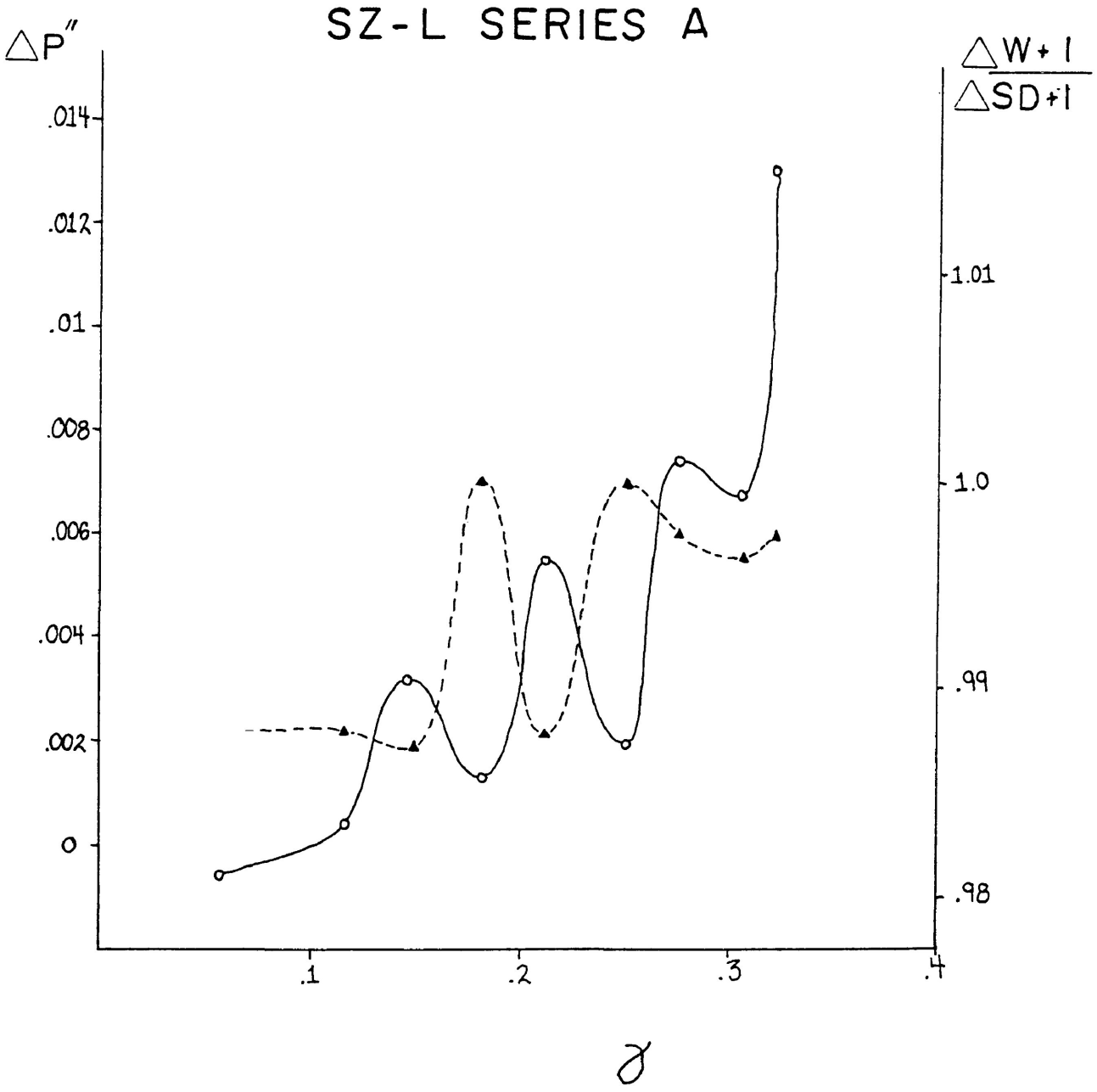

Figure 5-3. In order to assess the effect of the width change occuring within the shear zone on the degree of anisotropy, a comparison of the change in the degree of anisotropy between increments of shear deformation ($\Delta P''$, solid lines) and the relative importance of the change of width of the shear zone on the deformation within the shear zone ($[\Delta W+1]/[\Delta SD+1]$; dashed lines) made. The results here are for SZ-L of the sand-cement Series A.

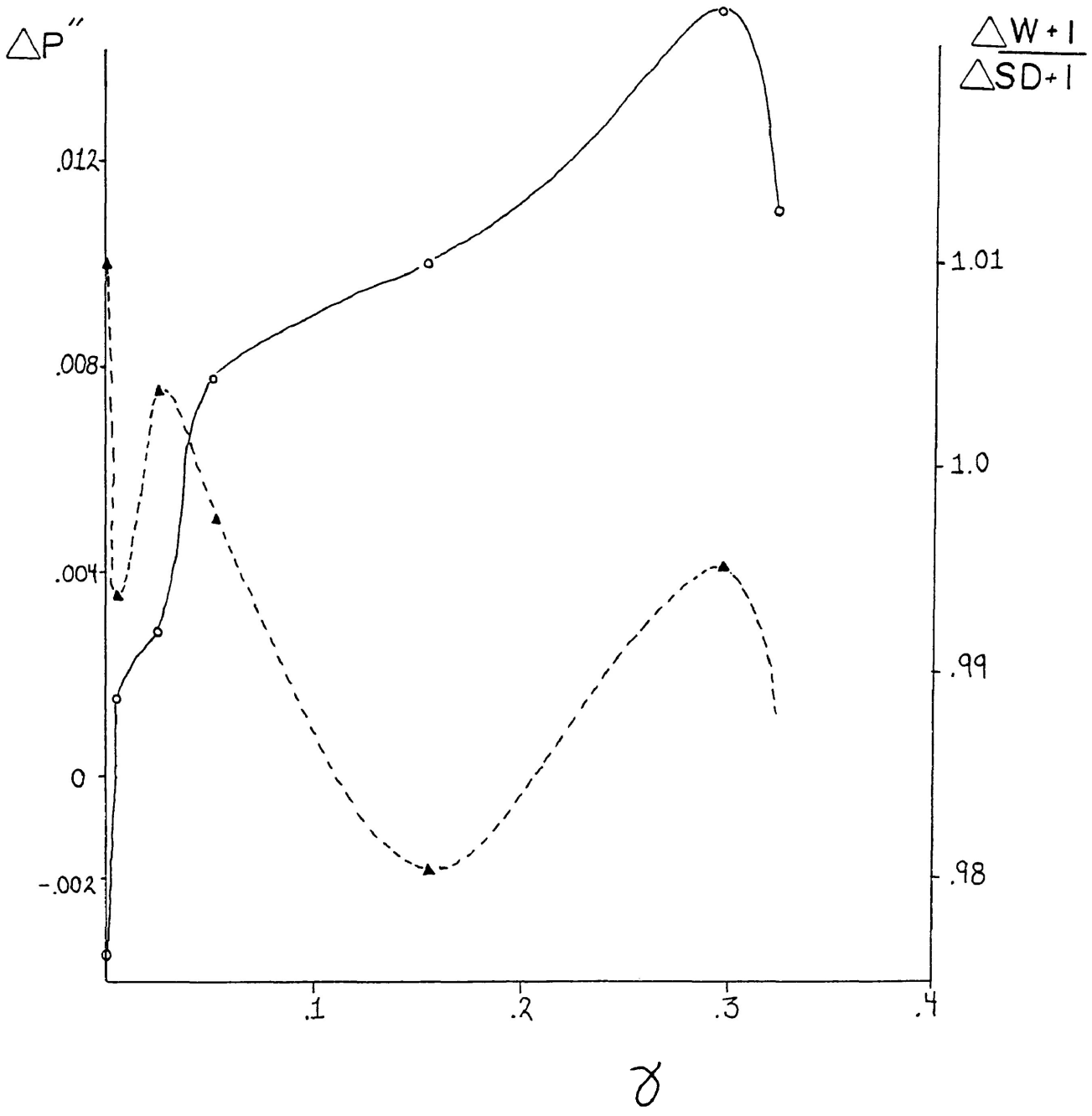

Figure 5-4. Comparison of the change in the degree of anisotropy between increments of shear deformation ($\Delta P''$; solid lines) and the relative importance of the change of width of the shear zone on the deformation within the shear zone ($[\Delta W+1]/[\Delta SD+1]$; dashed lines) for SZ-3 of the sand-cement Series B.

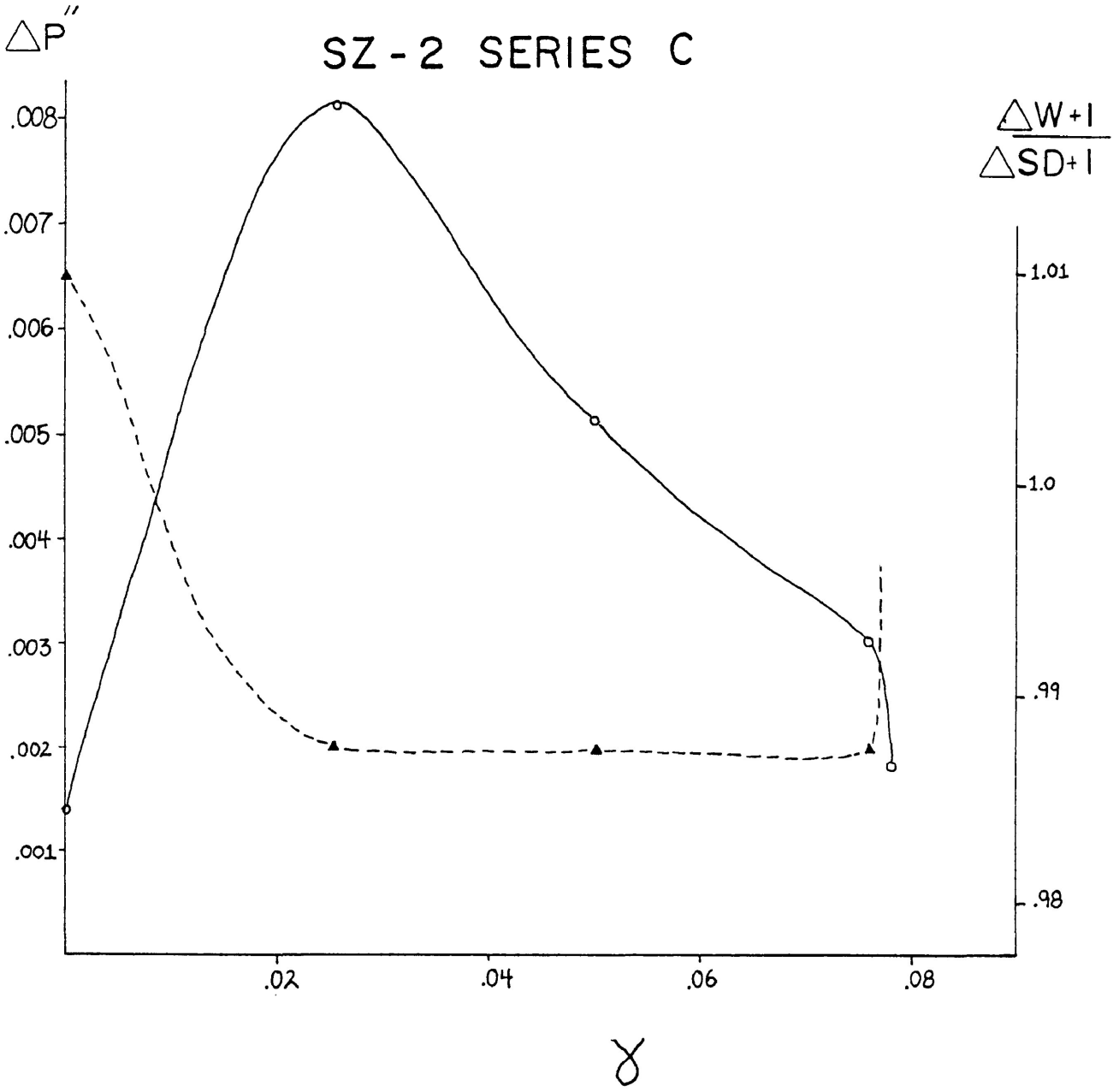

Figure 5-5. Illustrating the change in the degree of anisotropy between increments of shear deformation ($\Delta P''$; solid lines) against the relative importance of the change of width of the shear zone on the deformation within the shear zone ($[\Delta W+1]/[\Delta SD+1]$; dashed lines) for SZ-2 of the sand-cement Series C.

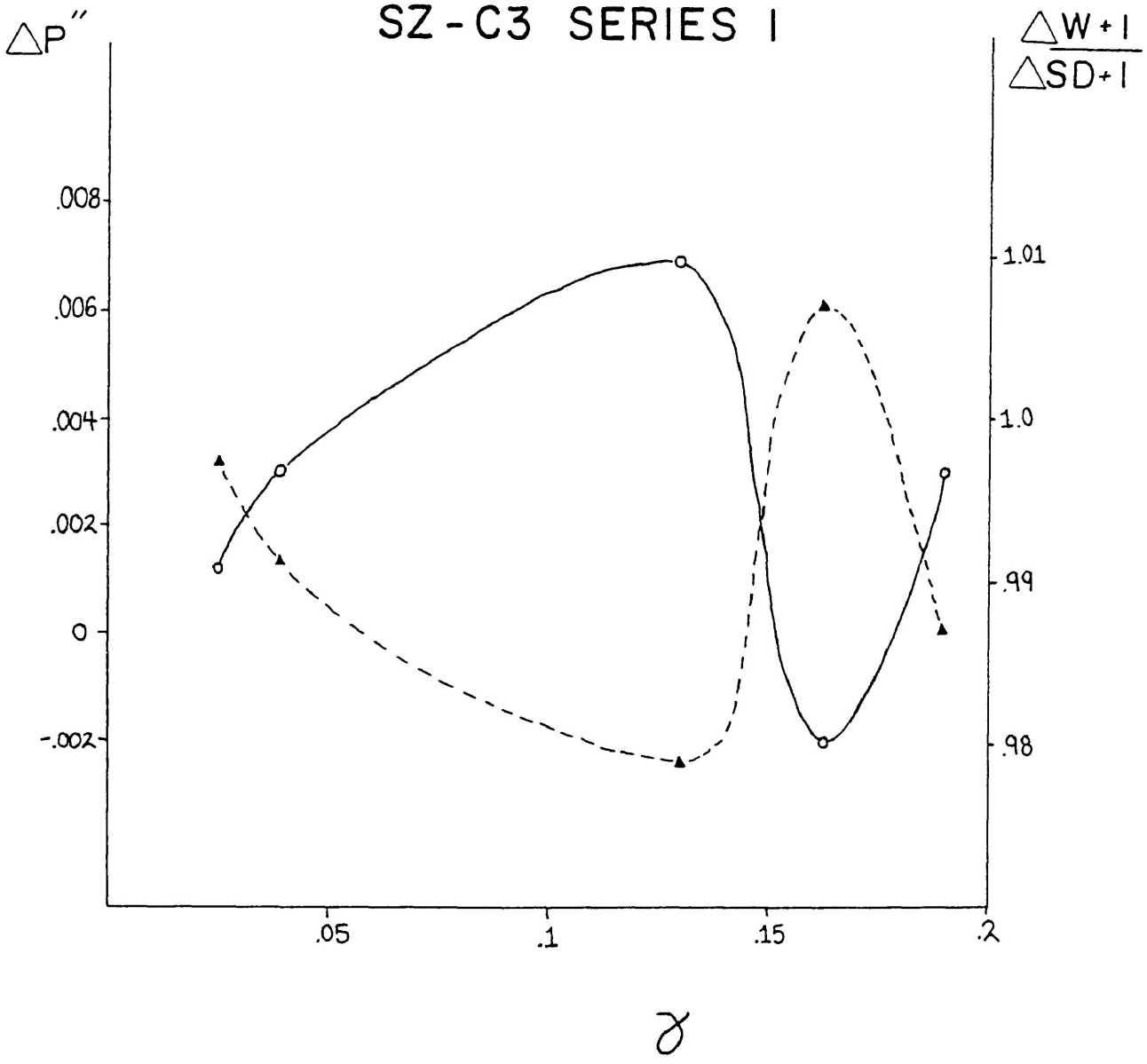

Figure 5-6. Illustrating the change in the degree of anisotropy between increments of shear deformation ($\Delta P''$; solid lines) against the relative importance of the change of width of the shear zone on the deformation within the shear zone ($[\Delta W+1]/[\Delta SD+1]$; dashed lines) for SZ-C3 of the calcite-cement Series 1.

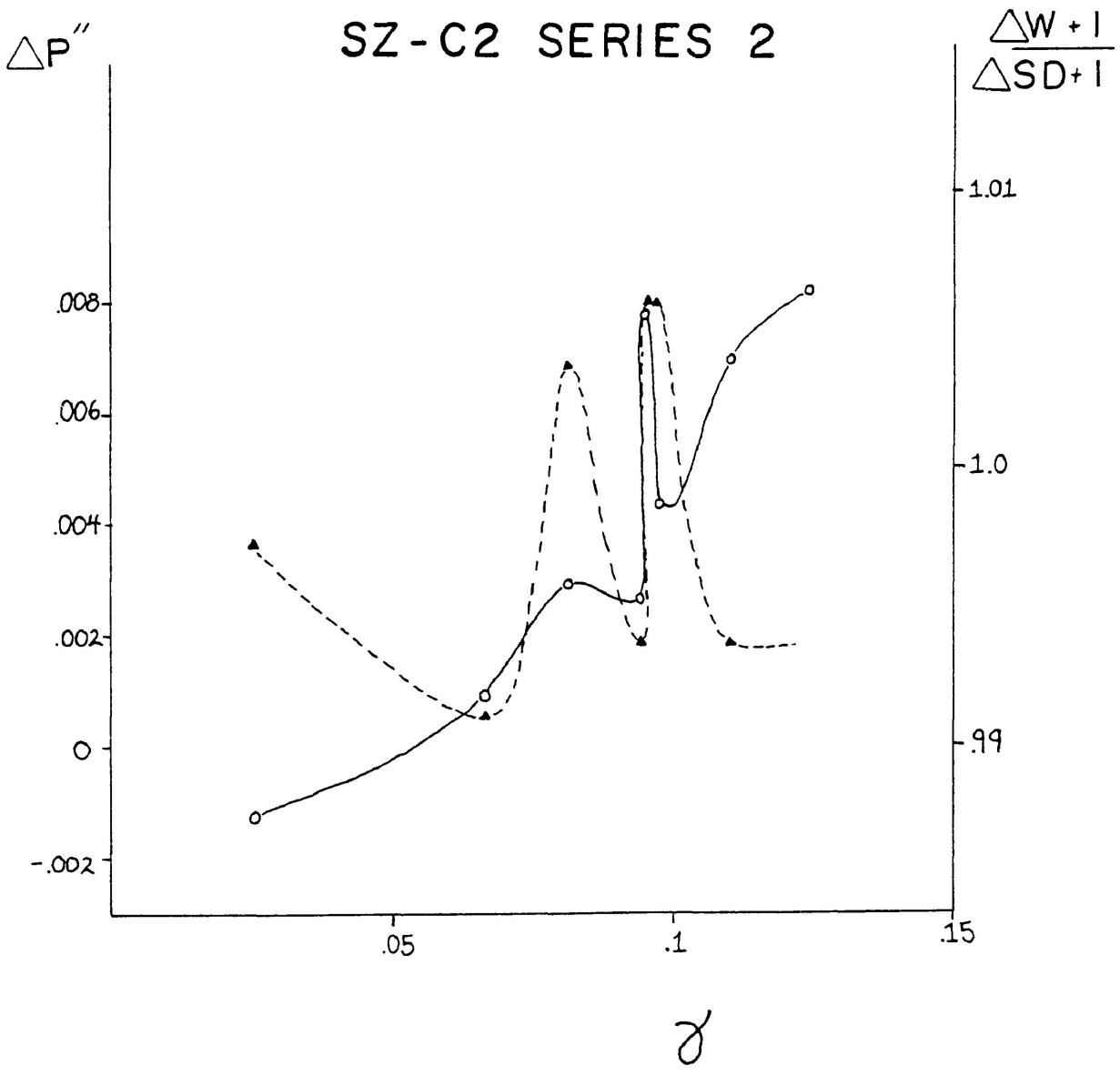

Figure 5-7. Illustrating the change in the degree of anisotropy between increments of shear deformation (ΔP"; solid lines) against the relative importance of the change of width of the shear zone on the deformation within the shear zone ([ΔW+1]/[ΔSD+1]; dashed lines) for SZ-C2 of the calcite-cement Series 2.

within the experimental shear zones, will result from deformation possessing both a flattening and a shearing character.

The net deformation can then be considered to be equivalent to a simple shear deformation with negative dilatancy. So, although the experiments are not truly simple shear, the experimental deformation, combining pure and simple shear, may more closely represent natural situations.

Pure Shear- During the deformation of the cylindrical specimens there is a tendancy for the specimens to take on a slightly hour-glassed shape during the initial stages of deformation and a slight barrel-shape after approximately 15% shortening. However, for most specimens the experimental shortening approximates deformation by homogeneous pure shear.

Changes in orientation of the magnetic susceptibility ellipsoid with respect to strain:

Shear Zone Experiments:

Sand-Cement Shear Zones- During the three series of experiments on the sand-cement shear zones a consistent pattern of rotation of the principal susceptibility directions was observed.

The progressive rotations of the three principal susceptibility directions were commonly clockwise during deformation, although in the first increments of deformation some counter-clockwise

rotations were observed. K_{max} would commonly rotate towards a orientation that was nearly perpendicular to the primitive plane of the stereonet while K_{int} and K_{min} would often rotate toward or within this plane (ie. Figure 5-8). The direction of the minimum susceptibility axes, K_{min}, would usually rotate toward a position that had an angular orientation of approximately 60^{o} to the shear zone. The 'typical' orientation of K_{max} was sometimes occupied by the K_{int} principal susceptibility direction and vice versa, however, the K_{max} direction appears to be the most favourable for this position. In one experiment (SZ-H of Series A) the orientation of the K_{int} and K_{max} principal susceptibility directions were exchanged during deformation (Figure 5-9).

The rate of rotation experienced by the susceptibility axes in the sand-cement material were shown, except for the initial increments of deformation, to be much like that of a similarily oriented material line. Ghosh and Ramberg (1976) have shown that for deformation by simultaneous pure and simple shear the rate of rotation of a rigid elliptical inclusion varies according to its orientation and axial ratio. This also appears to be true of the magnetic susceptibility ellipsoid, however it must be remembered that the susceptibility ellipsoid is the combined result of each magnetic grain within the material. Knowing that such grains are originally randomly oriented, indicates the effectiveness of the

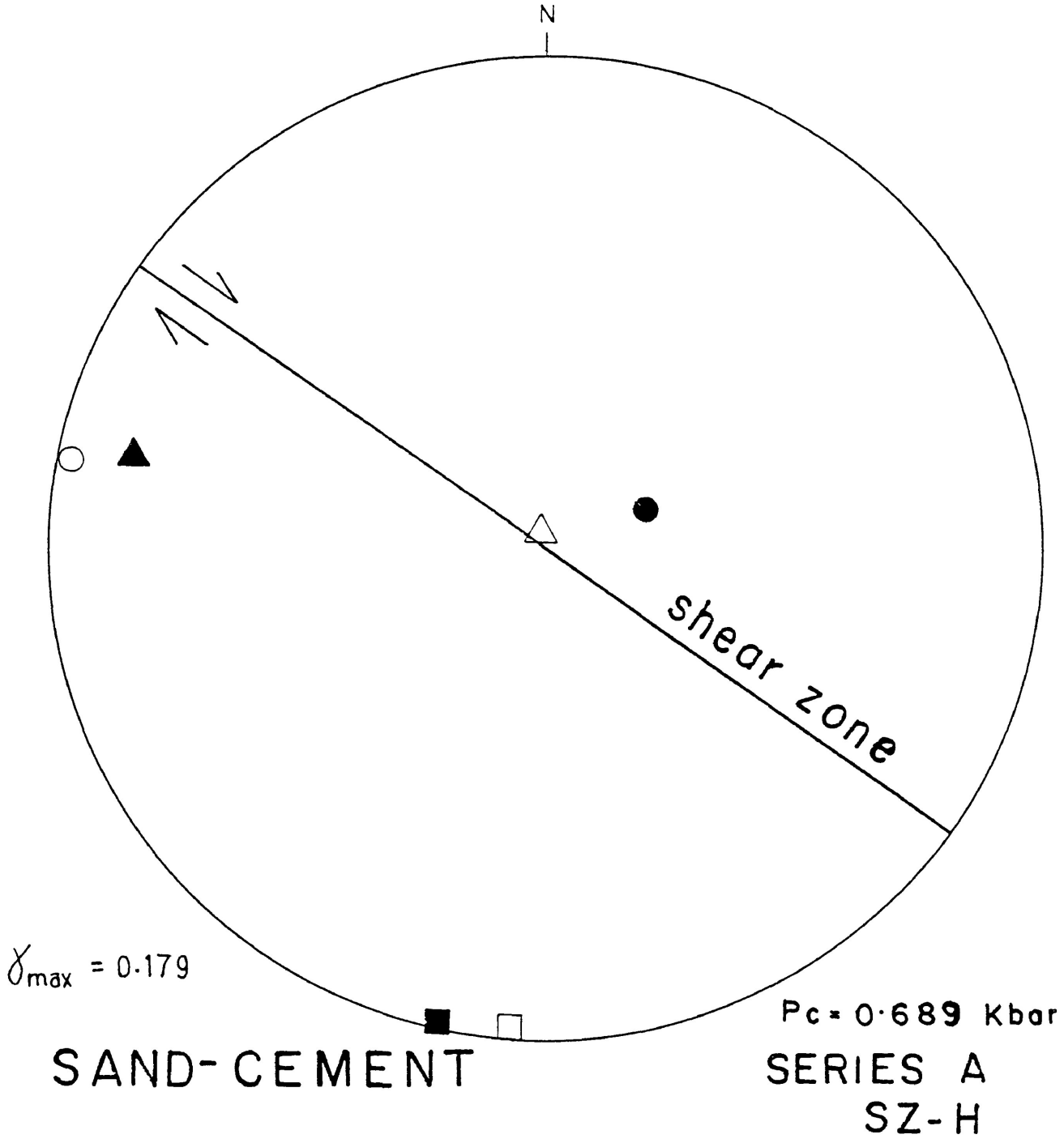

Figure 5-8. The change in the orientation of the principal susceptibility directions for SZ-H of the single-step sand-cement simple shear deformation Series A. Note that the orientation of the K_{max} and K_{int} susceptibility directions have been exchanged during deformation.

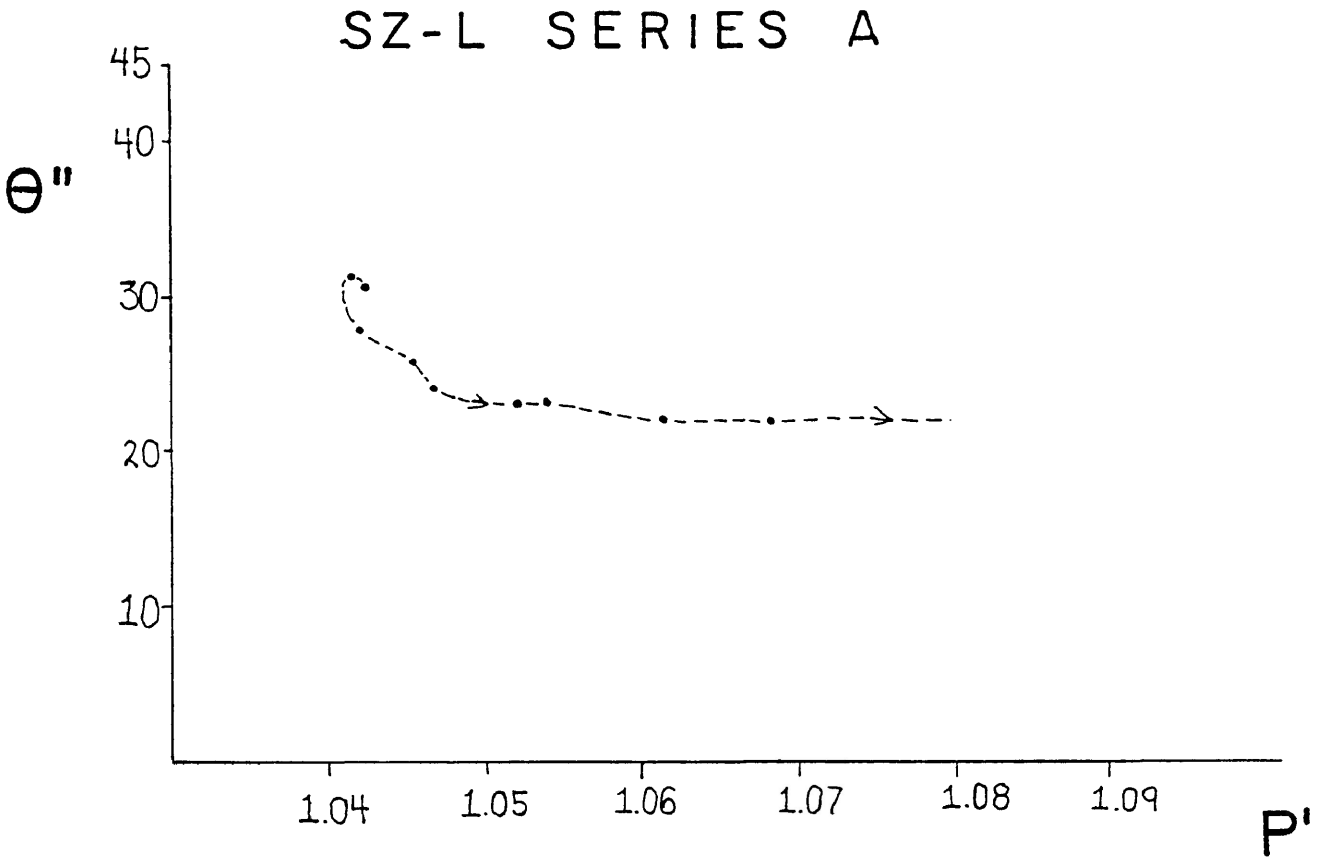

Figure 5-9. Illustrating the angular position of the K_{max}-K_{int} plane with respect to the shear zone (θ") as the degree of anisotropy (P') changes for SZ-L of the sand-cement Series A.

re-orientating mechanisms during the experimental deformation.

The plane containing K_{max} and K_{int}, measured on the primitive plane of the stereonet from the shear zone, would typically rotate towards the shear zone as the anisotropy increased (ie. Figures 5-10 to 5-12). As the ellipsoid became 'fixed' the rotation of the K_{max}-K_{int} plane would decelerate. This effect is most likely due to the combination of simple and pure shear deformation within the shear zone, the simple shear causing the plane to rotate clockwise towards the shear zone, while the pure shear effect would oppose this when the K_{max}-K_{int} plane attempts to rotate beyond the principal plane of flattening corresponding to the compaction influence.

Calcite-Cement Shear Zones- Although the progressive rotations experienced by the principal susceptibility directions in the two series of calcite-cement shear zones are more varied than those in the sand-cement material, a common orientation of the K_{min} direction and the plane containing the intermediate and maximum susceptibility directions appears to exist. K_{min}, in each of the experiments rotates toward the primitive plane of the stereonet, to a direction within this plane that has an angular position of approximately 70^{o} to the direction of shear. K_{max} and K_{int} commonly rotate toward or within the shear plane (ie. Figure 5-13), and in some instances the plane containing these two

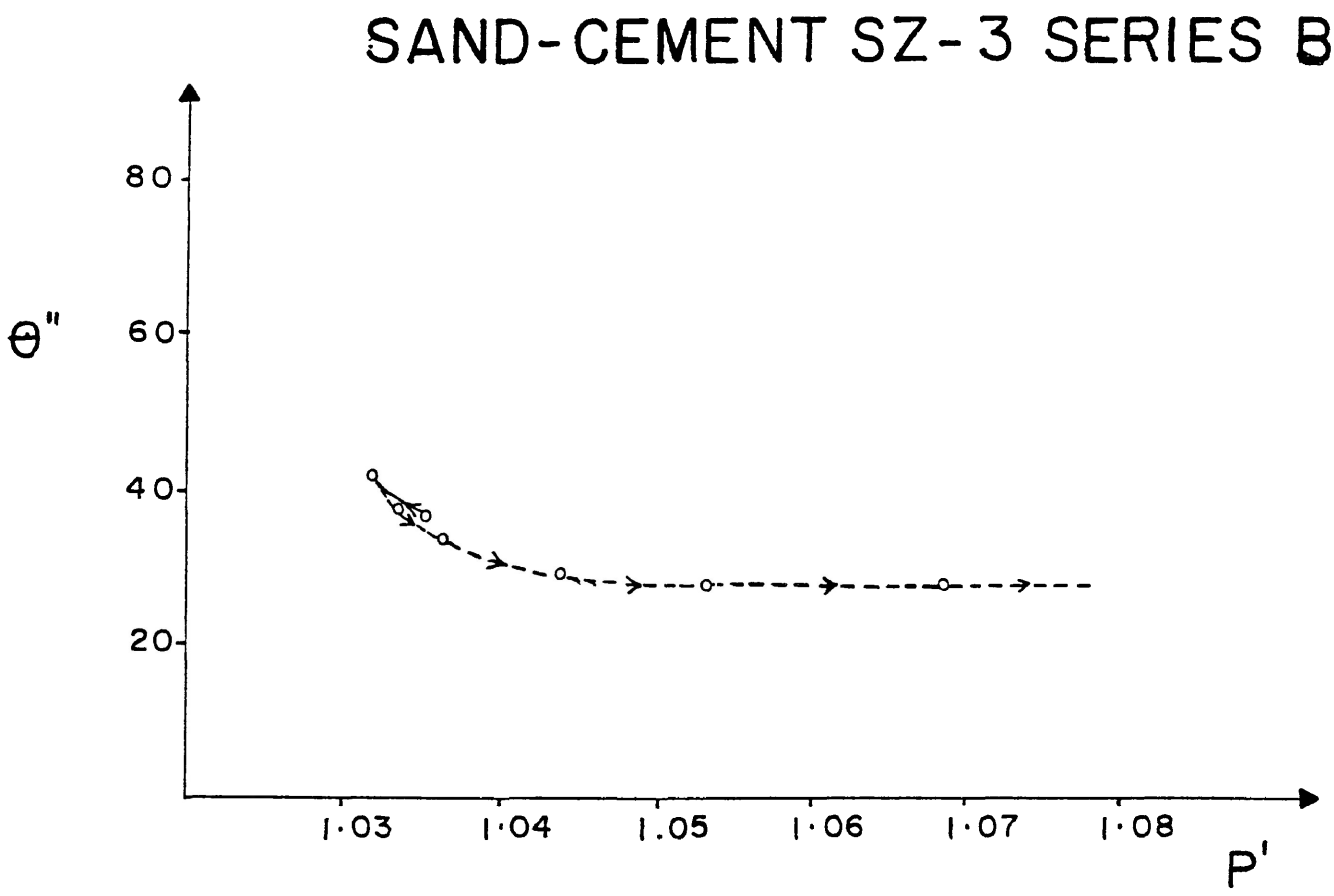

Figure 5-10. Illustrating the angular position of the K_{max}-K_{int} plane with respect to the shear zone (θ") as the degree of anisotropy (P') changes for SZ-3 of the sand-cement Series B.

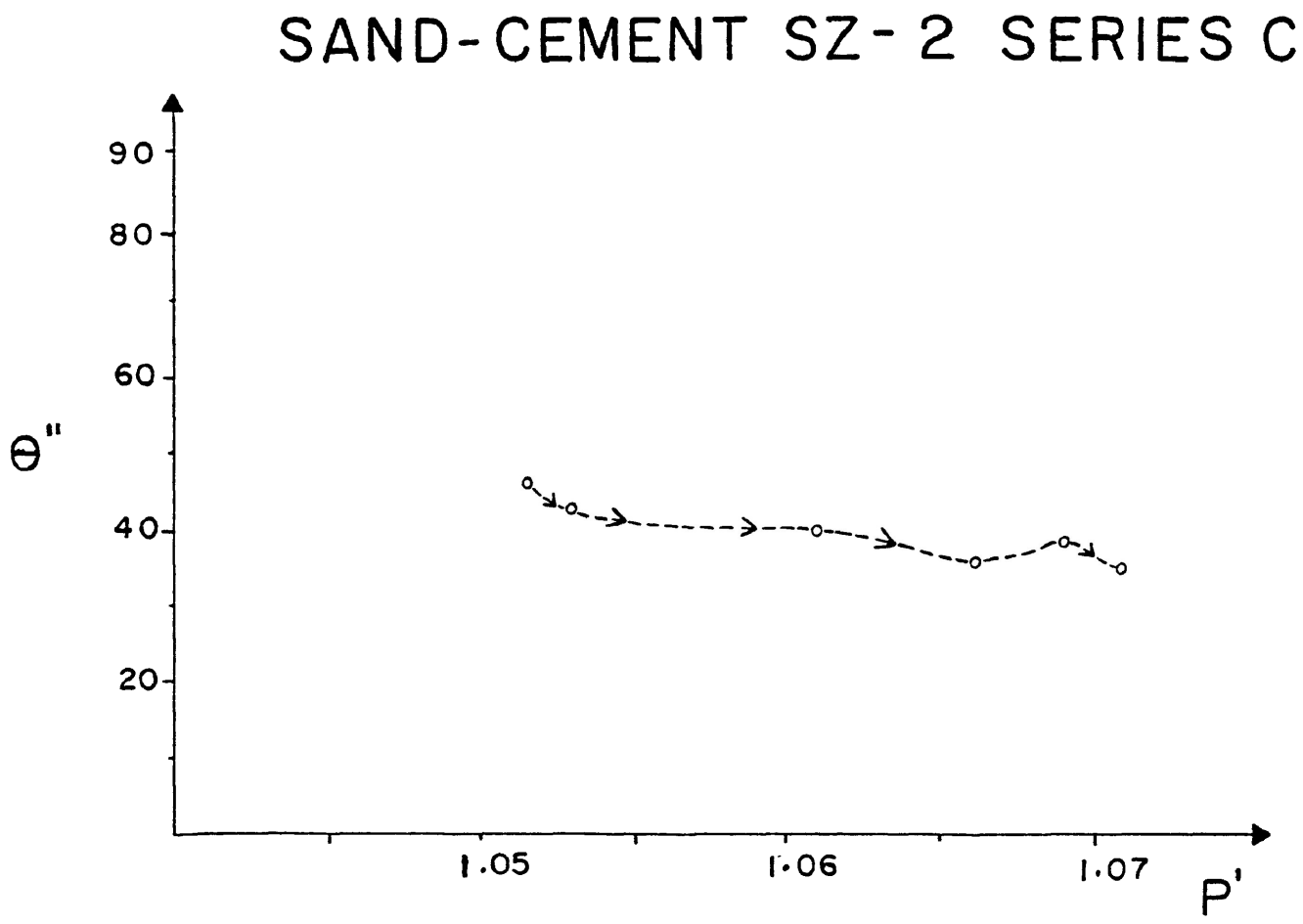

Figure 5-11. Illustrating the angular position of the K_{max}-K_{int} plane with respect to the shear zone (θ") as the degree of anisotropy (P') changes for SZ-2 of the sand-cement Series C.

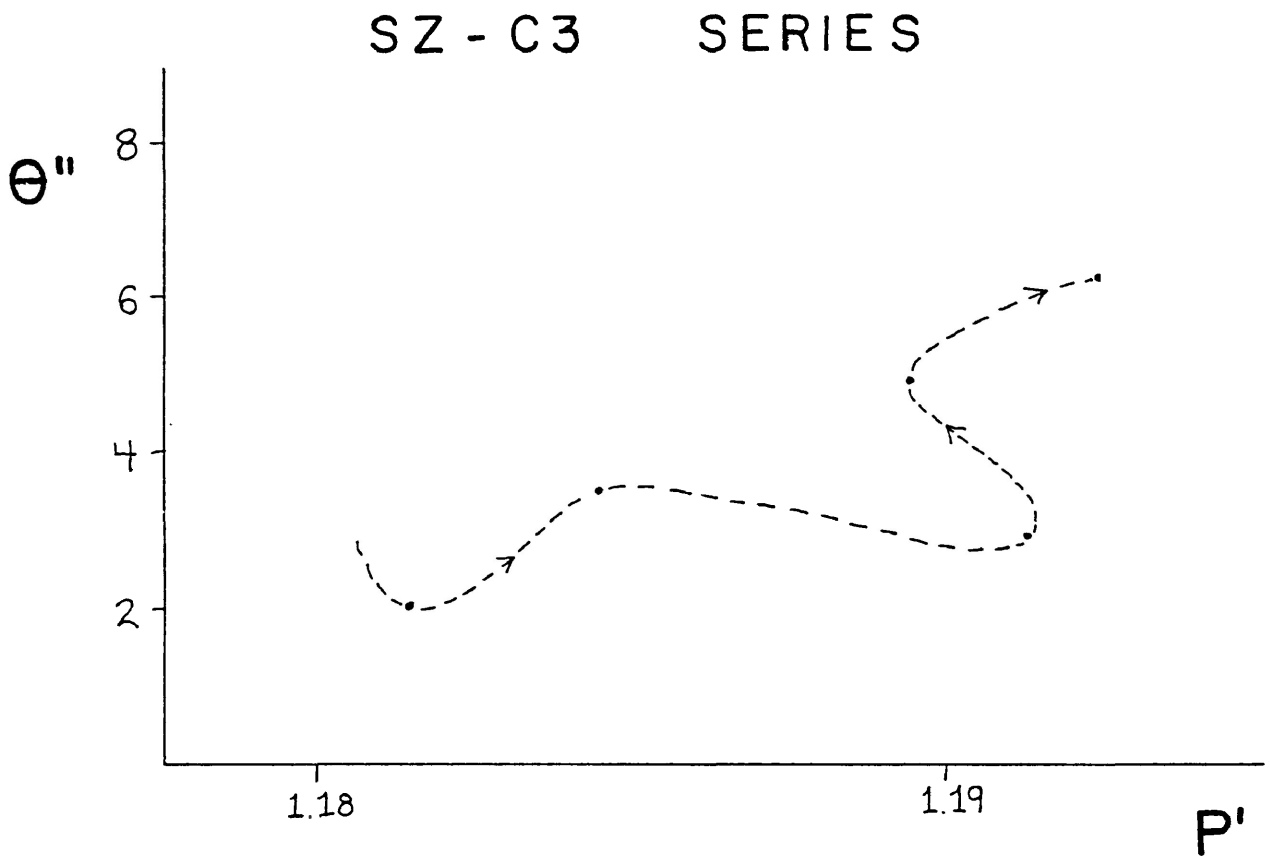

Figure 5-12. Illustrating the angular position of the Kmax-Kint plane with respect to the shear zone (θ") as the degree of anisotropy (P') changes for SZ-C3 of the calcite-cement Series 1.

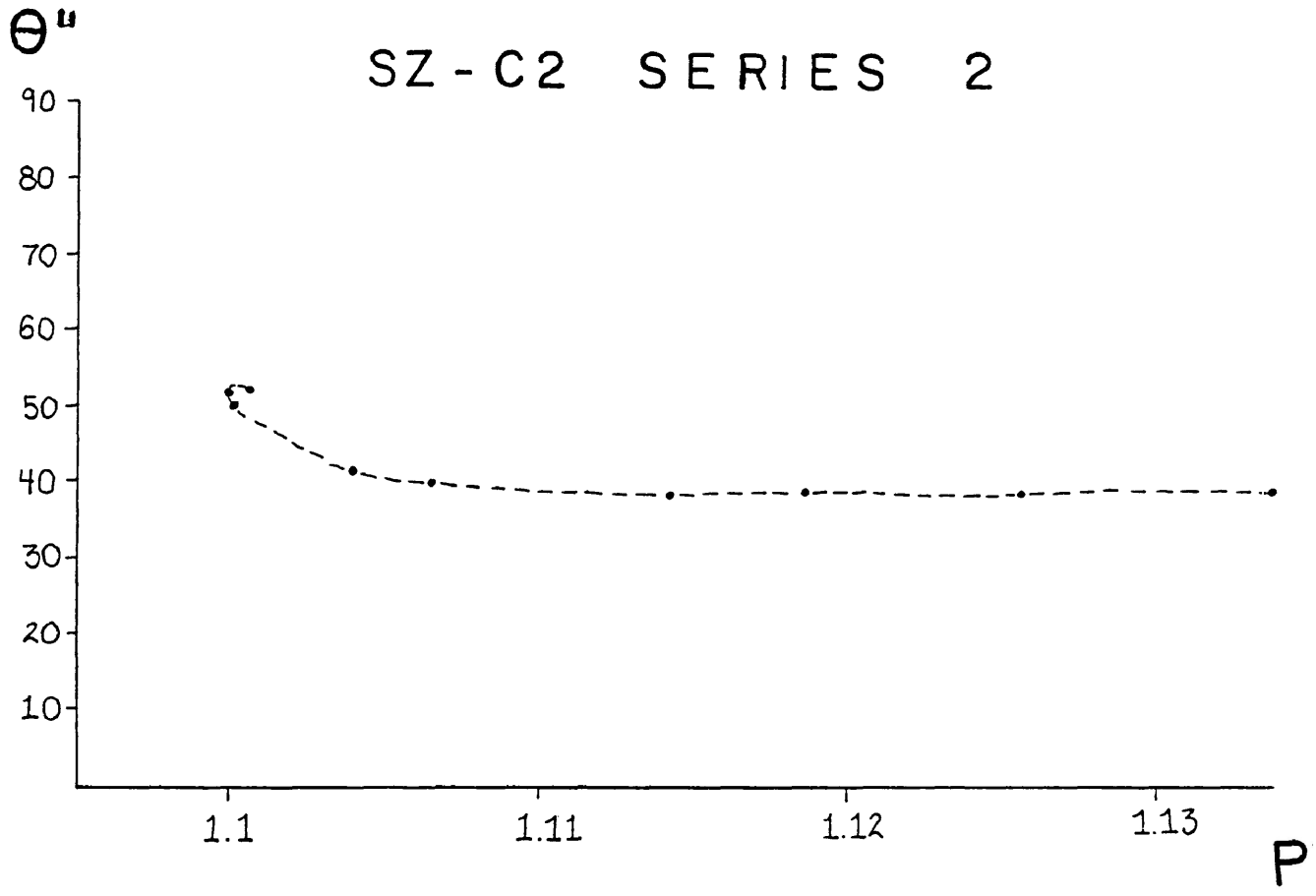

Figure 5-13. Illustrating the angular position of the Kmax-Kint plane with respect to the shear zone (θ'') as the degree of anisotropy (P') changes for SZ-C2 of the calcite-cement Series 2.

susceptibility directions was nearly coplannar with the shear plane (ie. Figure 5-12).

In the calcite-cement shear zones the rate of rotation of the susceptibility axes was usually much different and in some cases their rotation was toward a direction opposite to that of the shear zone. This later effect is attributed to the rotation of the principal susceptibiltiy axes into preferred orientations generated by the combination of pure and simple shear deformation.

Pure Shear Experiments:

Within the Calcite-cement pure shear tests a common pattern to the progressive rotation of the pricipal susceptibility directions was distinguished: K_{min} rotates toward the centre of the stereonet, corresponding to the axis of maximum shortening (Z-axis) and both K_{max} and K_{int} rotate away from the Z-axis, toward the primitive plane of the stereonet which corresponds the plane of flattening for the specimen. During the initial increments of deformation, some specimens displayed a rotation of the magnetic susceptibility axes opposite to the typical pattern. This effect has been noted in the pure shear experiments within the elastic range by Nagata (1970) and for experiments involving large strains (Borradaile and Alford 1987).

For the calcite-cement material, the rotation of the K_{min}

susceptibility axis has been shown to be faster than would be inferred from the effects of homogenous strain on a linear element when it is within approximately 30^{o} to the principal strain axes. When the susceptibilty axes are beyond this apparent 30^{o} limit they tend to rotate at rate slower than or equal to that expected from a material linear element.

Within the sand-cement pure shear tests of Borradaile and Alford (1987) the rotations of the K_{min} susceptibility axis within 40^{o} of the Z-axis were shown to be much faster than the rotation of linear material elements.

Thus the rate of rotation of the susceptibility axis within the calcite-cement material appear to be not only orientation dependent, but overall, slower than similar rotations in a sand-cement material.

Changes in shape and anisotropy of the Magnetic Susceptibility's Magnitude Ellipsoid:

Shear Zone Experiments:

Sand-Cement Shear Zones- Within the sand-cement shear zones deformation of the susceptibility ellipsoid was predominantly of a flattening character. In both the Flinn type of susceptibility plot and the Hrouda-Jelinek anisotropy plot progressive deformation within the shear zones consistently moved the susceptibility

ellipsoid into or further into the field of flat-shaped ellipsoids. In quite a number of shear zones the initial increment of deformation caused the susceptibility ellipsoid to become slightly prolate and in some instances less anisotropic.

Calcite-Cement Shear Zones- Much like the sand-cement shear zones, the deformation of the magnetic susceptibility ellipsoids within the calcite-cement material produces progressively more anisotropic and flat-shaped ellipoids, except in some specimens during the initial increments of deformation.

Ramsay and Wood (1973) predicted, using a modified Flinn diagram, the deformation path of a sphere deforming by conditions of plane strain including those with an initial and incremental volume loss.

Like plain strain, simple shear deformation occurs along two (the Z and X) of the three pricipal strain directions. Thus, if we are to imagine a sphere deforming by simple shear we need only observe the change in shape of the ellipsoid in the plane containing these two directions (perpendicular to the Y pricipal strain direction). In the case of a sphere deforming by simple shear with no loss in volume the deformation path on a natural log Flinn diagram (ln(X/Y) vs ln(Y/Z)), will be a line originating from the origin with a slope of 45^{o}. Subsequently, if a volume loss were to occur before the onset of simple shear, the result will be a

deformation path again possessing a 45^{o} slope, but originating at a position along the abscissa corresponding to the initial Y/Z ratio. The present shear zone experiments are equivalent to a simple shear deformation with progressive loss of volume. The results of experimental deformation exhibit a deformation path akin to that calculated by Ramsay and Wood (1973), who indicated that for simple shear with progressive volume loss, the deformation path on the Flinn-type susceptibility plot would possess a slope of less than unity and curve toward the axis of foliation, hence the ellipsoid shape becomes progressively more flattened than rod-shaped.

Correlation of the change in magnetic anisotropy with strain:

There exists, for both the shear zone and pure shear experiments, a power-law correlation between the change in the degree of anisotropy of susceptibility ($\Delta P'$) and the bulk strain ratio.

The increase in anisotropy of the susceptibility ellipsoids is believed to be principally due to the aligning effect of deformation on the slightly elongate magnetite grains.

Within the sand-cement material the rotations of the pricipal susceptibility directions have been shown to be much like that of real material lines, this may indicate that within this material the grains are simply rotating and rolling (ie. particulate flow).

Thin sections of the sand-cement material indicate a moderate preferred dimensional orientation of the magnetite grains, thus the magnetite has suffered an alignment either by 1) an intact grain rotation or by 2) a 'passive' flow of the magnetite.

Within the calcite-cement shear zones a weak to no preferred alignment of the magnetite was observed in thin section, yet the measured change in anisotropy occurring within simple shear experiments is much like from the sand-cement tests.

The fact the magnetite grains do not show as preferred an orientation within the calcite-cement material as within the sand-cement material may be due to the strain compatibility contrast of the grains within the cement mixtures. Within the sand-cement, the grains are roughly the same shape (sub-sphereical) and roughly possess similar 'hardnesses', thus during deformation a particular grain could jostle about much like its neighbour. In the calcite-cement material, the calcite grains shape and much 'softer' nature would hinder the rotation of the sub-spherical magnetite by becoming elongate, hence 'pinning' the magnetite by impeding its rotation.

Comparison of Experimental Results with Natural Examples:

Primarily, natural deformation appears to produce flat-shaped magnetic susceptibility ellipsoids. Experimental deformation in

either pure shear (this study; Borradaile & Alford 1987) or under conditions approximating simple shear both exhibit a flattening of the magnetic susceptibility magnitude ellipsoid.

Coward (1976) described the change in the orientation, anisotropy and shape of the magnetic susceptibility ellipsoid for rocks across a natural shear zone in North Uist, Scotland. Here Coward estimated that the character of deformation was not simple shear alone but a combination of pure and simple shear. The magnetic susceptibility ellipsoids were shown to become flattened and suffer and increase in anisotropy toward the centre of the shear zone. In studying the magnetic fabric of shear zones Rathore (1980; with Becke, 1980; and Rathore et al., 1983), has found that the K_{min} direction consistently parallels the cleavage poles throughout shear zones, and has used the rotation of the principal susceptibility directions to analyze the sense of movement along a shear zone.

Susceptibility directions have been shown to parallel principal strain directions in nature. Within the pure shear experiments, the rotations of the principal susceptibility directions are clearly toward the orientations of the principal strains and the results from the simple shear experiments show the susceptibility directions rotating as would a ellipsoidal marker.

Thus the susceptibility fabrics produced by both the sand-cement and calcite-cement materials in this study are

similar in orientation and shape to the fabrics produced in most naturally deformed rocks.

Stress Relaxation and Microscopic Observations with inferences on deformation mechanisms:

Stress relaxation of cement mixtures have been previously conducted (ie. Klug & Whittman 1970; Brooks & Neville 1976), however examination of such materials has been predominately for material strength research and not towards the understanding of the predominant mechanisms of deformation within the cement gel. Nevertheless, deformation within the sand-cement and calcite-cement materials undoubtably involves deformation of the cement gel, microcracking at the cement-grain boundary and rotation and other intergrannular motions of the grains within the cement matrix.

Cataclasis appears to be the dominant mechanism of deformation of the grains in the sand-cement material. Supporting evidence for this are the numerous broken grains in thin section, also a high n value or slope on the stress relaxation graphs indicating that the materials strength is independent of strain-rate. This is a commonly reported feature of cataclasis.

The n value recorded within the experimental strain-rates ranges from approximately 42 to 50, thus for this material that value of n may describe a flow law wherein cataclasis and

particulate flow predominate for this material.

Rotation of the magnetite grains, supported by their preferred direction indicates that deformation by particulate flow is also occurring within the sand-cement material. Previous work on the deformation of magnetite (Muller & Siemes 1972; Hennig-Michaeli & Siemes 1975) indicates that plastic deformation of magnetite may occur at room temperature. Although evidence for 'flow' of a magnetite grain was discovered in SZ-3 of Series B, it is doubtful, due to the rate of rotation of the susceptibility axes which are most like material lines, that this mechanism predominates in the deformation of the magnetite within the sand-cement shear zones.

Within the calcite-cement shear zones, intra-crystalline glide appears to be the dominant deformation mechanism affecting the grains. Evidence for this is supplied in thin section, as the calcite grains have changed shape and display new twin lamellae.

The slope of the relaxation data within the range of the experimental strain-rates ranged from approximately 22-26. This relative insensitivity of strain-rate upon differential stress suggests that cataclasis may be important. However, microscopic observations indicate that deformation by dislocation slip, twinning and particulate flow have also occured. Thus, such a range of n values perhaps describes the stress exponent for a flow law which incorporates complex inter- and intra-grannular deformation mechanisms within this material.

It is uncertain, however, by what mechanism the magnetite

within the calcite shear zones is deforming. The degree of magnetic anisotropy is increasing within the material, thus the magnetite grains are undoubtably being affected by deformation either by 1) rotating towards some preferred direction, or 2) are undergoing a re-arrangment of their grain shape by some dislocation glide process, much like the calcite. The second hypothesis is unlikely, however, since the magnetite grains are apparently much 'stronger' than the calcite grains and are thus acting more or less like rigid particles in a 'softer' matrix. Although the first hypothesis is seemingly correct, no marked preferred alignment of the magnetite grains within the deformed calcite-cement shear zones was observed.

The question of the validity of quoting the stress relaxation results (preformed in pure shear geometry) for the shear zone deformation still remains. Thin section examination of the calcite-cement material deformed in pure shear reveals similar deformation mechanisms as were described in the shear zone experiments. Thus, although the shear zone geometry must undoubtably possess a slightly different stress-to-permanent strain relationship during relaxation, the tests appear valid for the experimental strain-rates employed.

Summation

Under experimental conditions:

Simple Shear

1-The character of deformation within the experimental shear zones is transpressive, combining both simple and pure shear.

2- The original susceptibility's magnitude ellipsoid becomes progressively flatter and more anisotropic with deformation, and thus behaves somewhat like an ellipsoidal strain marker in its shape and anisotropy changes toward the final susceptibility.

3-Within the sand-cement shear zones the rotations of the pricipal susceptibility directions are directed toward a consistent orientation. Their rate of rotation is much like that expected of a line element.

4-Within the calcite-cement shear zones the rotations of the K_{min} principal susceptibility direction and the plane containing the K_{max} and K_{int} directions are directed towards a consisted orientation. The principal susceptibility directions rotate much differently than would be expected from line elements.

5-There exists a correlation between the change in the degree of anisotropy of susceptibility ($\Delta P'$) and the bulk shear strain ratio (ln X/Z) within the experimental shear zones.

6-The predominant deformation mechanisms for the two materials differ, the sand-cement material deforming by a combination of particulate flow and cataclasis, while the calcite-material by twinning, dislocation slip and perhaps some inter-crystalline mechanism. Although the rate of rotation of the susceptibility ellipsoids may differ, within both materials the experimentally produced susceptibility fabrics are similar to those produced in naturally deformed materials.

Pure Shear

1-The magnetic susceptibility's magnitude ellipsoid behaves somewhat like an ellipsoidal strain marker in its rotations, anisotropy and shape changes.

2-The rate of rotation of the principal susceptibility directions for the calcite-cement material appear to be orientation dependent. Those susceptibility ellipsoids having their K_{min} directions within 30^{o} of the maximum shortening direction (Z-axis) rotate faster than would be expected from hypothetical line elements while those ellipsoids possessing an angle greater

than 30^{o} between their K_{min} susceptibility direction and the Z-axis rotate slower.

3-There exists a correlation between the change in the degree of anisotropy of susceptibility ($\Delta P'$) and the bulk strain ratio for pure shear.

4-Comparison of the calcite-cement pure shear experiments to the sand-cement pure shear tests of Borradaile and Alford (1987) illustrates as do the two materials in simple shear that although the deformation mechanism differ, the magnetic fabrics produced are similar to each other and to those produced in natural situations. This suggests that the orientation of the susceptibility fabric may be essentially independent of the bulk deformation fabric when the carrier of susceptibility is a disseminated accessory mineral.

References

Ashby, M.F., 1972: A first report on Deformation-Mechanism Maps; Acta Metallurgica, v.20, p.887-897.

Ashby, M.F. and Verrall, R.A., 1977: Micromechanisms of flow and fracture, and their relavance to the Rheology of the Upper Mantle; Phil. Trans. R. Soc. Lond. Ser. A., v.288, p.59-95.

ASTM STP 676.Stress Relaxation Testing, Alfred Fox, Editor. Am. Soc. for Testing and Materials, 1979.

Borg, I., Friedman, M., Hadin, J. and Higgs, D.V., 1960: Experimental Deformation of St. Peter sand: a study of cataclastic flow; in D. Griggs and J. Handin, Editors, Rock Deformation. Geol. Soc. Am. Mem. 79, p.133-192.

Borradaile, G.J., 1981: Particulate Flow of Rock and the Formation of Cleavage; Tectonophysics, v.72, p.305-321.

Borradaile, G.J. and Tarling, D.H., 1981: The influence of Deformation Mechanisms on Magnetic Fabrics in weakly Deformed Rocks; Tectonophysics, v.77, p.151-168.

Borradaile, G.J. and Mothersill, J.S., 1984: Coaxial deformed and

magnetic fabrics without simply correlated magnitudes of principal values; Phys. Earth Planet. Interiors, v.35, p.294-300.

Borradaile, G.J. and Tarling, D.H., 1984: Strain partitioning and magnetic fabrics in particulate flow; Can. J. Earth Sci., v.21, p.694-697.

Borradaile, G.J., Mothersill, J.S., Tarling, D.H. and Alford, C.S., 1985: Sources of Magnetic Susceptibility in a Slate; Earth Planet. Sci. Lett., v.76, p.336-340.

Borradaile, G.J. and Alford, C.S., 1987: Relationship between Magnetic Susceptibility and Strain in laboratory experiments; Tectonophysics, v.133, p.121-135.

Borradaile, G., Keeler, W., Alford, C. and Sarvas, P., in press: Anisotropy of Magnetic Susceptibility of Some Metamorphic Minerals; Phys. Earth Planet. Interiors.

Brooks, J.J. and Neville, A.M., 1976: Relaxation of Stress in Concrete and its Relation to Creep; Proc. of the American Conrete Institute, v.73, n.4, p.227-232.

Carter, N.L., 1976: Steady State Flow of Rocks; Reviews of Geophysics and Space Physics, v.14, pp.301-360.

Chlupacova, M., Hrouda, F., Janak, F. and Rejl, L., 1975: The Fabric, Gensis and Relative-age Relations of the Granitic Rocks of the Cista-Jesenice Massif (Czech.) as Indicated by Magnetic Anisotropy; Gerl. Beitr. Geophys., v.84, p.487-500.

Coates, M.E., 1972: Geology of the Black Sturgeon River Area, District of Thunder Bay; Ont. Dept. Mines and Northern Affairs, Geol. Report 98. 41 pages.

Coward, M.P., 1976: Strain Within Ductile Shear Zones; Tectonophysics, v.34, p.181-197.

Dahlstron, C.D.A., 1970: Structural geology in the eastern margin of the Canadian Rocky Mountains; Bull. Can. Pet. Geol., v.18, n.3, p.332-406.

Donath, F.A., 1970: Rock Deformation apparatus and experiments for Dynamic Structural Geology; Journal of Geologic Education, v.18, p.3-12.

Donath, F.A. and Fruth, L.S., 1971: Dependance of Strain-Rate effects on Deformation Mechanism and Rock Type; J. Geol., v.79, n.3, p.347-371

Donath, F.A. and Guven, N., 1971: Data Reduction in Experimental Rock Deformation; Contributions to Geology, v.10, p.89-116.

Donath, F.A. and Wood, D.S., 1976: Experimental evaluation of the deformation path concept; Phil. Trans. R. Soc. Lond. Ser. A., v.283, p.187-201.

Dorn, J.E., 1957: The spectrum of activation energies for creep, in Creep and Recovery. Am. Soc. for Metals, Cleveland, Ohio. p.259.

Elliot, D., 1973: Diffusional flow laws in metamorphic rocks; Geol. Soc. Am. Bull., v.84, p.2645-2664.

Ellwood, B.B., 1975: Analysis of Emplacement Mode in Basalt from DSDP Holes 319A and 321 Using Anisotropy of Magnetic Susceptibility; J. Geophys. Res., v.80. p.4805-4808.

Ellwood, B.B., 1979: Anisotropy of Magnetic Susceptibility Variations in Icelandic Columnar Basalts; Earth Planet. Sci. Lett., v.42, p.209-212.

Elwood, B.B. and Ledbetter, M.T., 1979: Paleocurrent Indicators in Deep-sea Sediment; Science, v. , p.1335-1337.

Ferguson, C.C., 1983: Composite Flow Laws Derived from High

Temperature Experimental Data on Limestone and Marble; Tectonophysics, v.95, p.253-266.

Flinn, D., 1962: On folding during three-dimensional progressive deformation; Quarterly J. Geol. Soc. Lond., v.118, p.385-433.

Friedman, M., 1963: Petrofabric Analysis of Experimentally Deformed Calcite-Cemented Sandstones; J. Geol., v.71, p.12-37.

Friedman, M., Teufel, L.W. and Morse, J.D., 1976: Strain and stress analyses from calcite twin lamellae in experimental buckles and faulted drape-folds; Phil. Trans. R. Soc. London. Ser. A., v.283, p.87-107.

Friedman, M. and Higgs, N.G., 1981: Calcite Fabrics in Experimental Shear Zones; in N.L. Carter, M. Friedman, J.M. Logan and D.W. Stearns, Editors, Mechanical Behavior of Crustal Rocks. Geophys. Monogr. 24, Am. Geophys. Union, p.11-27.

Ghosh, S.K. and Ramberg, H., 1976: Reorientation of inclusions by Combination of Pure and Simple Shear; Tectonophysics, v.34, p.1-70.

Graham, J.W., 1954: Magnetic susceptibility anisotropy, an unexploited petrofabric element; Bull. Geol. Soc. Am., v.65,

p.1257-1258.

Graham, J.W., 1966: Significance of magnetic anisotropy ion Appalachian sedimentary rocks; in J.S. Steinhard and T.J. Smith (Editors) The Earth Beneath the Continents. Geophys. Monogr. 10, Am. Geophys. Union. p.627-648.

Griggs, D.T. and Blacic, J.D., 1965: Quartz: anomalous weakness of synthetic crystals; Science, v.147, p.292-295.

Guiu, F. and Pratt, P.L., 1964: Stress Relaxation and the Plastic Deformation of Solids; Physica Status Solidi, v.6, p.111-120.

Gupta, I. and Li, J.C.M., 1970: Stress relaxation, internal stress and work hardening in LiF and NaCL crystals; Mater. Sci. Eng., v.6, p.20-26.

Hadizadeh, J. and Rutter, E.H., 1983: The low temperature brittle-ductile transition in a Quartzite and the occurrence of cataclastic flow in nature; Geol. Rundsch., v.72, n.2, p.493-509.

Haimson, B.C., 1975: The state of stress in the Earths Crust; Rev. Geophys. Space Phys., v.13, p.350-352.

Halvorsen, E., 1974: The Magnetic Fabric of Some Dolerite

Intrusions, NE. Spitsbergen, Implications for their mode of Emplacement; Earth Planet. Sci. Lett., v.21, p.127-133.

Hamilton, N. and Rees, A.I., 1971: The Anisotropy of Magnetic Susceptibility of the Franciscan Rocks of the Diablo Range, Central California; Geol. Rundsch., v.60, p.1103-1124.

Hamilton, N., Owens, W.H. and Rees, A.I., 1968: Laboratory Experiments on the Production of Grain Orientation in Shearing Sand; J. Geol., v.76, p.465-472.

Hennig-Michaeli, C. and Siemes, H., 1975. Zwillugsgleitung beim Magnetit; Neues Jahrb. Mineral. Abh., v.123, p.330-334.

Hobbs, B.E., 1968: Recrystallization of single crystals of quartz; Tectonophysics, v.6, p.353-401.

Hrouda, F., 1976: The origin of cleavage in the Light of Magnetic Anisotropy Investigations; Phys. Earth Planet. Interiors, v.13, p.132-142.

Hrouda, F. and Janak, F., 1976: The Changes in Shape of the Magnetic Susceptibility Ellipsoid During Progressive Metamorphism and Deformation; Tectonophysics, v.34, p.135-148.

Hrouda, F., Janak, F. and Rejl, L., 1978: Magnetic Anisotropy and Ductile Deformation of Rocks in zones of Progressive Regional Metamorphism; Gerl. Beitr. Geophys., v.87, p.126-134.

Hrouda, F., 1982: Magnetic Anisotropy of Rocks and its application in Geology and Geophysics; Geophysical Surveys, v.5, p.37-82.

Hull, D., 1965: Introduction to dislocations. Pergamon Press, Oxford. 2nd Edition. 259 pages.

Ising, E.,1942: On the Magnetic Properties of Varved Clay; Arkiv Astron. Fysik, v.29A, n.5, p.1-37.

Janak, F., 1972: Magnetic susceptibility anisotropy of various rock types and its significance for geophysics and geology; Geophys. Prospect., v.20, p.375-384.

Jelinek, V., 1981: Characterization of magnetic fabrics of rocks; Tectonophysics, v.79, p.T63-T67.

Kern, J.W., 1961: Th effect of stress on the susceptibility and magnetization of a partially magnetized multidomain system; J. Geophys. Res., v.66, p.3807-3816.

Kligfield, R., Owens, W.H. and Lowrie, W., 1982: Magnetic

susceptibility anisotropy, strain and progressive deformation in Permian sediments from the Maritime Alps (France); Earth Planet. Sci. Lett., v.55, p.181-189.

Klug, P. and Wittman, F., 1970: The correlation between creep deformation and Stress Relaxation in Concrete; Materiaux et Constructions; essais et recherches, v.3, n.14, p.75-80.

Knapp, S.T., Friedman, M. and Logan, J.M., 1987: Slip and Recrystallization of Halite gouge in Experimental Shear Zones; Tectonophysics, v.135, p.171-183.

Kolofikova, O., 1976: Geological Interpretation of Measurements of Magnetic Properties of Basalts on Example of the Chribsky Les Lava Flow of the Velky Roudny Volcano (Nizky Jesenik); Cas. Mineral. geol., v.21, p.387-396.

Means, W.D., 1977: A Deformation experiment in Transmitted Light; Earth Planet. Sci. Lett., v.35, p.169-179.

Muller, P. and Siemes, H., 1972: Zur Festigkeit und Gefugeregulung von experimentell verformten Magnetiterzen; Neues Jahrb. Mineral. Abh., v.117, p.39-60.

Nagata, T., 1964: Magnetic Susceptibility of Compressed Rocks;

Journal of Geomagnetism and Geoelectricity, v.48, p.73-80.

Nagata, T., 1970: Anisotropic Magnetic Susceptibility of rocks under Mechanical Stress; Pure and Applied Geophysics, v.78, p.110-122.

Nicolas, A. and Poirrer, J.P., 1976: Crystalline Plasticity and Solid State Flow in Metamorphic Rocks. Wiley-Interscience, Toronto. 444 pages.

Neville, A.M. 1981: Properties of Concrete. 3rd Edition. Copp Clark Pitman, Toronto. 779 pages.

Owens, W.H. and Bamford, D., 1976: Magnetic, seismic, and other anisotropic properties of rock fabrics; Phil. Trans. R. Soc. London Ser. A., v.283, p.55-68.

Owens, W.H. and Rutter, E.H., 1978: The Development of Magnetic Susceptibility Anisotropy through Crystallographic Prefferred Orientation in a Calcite Rock; Physics of the Earth and Planetary Interiors, v.16, p.215-222.

Paterson, M.S., 1976: Some current aspects of experimental rock deformation; Phil. Trans. R. Soc. London Ser. A., v.283, p.163-172.

Paterson, M.S. 1978: Experimental Rock Deformation - The Brittle Field. Minerals and Rocks 13. Springer-Verlag, New York. 254 pages.

Paterson, M.S., 1987: Problems in the extrapolation of Laboratory Rheological Data; Tectonophysics, v.133, p.33-43.

Phakey, P., Dollinger, G. and Christie, J., 1972: Transmission electron microscopy of experimentally deformed Olivine crystals; in Flow and Fracture of Rocks. Am. Geophys. Union, Geophys. Monograph 16, p.117-138.

Porath, H., Stacey, F.D. and Cheam, A.S., 1966: The choice of Specimen shape for magnetic anisotropy measurements of rocks; Earth Planet Sci. Lett., v.1, p.92.

Porath, H., 1968: The Magnetic Anisotropy of the Yampi Sound Hematite Ores; Pure Appl. Geophys., v.69, p.168-178.

Ramsay, J.G., 1967: Folding and Fracturing of Rocks, McGraw-Hill, New York. 568 pages.

Ramsay, J.G. and Wood, D.S., 1973: The Geometric Effects of Volume Change During Deformation Processes; Tectonophysics,

v.16, p.263-277.

Ramsay, J.G. and Huber, M.I., 1983: The Techniques of Modern Structuaral Geology-Volume 1: Strain Analysis. Academic Press, New York. 307 pages.

Rathore, J.S., 1979: Magnetic susceptibility anisotropy in the Cambrian Slate Belt of N. Wales and correlation with strain; Tectonophysics, v.53, p.83-98.

Rathore, J.S., 1980: Evidence for Sinistral Movements along the Judicarian Line drawn from a study of Magnetic Fabrics in the Regions of Mt. Croce and Asten (South Tyrol); Geol. Rundsch., v.69, p.674-694.

Rathore, J.S. and Becke, M., 1980: Magnetic Fabric Analyses in the Gail Valley (Carinthia, Austria) for the Determination of the sense of movements along this region of the Periadriatic Line; Tectonophysics, v.69, p.349-368.

Rathore, J.S. and Henry, B., 1982; Comparison of strain and magnetic fabrics in Dalradian rocks from the southwest Highlands of Scotland; J. Struct. Geol., v.4, p.373-384.

Rathore, J.S., Courriox, G. and Choukroune, P., 1983; Study of

ductile shear zones (Galicia, Spain) using texture goiometry and magnetic fabric methods; Tectonophysics, v.98, p.87-109.

Rees, A.I., 1966: The Effects of Depositional Slopes on the Anisotropy of Magnetic Susceptibility of Laboratory Deposited Sands; J. Geol., v.74, p.856-867.

Rees, A.I. and Woodall, W.A., 1975: The Magnetic Fabric of some Laboratory-deposited Sediments; Earth Planet. Sci. Lett., v.25, p.121-130.

Rutter, E.H., 1972: The influence of inerstitial water on the rheological behaviour of calcite rocks; Tectonophysics, v.14, p.13-33.

Rutter, E.H. 1976: The Kinetics of rock deformation by Pressure Solution; Phil. Trans. R. Soc. London Ser. A, v.283, p.203-219.

Rutter, E.H. and Mainprice, D.H., 1978: The effect of Water on Stress Relaxation of Faulted and Unfaulted Sandstone; Pure and Applied Geophysics, v.116, p.634-654.

Rutter, E.H., Atkinson, B.K. and Mainprice, D.H., 1978: On the use of the stress relaxation testing method in studies of the mechanical behaviour of geologic materials; Geophys. J. R. Astron.

Soc., v.55, p.155-170.

Rutter, E.H., Peach, G.J., White, S.H. and Johnston, D., 1985: Experimental 'syntectonic' hydration of Basalt; J. Struct. Geol. v.7, n.2, p.251-266.

Sbar, M.L. and Sykes, L.R., 1972: Contemporary compressive stress and sensitivity in eastern North America; Geol. Soc. Am. Bull., v.84, p.1861-1882.

Schmid, S.M., 1976: Rheological evidence for changes in the deformation mechanism of Solnhofen Limestone towards low stresses; Tectonophysics, v.31, p.T21-T28.

Schwarz, E.J., 1974: Magnetic Fabric in Massive Sulphide Deposits; Can. J. Earth Sci., v.11, p.1699-1675.

Singh, J., Anderson, D.J. and Tarling, D.H., 1975: The magnetic susceptibility anisotropy of deformed rocks from North Cornwall, England; Tectonophysics, v.27, p.141-153.

Stupavsky, M., 1983: SI-1 Magnetic Susceptibility Instrument Handbook, Saphire Instruments, P.O. Box 385, Ruthven, Ont., Canada. 92 pages.

Tullis, J., 1978: Processes and conditions of mylonite formation as inferred from experimental deformation studies; Geol. Soc. Am. Short Course, Mylonites Natural and Experimental. Boston, March 7 & 8, 1978.

White, S., 1976: Estimation of strain rates from microstructural features; Q.J. Geol. Soc. London, v.133, p.577-583.

Wood, D.S., Oertel, G., Singh, J. and Bennett, H.F., 1976; Strain and anisotropy in rocks; Phil. Trans. R. Soc. London, Ser. A., v.283, p.27-42.

Wyss, M., 1970: Stress estimates for South American shallow and deep earthquakes; J. Geophys. Res., v.75, p.1529-1544.

APPENDIX A

BASIC PROGRAM "NATSR"; G. Borradaile & C. Alford (22/10/85)

Another version of this program exists: "DISPR" for constant displacement rate.

BASIC LINE(S): note in this version of basic (AIM) variable/constant names are only recognised by the first two characters.

01 PROGRAM TITLE

10 Turns off the analog output converter and hence the pump motor (when in remote mode). The converter output is held at zero volts until USR(9) is called. Also sets K% used in the time loop to zero.

Allows user to account for the cross-sectional area change through the specimen during constant volume deformation (QA set to 1) if not desired (QA=0) at the beginning of the experiment, it can be later accounted for (see line 910) presumably after volume change in the specimen has ceased.

12-19 Allows user to set the variable parameters of specimen length and diameter, confining pressure, specimen shortening due to confining pressure, strain rate and percent strain to be achieved. Also sets the averaging time desired per printout of strain rate and sets a voltage factor which is necessary

in altering the speed of the pump when the strain rate is outside the possible rates attainable by the present upper and lower voltages. (A good voltage factor is 0.7, when strain rate is 5×10^{-6} sec^{-1} for Berea sandstone with time gap of 40 seconds). These can be changed during a test, see line 902-908.

20 Sets a 10% window about the desired strain rate (ED), defined by 5% below ED (the lower estimate LE) and 5% above (the upper estimate UE).

21 Calculates the area (AR) of cross-section of the cylindrical specimen.

22-23 Sets the constants of machine distortion in inches/volt. Note - these will differ for individual apparatus. (constant k1 x k2 = k12).

24 Calculates the specimen length under confining pressure: Sets LØ equal to this length.

26-29 Sets to zero several parameters.

30 Informs the computer to go to a gain setting subroutine at 1500.

(subroutine) 1500 to 1550 — Allows user to set the gains for the load and displacement channels. The gains are set at 1, 10 or 100. This subroutine can also be used to alter the gains settings during an experiment when CA=1. The later part of the subroutine allows the user to adjust the position of the linear variable differential transformer (LVDT) so that the displacement 'D' value on the screen is close to zero. When this is done , press "E" and the program will return to line 60.

60 — Sets CA=1

62-70 — Reads the average initial load valve over a period of 10 loops, so reducing the effect of voltage fluctuations. This initial load will later be used as the "zero" point for calculating the axial differential load on the specimen during the experiment.

102-112 — Starts the pump with a voltage proportional to the integer "8000" thus the pump will start at a high speed and should give the specimen a good seating.

113 — Sets values for the upper voltage (UV) and the lower voltage (LV). These are an estimate of the voltages which will produce strain rates bracketing the desired strain-rate.

120-134 . Reads the average displacement and load values and sets any previous strain rate (S2) to S1.

136-142 Commands the computer to display the current displacement and load values on the screen.

150-165 The time loop. This introduces a delay of a desired integral number of seconds (the time gap-DT%) before reading the new displacement and load voltages. The counter GB keeps a total of the number of seconds passed during the averaging time.

500-512 Reads the new displacement and load at the end of the delay time, DT%.

514 If for some reason (electronic fluctuation) the new displacement is less than the old one, then the computer will subtract 1 from AK% and go back and read displacement and load all over again, thereby allowing proper control of the strain rate.

515 If it is the first recording of displacement and load in an averaging time (AK%=1) then the computer will store the load value (L1) for later calculation of the change in differential stress over an averaging time.

520 Prints the new displacement and load on the screen.

600-630 Calculates the strain rate over the time interval DT. The total displacement measured (Y) is a combination of machine distortion (Z) and the shortening of the specimen (D). The distortion of the machine must be subtracted from the total displacement to give the actual displacement of the specimen (D=Y-Z).

If for some reason D is less than zero (Z>Y) then the strain rate is fixed at zero (negative values not permitted).

632 Displays the strain rate on the screen.

634 Sums the strain rates.

636 Sets the strain-rate SR equal to S2 for purposes of comparison with the previous strain rate, S1.

640 When the number of strain rates desired (AT) have been recorded this line informs the computer to go to the strain rate averaging subroutine.

(subroutine)

980-1010 Strain rate averaging subroutine where the cross-section area of the specimen is modified if QA=1 and the

average strain rate (ASR), the percentage shortening (RS), the axial differential load on the specimen (W), the change in axial differential load (SG) and the total time in seconds (GB) are calculated and are printed.

700-901 Refer to section and flow chart on the "Funnel" procedure. This essentially sends a voltage to the pump, which produces a small deformation for which the strain rate is determined. If it does not produce the suitable strain rate it reduces or increases the voltage by using the average of the last lowest and present voltage or by using the average of the present voltage and the last highest voltage respectively.

902-910 If, during the experiment any of the input parameters need to be changed, this can be accomplished by pressing the appropriate key.
(S = strain rate, T = time gap, V=voltage factor, E=% strain, A=time over which average strain rate is fixed, G=the gains, F1=break from program).
"C" is depressed if the correction for change of cross-sectional area is desired from that time onwards. Furthermore, if the user wishes to perform a stress relaxation text, "R" is depressed (see line 1990).

911 Determines the percent strain that has occured. It if is greater than that desired (PS) the program returns to line 10 and stops the pump, ending the experiment.

922 If the percent strain that has occured is less than that desired the computer returns to line 120.

1990 Begins the stress relaxation program.

1991 STOPS THE PUMP

1992 Inputs the elastic rock compliance value (KR) for the material. (See notes).

1993 If the correction for change in cross-sectional area had not already been made, the computer now begins to make the correction.

1994-1995 Informs the computer to turn on the printer so that subsequent calls of the print statement will output data to the printer as well as the display.

1997-2003 Calculated and prints the percent strain of the specimen and the axial differential stress acting at the start of stress relaxation.

2004 Remark to remind the user to close valve 6, thus locking the lower piston into place with respect to σ_{max}.

2005-2009 Sets the time gap (TG%) over which readings of displacement and load change are made. Initially the value is set at 10 seconds, afterwards the time gap is set according to the rate of strain to allow for optimum machine performance (see notes).

2010-2015 Reads the average displacement and load values.

2020-2040 The time loop. Performs the same function as the time loop on the main program (lines 150-165) with the option to return to the main program, if "0" Key is depressed. The time loop will be repeated a number of times equal to the value of CA which is dependent upon the strain rate (lines 2400-2404).

2045-2055 Reads the new displacement and load at the end of the desired delay time.

2060-2068 Calculates the strain rate over the set time interval, T6%. the displacement measured (DD) will not account for total shortening of the specimen (SD), which is a sum of the displacement measured, the elastic compliance of the machine (2) and the elastic compliance of the rock (KR). See notes.

2069 If for some reason (electronic fluctuation) the SR is calculated to be negative the computer is instructed to return to 2010.

2070 Determines the new length of the specimen.

2071 Determines the new area of cross-section of the specimen.

2072-2076 Calculates the axial differential stress (DS) and the change in DS over the delay time.

2111-2118 Prints the strain rate, the change in axial differential stress, the new area of cross-section, the average axial differential stress and the time elapsed in seconds.

2400-2404 Since the maximum allowable time gap is 32767 seconds and the amount of time necessary for strain rates below 1.84×10^{-8} exceeds this, it is necessary to set the counter CA to an increasingly greater value as the strain rates decrease. This counter represents the amount of times the time gap must be repeated for the proper duration of time to elapse.

2406 When the SR rate has decreased below 1.0×10^{-9} sec^{-1} the precision/accuracy of the reading is in question due to the lengthy period of time between readings. Thus the experiment is terminated.

2500 Informs the computer to return to line 2006.

3000 END.

The funnel procedure (lines 700-710 and 800-808)

This is the procedure for adjusting the voltage output to the pump so that the strain rate (SR) is adjusted to be close to that desired (ED).

Basic Theory

We can consider the unknown relationship between strain-rate and input voltage on a graph (Fig. 1).

The desired strain rate is ED, with a range of acceptability UE to LE where UE=1.05 x ED and LE=0.95 x ED (line 20).

Initially a high voltage is input to the pump and the strain rate determined (A on graph). Then a low voltage is input and the strain rate is redetermined (B on graph).

A new voltage is chosen which is the average of the two first input voltages (Upper voltage UV_1 and Lower voltage LV_1). This average voltage causes a certain strain-rate which is determined as SR1 (point C on graph).

By now the properties of the rock could have changed and the new relationship between voltage and strain-rate may be elsewhere (see graph). If SR_1 was too low (<ED) then the last input voltage $(LV_1 + UV_1)2$ now becomes the new low voltage LV_2 and the old UV_1 becomes the new UV_2. Another voltage is input to the pump which is the average of UV_2 and LV_2. This causes a strain A13

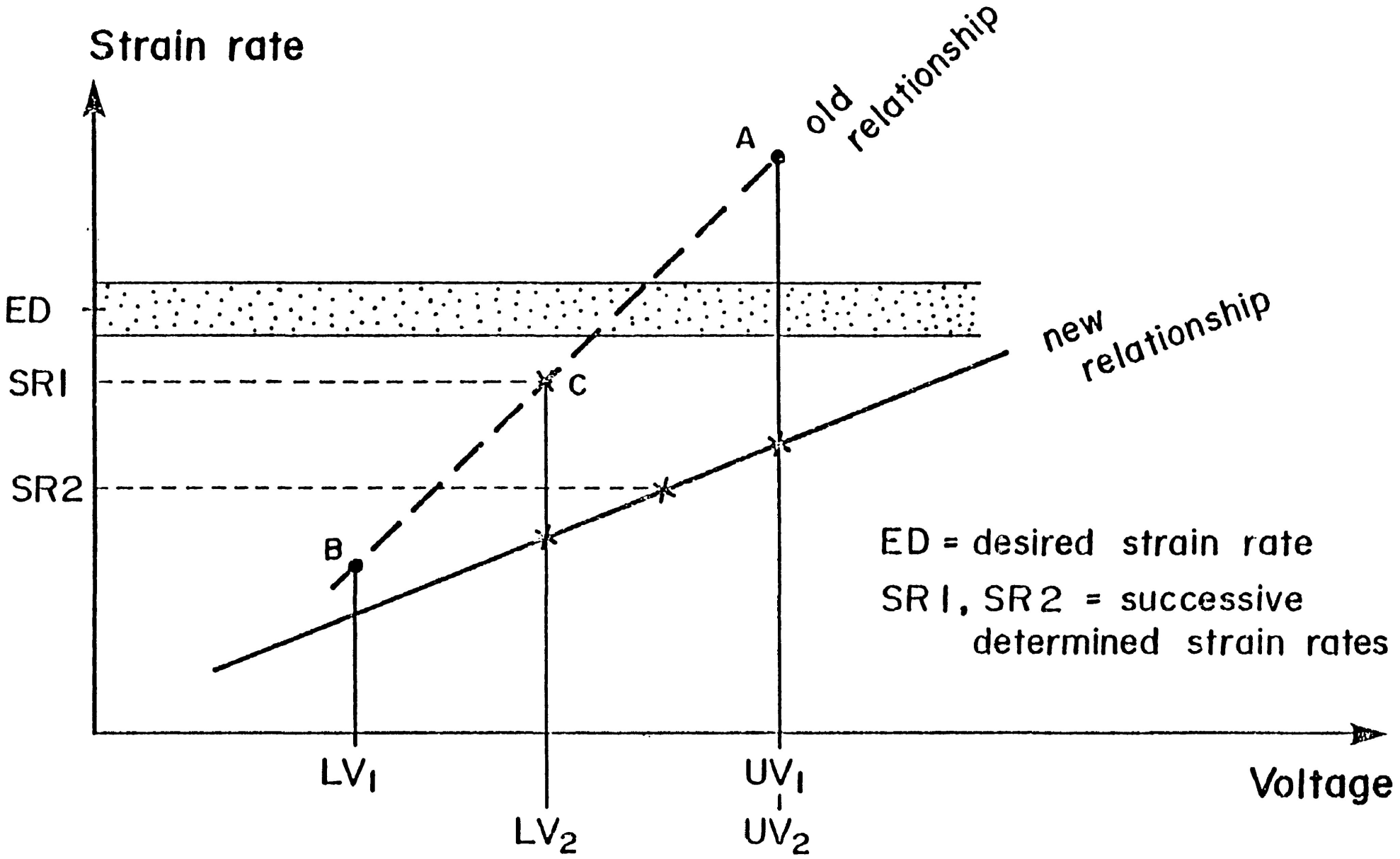
Strain rate
old relationship
A
ED
SR1
C
new relationship
SR2
B
ED = desired strain rate
SR1, SR2 = successive determined strain rates
LV1
LV2
UV1
UV2
Voltage

Figure A1.

rate SR_2. In a troublesome case as shown, $SR_2 < SR_1$, which is even further away from ED. Thus the upper voltage UV_2 is increased by a factor VF to LV_2 x (2-VF) (line 807).

The procedure is then repeated. This procedure continually attempts to restore a strain rate which is close to ED; if the strain rate lies between UE and LE the voltage to the pump is not changed. However, in that situation the rock properties will eventually change and a new relationship on the strain-rate versus voltage graph will cause the strain rate to wander outside the limits of acceptibility on either side of ED. Then the funnel procedure, outlined above, is again invoked.

Note that the procedure works also if the determined strain-rates are too high, but then in the worst case successive strain rates SR_2 and SR_1 are progressively higher than ED, and the lower voltage is reduced by the factor VF, thus becoming LVxVF (line 805).

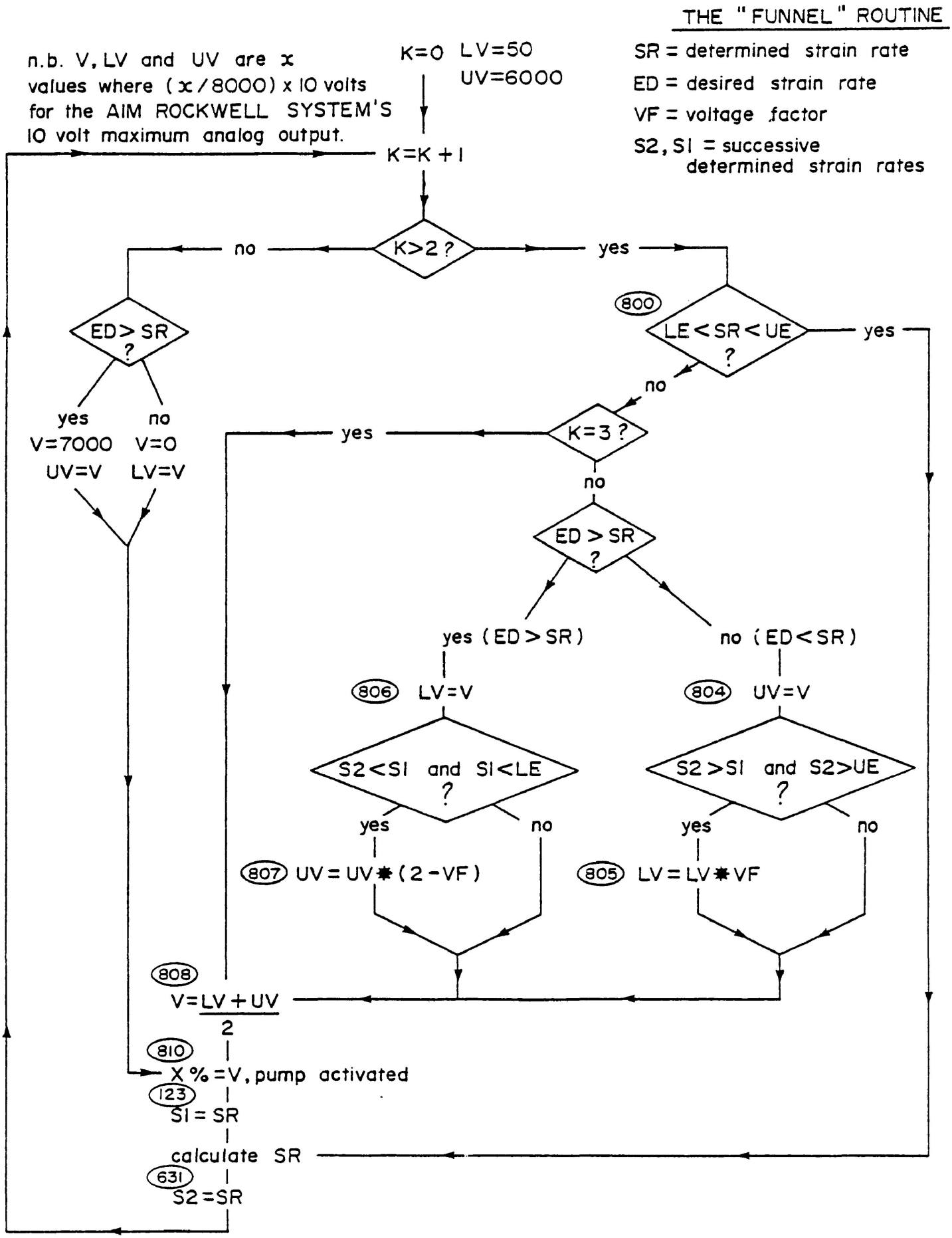
THE "FUNNEL" ROUTINE
SR = determined strain rate
ED = desired strain rate
VF = voltage factor
S2, S1 = successive determined strain rates
n.b. V, LV and UV are x values where (x/8000) x 10 volts for the AIM ROCKWELL SYSTEM'S 10 volt maximum analog output.
K=0 LV=50 UV=6000
K=K+1
K>2 ?
no
yes
ED > SR ?
yes V=7000 UV=V
no V=0 LV=V
800
LE < SR < UE ?
yes
no
K=3 ?
yes
no
ED > SR ?
yes (ED > SR)
no (ED < SR)
806 LV=V
804 UV=V
S2<S1 and S1<LE ?
S2>S1 and S2>UE ?
yes
no
807 UV = UV * (2 - VF)
805 LV = LV * VF
808
V = LV + UV / 2
810
X % = V, pump activated
123
S1 = SR
calculate SR
631
S2 = SR

Figure A2.

The correction for apparatus distortion

The apparatus distortion is given by the constant K_{12} (=K1xK2) and the change in load L_2-L_1.

thus: $K_{12} \times (L_2-L_1)$. (line 616 Z=L2-L1)

Note that the load may increase or decrease. The displacement measured (D_2-D_1), is always > 0 (except for electronic fluctuations), and is the sum of the effects of apparatus distortion and rock distortion.

Given: total distortion $s = s_2-s_1$

apparatus distortion $a = a_2-a_1$

rock distortion $r = r_2-r_1$

we can idedntify the following conditions.

$s_2-s_1=(r_2-r_1) + (a_2-a_1)$ (load increasing)

or

$+ (a_1-a_2)$ (load decreasing)

?. $s_2-s_1 = r_2-r_1$ no apparatus distortion, since no change in load.

. $s_2-s_1 = (a_2-a_1) - (r_1-r_2)$ because apparatus distortion has now changed sense such that it helps rock deformation.

Thus we use 622:

$$D = ABS\ (Y - Z)$$

where $Y=f\ (D_2-D_1)$

$Z=f\ (L_2-L_1)$

The changes in sign in lines (1) to(3) above are taken care of by the signs of Y and of Z.

PROGRAM SYMBOLS

Specimen parameters

OL original length (under P_c also)

OD original diameter

DP apparent shortening due to P_c

LO = current length of specimen

VL volume of specimen

AR = area of the end of the cylindrical specimen

XR = elastic compliance of rock type

RS = present total axial strain on the specimen

Condition parameters

PC = the confining pressure in psi

DS,W = the axial differential stress in bars

SG the change on axial differential stress in bars over the averaging time

SR = the current strain rate

ASR = the average strain rate over the averaging time

Program Parameters

(Variables with certain values which cause the operation of certain parts of the program)

involved with gain setting subroutine and the large time gap necessary for strain-rates less than 1.84 E-8.
(necessary because the AIM computer will not count in a loop involving more than approximately 32,000 cycles).

involved in area correction during shortening of the specimen.

K% = counter involved in early stages of voltage setting for motor control.

PS total percent strain of specimen desired, program will end if value exceeded.

" set value of strain rate

Counters: AK% counts number of times through time loop

J% used in time loop

N used for reading average values of displacement and load

GB adds accumulated time in seconds during an averaging time

LSUM, DSUM = sums the load and displacement readings

SSR = sums the strain rate readings

Performance Parameters

(Values which contribute to the accuracy and performance of the program)

X%,V — the output voltage to the parajust motor control unit

' ' — the lower limit of rate of strain permissable before a change of voltage

the upper limit of rate of strain permissable fore a change of voltage

the factor in which the voltage is ultiplied according to the comparison of S2 + S1

S2 — the current strain rate

S1 — the previous strain rate

displacement gain setting

load of gain relating to channel 0 (Displacement)

value of gain relating to channel 1 (Load)

PD,PL — numbers which sets the gain for one channel of the analog to digital converter

TG%,DT% = value of delay time between readings of displacement and load, set according to machine accuracy needs

the averaging time over which the data is calculated

the previous voltage to the parajust that was less than the current voltage

the previous voltage to the parajust that was greater than the current voltage

Calculation Variables (values used in the calculation of strain rate etc.)

Y,DD = the total displacement in inches measured by the LVDT during a time gap loop

the displacement of the LVDT caused by machine distortion during a time gap loop

D,SD = the change in length of the specimen in inches during a time gap loop

the new axial load in lb/in^2 after an averaging time

the average value of axial load during a time gap loop for stress relaxation

LVDT and Load Cell Output (in volts)

the value of the Linear Voltage Displacement Transducer at the beginning of a time gap loop.

the value of the LVDT at the end of a time gap loop.

L1 = the value of axial load at the start of a time gap loop.

L4 the value of axial load at the beginning of a averaging time loop.

L2 the value of axial load before the pistons begin to advance (equal to P_C).

the value of axial load at the end of a time gap and/or averaging time loop.

Machine constants

K12 = the machine distortion value for increases in differential stress

K3 = the displacement constant for the LVDT

K4 = the machine distortion value for increases in confining pressure

For load cell TP 795 and the standard pressure vessel without extension piece for high temperature work, the following are examples of the values in the Fall of 1985:

K12 = 1.897 in/volt

(note the AIM BASIC Complier only recognises variables or constants with two characters but K12 is still used to remind us that K12 = K1 x K2).

The actual apparatus constant K1 = 189.7 x 10^{-8} in/lb. K2 = 10^{6}, is a factor due to the fact that the input to the load cell is adjusted so that the loadcell's output is 1mVolt per 1000 lbs of load (hence 10^{6} lbs/volt).

K3 = 0.1374

K4 = 1.897 x 10^{-7} in/p.s.i. (K4 is derived from an apparatus constant which is approximately 0.1 x K12).

Specimen constant (KR)

For stress relaxation texts, that use the last part of the program, i is necessary to know the elastic constant for the rock. This is usually obtained from the unloading curve of a sample of the rock.

As an example, for the cemented sand-magnetite mixture used by Corradaile and Alford in the Summer and Fall of 1985 KR = 0.201 in/volt.

CONSTANT STRAIN-RATE PROGRAM

```
 1  REM..NATSR WITH AR CHANGE & STRESS RELAX
10  A=USR(12): K%=0
11  INPUT "AREA CHANGE, 1/0";QA
12  INPUT "CONFINING PRESSURE IN PSI";PC
13  INPUT "TIME GAP";DT%
14  INPUT "AVERAGING TIME";AT
15  INPUT "VOLTAGE FACTOR";VF
16  INPUT "ORIGINAL LENGTH";OL: INPUT "SHORTENING UNDER
PC";DP
17  INPUT "DIAMETER";OD
18  INPUT "STRAIN RATE";ED
19  INPUT "PERCENT STRAIN";PS
20  UE=1.05*ED:LE=0.95*ED
21  AR=3.1416*(OD/2)*(OD/2)
22  K12=1.897
23  K3=.1374:K4=1.897E-7
24  OL=OL-DP+ (PC*K4): LO=OL
26  AK%=0: VL=OL*AR
27  SSR=0
28  ASR=0
29  CA=0:GB=0
30  GOTO 1500
```

```
60 CA=1
62 LSUM=0
64 FOR M=1 TO 10
66 L3=USR(.1): LSUM=LSUM+L3
68 NEXT M
70 L3=LSUM/10.0
102 REM..START PUMP
110 A=USR(9)
112 A=USR(4096*6+8000)
113 UV=7000:LV=50
120 REM..READ DISPL & LOAD
122 DSUM=0: LSUM=0
123 S1=S2
124 FOR M=1 TO 10
126 D1=USR(0): DSUM=DSUM+D1
128 L1=USR(1): LSUM=LSUM+L1
130 NEXT M
132 D1=DSUM/10.0
134 L1=LSUM/10.0
136 A=USR(10)
142 PRINT D1;L1
150 REM..START TIME GAP LOOP
152 GB=GB+DT%
```

```
155 J%=0: K%=K%+1
156 AK%=AK%+1
160 IF (USR(8))=0 THEN J%=J%+1
162 IF J%=DT% THEN 500
165 GOTO 160
500 DSUM=0: LSUM=0
502 FOR M=1 TO 10
504 D2=USR(0): DSUM=DSUM+D2
506 L2=USR(1): LSUM=LSUM+L2
508 NEXT M
510 D2=DSUM/10.0
512 L2=LSUM/10.0
514 IF D2<D1 THEN AK%=AK%-1: GOTO 120
515 IF AK%=1 THEN L4=L1
520 PRINT D2;L2
600 REM..CALC STRAIN RATE
609 REM..TOTAL DISPL
610 Y=((D2-D1)/4096)*(10/GD)*K3
612 REM..MACH DISTORTION
616 Z=((L2-L1)/4096)*(10/GL)*K12
620 REM..REAL DISPL
622 D=Y-Z
624 IF Z>Y THEN D=0
```

```
626 DT=DT%
628 SR=(D/LO)/DT
630 LO=LO-D
632 PRINT SR
634 SSR=SSR+SR
636 S2=SR
640 IF AK%>=AT THEN 980
700 IF K%>2 THEN 800
702 IF ED<SR THEN V=1: LV=V
706 IF ED>SR THEN V=7000: UV=V
710 GOTO 810
800 IF SR<UE AND SR>LE GOT 902
802 IF K%=3 GOTO 808
804 IF ED<SR THEN UV=V
805 IF S2>S1 AND S1>UE THEN LV=LV*VF
806 IF ED>SR THEN LV=V
807 IF S2<S1 AND S1<LE THEN UV=UV*(2-VF)
808 V=(LV+UV)/2.0
809 IF V>8100 THEN V=8100
810 X%=V
900 REM..OUTPUT VOLTAGE TO PUMP
901 A=USR(4096*6+X%)
902 GET A$
```

```
903  IF A$="S" THEN INPUT "STR RATE";ED:
UE=1.05*ED:LE=ED*0.95
904  IF A$="T" THEN INPUT "TIME GAP";DT%
905  IF A$="V" THEN INPUT "VOLTAGE FACTOR";VF
906  IF A$="E" THEN INPUT "PERCENT STRAIN";PS
907  IF A$="A" THEN INPUT "AVERAGING TIME";AT
908  IF A$="G" THEN 1500
909  IF A$="R" THEN 1990
910  IF A$='C" THEN QA=1: VL=L0*AR
911  IF PS<((1-(L0/0L))*100) THEN 10
922  GOTO 120
980  IF QA=1 THEN AR=VL/L0
982  DK=(((L2-L4)/4096)*(10/GL)*1E6)/AR
985 SG=DK/14.5
1000  ASR=SSR/AK%
1001  RS=(1-(L0/0L))*100
1002  W=(((L2-L3)/4096)*(10/GL)*1E6)/AR
1003  W=W/14.5
1004  A=USR(14)
1005  PRINT "A.S.R.=";ASR
1006  PRINT "RS=";RS
1007  PRINT "DS=";W
1008  PRINT "DELTA DS=";SG: PRINT "TIME=";GB
```

```
1009 SSR=0: AK%=0
1010 GB=0: GOTO 700
1500 REM..SET GAINS
1502 INPUT "DISPL GAIN";GD
1504  INPUT "LOAD GAIN";GL
1506 IF GD=1 THEN G0=0
1508 IF GL=1 THEN G1=0
1510 IF GD=10 THEN G0=1
1512 IF GL=10 THEN G1=1
1513 IF GD=100 THEN G0=2
1514 IF GL=100 THEN G1=2
1524 PD=64*G0+0
1526 PL=64*G1+1
1528 A=USR(4096*1+PD)
1530 A=USR(4096*1+PL)
1532 IF CA=1 THEN 911
1534 DSUM=0
1536 FOR M=1 TO 5
1538 D3=USR(0): DSUM=DSUM+D3
1540 NEXT M
1542 D3=DSUM/5.0
1544 A=USR(10)
1546 PRINT D3
```

```
1548 GET A$: IF A$="B" THEN 60
1550 IF A$="" THEN 1534
1990 REM..STRESS RELAXATION
1991 A=USR(12)
1992 INPUT "ROCK CONSTANT";KR
1993 IF QA=0 THEN VL=L0*AR: QA=1
1994 A=USR(9)
1995 A=USR(14)
1997 LSUM=0
1998 FOR M=1 TO 8
1999 L5=USR(1): LSUM+L5
2000 NEXT M
2001 L5=LSUM/8.0
2002 RS=(1-(L0/0L))*100: PRINT "RS=";RS
2003 DS=((((L5-L3)/4096)*(10/GL)*1E6)/AR)/14.5: PRINT
"DS=";DS
2004 PRINT "CLOSE VALVE 6!!"
2005 TG%=10: GOTO 2010
2006 TG%=(6.0E-4/SR)/CA
2010 DSUM=0: LSUM=0
2011 FOR M=1 TO 20
2012 D1=USR(0): DSUM=DSUM+D1
2013 L1=USR(1): LSUM=LSUM+L1
```

```
2014 NEXT M
2015 D1=DSUM/20.0: L1=LSUM/20.0
2020 REM..TIME GAP
2025 J%=0
2026 IF (USR(8))=0 THEN J%=J%+1
2028 IF J%=TG% THEN 2040
2029 GET A$: IF A$="0" THEN CA=1: GOTO 102
2030 GOT 2026
2040 NEXT M
2045 DSUM=0: LSUM=0
2046 FOR M=1 TO 20
2048 D2=USR(0): DSUM=DSUM+D2
2050 L2=USR(1): LSUM=LSUM+L2
2051 NEXT M
2055 D2=DSUM/20.0: L2=LSUM/20.0
2060 REM..CALC STR RATE & DIFF STRESS
2061 Z=((L2-L1)/4096)*(10/GL)*K12
2062 DD=((D2-D1)/4096)*(10/GD)*K3
2063 SD=DD-Z-((KR*Z)/K12)
2064 LL=((L2+L1)/2)-L3
2066 LL=(LL/4096)*(10/GL)*1E6
2068 SR=((SD/L0)/TG%)/CA
2069 IF SR<0 THEN 2010
```

```
2070 L0=L0-SD
2071 AR=VL/L0
2072 DS=(LL/14.5)/AR
2075 DK=(((L2-L1)/4096)*(10/GL)*1E6)/AR
2076 SG=DK/14.5
2111 PRINT "SR=";SR
2113 PRINT "DELTA DS=";DS
2114 PRINT "AR=";AR
2116 PRINT "DS=";DS
2118 PRINT "TIME=";TG%*CA
2400 IF SR<1.84E-8 AND SR>1.0E-8 THEN CA=5: GOTO 2006
2402 IF SR<1.0E-8 AND SR>5.0E-9 THEN CA=4: GOTO 2006
2404 IF SR<5.0E-9 AND SR>1.0E-9 THEN CA=20:GOTO 2006
2406 IF SR<1.0E-9 THEN 10
2500 GOTO 2006
3000 END
```

Notes on Stress-Relaxation

Relaxation testing can be conducted at any point in the history of a constant strain rate test, however testing is commonly performed once 5 or 10 percent axial strain has occurred in a specimen.

Stress relaxation is achieved by first stopping any further advance of the pistons in contact with the specimen and 'locking' them into place. With time the total axial differential stress will decrease as the rock is furtner strained.

If we think of the specimen and machine as a system we can define an equation relating the strain rate and stress drop. (Figure 3)

The elastic compliance (K12) of the machine can be found by experimental loading of some standard sample. The elastic compliance of the rock will have to be discovered through earlier testing by the examination of a load vs. displacement graph for the rock type. (Figure 4)

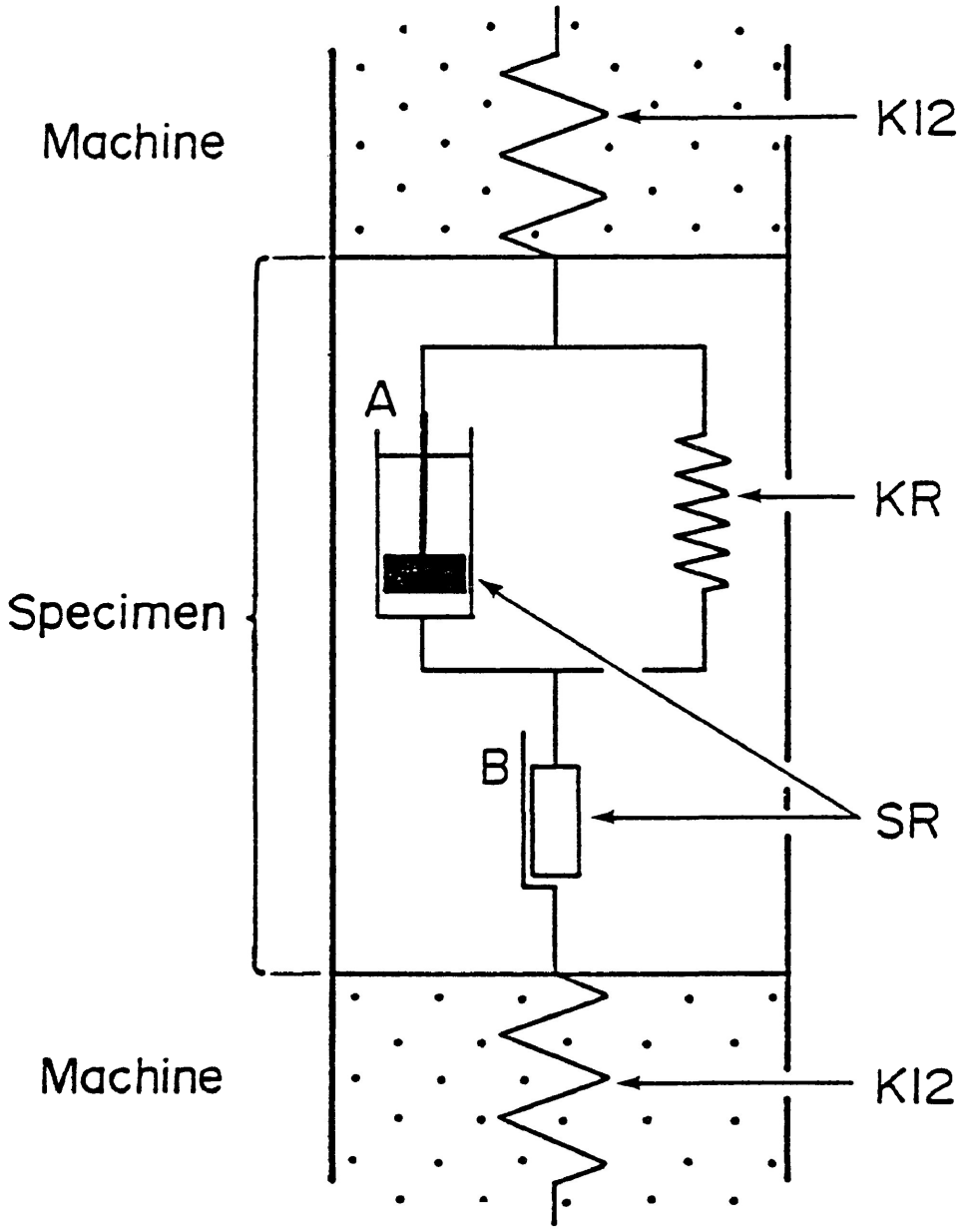

Figure A3.
Schematic representation of the machine sample system.

K12 the elastic compliance of the machine.

the elastic compliance of the rock

the samples displacement which is a result of a viscous (A and a plastic (B) component.

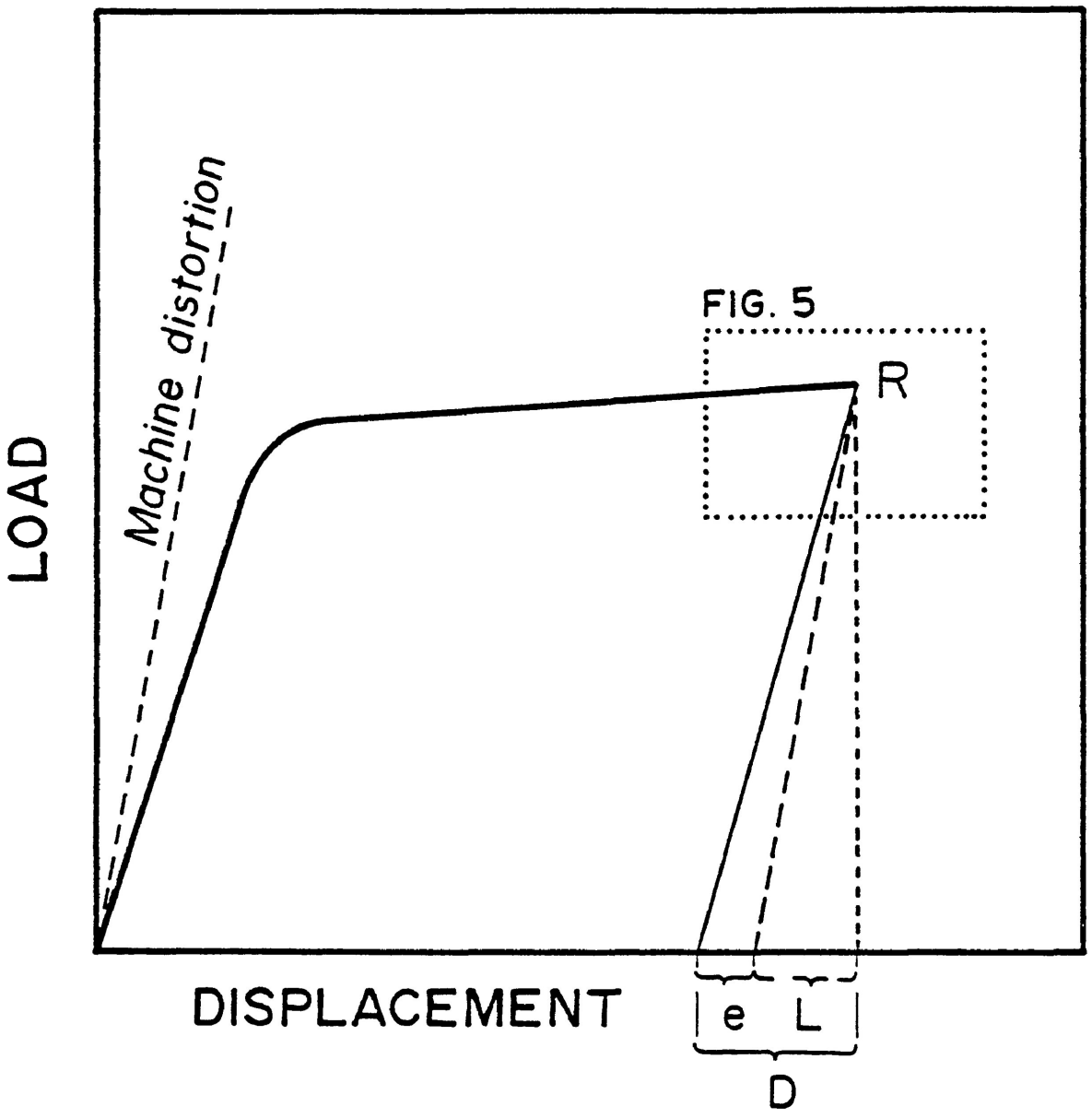

Figure A4.

Theoretical load versus displacement graph, upon unloading the rock appears to spring back a distance 'D' from point 'R'.

The distance D is the sum of the slope due to machine distortion 'L' and that due to the actual elastic compliance of the rock 'e'

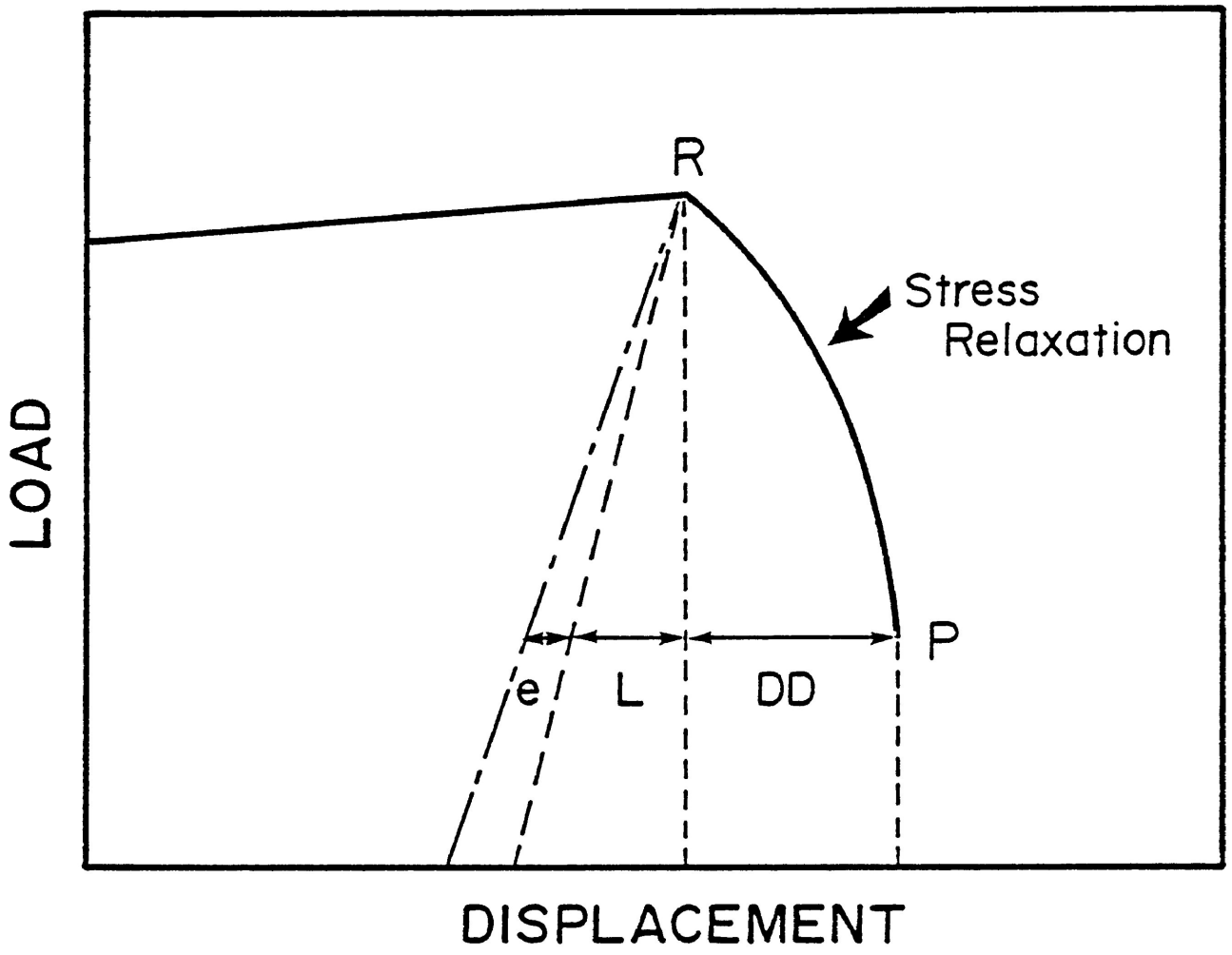

Figure A5.

Enlarged section from previous graph displaying typical stress relaxation curve. Note how when load is reduced KR and K12 assist in the shortening of the rock which is not strictly DD. Thus even if line R-P was vertical (DD=0) then some shortening of the sample will still occur.

However during relaxation the LVDT records some shortening on the sample, Figure 3, thus from the load vs. displacement graph we can now write:

total sample shortening = DD + L + e

L and e are values of displacement dependent upon the change in stress.

Thus $L = (\sigma'_f - \sigma'_i)$ (K12)

$e = (\sigma'_f - \sigma'_i)$ (KR)

where σ'_f and σ'_i are successive (initial, final) differential stresses. Since the stress is dropping, the values for L and e will be negative thus equation (1) can be rewritten as:

(2) total sample shortening = DD - L - e

which can be written in terms of strain rate as

(3) $\dot{e} = ((DD - L - e)/L\emptyset)/TG$

where LØ is the length of the specimen previous to the samples shortening at that increment and TG is the time gap.

APPENDIX B

ACCURACY AND PRECISION

In quoting results from measurements taken from the SI-1 AMS unit, the graticule, micrometers, the LVDT and the load cell throughout this study some mention of the accuracy of the measurements must be made. In the case of the SI-1 AMS unit and the triaxial rig apparatus a brief review of the proceedures in data processing is in order.

Sensitivity and Accuracy of the Sapphire Instruments SI-1 AMS unit:

The SI-1 unit calculates the magnetic susceptibility (MS) of a sample essentially by recording the inductance of the sensing coil with the specimen within the coil, L_s, and then subtracting from that the inductance of the air and background, L_a, measured with the coil empty.

The SI-1 measures L_s and L_a to 7 significant digits (Stupavsky 1983). The precision of the SI-1 Ms measurement is, for the most part, dependent on three inter-related factors;

1. Volume of the sample,

2. Measurement time,

3. The bulk susceptibility of the sample,

and one independent factor;

4. Background noise.

The first three factors are related as: when the bulk susceptibility of a sample is high, the need for a large volume of the sample or a long measuring time would be significantly lessened than if the bulk susceptibility of that sample were low.

Volume-The precision of the MS measurement increases as a specimens' volume approaches that of the sensing coil.

The volume of the SI-1 sensing coil is 160 cm^3 and throughout this investigation the volume the simple shear and pure shear specimens ranged from approximately 4.5 to 8 cm^3. When the specimens fill only a fraction of the coil volume, as is the case in this study, the SI-1 unit determines the susceptibility of the specimen using a coil calibration factor recorded by measuring the MS of an equal sized sample of MnO_2.

Measurement time-The precision of the MS of a sample is usually increased if the measuring time is lengthened. Four separate measuring times are available on the SI-1 unit 2, 4, 6, and 8 seconds.

Repeat MS measurements on a 1 inch long, 0.75 inch diameter sample of the high bulk susceptibility sand-cement material has shown that the degree of accuracy is not significantly improved by increasing the measuring time from 4 seconds to 6 or 8. Thus the 4 second measuring time was used exclusively for the determination of the AMS for the simple and pure shear experiments.

For the measurement of the low bulk susceptibility materials, the calcite and cement, a 6 second measuring time was employed as well as a sample volume equal to that of the sensing coil.

Bulk Susceptibility- The bulk susceptibility values of the sand-cement material and the calcite-cement material are both greater than 3×10^{-3} c.g.s./cm^3. Stupavsky (1983) has indicated that the absolute accuracy of MS measurement for materials having MS > 3×10^{-5} c.g.s./cm^3 is better than 95% and that for a 2 second measurement time the number of significant figures for such high susceptibility materials is at least 4 and longer measuring times may improve the accuracy.

Background noise-The measurement proceedure involves comparison of a sample and an air-background reading. Thus the precision of the instrument may decrease if significant changes in external conditions occur within the sensing range of the inducting coil between the two readings or between consecutive measurements.

That is, the air-background reading is considered a "null" reading. If any two air-background readings are not the same, the deviation is due to external factors termed "background noise".

Measurement of the MS of the specimens occurred under conditions of constant temperature and relatively low background noise conditions (ie. no moving objects). Also the measurement procedure is such that L_s and L_a are measured within a few seconds of each other so that the influence of backgound noise on the determined MS is minimal.

The AMS of a sample is determined by MS measurements for either 6, 12 or 24 specified orientations inside the measuring coil. The degree of accuracy of the individual MS measurements of the experimental materials appears to be ensured, but what of the orientation of the principal susceptibility directions.

When employing the 12 or 24 orientation measurment of AMS the SI-1 program will give the 95% confidence limits for the magnitude and directions of the principal susceptibilities. Typically the indicated 95% confidence limits of the orientations are remarkably good, sometimes being on the order of 1/100 of a degree.

To test the "true' precision of the given orientations the AMS of

one specimen was repeatedly measured; 10 measurements were made of the sample with the sample left in its holder between measurements, also great care was taken during these readings so that the sample and 'boat' were being placed in exactly the same position inside the sensing coil; a further 10 measurements were made in conditions equally that of a normal reading, with the sample removed from its holder between each measurement and a slightly lesser amount of care in placing the sample and 'boat' in exactly the same position inside the coil. For both of the10 measurements Fisherean radii (α_{95}) were statistically determined for the principal susceptibility directions.

The results from the first 10 readings (Table B-1) indicate perhaps the most precise 95% confidence limits the SI-1 is capable of for orientation determination. The α_{95} radius of 'cone of confidence' in each case is less than 1^{o}. The second 10 readings (Table B-2) reveal a slightly larger α_{95} radius for the principal susceptibility directions. These readings are problably more realistic in their estimation of the cone of confidence about the susceptibility directions determined from the SI-1 unit ($>1.5^{o}$). However, in the authors estimation, during the course of data collection a 95% confidence limit of at least 3^{o} should be ascribed to the derived susceptibility directions, which, although quite

TABLE B-1
SPECIMEN LEFT IN HOLDER BETWEEN READINGS

	MINIMUM			INTERMEDIATE			MAXIMUM		
NO.	DEC	INC	EV^{-3}	DEC	INC	EV^{-3}	DEC	INC	EV^{-3}
1	43.08	80.59	1.1272	20.68	-8.74	1.1903	291.25	3.52	1.1992
2	43.97	80.23	1.1269	23.89	-9.1	1.1899	294.35	3.35	1.1993
3	42.91	79.74	1.1265	23.32	-9.74	1.1898	293.95	3.34	1.1987
4	43.4	80.66	1.127	23.07	-8.84	1.1898	293.62	3.16	1.1984
5	43.53	79.95	1.127	22.39	-9.43	1.1896	293.02	3.54	1.1984
6	42.31	79.55	1.126	22.03	-9.76	1.1894	292.6	3.58	1.1986
7	42.87	79.92	1.1252	22.68	-9.56	1.1886	293.33	3.37	1.1975
8	41.37	79.53	1.1257	23.67	-10.0	1.1889	294.24	3.11	1.1982
9	42.63	79.87	1.1259	22.47	-9.55	1.1896	293.08	3.41	1.1979
10	43.66	79.78	1.126	20.28	-9.51	1.1896	292.05	3.93	1.1988
	AVERAGE			AVERAGE			AVERAGE		
	42.96	79.98		22.45	-9.42		299.57	3.8	
	95 radius= 0.24^0			95 radius= 0.74^0			95 radius= 0.11^0		

TABLE B-2
SPECIMEN REMOVED FROM HOLDER BETWEEN READINGS

	MINIMUM			INTERMEDIATE			MAXIMUM		
NO.	DEC	INC	EV^{-3}	DEC	INC	EV^{-3}	DEC	INC	EV^{-3}
1	39.34	81.63	1.128	22.97	-7.99	1.1902	293.27	2.35	1.1988
2	20.02	79.48	1.1282	23.12	-10.3	1.1904	292.98	-0.51	1.2009
3	23.22	80.42	1.1284	22.18	-9.32	1.1909	292.1	0.28	1.2002
4	20.82	80.67	1.1285	23.1	-9.4	1.191	293.06	-0.39	1.2002
5	21.15	80.33	1.1285	22.61	-9.52	1.1915	292.51	-0.18	1.2003
6	43.92	78.71	1.1283	19.52	-10.3	1.1928	290.4	4.54	1.2005
7	58.18	81.91	1.1284	21.67	-6.35	1.191	292.07	4.84	1.2005
8	58.39	81.79	1.1287	21.05	-6.42	1.1908	291.51	4.99	1.2005
9	38.64	83.18	1.1297	24.67	-6.62	1.1911	294.86	1.63	1.2
10	34.56	82.83	1.1293	24.96	-7.09	1.1911	295.12	1.17	1.2009
	AVERAGE			AVERAGE			AVERAGE		
	38.73	81.52		22.59	-8.35		292.8	1.87	
	$_{95}$ radius= 1.62^0			$_{95}$ radius= 1.36^0			$_{95}$ radius= 1.58^0		

large, is approximately the size of the sybol used to indicate the directions on the stereonet projections.

Stress Relaxation:

Voltages, indicating displacement in inches, from the LVDT, or pounds from the load cell, are converted into digital readings on a scale of 1 to 4096.

The LVDT is accurate to .0005 inches, thus this displacement can be said to be the smallest reliable measurement. Since the accuracy of the control system is only as good as 1 part in 4096, to have reliable strain-rates it is necessary to allow the amount of time necessary for this small increment of displacement to occur.

If 5×10^{-4} inches is the smallest displacement allowable, the necessary time to elapse for this displacement to occur can be determined according to the strain rate:

re: $$SR = \frac{5 \times 10^{-4}}{dt}$$

or $$dt = \frac{5 \times 10^{-4}}{SR}$$

$$\text{ie.} \quad dt = \frac{5 \times 10^{-4}}{SR} = 500 \text{ seconds}$$

Since this value (dt) is at the very limit of machine sensitivity the dt value are given an added 20%. Thus, during a relaxation test, the time gap is set at a value proportional to an expected strain-rate lower than the previously measured strain-rate in order to 'capture' a precise reading.

However, as the rate of permanent strain accumulation continually decreases the amount of time necessary to receive a meaningful result becomes in itself a problem. During rather long time gaps (those over 1 hour) significant fluctuations may occur in the voltage supplying the LVDT and load cell.

Line voltage was monitored on several occasions by first setting the LVDT at a fixed position and conecting it and the load cell to the computer and the strip chart recorder. Results indicated that for a period of one day the drift experienced by the load cell was negligable (at worst; ±1 unit in 4096) while the drift experienced by the LVDT could be extreme (± 50 units in 4096). However, it was noted that for the LVDT the worst drift occurred during 'peak' hours of electrical demand (between 8:00 and 9:00 am, and between 4:00 and 6:00 pm). Beyond these fairly drastic times of fluctuation, and during the weekend, when demand is

lowest, the drift was within the expected range for the unit (± 0.22 %).

Thus relaxation test were always conducted during the weekend in order to minimize errors due to line voltage fluctuations. Nevertheless, during each test any potential drift was monitored on the strip chart record such that results could be dismissed if any significant drift did occur.

Specimen Measurement:

0-1 inch and 1-2 inch micrometers were used for the measurement of specimen length and width. Both micrometers are accurate to 0.0005 inches, hence specimen sizes quoted for tests are reliable.

Determination of shear zone displacements and width were achieved by the use of a graticule with a measuring accuracy of 0.05 mm. However, since the specimens are cylindrical the measuring surface is round, hence the graticule could be placed in a variety of locations along the circumferance of the specimen thus making it difficult to accurately record the incremental changes in shear zone width and displacement. Subsequently, measurements were often repeated and throughout each recording great care was taken in ensuring the graticule was placed at an appropriate tangent in order to view the shear zone.

APPENDIX C
Experiments

SAND-CEMENT SHEAR ZONES

Series A (0.689 kbars P_c)

Single Step Tests

# Experiment No.	W_o Initial Width (cm)	W_f Final Width (cm)	SD Shear Displacement (cm)	γ Shear Strain	$\Delta P'$ Change in Anisotropy
SZ-A	0.508	0.495	0.013	.025	.002
SZ-B	0.521	0.483	0.044	.092	.0184
SZ-C	0.457	0.419	0.051	.121	.0146
SZ-D	0.495	0.457	0.038	.083	.0165
SZ-E	0.445	0.419	0.013	.03	.0007
SZ-F	0.469	0.432	0.025	.058	.0053
SZ-G	0.508	0.483	0.063	.13	.0237
SZ-H	0.546	0.495	0.089	.179	.0182
SZ-I	0.483	0.438	0.064	.146	.0332
SZ-J*	0.521	0.469	0.139	.297	.0395
SZ-K	0.521	0.469	0.178	.378	.0373

*faulted during deformation

Multiple Step Tests

#	W_o (cm)	W_{min} Minimum Width (cm)	SD (cm)	γ_{max} Max.Shear Strain	$\Delta P'$
SZ-L	0.457	0.394	0.127	.322	.0388
SZ-M	0.49	0.435	0.114	.263	.0291

SAND-CEMENT SHEAR ZONES

Series B (1.0 kbar P_c)
Multiple Step Tests

#	W_o (cm)	W_{min} (cm)	SD (cm)	γ_{max}	$\Delta P'$
SZ-1	0.465	0.43	0.051	.118	.0314
SZ-2	0.5	0.465	0.038	.085	.0227
SZ-3	0.52	0.47	0.152	.324	.044

SAND-CEMENT SHEAR ZONES

Series C (1.5 kbars P_c)
Multiple Step Tests

#	W_o (cm)	W_{min} (cm)	SD (cm)	γ_{max}	$\Delta P'$
SZ-1	0.51	0.49	0.051	.104	.0306
SZ-2	0.51	0.49	0.038	.078	.0194
SZ-3	0.39	0.32	0.032	.099	.0175

CALCITE-CEMENT SHEAR ZONES

Series 1 (1.0 kbars P_c)
Multiple Step Tests

#	W_o (cm)	W_{min} (cm)	SD (cm)	γ_{max}	$\Delta P'$
SZ-C1	0.44	0.4	0.044	.111	.0341
SZ-C2	0.51	0.49	0.038	.077	.0241
SZ-C3	0.52	0.47	0.089	.189	.0121

CALCITE-CEMENT SHEAR ZONES

Series 2 (1.5 kbars P_c)
Multiple Step Tests

#	W_o (cm)	W_{min} (cm)	SD (cm)	γ_{max}	$\Delta P'$
SZ-C2	0.5	0.46	0.057	.124	.0332
SZ-C3	0.49	0.44	0.057	.129	.0563
SZ-C4	0.54	0.5	0.025	.051	.0141

C1 faulted during early stages of deformation

CALCITE-CEMENT
PURE SHEAR EXPERIMENTS

Single Step Tests

# Experiment No.	L_o Initial Length (cm)	L_f Final Length (cm)	e Percent Shortening (%)	$\Delta P'$ Change in Anisotropy
AC-1	1.912	1.786	6.64	.0009
AC-2	2.029	1.874	7.63	-.002
AC-3	1.953	1.867	4.42	.0028
AC-4	2.151	1.994	7.32	.0037
AC-5	2.037	1.829	10.22	.0205
AC-6	2.456	2.167	11.78	-.008
AC-7	1.816	1.704	6.15	.0022
AC-8	2.098	1.719	18.03	.0213
AC-9	1.953	1.694	13.26	.0022

CALCITE-CEMENT
PURE SHEAR EXPERIMENTS

Multiple Step Tests

# Experiment No.	L_o Initial Length (cm)	L_{min} Minumum Length (cm)	e Percent Shortening (%)	$\Delta P'$ Change in Anisotropy
AC-10	1.948	1.592	18.3	.0181
AC-11	2.327	1.925	17.25	.0108

APPENDIX D

MSA DATA AND THIN SECTION LIST

MAGNETIC SHAPE TESTS OF INCLINED DISKS FOR SHEAR ZONE TESTING

SI-1 AMS DATA SHEET

FIRST TEST INVOLVES A WIDE INCLINED DISK (D) CUT FROM A CYLINDER (C) OF THE SAND-CEMENT MATERIAL
- NOTE VOLUME LOSS

SN	k MINIMUM			k INTERMEDIATE			k MAXIMUM			PARAMETERS						
	DEC	INC	EV	DEC	INC	EV	DEC	INC	EV	T	P'	W	SD	Vol.	ln X/Z	γ
C	282.5	-75.6	4.5351^{-3}	356.1	4.1	4.6257^{-3}	85.3	-13.7	4.634^{-3}	0.8327	1.0241			5.89		
	R95	0.06	Ev95	6.0^{-6}	R95	2.53	Ev95	6.72^{-6}	R95	0.67	Ev95	2.39^{-5}					
D	81.4	81.6	4.6927^{-3}	339.1	-3.6	4.7226^{-3}	71.1	-9.4	4.7392^{-3}	0.0	1.0101	0.87		2.56		
	R95	0.29	Ev95	2.3^{-5}	R95	4.71	Ev95	3.03^{-5}	R95	3.49	Ev95	1.85^{-5}				

SI-1 AMS DATA SHEET

DECREASING WIDTH TEST WIDTH DESCRIBED BY RATIO W/D (WIDTH/DIAMETER)

SN	k MINIMUM			k INTERMEDIATE			k MAXIMUM			PARAMETERS						
	DEC	INC	EV	DEC	INC	EV	DEC	INC	EV	T	P'	W/D	SD	Vol.	ln X/Z	γ
0	27.1	-33.8	4.4479^{-3}	340.9	45.9	4.5867^{-3}	279.2	-24.7	4.661^{-3}	0.3131	1.0487	0.826		4.57		
	R95	0.65	Ev95	1.33 $^{-5}$	R95	0.79	Ev95	9.85^{-6}	R95	0.82	Ev95	1.73^{-5}					
1	24.1	-34.5	4.6406^{-3}	336.9	44.6	4.793^{-3}	275.0	-25.5	4.8683^{-3}	0.3489	1.05	0.759		4.0		
	R95	0.76	Ev95	1.67^{-5}	R95	0.78	Ev95	1.61^{-5}	R95	0.39	Ev95	6.27^{-6}					
2	25.6	-34.9	4.4062^{-3}	333.4	41.8	4.5547^{-3}	273.2	-29.1	4.6237^{-3}	0.3772	1.0505	0.713		3.94		
	R95	2.31	Ev95	4.92^{-5}	R95	4.41	Ev95	2.83^{-5}	R95	4.04	Ev95	5.82^{-5}					
3	26.7	-35.4	4.4051^{-3}	340.4	44.1	4.5541^{-3}	277.3	-25.0	4.6225^{-3}	0.3813	1.0505	0.632		3.34		
	R95	0.23	Ev95	5.12^{-6}	R95	0.39	Ev95	1.43^{-5}	R95	0.41	Ev95	1.35^{-5}					
4	25.3	-29.2	4.6226^{-3}	332.9	47.5	4.7856^{-3}	278.2	-27.8	4.8519^{-3}	0.4336	1.0511	0.536		2.82		
	R95	0.5	Ev95	8.96^{-6}	R95	0.7	Ev95	3.03^{-6}	R95	0.5	Ev95	1.06^{-5}					
5	25.8	-33.0	4.7282^{-3}	336.7	45.2	4.8814^{-3}	276.9	-26.6	4.9568^{-3}	0.352	1.0493	0.464		2.39		
	R95	0.42	Ev95	1.08^{-5}	R95	1.08	Ev95	1.57^{-5}	R95	1.15	Ev95	1.96^{-5}					
6	21.5	-30.1	4.8688^{-3}	346.4	54.8	5.0244^{-3}	281.6	-16.7	5.1064^{-3}	0.3202	1.0496	0.397		1.94		
	R95	0.44	Ev95	1.52^{-5}	R95	0.48	Ev95	2.27^{-5}	R95	0.19	Ev95	1.63^{-5}					
7	21.1	-24.4	4.3679^{-3}	331.9	55.2	4.4984^{-3}	279.9	-23.1	4.586^{-3}	0.2081	1.05	0.287		1.47		
	R95	0.76	Ev95	1.44^{-5}	R95	0.73	Ev95	1.5^{-5}	R95	0.36	Ev95	5.81^{-6}					

SINGLE STEP SAND-CEMENT SHEAR ZONES

SI-1 AMS DATA SHEET

SERIES SZ-A

SN	k MINIMUM			k INTERMEDIATE			k MAXIMUM			PARAMETERS						
	DEC	INC	EV	DEC	INC	EV	DEC	INC	EV	T	P'	W	SD	Vol.	ln X/Z	γ
0	11.6	-78.1	1.1362 $^{-3}$	16.6	11.9	1.176 $^{-3}$	286.4	1.0	1.2245 $^{-3}$	-.0798	1.0777	0.51	0.0	7.31	0	0
	R95 1.15		Ev 95 5.73 $^{-6}$	R95 1.64		Ev 95 2.97 $^{-6}$	R95 1.26		Ev 95 7.68 $^{-6}$							
1	354.9	-79.8	1.1481 $^{-3}$	18.7	9.2	1.1909 $^{-3}$	288.1	4.0	1.2396 $^{-3}$	-.0452	1.0797	0.49	.013	7.22	.025	.025
	R95 0.43		Ev 95 2.48 $^{-6}$	R95 0.35		Ev 95 3.29 $^{-6}$	R95 0.16		Ev 95 1.96 $^{-6}$							

SI-1 AMS DATA SHEET

SERIES .. SZ-B

SN	k MINIMUM			k INTERMEDIATE			k MAXIMUM			PARAMETERS						
	DEC	INC	EV	DEC	INC	EV	DEC	INC	EV	T	P'	W	SD	Vol.	ln X/Z	γ
0	12.5	51.9	1.2348^{-3}	297.8	-11.6	1.2496^{-3}	36.3	-35.6	1.2748^{-3}							
	R95 2.3		E95 1.15^{-5}	R95 1.78		E95 7.2^{-6}	R95 1.8		E95 9.85^{-6}	-.2566	1.0327	0.52	0.0	6.60	0	0
1	12.1	60.7	1.2232^{-3}	307.8	-13.7	1.2654^{-3}	44.5	-25.3	1.2842^{-3}							
	R95 0.15		E95 1.81^{-6}	R95 1.25		E95 3.1^{-6}	R95 0.24		E95 3.85^{-6}	.3955	1.0511	0.48	.044	6.60	.092	.092

SI-1 AMS DATA SHEET

SERIES n SZ-C

SN	k MINIMUM			k INTERMEDIATE			k MAXIMUM			PARAMETERS						
	DEC	INC	EV	DEC	INC	EV	DEC	INC	EV	T	P'	W	SD	Vol.	ln X/Z	χ
0	324.6	65.5	7.568^{-4}	65.9	5.1	9.9718^{-4}	338.1	-23.8	1.0104^{-3}	.5399	1.0586	0.46	0.0	7.27	0	0
	R95 1.03		Ev95 5.74^{-6}	R95 0.69		Ev95 2.53^{-6}	R95 1.19		Ev95 5.55^{-6}							
1	336.2	64.7	9.8388^{-4}	61.3	-2.3	1.0406^{-3}	330.2	-25.2	1.0504^{-3}	.7137	1.0732	0.42	.051	7.07	.121	.121
	R95 0.18		Ev95 2.98^{-7}	R95 2.65		Ev95 6.34^{-6}	R95 2.64		Ev95 6.58^{-6}							

SI-1 AMS DATA SHEET

SERIES SZ-D

SN	k MINIMUM			k INTERMEDIATE			k MAXIMUM			PARAMETERS						
	DEC	INC	EV	DEC	INC	EV	DEC	INC	EV	T	P'	W	SD	Vol.	ln X/Z	γ
0	331.1	50.0	1.0937^{-3}	275.4	-25.4	1.1275^{-3}	20.3	-28.9	1.1397^{-3}	.4782	1.0436	0.49	0.0	7.44	0	0
	R95 0.69	Ev95	1.76^{-6}	R95 0.62	Ev95	7.58^{-6}	R95 0.8	Ev95	7.55^{-6}							
1	11.6	64.2	1.1255^{-3}	66.6	-16.9	1.1707^{-3}	330.3	-21.8	1.1914^{-3}	.3839	1.0601	0.46	.038	7.21	.083	.083
	R95 1.49	Ev95	1.28^{-6}	R95 1.59	Ev95	6.48^{-6}	R95 2.04	Ev95	6.63^{-6}							

SI-1 AMS DATA SHEET

SERIES ,1 SZ-E

SN	k MINIMUM			k INTERMEDIATE			k MAXIMUM			PARAMETERS						
	DEC	INC	EV	DEC	INC	EV	DEC	INC	EV	T	P'	W	SD	Vol.	ln X/Z	γ
0	28.4	37.4	1.0013^{-3}	330.1	-34.5	1.0524^{-3}	87.5	-33.8	1.0747^{-3}	0.4067	1.0753	0.44	0.0	7.27	0	0
	R95	0.49	E_v95	2.87^{-6}	R95	0.77	E_v95	2.61^{-6}	R95	0.62	E_v95	1.87^{-6}				
1	18.8	38.8	1.0317^{-3}	324.2	-35.7	1.0839^{-3}	79.9	-31.1	1.1083^{-3}	0.3785	1.0761	0.42	.013	7.10	.029	.03
	R95	1.04	E_v95	5.78^{-6}	R95	1.36	E_v95	5.19^{-6}	R95	0.89	E_v95	3.47^{-6}				

SI-1 AMS DATA SHEET

SERIES .. SZ-F

SN	k MINIMUM			k INTERMEDIATE			k MAXIMUM			PARAMETERS						
	DEC	INC	EV	DEC	INC	EV	DEC	INC	EV	T	P'	W	SD	Vol.	ln X/Z	Y
O	311.5	56.3	1.0397^{-3}	38.9	-1.8	1.0925^{-3}	307.7	-33.6	1.1131^{-3}	0.4536	1.0730	0.47	0.0	6.98	O	O
	R95	0.86	Ev95 2.95^{-6}	R95	3.3	Ev95 3.11^{-6}	R95	3.3	Ev95 4.74^{-6}							
1	321.9	58.8	1.0606^{-3}	34.3	-10.4	1.1226^{-3}	298.5	-29.6	1.1391^{-3}	0.5909	1.0783	0.43	0.25	6.85	.058	058
	R95	1.08	Ev95 7.12^{-6}	R95	3.3	Ev95 1.17^{-5}	R95	3.47	Ev95 1.41^{-5}							

SI-1 AMS DATA SHEET

SERIES n SZ-G

SN	k MINIMUM			k INTERMEDIATE			k MAXIMUM			PARAMETERS						
	DEC	INC	EV	DEC	INC	EV	DEC	INC	EV	T	P'	W	SD	Vol.	ln X/Z	Y
0	73.5	89.0	4.129^{-2}	9.3	10.3	4.2269^{-2}	279.0	1.7	4.3334^{-2}	0.0	1.0495	0.51	0.0	7.12	0	0
	R95 5.94		Ev95 6.28^{-5}	R95 1.39		Ev95 1.15^{-4}	R95 0.3		Ev95 9.97^{-5}							
1	7.92	84.3	1.2632^{-3}	6.5	-6.2	1.3184^{-3}	276.5	0.1	1.355^{-3}	0.2204	1.0732	0.48	.063	6.84	0.131	.131
	R95 0.02		Ev95 1.22^{-6}	R95 0.13		Ev95 1.38^{-6}	R95 0.01		Ev95 1.68^{-6}							

SI-1 AMS DATA SHEET

SERIES ,, SZ-H

SN	k MINIMUM			k INTERMEDIATE			k MAXIMUM			PARAMETERS						
	DEC	INC	EV	DEC	INC	EV	DEC	INC	EV	T	P'	W	SD	Vol.	ln X/Z	χ
0	29.4	85.9	1.2049^{-3}	89.0	-2.2	1.3046^{-3}	2.79	-10.9	1.3112^{-3}	0.8818	1.0993	0.54	0.0	7.08	0	0
	R95 0.02		E,95 1.11^{-6}	R95 0.12		E,95 4.72^{-6}	R95 6.07		E,95 4.6^{-6}							
1	1.98	77.6	1.2557^{-3}	17.2	-12.0	1.381^{-3}	286.5	-3.2	1.3843^{-3}	0.9527	1.1175	0.49	.089	6.77	.179	.179
	R95 0.29		E,95 9.44^{-7}	R95 3.94		E,95 5.44^{-6}	R95 3.48		E,95 5.51^{-6}							

SI-1 AMS DATA SHEET

SERIES SZ-I

SN	k MINIMUM			k INTERMEDIATE			k MAXIMUM			PARAMETERS						
	DEC	INC	EV	DEC	INC	EV	DEC	INC	EV	T	P'	W	SD	Vol.	ln X/Z	Y
0	337.4	77.0	1.0863^{-3}	51.4	-3.6	1.1311^{-3}	320.6	-12.4	1.1448^{-3}	0.5409	1.0564	0.48	0.0	6.96	0	0
	R95 0.27	E$_v$95	1.53^{-6}	R95 5.41	E$_v$95	1.69^{-5}	R95 5.39	E$_v$95	1.7^{-5}							
1	355.5	72.0	1.135^{-3}	47.2	-11.4	1.2174^{-3}	314.4	-13.7	1.2272^{-3}	0.7958	1.0896	0.44	.063	6.57	.145	145
	R95 0.33	E$_v$95	2.25^{-6}	R95 7.25	E$_v$95	1.96^{-5}	R95 7.2	E$_v$95	1.98^{-5}							

SI-1 AMS DATA SHEET

SERIES A SZ-J

SN	k MINIMUM			k INTERMEDIATE			k MAXIMUM			PARAMETERS						
	DEC	INC	EV	DEC	INC	EV	DEC	INC	EV	T	P'	W	SD	Vol.	ln X/Z	Y
0	291.1	-73.7	1.1468^{-3}	16.2	1.4	1.1822^{-3}	285.8	16.2	1.2059^{-3}	0.2101	1.0517	0.52	0.0	6.73	0	0
	R95 0.27		Ev95 1.49^{-6}	R95 0.55		Ev95 3.9^{-6}	R95 0.59		Ev95 3.77^{-6}							
1	52.0	77.4	1.2384^{-3}	13.8	-9.9	1.3244^{-3}	285.2	7.6	1.3442^{-3}	0.6387	1.0912	0.47	.139	6.11	.296	.297
	R95 0.14		Ev95 1.44^{-6}	R95 1.0		Ev95 2.2^{-6}	R95 0.98		Ev95 3.33^{-6}							

SI-1 AMS DATA SHEET

SERIES A SZ-K

SN	k MINIMUM			k INTERMEDIATE			k MAXIMUM			PARAMETERS						
	DEC	INC	EV	DEC	INC	EV	DEC	INC	EV	T	P'	W	SD	Vol.	ln X/Z	γ
0	22.2	66.3	1.2591 -3	35.9	-23.1	1.3144 -3	303.8	-5.0	1.3364 -3	0.4435	1.0633	0.52	0.0	6.63	0	0
	R95 0.16		Ev95 1.49 -6	R95 1.24		Ev95 4.61 -6	R95 1.26		Ev95 4.95 -6							
1	21.9	71.0	1.409 -3	32.4	-18.7	1.5163 -3	301.2	-3.2	1.5418 -3	0.6301	1.1006	0.47	.178	5.83	.376	.378
	R95 0.1		Ev95 1.85 -6	R95 1.75		Ev95 8.92 -6	R95 1.75		Ev95 9.05 -6							

MULTIPLE STEP SAND-CEMENT SHEAR ZONES

SI-1 AMS DATA SHEET

SERIES SZ-L

SN	k MINIMUM			k INTERMEDIATE			k MAXIMUM			PARAMETERS						
	DEC	INC	EV	DEC	INC	EV	DEC	INC	EV	T	P'	W	SD	Vol.	ln X/Z	Y
0	68.4	77.5	1.0115 $^{-3}$	6.5	-5.9	1.0412 $^{-3}$	277.6	10.9	1.0529 $^{-3}$	0.4431	1.0422	0.46	0.0	7.35	0	0
	R95 0.27	Ev95	1.08 $^{-6}$	R95 0.57	Ev95	8.38 $^{-7}$	R95 0.49	Ev95	1.98 $^{-6}$							
1	45.1	76.4	1.0667 $^{-3}$	2.7	-4.2	1.0933 $^{-3}$	271.8	9.4	1.1108 $^{-3}$	0.2155	1.0416	0.44	.025	7.07	.057	.057
	R95 0.48	Ev95	3.59 $^{-6}$	R95 14.2	Ev95	4.79 $^{-6}$	R95 0.36	Ev95	2.68 $^{-6}$							
2	51.2	77.5	1.0784 $^{-3}$	2.8	-8.1	1.107 $^{-3}$	274.1	9.2	1.1232 $^{-3}$	0.2868	1.042	0.43	.051	7.0	.117	.117
	R95 0.28	Ev95	2.81 $^{-6}$	R95 1.02	Ev95	4.58 $^{-6}$	R95 0.26	Ev95	2.73 $^{-6}$							
3	40.5	76.4	1.0851 $^{-3}$	1.7	-9.7	1.117 $^{-3}$	272.9	8.4	1.1333 $^{-3}$	0.3333	1.0452	0.43	.064	6.95	.147	.147
	R95 0.62	Ev95	3.44 $^{-6}$	R95 1.16	Ev95	4.38 $^{-6}$	R95 0.31	Ev95	1.79 $^{-6}$							
4	27.2	78.0	1.0961 $^{-3}$	7.7	-11.4	1.128 $^{-3}$	278.5	3.9	1.1465 $^{-3}$	0.2762	1.0465	0.42	.076	6.87	.181	.182
	R95 0.36	Ev95	2.06 $^{-6}$	R95 0.79	Ev95	4.5 $^{-6}$	R95 0.46	Ev95	4.4 $^{-6}$							
5	36.1	77.3	1.0875 $^{-3}$	358.0	-11.0	1.1261 $^{-3}$	89.8	-7.6	1.1425 $^{-3}$	0.4139	1.052	0.42	.089	6.79	.211	.212
	R95 0.41	Ev95	3.44 $^{-6}$	R95 2.82	Ev95	5.92 $^{-6}$	R95 0.13	Ev95	4.22 $^{-6}$							
6	31.5	76.1	1.1094 $^{-3}$	0.8	-12.4	1.1499 $^{-3}$	272.4	6.8	1.1676 $^{-3}$	0.4025	1.0539	0.41	.102	6.69	.249	.25
	R95 0.16	Ev95	1.81 $^{-6}$	R95 1.92	Ev95	3.52 $^{-6}$	R95 0.16	Ev95	3.75 $^{-6}$							
7	16.8	76.6	1.1032 $^{-3}$	4.6	-13.2	1.1512 $^{-3}$	275.3	2.7	1.1683 $^{-3}$	0.4857	1.0613	0.40	.114	6.61	.275	.276
	R95 0.1	Ev95	1.35 $^{-6}$	R95 0.4	Ev95	2.46 $^{-6}$	R95 0.2	Ev95	2.52 $^{-6}$							

SI-1 AMS DATA SHEET

SERIES SZ-L continued

SN	k MINIMUM			k INTERMEDIATE			k MAXIMUM			PARAMETERS						
	DEC	INC	EV	DEC	INC	EV	DEC	INC	EV	T	P'	W	SD	Vol.	ln X/Z	δ
8	15.9	78.1	1.1305^{-3}	2.3	-12.2	1.187^{-3}	273.0	2.7	1.2036^{-3}							
	R95 0.11		E95 1.59^{-6}	R95 1.38		E95 3.03^{-6}	R95 0.13		E95 3.22^{-6}	0.5568	1.068	0.39	.121	6.51	.305	.306
9	23.4	74 8	1.1458^{-3}	2.5	-13.9	1.2184^{-3}	273.6	5.2	1.2316^{-3}							
	R95 0.52		E95 2.14^{-6}	R95 1.09		E95 5.35^{-6}	R95 0.23		E95 3.02^{-6}	0.7016	1.081	0.39	.127	6.37	.32	.322

SI-1 AMS DATA SHEET

SERIES SZ-M

SN	k MINIMUM			k INTERMEDIATE			k MAXIMUM			PARAMETERS						
	DEC	INC	EV	DEC	INC	EV	DEC	INC	EV	T	P'	W	SD	Vol.	ln X/Z	γ
0	326.4	76.2	1.0992^{-3}	336.4	-13.6	1.1492^{-3}	65.8	2.3	1.1803^{-3}	0.2497	1.0745	0.52	0.0	7.75	0	0
	R95 0.33	Ev95	1.97^{-6}	R95 0.87	Ev95	2.05^{-6}	R95 0.82	Ev95	3.43^{-6}							
1	321.3	75.3	1.151^{-3}	337.9	-14.2	1.2069^{-3}	66.9	4.0	1.2407^{-3}	0.2639	1.0788	0.49	0.0	7.49	0	0
	R95 0.08	Ev95	8.14^{-7}	R95 0.54	Ev95	2.66^{-6}	R95 0.55	Ev95	3.18^{-6}							
2	324.8	73.7	1.1621^{-3}	338.2	-15.8	1.2169^{-3}	67.2	3.6	1.2511^{-3}	0.2488	1.0773	0.48	0.0	7.43	0	0
	R95 0.49	Ev95	2.16^{-6}	R95 0.89	Ev95	3.42^{-6}	R95 0.75	Ev95	4.44^{-6}							
3	328.4	74.8	1.1784^{-3}	335.9	-15.0	1.236^{-3}	65.5	1.9	1.2705^{-3}	0.2682	1.0791	0.48	.013	7.33	.026	.026
	R95 0.39	Ev95	2.56^{-6}	R95 0.71	Ev95	2.1^{-6}	R95 0.6	Ev95	2.31^{-6}							
4	327.3	73.6	1.187^{-3}	338.8	-16.1	1.2485^{-3}	67.9	3.1	1.2831^{-3}	0.2977	1.0822	0.475	.013	7.25	.027	.027
	R95 0.43	Ev95	6.7^{-7}	R95 0.77	Ev95	4.16^{-6}	R95 0.65	Ev95	4.68^{-6}							
5	328.7	73.8	1.1864^{-3}	338.7	-15.9	1.2542^{-3}	67.9	2.6	1.2872^{-3}	0.3629	1.0868	0.465	.025	7.19	.055	.055
	R95 0.21	Ev95	2.38^{-6}	R95 0.88	Ev95	6.24^{-6}	R95 0.85	Ev95	6.07^{-6}							
6	342.2	76.7	1.2082^{-3}	337.1	-13.2	1.2876^{-3}	67.4	-1.1	1.3202^{-3}	0.436	1.0957	0.46	.076	7.03	.165	.166
	R95 0.14	Ev95	9.52^{-7}	R95 0.73	Ev95	3.33^{-6}	R95 0.71	Ev95	3.71^{-6}							
7	339.9	73.7	1.233^{-3}	335.8	-16.3	1.3275^{-3}	66.1	-1.1	1.3598^{-3}	0.5395	1.1079	0.435	.114	6.83	.262	.263
	R95 0.1	Ev95	2.01^{-6}	R95 0.37	Ev95	3.17^{-6}	R95 0.34	Ev95	3.52^{-6}							

#0 represents precompacted specimen

SI-1 AMS DATA SHEET

SERIES B SZ-1

SN	k MINIMUM			k INTERMEDIATE			k MAXIMUM			PARAMETERS						
	DEC	INC	EV	DEC	INC	EV	DEC	INC	EV	T	P'	W	SD	Vol.	ln X/Z	γ
0	318.5	82.1	1.1701^{-3}	338.3	-7.5	1.2405^{-3}	67.9	2.6	1.2779^{-3}	0.3258	1.0938	0.465	0.0	6.42	0	0
	R95 0.04		Ev95 9.52^{-7}	R95 0.38		Ev95 2.11^{-6}	R95 0.38		Ev95 2.39^{-6}							
1	337.7	82.2	1.1763^{-3}	337.5	-7.7	1.2504^{-3}	67.5	-0.0	1.2879^{-3}	0.3479	1.0968	0.45	0.0	6.37	0	0
	R95 0.04		Ev95 1.46^{-6}	R95 0.23		Ev95 2.98^{-6}	R95 0.2		Ev95 2.11^{-6}							
2	347.1	77.9	1.0502^{-3}	340.8	-12.1	1.1218^{-3}	71.1	-1.31	1.1549^{-3}	0.388	1.1022	0.44	.013	6.29	.029	.029
	R95 0.09		Ev95 9.24^{-7}	R95 0.43		Ev95 2.62^{-6}	R95 0.44		Ev95 2.7^{-6}							
3	343.6	77.5	1.1893^{-3}	341.2	-12.5	1.2815^{-3}	71.4	-0.5	1.3181^{-3}	0.4522	1.1121	0.43	.025	6.18	.059	.059
	R95 0.34		Ev95 1.85^{-6}	R95 0.61		Ev95 1.37^{-6}	R95 0.52		Ev95 2.72^{-6}							
4	351.4	77.1	1.2012^{-3}	340.1	-12.6	1.2984^{-3}	70.6	-2.4	1.3338^{-3}	0.4862	1.1148	0.43	.038	6.09	.088	.089
	R95 0.13		Ev95 6.86^{-7}	R95 0.39		Ev95 3.67^{-7}	R95 0.38		Ev95 1.69^{-6}							
5	1.1	77.5	1.2355^{-3}	340.8	-11.6	1.3471^{-3}	71.6	-4.2	1.383^{-3}	0.5336	1.1252	0.43	.051	5.86	.118	.118
	R95 0.35		Ev95 1.01^{-6}	R95 0.23		Ev95 2.26^{-6}	R95 0.17		Ev95 1.58^{-6}							

SI-1 AMS DATA SHEET

SERIES B SZ-2

SN	k MINIMUM			k INTERMEDIATE			k MAXIMUM			PARAMETERS						
	DEC	INC	EV	DEC	INC	EV	DEC	INC	EV	T	P'	W	SD	Vol.	ln X/Z	Y
0	276.8	83.5	1.1566^{-3}	77.6	6.2	1.1885^{-3}	347.8	-1.9	1.2141^{-3}	0.1215	1.0498	0.50	0.0	7.25	0	0
	R95 0.03		Ev95 2.5^{-6}	R95 0.23		Ev95 3.7^{-6}	R95 0.27		Ev95 3.13^{-6}							
1	311.5	81.3	1.1706^{-3}	74.1	4.7	1.2066^{-3}	344.7	-7.35	1.2261^{-3}	0.3077	1.0481	0.48	0.0	7.18	0	0
	R95 0.19		Ev95 1.04^{-6}	R95 1.1		Ev95 4.1^{-6}	R95 1.07		Ev95 4.55^{-6}							
2	334.4	81.3	1.1701^{-3}	71.7	1.1	1.218^{-3}	341.9	-8.6	1.2367^{-3}	0.4486	1.0587	0.475	.013	7.13	.026	.0267
	R95 0.25		Ev95 1.99^{-6}	R95 0.9		Ev95 2.19^{-6}	R95 0.95		Ev95 3.46^{-6}							
3	330.3	79.6	1.1645^{-3}	73.2	2.3	1.2197^{-3}	343.6	-10.1	1.2372^{-3}	0.5296	1.0653	0.465	.025	7.08	.054	.0546
	R95 0.15		Ev95 9.22^{-7}	R95 1.6		Ev95 5.44^{-6}	R95 1.58		Ev95 5.87^{-6}							
4	348.8	77.7	1.1709^{-3}	68.9	-2.14	1.2371^{-3}	338.5	-12.1	1.2497^{-3}	0.6889	1.0725			7.03		
	R95 0.13		Ev95 1.29^{-6}	R95 0.76		Ev95 2.71^{-6}	R95 0.81		Ev95 1.85^{-6}							

SI-1 AMS DATA SHEET

SERIES B SZ-3

SN	k MINIMUM			k INTERMEDIATE			k MAXIMUM			PARAMETERS						
	DEC	INC	EV	DEC	INC	EV	DEC	INC	EV	T	P'	W	SD	Vol.	ln X/Z	γ
0	272.8	-55.3	1.1892^{-3}	299.7	31.7	1.2079^{-3}	21.7	-12.7	1.2314^{-3}	0.1051	1.0355	0.52	0.0	7.22	0	0
	R95 1.91	Ev95	8.19^{-6}	R95 2.12	Ev95	7.94^{-6}	R95 1.05	Ev95	2.87^{-6}							
1	278.8	-52.6	1.2015^{-3}	295.6	36.1	1.2171^{-3}	19.6	-8.2	1.2398^{-3}	-.1779	1.032	0.51	0.0	7.17	0	0
	R95 1.81	Ev95	7.28^{-6}	R95 2.07	Ev95	6.28^{-6}	R95 1.16	Ev95	3.91^{-6}							
2	273.1	-63.0	1.2027^{-3}	293.7	25.4	1.2213^{-3}	19.7	-8.3	1.2425^{-3}	0.0	1.0335	0.51	0.0	7.14	0	0
	R95 1.15	Ev95	6.22^{-6}	R95 1.33	Ev95	6.97^{-6}	R95 0.76	Ev95	2.98^{-6}							
3	86.7	66.3	1.2145^{-3}	298.0	20.5	1.2361^{-3}	23.7	-11.3	1.2587^{-3}	0.0	1.0363	0.50	.013	7.06	.025	.0254
	R95 1.2	Ev95	5.78^{-6}	R95 1.88	Ev95	2.64^{-6}	R95 1.48	Ev95	5.36^{-6}							
4	69.6	70.0	1.2178^{-3}	301.3	12.7	1.2485^{-3}	27.8	-15.2	1.2712^{-3}	.160	1.044	0.49	.025	6.98	.052	.0518
	R95 0.39	Ev95	2.76^{-6}	R95 0.35	Ev95	3.24^{-6}	R95 0.24	Ev95	1.2^{-6}							
5	63.6	74.5	1.2181^{-3}	297.7	9.25	1.2596^{-3}	25.6	-12.3	1.2822^{-3}	.3065	1.0534	0.49	.076	6.94	.156	.1555
	R95 0.4	Ev95	1.43^{-6}	R95 1.16	Ev95	4.99^{-6}	R95 1.11	Ev95	5.37^{-6}							
6	64.1	76.3	1.2717^{-3}	294.7	8.8	1.3322^{-3}	23.1	-10.4	1.3566^{-3}	.4384	1.0689	0.47	.139	6.53	.296	.2972
	R95 0.2	Ev95	7.69^{-7}	R95 0.9	Ev95	4.22^{-6}	R95 0.88	Ev95	4.39^{-6}							
7	52.3	78.6	1.2572^{-3}	291.2	5.9	1.33^{-3}	20.2	-9.7	1.3532^{-3}	.530	1.0799	0.47	.152	6.53	.322	.3242
	R95 0.23	Ev95	1.8^{-6}	R95 1.1	Ev95	3.96^{-6}	R95 1.08	Ev95	4.72^{-6}							

SI-1 AMS DATA SHEET

SERIES C SZ-1

SN	k MINIMUM			k INTERMEDIATE			k MAXIMUM			PARAMETERS						
	DEC	INC	EV	DEC	INC	EV	DEC	INC	EV	T	P'	W	SD	Vol.	ln X/Z	γ
0	81.8	83.5	1.1616 $^{-3}$	28.9	-4.1	1.1926 $^{-3}$	299.4	5.1	1.2037 $^{-3}$	0.480	1.0376	0.51	0.0	7.38	0	0
	R95 0.14	Ev95	3.41 $^{-6}$	R95 0.46	Ev95	6.86 $^{-6}$	R95 0.17	Ev95	6.10 $^{-6}$							
1	84.0	84.9	1.1639 $^{-3}$	25.3	-2.38	1.1942 $^{-3}$	295.4	4.4	1.2063 $^{-3}$	0.4373	1.0375	0.50	0.0	7.35	0	0
	R95 0.16	Ev95	3.44 $^{-6}$	R95 1.79	Ev95	3.81 $^{-6}$	R95 1.73	Ev95	1.19 $^{-6}$							
2	52.9	83.5	1.1646 $^{-3}$	21.4	-5.54	1.2035 $^{-3}$	291.7	3.4	1.216 $^{-3}$	0.521	1.0461	0.49	0.0	7.29	0	0
	R95 0.07	Ev95	1.89 $^{-6}$	R95 1.24	Ev95	4.92 $^{-6}$	R95 1.24	Ev95	4.88 $^{-6}$							
3	36.8	84.0	1.1534 $^{-3}$	20.8	-5.7	1.1987 $^{-3}$	290.9	1.7	1.2119 $^{-3}$	0.5578	1.0533	0.49	.013	7.27	.026	.026
	R95 0.12	Ev95	1.15 $^{-6}$	R95 0.56	Ev95	2.1 $^{-6}$	R95 0.45	Ev95	6.39 $^{-7}$							
4	38.8	82.8	1.1495 $^{-3}$	19.5	-6.9	1.199 $^{-3}$	289.8	2.3	1.2106 $^{-3}$	0.6276	1.0567	0.49	.025	7.27	.052	.052
	R95 0.27	Ev95	1.09 $^{-6}$	R95 1.6	Ev95	4.56 $^{-6}$	R95 1.55	Ev95	5.47 $^{-6}$							
5	33.9	83.0	1.139 $^{-3}$	19.6	-6.6	1.1934 $^{-3}$	289.8	1.7	1.2044 $^{-3}$	0.672	1.0617	0.49	.044	7.27	.091	.091
	R95 0.09	Ev95	1.7 $^{-6}$	R95 0.37	Ev95	4.57 $^{-6}$	R95 0.26	Ev95	3.72 $^{-6}$							
6	41.1	80.3	1.1303 $^{-3}$	20.2	-9.0	1.1924 $^{-3}$	290.7	3.4	1.2007 $^{-3}$	0.772	1.0682	0.49	.051	7.27	.104	.104
	R95 0.1	Ev95	1.06 $^{-6}$	R95 1.18	Ev95	1.78 $^{-6}$	R95 1.1	Ev95	6.69 $^{-7}$							

SI-1 AMS DATA SHEET

SERIES C SZ-2

SN	k MINIMUM			k INTERMEDIATE			k MAXIMUM			PARAMETERS						
	DEC	INC	EV	DEC	INC	EV	DEC	INC	EV	T	P'	W	SD	Vol.	ln X/Z	γ
0	25.1	-78.2	1.1717 -3	49.3	10.8	1.2189 -3	318.4	4.7	1.2277	0.6926	1.0515	0.51	0.0	7.03	0	0
	R95 0.5		Ev95 2.85 -6	R95 2.08		Ev95 4.11 -6	R95 2.14		Ev95 5.75-6							
1	30.1	-80.3	1.0859 -3	36.5	9.99	1.1289-3	306.4	1.3	1.1403-3	0.5888	1.0529	0.50	0.0	7.00	0	0
	R95 0.37		Ev95 3.24-6	R95 1.07		Ev95 8.18-6	R95 0.9		Ev95 7.63-6							
2	52.9	-84.3	1.0824-3	28.0	5.3	1.1322-3	298.3	-2.3	1.1447 -3	0.6087	1.061	0.50	.013	6.95	.025	.0254
	R95 0.1		Ev95 1.67-6	R95 1.01		Ev95 4.88-6	R95 0.95		Ev95 4.78-6							
3	285.8	88.3	1.0825-3	34.5	0.21	1.138 -3	304.4	-1.75	1.149 -3	0.6793	1.0661	0.50	.025	6.88	.049	.05
	R95 0.03		Ev95 2.44-6	R95 1.41		Ev95 5.31-6	R95 1.31		Ev95 4.68-6							
4	50.9	-86.8	1.0744-3	34.9	3.1	1.1316-3	305.0	-0.9	1.1437-3	0.6593	1.0691	0.50	.038	6.88	.076	.076
	R95 0.04		Ev95 1.58-6	R95 0.21		Ev95 4.11-6	R95 0.12		Ev95 3.75-6							
5	88.6	-88.0	1.0687-3	36.2	1.2	1.1283-3	306.2	-1.6	1.1388-3	0.7082	1.0709	0.49	.041	6.88	.083	.083
	R95 0.0		Ev95 1.01 -6	R95 1.74		Ev95 3.57-6	R95 1.75		Ev95 3.78-6							

SI-1 AMS DATA SHEET

SERIES SZ-3

SN	k MINIMUM			k INTERMEDIATE			k MAXIMUM			PARAMETERS						
	DEC	INC	EV	DEC	INC	EV	DEC	INC	EV	T	P'	W	SD	Vol.	ln X/Z	γ
0	89.3	-74.7	9.4303^{-4}	46.1	11.3	1.0114^{-3}	318.1	-10.2	1.0536^{-3}	0.2628	1.1186	0.39	0.0	7.30	0	0
	R95 0.06		E_v95 3.46^{-7}	R95 0.45		E_v95 2.24^{-6}	R95 0.44		E_v95 2.32^{-6}							
1	295.5	78.0	9.4206^{-4}	61.9	7.17	1.0318^{-3}	333.1	-9.5	1.040^{-3}	0.8407	1.1161	0.38	0.0	7.28	0	0
	R95 0.13		E_v95 1.07^{-6}	R95 3.07		E_v95 6.93^{-6}	R95 3.08		E_v95 7.15^{-6}							
2	310.6	77.0	9.4692^{-4}	53.4	2.9	1.0426^{-3}	324.1	-12.6	1.0493^{-3}	0.8756	1.1218	0.37	.013	7.17	.034	.034
	R95 0.16		E_v95 1.20^{-6}	R95 0.14		E_v95 2.93^{-6}	R95 0.22		E_v95 3.16^{-6}							
3	310.5	78.3	9.4095^{-4}	59.0	3.7	1.0404^{-3}	329.7	-11.0	1.0471^{-3}	0.8806	1.1273	0.36	.019	7.12	.053	.053
	R95 0.09		E_v95 7.83^{-7}	R95 4.16		E_v95 8.28^{-6}	R95 4.14		E_v95 8.43^{-6}							
4	308.1	77.9	9.3686^{-4}	61.5	4.9	1.0385^{-3}	332.5	-11.0	1.0451^{-3}	0.8851	1.1305	0.35	.025	7.12	.0725	.0725
	R95 0.17		E_v95 1.22^{-6}	R95 3.83		E_v95 8.63^{-6}	R95 3.86		E_v95 8.76^{-6}							
5	305.2	79.8	9.294^{-4}	59.1	4.1	1.0349^{-3}	329.8	-9.3	1.041^{-3}	0.8962	1.1361	0.32	.032	7.12	.099	.099
	R95 0.08		E_v95 1.0^{-6}	R95 0.54		E_v95 1.99^{-6}	R95 0.53		E_v95 2.10^{-6}							

MULTIPLE STEP CALCITE-CEMENT SHEAR ZONES

SI-1 AMS DATA SHEET

SERIES 1 SZ-C1

SN	k MINIMUM			k INTERMEDIATE			k MAXIMUM			PARAMETERS						
	DEC	INC	EV	DEC	INC	EV	DEC	INC	EV	T	P'	W	SD	Vol.	ln X/Z	γ
0	315.1	67.6	1.3218 -3	278 9	-48.4	1.3901 -3	13.1	-12.3	1.4303 -3	0.2773	1.0831	0.44	0.0	7.32	0	0
	R95 0.1		Ev95 2.35 -7	R95 0.2		Ev95 1.62 -6	R95 0.18		Ev95 1.01 -6							
1	316.8	66.9	1.3315 -3	278 8	-18.6	1.4077 -3	13.3	-13.2	1.4457 -3	0.3526	1.0875	0.43	0.0	7.27	0	0
	R95 0.29		Ev95 1.96 -6	R95 0.34		Ev95 3.02 -6	R95 0.22		Ev95 5.43 -7							
2	323.6	68.6	1.3381 -3	281.6	-16.1	1.4231 -3	15.1	-13.8	1.4611 -3	0.4006	1.0944	0.41	.013	7.20	.0308	.0309
	R95 0.08		Ev95 2.52 -6	R95 0.06		Ev95 5.97 -6	R95 0.06		Ev95 2.72 -6							
3	333.4	69.9	1.3307 -3	284.9	-13.6	1.4313 -3	18.5	-14.5	1.465 -3	0.5159	1.1055	0.41	.025	7.17	.0618	.0619
	R95 0.15		Ev95 1.26 -6	R95 0.27		Ev95 1.79 -6	R95 0.25		Ev95 2.49 -6							
4	338.6	69.9	1.3373 -3	286.5	-12.6	1.4523 -3	20.0	-15.3	1.4859 -3	0.5659	1.1172	0.40	.044	7.07	1109	111
	R95 0.08		Ev95 1.15 -6	R95 0.37		Ev95 1.77 -6	R95 0.37		Ev95 2.96 -6							

SI-1 AMS DATA SHEET

SERIES - SZ-C2

SN	k MINIMUM			k INTERMEDIATE			k MAXIMUM			PARAMETERS						
	DEC	INC	EV	DEC	INC	EV	DEC	INC	EV	T	P'	W	SD	Vol.	ln X/Z	γ
0	62.0	55.9	1.3321 $^{-3}$	320.3	7.8	1.452 $^{-3}$	45.2	-32.9	1.4884 $^{-3}$	0.5545	1.1234	0.51	0.0	7.75	0	0
	R95 0.64	Ev95	6.79 $^{-6}$	R95 0.62	Ev95	8.26 $^{-7}$	R95 0.75	Ev95	7.77 $^{-6}$							
1	58.5	55.7	1.3491 $^{-3}$	322.1	4.4	1.4725 $^{-3}$	49.2	-33.9	1.5125 $^{-3}$	0.5317	1.1268	0.51	.013	7.66	.025	025
	R95 0.48	Ev95	4.98 $^{-6}$	R95 0.33	Ev95	4.97 $^{-6}$	R95 0.53	Ev95	6.39 $^{-6}$							
2	55.3	59.0	1.3361 $^{-3}$	321.8	2.1	1.4767 $^{-3}$	50.6	-30 8	1.5097 $^{-3}$	0.6387	1.1389	0.50	.025	7.65	.051	.051
	R95 0.49	Ev95	5.68 $^{-6}$	R95 0.12	Ev95	9.67 $^{-6}$	R95 0.5	Ev95	6.94 $^{-6}$							
3	49.2	60.1	1.348 $^{-3}$	316.4	1.6	1.4991 $^{-3}$	45.4	-29.9	1.5335 $^{-3}$	0.6487	1.1475	0.49	.038	7.53	.077	.077
	R95 0.5	Ev95	6.21 $^{-6}$	R95 0.87	Ev95	3.47 $^{-6}$	R95 1.0	Ev95	8.46 $^{-6}$							

no further experimentation due to development of faults within specimen

SI-1 AMS DATA SHEET

SERIES 1 SZ-C3

SN	k MINIMUM			k INTERMEDIATE			k MAXIMUM			PARAMETERS						
	DEC	INC	EV	DEC	INC	EV	DEC	INC	EV	T	P'	W	SD	Vol.	ln X/Z	γ
0	321.6	51 8	1.4016 -3	63.3	9.0	1.5984 -3	340.1	-36.7	1.6336 -3	0.7158	1.1802	0.52	0.0	7.58	0	0
	R95 1.91	Ev95	2.55 -5	R95 1.02	Ev95	1.44 -5	R95 1.65	Ev95	2.51 -5							
1	322.7	51.6	1.4107 -3	63.9	8.8	1.6123 -3	340.7	-37.0	1.6442 -3	0.7439	1.1814	0.51	.013	7.54	.025	.025
	R95 1.32	Ev95	1.76 -5	R95 0.67	Ev95	9.71 -6	R95 1.15	Ev95	1.78 -5							
2	323.6	52.3	1.4261 -3	64.1	7.9	1.6364 -3	340.0	-36.5	1.6641 -3	0.7827	1.1844	0.50	.032	7.46	.038	.038
	R95 1.32	Ev95	1.78 -5	R95 1.04	Ev95	8.96 -6	R95 1.39	Ev95	1.85 -5							
3	327.6	53.5	1.4253 -3	71.0	9.7	1.6490 -3	347.9	-34.7	1.6675 -3	0.858	1.1913	0.49	.063	7.37	.129	.129
	R95 0.81	Ev95	1.03 -5	R95 0.87	Ev95	7.33 -6	R95 0.93	Ev95	1.09 -5							
4	326.6	55.1	1.429 -3	83.8	17.7	1.6537 -3	3.96	-29.0	1.6672 -3	0.8953	1.1893	0.47	.076	7.32	.161	.162
	R95 0.65	Ev95	7.86 -6	R95 3.64	Ev95	1.08 -5	R95 3.48	Ev95	1.50-5							
5	327.6	56.7	1.4203 -3	280.2	-23.9	1.647 -3	20.4	-21.7	1.6607 -3	0.8942	1.1923	0.47	.089	7.32	.188	.189
	R95 0.6	Ev95	6.94 -6	R95 6.16	Ev95	2.09 -5	R95 6.13	Ev95	2.3 -5							

SI-1 AMS DATA SHEET

SERIES 2 SZ-C2

SN	k MINIMUM			k INTERMEDIATE			k MAXIMUM			PARAMETERS						
	DEC	INC	EV	DEC	INC	EV	DEC	INC	EV	T	P'	W	SD	Vol.	ln X/Z	γ
0	288.2	-45.9	1.5577^{-3}	1.0	15.9	1.6683^{-3}	77.3	-39.7	1.7084^{-3}	0.4856	1.1006	0.50	0	6.92	0	0
	R95 1.75		Ev95 2.09^{-5}	R95 0.84		Ev95 4.9^{-6}	R95 1.9		Ev95 2.25^{-5}							
1	288.0	-48.0	1.5924^{-3}	358.6	16.6	1.7018^{-3}	75.6	-37.2	1.7453^{-3}	0.4494	1.0993	0.49	.013	6.81	.0259	.0259
	R95 1.44		Ev95 1.76^{-5}	R95 0.55		Ev95 4.39^{-6}	R95 1.47		Ev95 1.79^{-5}							
2	285.4	-51.7	1.5946^{-3}	353.2	16.6	1.7059^{-3}	71.9	-33.3	1.7489^{-3}	0.461	1.1002	0.48	.032	6.80	.0661	.0661
	R95 0.88		Ev95 1.07^{-5}	R95 0.35		Ev95 5.11^{-6}	R95 0.82		Ev95 9.99^{-6}							
3	278.8	-54.8	1.860^{-3}	347.6	14.3	1.9921^{-3}	68.7	-31.4	2.0473^{-3}	0.4303	1.1039	0.47	.038	5.78*	.081	.081
	R95 1.23		Ev95 1.77^{-5}	R95 1.21		Ev95 3.67^{-6}	R95 1.59		Ev95 1.92^{-5}							
4	278.1	-57.7	1.6055^{-3}	342.3	15.4	1.7284^{-3}	64.0	-27.7	1.7689^{-3}	0.522	1.1065	0.47	.044	6.67	.0944	.0945
	R95 0.96		Ev95 1.18^{-5}	R95 1.28		Ev95 4.84^{-6}	R95 1.46		Ev95 1.34^{-5}							
5	273.1	-60.4	1.6055^{-3}	339.8	12.7	1.7384^{-3}	63.4	-26.2	1.7805^{-3}	0.5375	1.1143	0.465	.044	6.61	.0955	.0956
	R95 1.15		Ev95 1.46^{-5}	R95 1.97		Ev95 1.03^{-5}	R95 2.13		Ev95 1.89^{-5}							
6	274.7	-60.8	1.6128^{-3}	337.5	14.3	1.754^{-3}	60.7	-24.9	1.7939^{-3}	0.5773	1.1186	0.46	.044	6.54	.0965	.0966
	R95 0.84		Ev95 1.09^{-5}	R95 0.89		Ev95 3.64^{-6}	R95 1.02		Ev95 1.11^{-5}							
7	275.7	-64.8	1.5951^{-3}	334.6	13.7	1.7463^{-3}	59.3	-20.7	1.7828^{-3}	0.6281	1.1256	0.46	.051	6.54	.109	.110
	R95 0.73		Ev95 9.52^{-6}	R95 1.40		Ev95 6.26^{-6}	R95 1.46		Ev95 1.22^{-5}							

* incorrect volume (should be 6.78) however this does not alter the orientation nor the ratios of the magnetic susceptibilities magnitude ellipsoid

SI-1 AMS DATA SHEET

SERIES 2 SZ-C2 continued

SN	k MINIMUM			k INTERMEDIATE			k MAXIMUM			PARAMETERS						
	DEC	INC	EV	DEC	INC	EV	DEC	INC	EV	T	P'	W	SD	Vol.	ln X/Z	χ
8	276.4	-65.3	1.5785^{-3}	334.2	13.7	1.7414^{-3}	59.1	-20.1	1.7744^{-3}	0.679	1.1338	0.46	.057	6.54	.123	.124
	R95	0.87	E.95 1.15^{-5}	R95	2.7	E.95 1.49^{-5}	R95	2.81	E.95 1.96^{-5}							

SI-I AMS DATA SHEET

SERIES 2 SZ-C3

SN	k MINIMUM			k INTERMEDIATE			k MAXIMUM			PARAMETERS						
	DEC	INC	EV	DEC	INC	EV	DEC	INC	EV	T	P'	W	SD	Vol.	ln X/Z	γ
0	53.9	62.7	1.3991 $^{-3}$	37.5	-26.3	1.4534 $^{-3}$	310.8	6.7	1.4834 $^{-3}$	0.3016	1.0611	0.49	0.0	7.34	0	0
	R95 0.82	Ev95	4.98 $^{-6}$	R95 1.61	Ev95	6.04 $^{-6}$	R95 1.38	Ev95	8.24 $^{-6}$							
1	49.1	63.4	1.4117 $^{-3}$	35.5	-25.9	1.4739 $^{-3}$	308.1	5.4	1.5047 $^{-3}$	0.3518	1.0672	0.48	.019	7.25	.0396	.0396
	R95 0.32	Ev95	1.71 $^{-6}$	R95 1.59	Ev95	8.83 $^{-6}$	R95 1.59	Ev95	9.17 $^{-6}$							
2	45.7	65.3	1.4164 $^{-3}$	33.2	-24.2	1.4869 $^{-3}$	305.4	4.7	1.5189 $^{-3}$	0.3904	1.0742	0.47	.038	7.19	.081	.081
	R95 0.82	Ev95	6.15 $^{-6}$	R95 2.36	Ev95	1.08 $^{-5}$	R95 2.23	Ev95	1.28 $^{-5}$							
3	39.7	67.4	1.4045 $^{-3}$	31.7	-22.3	1.4895 $^{-3}$	302.8	2.8	1.5219 $^{-3}$	0.4638	1.0866	0.46	.044	7.16	.096	.096
	R95 0.42	Ev95	4.15 $^{-6}$	R95 1.31	Ev95	3.85 $^{-6}$	R95 1.25	Ev95	6.14 $^{-6}$							
4	39.4	69.3	1.4181 $^{-3}$	33.2	-20.6	1.5159 $^{-3}$	304.0	2.02	1.5477 $^{-3}$	0.5253	1.0956	0.46	.051	7.16	.110	.110
	R95 0.46	Ev95	4.31 $^{-6}$	R95 2.15	Ev95	1.05 $^{-5}$	R95 2.1	Ev95	1.18 $^{-5}$							
5	30.4	70.2	1.379 $^{-3}$	38.4	-19.6	1.4847 $^{-3}$	307.5	-2.5	1.5143 $^{-3}$	0.5782	1.1036	0.45	.051	7.16	.113	.113
	R95 0.12	Ev95	4.75 $^{-7}$	R95 1.74	Ev95	8.63 $^{-6}$	R95 1.74	Ev95	9.02 $^{-6}$							
6	38.8	72.1	1.3603 $^{-3}$	36.9	-17.8	1.4816 $^{-3}$	307.1	0.54	1.5097 $^{-3}$	0.6395	1.1174	0.44	.057	7.16	.129	.129
	R95 0.15	Ev95	7.10 $^{-7}$	R95 1.53	Ev95	8.09 $^{-6}$	R95 1.52	Ev95	8.38 $^{-6}$							

SI-1 AMS DATA SHEET

SERIES 2 SZ-C4

SN	k MINIMUM			k INTERMEDIATE			k MAXIMUM			PARAMETERS						
	DEC	INC	EV	DEC	INC	EV	DEC	INC	EV	T	P'	W	SD	Vol.	ln X/Z	χ
0	41.3	30.4	1.5055^{-3}	332.0	-31.1	1.5553^{-3}	277.1	43.7	1.6159^{-3}							
	R95 1.2	Ev95	9.27^{-6}	R95 1.57	Ev95	6.14^{-6}	R95 1.38	Ev95	1.18^{-5}	-0.0795	1.0733	0.54	0.0	7.39	0	0
1	42.34	34.04	1.5277^{-3}	336.4	-31.1	1.5815^{-3}	277.3	40.4	1.6419^{-3}							
	R95 0.83	Ev95	7.44^{-6}	R95 1.11	Ev95	5.76^{-6}	R95 1.13	Ev95	9.83^{-6}	0.0	1.0747	0.53	0.0	7.29	0	0
2	39.3	39.4	1.5293^{-3}	343.7	-34.5	1.5855^{-3}	278.8	31.7	1.6448^{-3}							
	R95 0.93	Ev95	6.99^{-6}	R95 0.99	Ev95	7.3^{-6}	R95 0.33	Ev95	1.56^{-6}	0.0	1.0755	0.52	.006	7.25	.012	.0122
3	41.8	44.0	1.5387^{-3}	350.7	-33.0	1.6003^{-3}	280.9	27.9	1.6611^{-3}							
	R95 0.76	Ev95	5.97^{-6}	R95 0.84	Ev95	3.66^{-6}	R95 0.59	Ev95	5.79^{-6}	0.0	1.0795	0.52	.013	7.15	.024	.0244
4	42.6	47.5	1.533^{-3}	354.1	-31.2	1.5979^{-3}	281.0	25.6	1.6579^{-3}							
	R95 1.12	Ev95	8.81^{-6}	R95 1.24	Ev95	8.34^{-6}	R95 0.53	Ev95	3.93^{-6}	0.0586	1.0815	0.51	.013	7.15	.025	.0249
5	42.9	48.7	1.5238^{-3}	357.5	-31.6	1.5947^{-3}	283.1	23.5	1.6509^{-3}							
	R95 1.28	Ev95	1.05^{-5}	R95 1.43	Ev95	9.12^{-6}	R95 0.79	Ev95	6.24^{-6}	0.1353	1.0836	0.51	.025	7.15	.049	.0498
6	44.2	53.6	1.5139^{-3}	357.1	-29.5	1.5913^{-3}	281.9	21.4	1.6454^{-3}							
	R95 0.99	Ev95	8.3^{-6}	R95 4.38	Ev95	6.42^{-6}	R95 0.67	Ev95	6.03^{-6}	0.1973	1.0874	0.50	.025	7.15	.051	.0508

SINGLE STEP CALCITE-CEMENT PURE SHEAR TESTS

SI-1 AMS DATA SHEET

AC-1

SN	k MINIMUM			k INTERMEDIATE			k MAXIMUM			PARAMETERS						
	DEC	INC	EV	DEC	INC	EV	DEC	INC	EV	T	P'	L	D	Vol.	ln X/Z	e
0	78.9	-53.9	6.5891^{-3}	344.5	-3.2	7.1806^{-3}	72.1	35.8	7.3321^{-3}	0.6096	1.120	1.913	1.892	5.38	—	—
	R95 0.45		Ev95 2.41^{-5}	R95 0.41		Ev95 1.08^{-5}	R95 0.59		Ev95 2.78^{-5}							
1	80.8	-58.7	7.0625^{-3}	345.1	-3.5	7.7187^{-3}	72.9	31.0	7.856^{-3}	0.6686	1.1209	1.786	1.892	5.02	0.103	6.64%
	R95 0.32		Ev95 1.80^{-5}	R95 0.51		Ev95 1.54^{-5}	R95 0.59		Ev95 2.56^{-5}							

SI-1 AMS DATA SHEET

AC - 4

SN	k MINIMUM			k INTERMEDIATE			k MAXIMUM			PARAMETERS						
	DEC	INC	EV	DEC	INC	EV	DEC	INC	EV	T	P'	L	D	Vol.	ln X/Z	e
0	276.5	52.2	6.1449-3	9.3	2.1	6.6771-3	281.0	-37.7	7.0195-3	-.8253	1.0626	2.029	1.897	5.74	—	—
	R95	2.7	E.95	5.99-5	R95	2.52	E.95	1.70-5	R95	1.59	E.95	6.44-5				
1	279.1	54.4	7.5284-3	9.9	0.4	7.567-3	280.3	-35.6	7.9407-3	-.8091	1.0606	1.874	1.867	5.13	.119	7.63%
	R95	1.26	E.95	2.0-5	R95	0.77	E.95	3.41-5	R95	0.87	E.95	4.07-5				

SI-1 AMS DATA SHEET

AC-3

SN	k MINIMUM			k INTERMEDIATE			k MAXIMUM			PARAMETERS						
	DEC	INC	EV	DEC	INC	EV	DEC	INC	EV	T	P'	L	D	Vol.	ln X/Z	e
0	26.9	-45.0	6.7066^{-3}	85.4	29.1	6.6771^{-3}	334.2	32.8	6.8255^{-3}	0.0905	1.0177	1.953	1.897	5.52	—	—
	R95	0.67	Ev95	1.97^{-5}	R95	0.85	Ev95	2.68^{-5}	R95	1.49	Ev95	3.55^{-5}				
1	24.4	-42.1	7.4634^{-3}	84.4	29.6	7.5534^{-3}	332.0	34.9	7.6159^{-3}	0.1814	1.0205	1.867	1.844	4.98	.0678	4.42%
	R95	1.99	Ev95	5.37^{-6}	R95	1.77	Ev95	4.04^{-5}	R95	2.53	Ev95	4.09^{-5}				

SI-1 AMS DATA SHEET

AC-4

SN	k MINIMUM			k INTERMEDIATE			k MAXIMUM			PARAMETERS						
	DEC	INC	EV	DEC	INC	EV	DEC	INC	EV	T	P'	L	D	Vol.	ln X/Z	e
0	52.1	-76.4	6.7201 -3	76.8	12.8	7.046 -3	341.7	4.7	7.0947 -3	0.7464	1.0608	2.151	1.902	6.11	—	—
	R95 0.18		Ev95 4.81 -6	R95 0.93		Ev95 1.59 -5	R95 0.86		Ev95 1.72 -5							
1	55.9	-78.1	7.3442 -3	77.3	11.1	7.7272 -3	346.4	4.2	7.7760 -3	0.7799	1.0645	1.994	1.887	5.57	0.114	7.32%
	R95 0.09		Ev95 7.65 -6	R95 0.21		Ev95 1.94 -5	R95 0.18		Ev95 1.72 -5							

SI-1 AMS DATA SHEET

Ac - 5

SN	k MINIMUM			k INTERMEDIATE			k MAXIMUM			PARAMETERS						
	DEC	INC	EV	DEC	INC	EV	DEC	INC	EV	T	P'	L	D	Vol.	ln X/Z	e
0	81.7	73.4	6.7691 -3	333.3	5.4	6.9875-3	61.8	-15.6	7.1577-3	0.1379	1.0574	2.037	1.91	5.84	—	—
	R95 0.49	Ev95	1.88-5	R95 1.34	Ev95	3.18-5	R95 1.35	Ev95	3.74-5							
1	81.9	74.6	7.36 -3	332.5	5.24	7.7303-3	61.2	-14.5	7.9228-3	0.3323	1.0779	1.829	1.902	5.19	.162	10.22%
	R95 0.29	Ev95	1.19-5	R95 1.68	Ev95	5.06-5	R95 1.68	Ev95	5.3-5							

SI-1 AMS DATA SHEET

AC-6

SN	k MINIMUM			k INTERMEDIATE			k MAXIMUM			PARAMETERS						
	DEC	INC	EV	DEC	INC	EV	DEC	INC	EV	T	P'	L	D	Vol.	ln X/Z	e
0	312.0	-32.5	6.7626 -3	356.2	48.3	6.8896 -3	57.7	-22.9	7.147 -3							
	R95 0.95		Ev95 3.54 -5	R95 0.31		Ev95 1.54 -5	R95 0.96		Ev95 4.01 -5	-.3281	1.0577	2.456	1.899	6.96	—	—
1	318.4	33.1	7.8628 -3	336.6	55.5	7.971 -3	54.0	8.5	8.2429 -3							
	R95 2.97		Ev95 8.24 -5	R95 2.67		Ev95 5.17 -5	R95 1.54		Ev95 6.91 -5	-.4226	1.0497	2.167	1.885	6.04	.1881	11.78%

SI-1 AMS DATA SHEET

AC-7

SN	k MINIMUM			k INTERMEDIATE			k MAXIMUM			PARAMETERS						
	DEC	INC	EV	DEC	INC	EV	DEC	INC	EV	T	P'	L	D	Vol.	ln X/Z	e
0	316.0	-62.8	6.6848^{-3}	87.8	-18.9	6.8319^{-3}	4.5	18.8	7.1704^{-3}							
	R95	1.54	E95	3.94^{-5}	R95	1.56	E95	4.13^{-5}	R95	0.24	E95	4.59^{-5}	=3789	1.0743	1.816	1.905	5.17	—	—
1	316.9	-66.8	7.5427^{-3}	270.1	16.3	7.7152^{-3}	4.9	16.1	8.1077^{-3}							
	R95	0.84	E95	1.49^{-5}	R95	0.85	E95	1.0^{-5}	R95	0.18	E95	1.55^{-5}	=3746	1.0765	1.704	1.867	4.66	.095	6.15%

SI-1 AMS DATA SHEET

AC - 8

SN	k MINIMUM			k INTERMEDIATE			k MAXIMUM			PARAMETERS						
	DEC	INC	EV	DEC	INC	EV	DEC	INC	EV	T	P'	L	D	Vol.	ln X/Z	e
0	36.7	-66.4	6.5587-3	85.6	16.0	6.7775-3	350.5	16.7	6.8534-3							
	R95 0.2		Ev95 1.14-5	R95 0.18		Ev95 2.66-5	R95 0.4		Ev95 2.76-5	0.4925	1.0467	2.098	1.895	5.91	—	—
1	40.4	-75.1	7.5436-3	75.9	12.2	7.9397-3	344.1	8.3	8.0219-3							
	R95 0.01		Ev95 8.58-6	R95 0.02		Ev95 2.15-5	R95 0.09		Ev95 1.95-5	0.6663	1.068	1.719	1.912	4.94	.298	18.03%

SI-1 AMS DATA SHEET

AC- ,

SN	k MINIMUM			k INTERMEDIATE			k MAXIMUM			PARAMETERS						
	DEC	INC	EV	DEC	INC	EV	DEC	INC	EV	T	P'	L	D	Vol.	ln X/Z	e
0	293.7	41.6	6.5054 -3	348.4	-36.0	6.7381 -3	56.2	27.4	6.8702 -3	0.2875	1.0567	1.953	1.905	5.56	—	—
	R95 1.11		Ev95 3.63 -5	R95 1.8		Ev95 1.3 -5	R95 1.52		Ev95 3.8 -5							
1	292.5	74.5	7.7246 -3	359.0	-36.4	8.0045 -3	50.5	23.3	8.1752 -3	0.2553	1.0589	1.694	1.879	4.70	.213	13.26%
	R95 1.13		Ev95 4.12 -5	R95 2.01		Ev95 2.54 -5	R95 1.69		Fv95 4.93 -5							

MULTIPLE STEP CALCITE-CEMENT PURE SHEAR TESTS

SI-1 AMS DATA SHEET

AC-10

SN	k MINIMUM			k INTERMEDIATE			k MAXIMUM			PARAMETERS						
	DEC	INC	EV	DEC	INC	EV	DEC	INC	EV	T	P'	L	D	Vol.	ln X/Z	e
	311.8	62.2	6.4186 $^{-3}$	345.6	-23.4	6.5994 $^{-3}$	68.4	14.1	6.6938 $^{-3}$	0.3224	1.0435	1.948	1.897	5.50	—	—
	R95	0.98	Ev95	2.44 $^{-5}$	R95	0.93	Ev95	3.13 $^{-5}$	R95	0.55	Ev95	8.43 $^{-5}$				
A	317.0	58.0	7.1878 $^{-3}$	343.5	-28.7	7.3847 $^{-3}$	66.9	11.7	7.4933 $^{-3}$	0.2988	1.0431	1.854	1.854	5.0	.074	4.82%
	R95	0.56	Ev95	2.54 $^{-5}$	R95	0.74	Ev95	3.60 $^{-5}$	R95	0.39	Ev95	2.53 $^{-5}$				
B	306.2	56.8	7.2848 $^{-3}$	346.4	-26.5	7.4769 $^{-3}$	66.8	18.4	7.594 $^{-3}$	0.2546	1.0428	1.826	1.857	4.94	.096	6.25%
	R95	0.07	Ev95	1.81 $^{-5}$	R95	1.02	Ev95	7.11 $^{-6}$	R95	0.8	Ev95	2.02 $^{-5}$				
C	310.2	56.6	7.3959 $^{-3}$	347.6	-27.6	7.5957 $^{-3}$	68.3	17.2	7.7102 $^{-3}$	0.2830	1.0429	1.783	1.864	4.86	.133	8.47%
	R95	0.73	Ev95	2.38 $^{-5}$	R95	0.89	Ev95	2.23 $^{-5}$	R95	0.64	Ev95	9.73 $^{-6}$				
D	310.8	62.3	7.5033 $^{-3}$	347.2	-23.6	7.7226 $^{-3}$	68.2	13.6	7.834 $^{-3}$	0.3347	1.0447	1.75	1.864	4.78	.161	10.17%
	R95	0.46	Ev95	1.66 $^{-5}$	R95	0.42	Ev95	1.84 $^{-5}$	R95	0.24	Ev95	6.71 $^{-6}$				
E	312.3	61.9	7.6026 $^{-3}$	342.2	-24.9	7.8334 $^{-3}$	66.3	12.3	7.9548 $^{-3}$	0.3199	1.047	1.717	1.867	4.70	.189	11.86%
	R95	0.74	Ev95	2.43 $^{-5}$	R95	0.99	Ev95	1.97 $^{-5}$	R95	0.73	Ev95	1.55 $^{-5}$				
F	308.8	60.6	7.6252 $^{-3}$	340.5	-20.4	7.8897 $^{-3}$	65.7	12.7	8.0146 $^{-3}$	0.3526	1.0506	1.699	1.869	4.66	.205	12.77%
	R95	0.65	Ev95	2.71 $^{-5}$	R95	0.88	Ev95	3.14 $^{-5}$	R95	0.65	Ev95	1.42 $^{-5}$				
G	313.2	57.0	7.7113 $^{-3}$	338.5	-19.2	7.9902 $^{-3}$	63.0	6.5	8.1111 $^{-3}$	0.4058	1.0531	1.651	1.882	4.59	.248	15.25%
	R95	0.65	Ev95	2.71 $^{-5}$	R95	0.65	Ev95	2.1 $^{-5}$	R95	0.44	Ev95	1.18 $^{-5}$				

SI-1 AMS DATA SHEET

AC-10

SN	k MINIMUM			k INTERMEDIATE			k MAXIMUM			PARAMETERS						
	DEC	INC	EV	DEC	INC	EV	DEC	INC	EV	T	P'	L	D	Vol.	ln X/Z	e
H	313.6	72.7	7.7496 -3	334.4	-16.2	8.0855 -3	62.7	5.8	8.211 -3	0.4675	1.0616	1.593	1.899	4.52	.302	18.25%
	R95	0.37	E.95	1.64 -5	R95	0.67	E.95	1.73 -5	R95	0.55	E.95	3.69 -5				

SI-1 AMS DATA SHEET

AC-11

SN	k MINIMUM			k INTERMEDIATE			k MAXIMUM			PARAMETERS						
	DEC	INC	EV	DEC	INC	EV	DEC	INC	EV	T	P'	L	D	Vol.	ln X/Z	e
	21.2	60.5	6.7726 -3	275.5	8.8	7.0875 -3	0.7	-28.1	7.3191 -3							
	R95 0.28		Ev95 3.68 -6	R95 0.26		Ev95 4.64 -6	R95 0.73		Ev95 1.2 -5	0.1724	1.081	2.326	1.902	6.61	—	—
A	26.2	56.3	7.4667 -3	276.5	12.7	7.7781 -3	358.9	-30.7	8.0389 -3							
	R95 0.22		Ev95 3.71 -6	R95 0.32		Ev95 1.33 -5	R95 0.89		Ev95 1.82 -5	0.1071	1.0767	2.222	1.867	6.08	.069	4.47%
B	25.1	58.4	7.621 -3	277.8	10.4	7.9525 -3	1.8	-29.4	8.2154 -3							
	R95 0.34		Ev95 1.9 -6	R95 0.33		Ev95 1.64 -5	R95 0.34		Ev95 2.14 -5	0.1347	1.0781	2.197	1.859	5.96	.086	5.56%
C	23.6	59.3	7.754 -3	276.3	9.8	8.1186 -3	0.8	-28.7	8.3787 -3							
	R95 0.31		Ev95 1.54 -5	R95 0.2		Ev95 4.52 -6	R95 0.29		Ev95 1.93 -5	0.1843	1.0807	2.128	1.867	5.82	.133	8.51%
D	21.9	62.0	7.9397 -3	275.6	8.5	8.3448 -3	1.4	-26.6	8.5998 -3							
	R95 0.22		Ev95 1.58 -5	R95 0.21		Ev95 2.58 -5	R95 0.62		Ev95 1.52 -5	0.2459	1.0838	2.045	1.879	5.65	.193	12.12%
E	27.7	62.0	7.9501 -3	275.9	11.2	8.3705 -3	0.6	-25.4	8.6348 -3							
	R95 0.31		Ev95 8.02 -6	R95 0.3		Ev95 1.34 -5	R95 0.22		Ev95 1.25 -5	0.2809	1.088	1.989	1.897	5.62	.235	14.52%
F	28.3	63.5	8.0785 -3	276.5	10.6	8.5578 -3	1.7	-24.2	8.8071 -3							
	R95 0.19		Ev95 5.8 -6	R95 0.2		Ev95 1.50 -5	R95 0.14		Ev95 3.62 -5	0.3352	1.0918	1.925	1.905	5.48	.284	17.25%

LIST OF SLIDES

SLIDE NO.	SUBJECT
1	UNDEFORMED SAND-CEMENT MATERIAL
2	UNDEFORMED CALCITE-CEMENT MATERIAL

SAND-CEMENT SHEAR ZONES

SLIDE NO.	EXPERIMENT	SERIES	FINAL SHEAR STRAIN (ɣ)
5	SZ-A	A	.025
6	SZ-K	A	.378
7	SZ-1	C	.104
8	SZ-3	B	.324
9	SZ-1	B	.118

CALCITE-CEMENT SHEAR ZONES

SLIDE NO.	EXPERIMENT	SERIES	FINAL SHEAR STRAIN (ɣ)
10	SZ-C1	1	.111
11	SZ-C3	2	.129
12	SZ-C3	2	.129
13	SZ-C3	1	.189
14	SZ-C2	2	.124

CALCITE-CEMENT PURE SHEAR TESTS

SLIDE NO.	EXPERIMENT	FINAL STRAIN
20	AC-3	4.4%
21	AC-9	13.26%
22	AC-8	18.03%

Tectonophysics, 133 (1987) 121–135
Elsevier Science Publishers B.V., Amsterdam – Printed in The Netherlands

Relationship between magnetic susceptibility and strain in laboratory experiments

GRAHAM BORRADAILE and CRAIG ALFORD

Department of Geology, Lakehead University, Thunder Bay, Ont. P7B 5E1 (Canada)

(Received September 24, 1985; revised and accepted June 5, 1986)

Abstract

Borradaile, G. and Alford, C., 1987. Relationship between magnetic susceptibility and strain in laboratory experiments. *Tectonophysics*, 133: 121–135.

Under experimental conditions of 1.5 kbar confining pressure and at a strain-rate of 5×10^{-6} sec^{-1} at room temperature the principal directions of magnetic susceptibility of a dry, synthetic, magnetite-bearing sandstone rotate toward principal strain directions. The rotation is faster than that expected from rotation of a line in homogeneous strain. Fluid pressures of 200 or 700 bars do not appear to affect the development of anisotropy of susceptibility.

The *change* in bulk anisotropy shows a power law correlation with strain ratio where the initial susceptibility ellipsoid was nearly coaxial with the bulk strain axes during the experiment. More generally, in those situations, as well as ones in which the initial susceptibility ellipsoid was strongly inclined to the bulk strain axes there exists a common matrix M which relates the initial susceptibility tensor k_{ij}, the final susceptibility tensor k'_{ij} and the strain tensor e_{ij}:

$$e_{ij}k_{ij} = Mk'_{ij}$$

Introduction

Recently there has been considerable interest in the use of magnetic susceptibility in structural and tectonic geology. In brief, we know from the work of Graham (1954) and the schools of Tarling (e.g. Singh et al., 1975), Hrouda (e.g. Hrouda, 1982), Kligfield (e.g. Kligfield et al., 1977, 1982) and Owens (e.g. Owens and Bamford, 1976; Owens and Rutter, 1978), that the orientations of principal susceptibilities can correspond to the orientation of sedimentary, magmatic or tectonic fabrics. Furthermore, in the case of tectonically deformed rocks the principal susceptibilities often correspond to the principal strain directions determined from conventional strain markers (e.g. Rathore, 1979; Borradaile and Tarling, 1981, 1984; Borradaile and Mothersill, 1984). This correspondence has lead to the notion of a susceptibility ellipsoid, represented by the tensor components k_{ij}, whose principal directions may have tectonic significance.

We may rapidly and easily determine the susceptibility ellipsoid's orientation and magnitudes of susceptibility for a rock although conventional strain or fabric markers are absent. In this way it is possible to determine the cryptic fabric of the magnetic minerals and this may provide information on the principal strain orientations. Moreover, it has been suggested by Rathore (1979) and Rathore and Henry (1982) that the magnitudes of susceptibility (and thus the shape of the susceptibility ellipsoid given by ratios of magnitudes) may correspond to the shape of the strain ellipsoid.

To refine our knowledge of the correlations

0040-1951/87/$03.50

between susceptibility and strain in naturally deformed rocks we must focus our attention on the following items. Some literature citations indicate where these problems have been addressed to some degree:

(1) Which minerals are the source of the susceptibility? Are they matrix-forming minerals or minor phases? (e.g. Schwarz, 1974; Owens and Bamford, 1976; Wagner et al., 1981; Borradaile et al., 1986).

(2) What is the nature of the pre-tectonic susceptibility of rocks? (e.g. Graham, 1966; Rees, 1966, 1968; Hamilton et al., 1968; Rees and Woodall, 1975). Does this influence the post-tectonic susceptibility? (e.g. Borradaile and Tarling, 1981).

(3) What is the nature of the processes acting to change the original susceptibility k_{ij} to the final susceptibility k'_{ij} (Goldstein, 1980, touched on this problem). Were the magnetic minerals affected by recrystallisation processes (e.g. Borradaile et al., 1986), rotations (Owens, 1974), by pressure solution (Borradaile and Tarling, 1981) or other deformation mechanisms?

(4) What is the state of finite strain of the rock (e_{ij})?

In naturally deformed rocks there are inevitably problems in determining these four items and while this does not undermine the value of susceptibility studies it does leave questions unanswered in linking the four items.

We attempt to address the problems from susceptibility studies of experimentally deformed materials: (a) of known mineralogy; (b) of known original susceptibility (k_{ij}); (c) subjected to experimental deformation of a macroscopically ductile nature; so that (d) the bulk finite strains (e_{ij}) are known.

Owens and Rutter (1978) adopted a similar approach. However, they investigated the changes in diamagnetic susceptibility of marble and of single calcite crystals and the accompanying crystallographic fabrics. They calibrated crystallographic fabric in terms of susceptibility for single crystals. Our study focusses on the bulk strain effects upon a multigranular, polymineralic material with disseminated ferrimagnetic marker grains. We address the problem of calibrating bulk strain in terms of bulk susceptibility changes.

The material used

The specimens used in the experiments had to be of relatively small size (approx. 10 cm^3) to fit in the triaxial rig. Consequently, the bulk susceptibility had to be high so that the anisotropy of susceptibility could be determined accurately. Moreover, the initial anisotropy of susceptibility of the specimens before deformation had to be low, so that the difference in shapes of the specimen before and after strain did not produce a shape effect which adversely affected the determination of the susceptibility ellipsoid. Further, the material had to be suitably strong so that it permitted the pistons of the triaxial rig to be precisely seated against the specimen at the start of a test; suitably ductile at the range of confining pressures and strain rates permissible, and of a suitable grain-size to favour homogeneous deformation.

Being unable to find a natural material which met these requirements we synthesised an artificially cemented "sandstone". This was prepared by sieving a glacio-lacustrine beach sand to retain an aggregate in the grain-size range 3.0 to 3.5 Ø (0.125 to 0.088 mm). The sieved sand had at this stage an enhanced magnetite content of about 4 wt.% and a mineralogy dominated by quartz and feldspars. To improve the confidence of measurement of susceptibility directions, crushed magnetite was added to the mixture. These grains had similar shape ratios to the natural grains of the sieved beach sand and were sieved to give the same grain size as the naturally present magnetite. The magnetite is thus present in approximately the same size range as the other grains. Whilst this is not usually the case in natural metamorphic rocks, it was our intention to investigate the effects on magnetite "re-orientation" where the magnetite might be expected to behave in a broadly similar fashion to the matrix-forming grains.

The aggregate was cemented with 40% (dry volume proportion) of Portland cement which was distributed evenly through the well-mixed aggregate. The cement was set by the addition of warm water. The effects of "flow fabrics" produced by mixing the cement were reduced by setting the aggregate in a large shallow tray. This was re-

peatedly probed with a fine copper wire during setting to reduce any preferred orientation produced during mixing. The setting tray was also rotated to minimise the aligning effect of the earth's magnetic field on the magnetite. The set block had 8% magnetite by weight and was air-dried for 1 month. The specimens were then core-drilled from the block. Small bubbles at the surface of the cores were filled with the same mixture of the aggregate and cement. This was necessary to reduce the frequency of jacket failures during the triaxial rig tests. Cement on its own has a susceptibility of 7.26 (± 0.04 s.e.) $\times 10^{-6}$ cgs cm^{-3} (twenty determinations on a specimen of 143 cm^3). Thus it makes a negligible contribution to the susceptibility of the samples for which the bulk susceptibilities are about 3×10^{-3} cgs cm^{-3}.

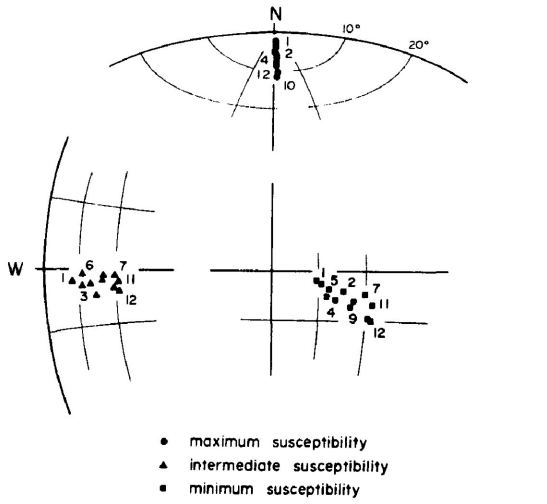

Fig. 1. Condensed parts of a lower hemisphere equal area steronet. This shows how the principal susceptibility directions of a single, never-deformed cylindrical sample change as the cylinder's length is gradually reduced by grinding. No. *1* indicates the greatest length, when the length/diameter ratio of the specimen was nearly 1.4. No. *12* indicates the shortest length when the specimen had a length/diameter ratio of just less than 0.6.

Determination of magnetic susceptibility

The magnetic susceptibility of cylindrical core specimens was determined before and after deformation in an SI-1 meter developed by Sapphire Instruments of Ruthven, Ont., described elsewhere (Borradaile and Mothersill, 1984).

Specimen shape, especially the length/diameter ratio ($1/d$), can influence the determination of anisotropy of susceptibility where the bulk susceptibility is low. Where $1/d > 0.82$ the maximum susceptibility will be parallel to the axis of the cylindrical specimen and where $1/d < 0.82$ the minimum susceptibility will be parallel to the axis (Stupavsky, 1983). Thus we have taken a somewhat longer than usual core of the material and determined its anisotropy of susceptibility repeatedly as its length was reduced gradually by grinding off the ends. There was little change in the orientations of the principal susceptibility directions (Fig. 1). Since the 95% cone of confidence about the determined principal directions can be as much as 3°, and in view of the data distribution in Fig. 1, we consider the shape effect upon the determination of susceptibility directions to be minor in this material. This permits us to determine anisotropy of susceptibility from the same specimen before deformation and after deformation, when its shape had changed. It should also be noted that the $1/d$ ratios actually used in our tests were in quite a narrow range ($1.2 > 1/d > 0.94$ at the start of the test).

The shape effect influences the magnitudes of anisotropy. We used the P' parameter of Jelinek (1981), expression of total degree of anisotropy given by:

$$P' = \exp\sqrt{2\left(a_1^2 + a_2^2 + a_3^2\right)}$$

where $a_1 = \ln(k_{11}/\bar{k})$ etc. and:

$$\bar{k} = (k_{11} \cdot k_{22} \cdot k_{33})^{1/3};\ k_{11} = k_{\max} \text{ etc.}$$

The way in which P' varies with the ratio $k_{\max}/k_{\text{int}}$ etc. is shown in Fig. 2.

We note a slight decrease in P' as the $1/d$ ratio was reduced from 1.4 to 0.6 (Fig. 3). Again we emphasise that this range of $1/d$ ratio is actually much greater than that used in the tests to be described subsequently.

A systematic change in the shape of the susceptibility ellipsoid also occurs as the specimens $1/d$ ratio changes. This change is expressed in terms of the single parameter T (Jelinek, 1981) which is given by:

$$T = \left[2(\ln k_{11} - \ln k_{22})/(\ln k_{22} - \ln k_{33})\right] - 1$$

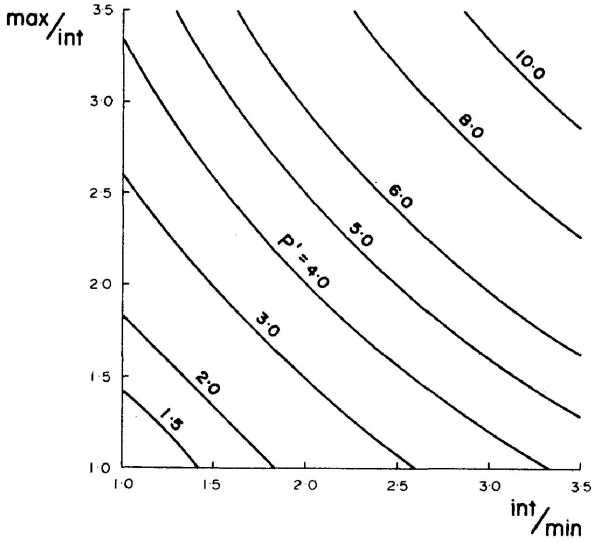

Fig. 2. Illustrating the variation of the anisotropy parameter, P', in terms of the ratios of the principal susceptibilities. P' expresses the degree of anisotropy (Jelínek, 1981).

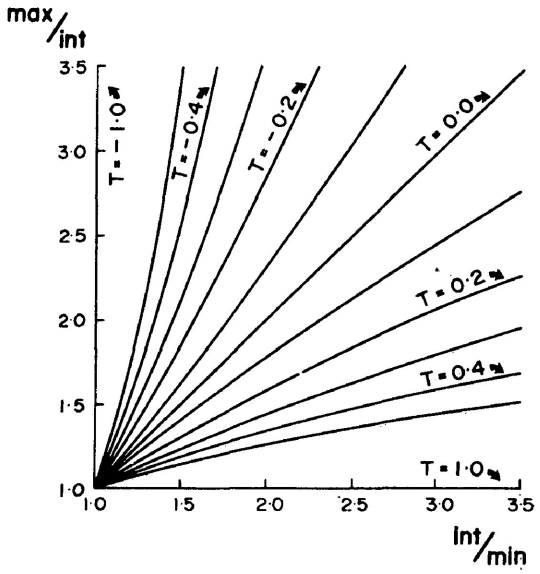

Fig. 4. Illustrating the variation of the sense of anisotropy parameter, T, with the ratios of the principal susceptibilities.

The variation in T with the ratios k_{max}/k_{int} etc. is shown in Fig. 4. The change in T shown by the specimen is indicated in Fig. 5. While this shape change appears substantial it should be realised that the ellipsoids described are very nearly spherical and plot near the origin of a graph of k_{max}/k_{int} against k_{int}/k_{min}, since their P' values are so low.

In the experimentally deformed samples a reference arrow was placed on one end of the cylindrical specimens to permit changes in susceptibility orientations to be detected.

Experimental deformation

The samples of known magnetic susceptibility were deformed in a triaxial rig designed by Donath (1970). The specimens were jacketed in Teflon or a combination of Teflon and heat-shrink tubing. Since these materials have negligible susceptibili-

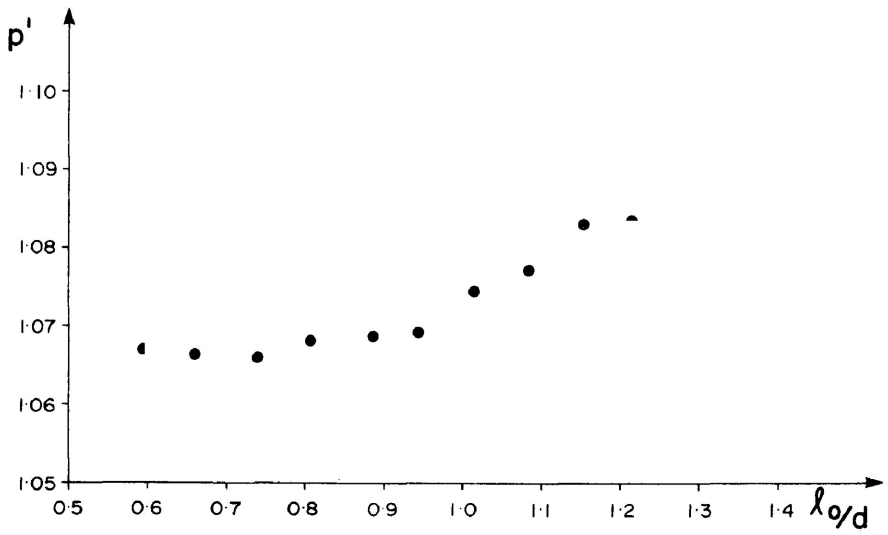

Fig. 3. Illustrating the shape effect upon the anisotropy parameter, P'. The ratio of length/diameter for a single, never-deformed specimen was changed by grinding away the ends of the specimen.

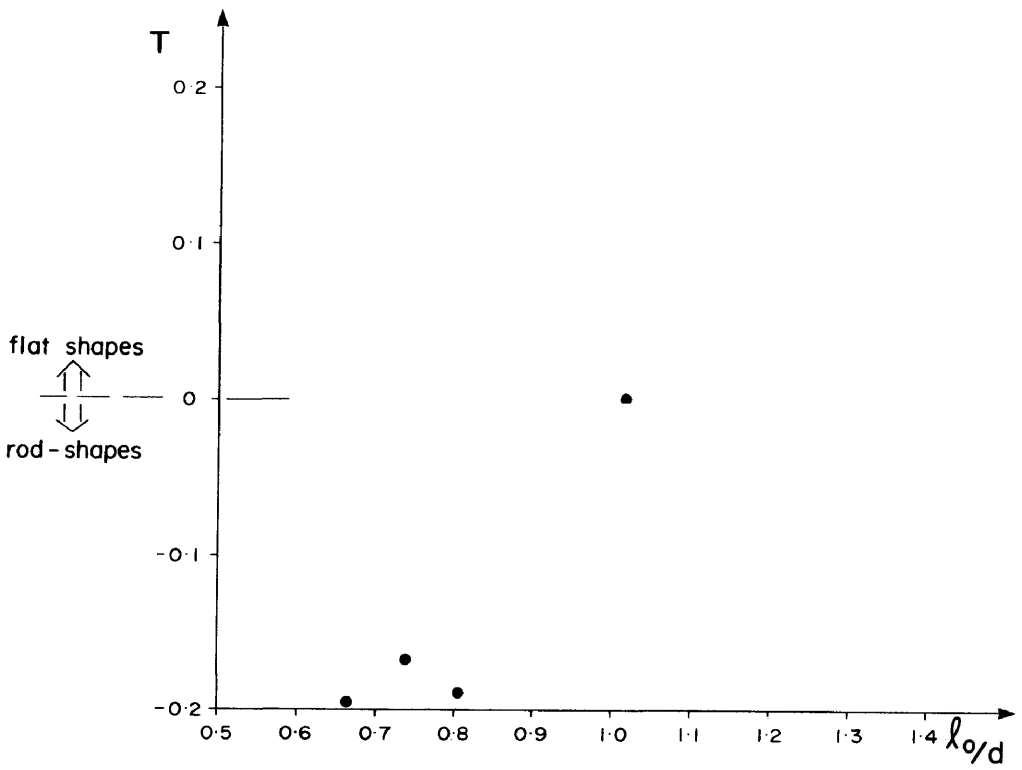

Fig. 5. Illustrating the shape effect upon the anisotropy parameter, T. The same specimen was used as in Fig. 3 as its length was reduced by grinding.

ties and the susceptibility of specimens is high (ca. 3×10^{-3} cgs cm^{-3}) it permitted us to leave the specimens in their jackets for the susceptibility determination after deformation. Some specimens could be removed from their jackets and this permitted us to reuse the same specimen with a new jacket for subsequent tests to examine the effects of progresive deformation in increments of several percent shortening.

The specimens were all deformed at a confining pressure of 1.5 kb (1.5×10^8 Pa) and at a strain-rate of 5.11 ± 0.25 (s.d.) $\times 10^{-6}$ sec^{-1}. The strain rate was a "natural" strain rate in which the incremental change in length was in a constant ratio to the length of the specimen at the start of that increment (Pfiffner and Ramsay, 1982). Loading was achieved hydraulically via a syringe pump driven electrically through a multi-rate gearbox. Separate chart recorders plotted load versus displacement and displacement versus time, and in the later tests a microcomputer system permitted automatic control of the strain-rate via a variable speed control to the loading pump. Synchronous data reduction and corrections were similar to those outlined by Donath and Guven (1971) and Rutter (1972) and used a microprocessor system supplied by Dr. J. Holder (C.G.S. Inc.). The constant strain-rate programs and stress relaxation programs were written by the authors in BASIC to utilise Dr. Holder's machine language subroutines.

The artificially cemented sandstone showed work hardening stress–strain curves without sharp yield points for all tests. Neville (1981, p. 364) attributes most deformation at low strains to microcracking at the boundaries between rock particles and the cement "gel" in concrete. The cement gel is a cryptocrystalline aggregate of hydrated calcium silicates and calcium aluminates which progressively crystallise over a period of months or years. The artificial cement that we used was a Portland variety which achieves nearly all of its ultimate strength after 28 days. During the next 28 days it only increases its strength by 5% and thereafter more slowly. Thus during our

tests, performed in this second interval of 28 days, the samples did not increase substantially in strength and we do not believe that any substantial change in the mode of deformation occurred over this period.

Stress-relaxation tests of the type used by Rutter et al. (1978) and Schmid (1976) were performed on the artificial cement-sand material. There is some indication that there is a change in deformation mechanism at a strain rate of about 7.9×10^{-7} sec^{-1} (Fig. 6b). Nevertheless, both the singly deformed material and the multiple deformed material (corresponding to pre-stressed concrete) show the same slope on the $\log_{10}$ (differential stress) versus $\log_{10}$ (strain-rate) graph at the strain rate used in the tests (5×10^{-6} sec^{-1}). This suggests a relationship between differential stress (in bars) and strain rate (e) of the form:

$$\dot{e} \propto \sigma^n$$

with $n \simeq 40$.

This weak effect of differential stress (strength) upon strain rate is typical of sandstones deforming by cataclastic flow (Donath and Fruth, 1971)

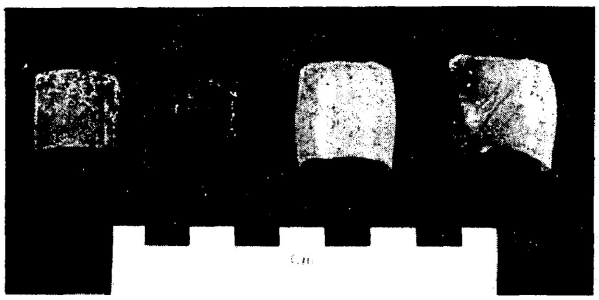

Fig. 7. A selection of specimens, from left to right these are not deformed, shortened by 13%, by 21%, and by 35%. The two specimens on the right are still encased in teflon jackets. The most deformed specimen shows shear zones that normally developed beyond 24% shortening.

but in our samples most of the deformation is confined to the cement gel.

For the constant strain-rate tests at 5×10^{-6} sec^{-1} we chose a specimen shape by experimentation which would suppress faulting as a mode of failure and instead fail in a macroscopically ductile fashion. The actual length varied from test to test so that the final $1/d$ ratio expected after a certain shortening would produce the least shape-effect

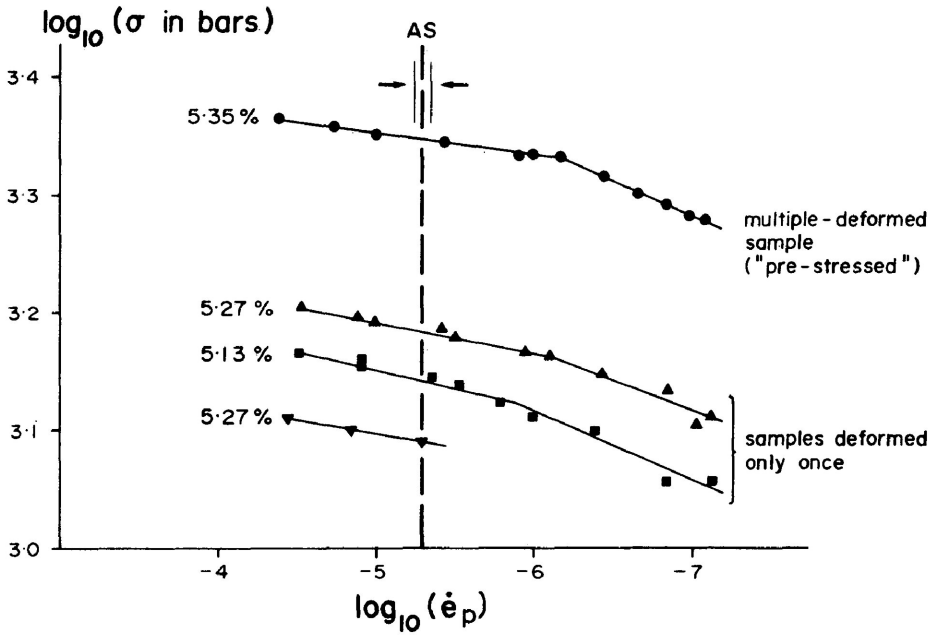

Fig. 6. Stress-relaxation results for the artificially cemented sandstone performed at the percentage strain indicated. Note that multiple deformed specimens (="pre-stressed concrete") are stronger than single deformed specimens. In the subsequent tests which were used to study the effects of strain on the magnetic susceptibility a strain-rate of 5×10^{-6} sec^{-1} was chosen; the actual average (AS) and standard deviation are indicated on the graph above. (σ = differential stress in bars, $\dot{e}_p$ = rate of accumulation of permanent strain).

upon the determination of the anisotropy of magnetic susceptibility.

Examples of the initial and deformed specimens are shown in Fig. 7.

Comparison of anisotropy of susceptibility before and after deformation

The principal susceptibilities and their orientations were determined for each specimen before deformation. A reference arrow was placed on one end of each cylindrical specimen so that the susceptibility could be determined relative to it after the experimental deformation. Susceptibility was determined immediately after each specimen was removed from the triaxial rig. To check whether any time-dependent inverse magnetostrictive (piezomagnetic) effects occurred during the release of stored strain energy, the susceptibility of two deformed specimens and a never-deformed control specimen were measured at repeated intervals for some time after the experiments (Fig. 8).

The value P' did not change significantly after experimental deformation. In fact the individual susceptibility values rarely moved beyond the 95% confidence limits of previous determinations. (As an example of the size of the confidence limits the values for a typical deformed specimen, B8520, were:

$k_{min} = 2.6698 \pm 0.002$

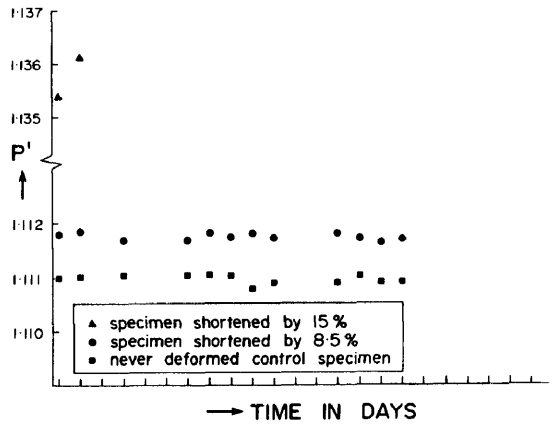

Fig. 8. This illustrates that the magnetic anisotropy shows no significant, consistent changes with time after a sample has been experimentally deformed.

$k_{int} = 2.8250 \pm 0.003$

$k_{max} = 3.0377 \pm 0.003$

all in units of 10^{-3} cgs cm^{-3}.)

Despite the lack of time-dependence on the susceptibility values within the time-frame concerned, post-deformation susceptibility tests were always performed immediately following removal of the specimen from the triaxial rig.

Changes in orientation of the principal susceptibilities during experimental deformation

Specimens have been deformed by axial shortening in the range 2% to 35%. Fully ductile behaviour in the macroscopic sense has been achieved to 25% axial shortening. It has thus been possible to monitor rotations of the principal susceptibilities in this range. However it is necessary to draw attention to the fact that the best attempts at bulk homogeneous deformation are merely approximations to that state. The typical sequence of events with progressive shortening is that, firstly, the cylindrical specimen takes on a very weak "hourglass shape". This accompanies a small volume reduction that we attribute largely to the collapse of bubbles in the cement matrix although pure cement gels are known to contract during creep (Neville, 1970, p. 260). At about 3.5% shortening this effect disappears and the specimen becomes progressively more barrel-shaped (see Fig. 7). At about 24% shortening some macroscopic faulting occurs. The load–displacement curve for the experiment usually indicated the onset of faulting so that it was possible to isolate partly the component of axial shortening due to bulk strain and that due to faulting where the net shortening exceeded this 24% limit.

A typical example of the effect of progressive movement of the susceptibility axes is illustrated by experiment B8513 (Fig. 9). This specimen was shortened along its axis by 3%, then further shortened in a subsequent test to a total shortening of 21%. The initial motion of the susceptibility axes shown by this and other specimens is that the minimum susceptibility (k_{min}) may not move toward the axis of shortening (the axis of the cylinder), Z, in the initial stage (Fig. 9a). This effect

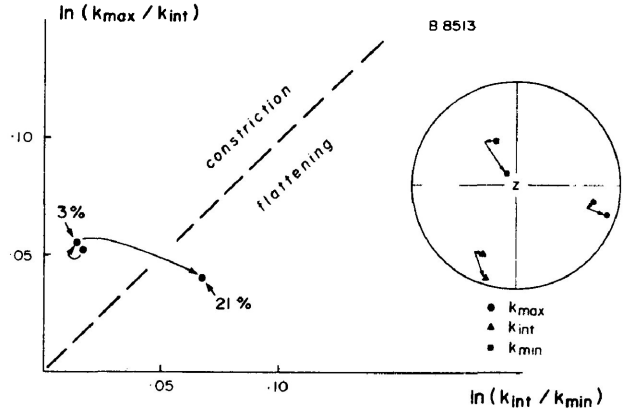

Fig. 9. Changes in anisotropy of susceptibility in a specimen shortened in two stages, first by 3% and then further to give a total shortening of 21%. a. (inset) Lower hemisphere stereonet showing the rotation of principal directions of susceptibility. b. Graph showing change in ratio of susceptibilities.

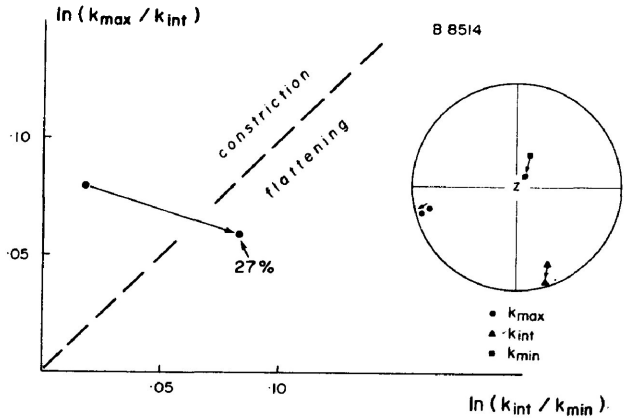

Fig. 10. Changes in anisotropy of susceptibility in a specimen shortened in a single test by a total of 27%. a. (inset) Lower hemisphere stereonet showing rotation of the principal directions. b. Graph showing change in ratio of susceptibilities.

persists to about 4% shortening while the specimen develops and keeps an hourglass shape. Further deformation beyond the 4% level produces a distinct rotation of k_{min} toward the Z axis and k_{max} and k_{int} away from the Z axis.

Moreover, the shape of the susceptibility ellipsoid does not always become progressively more eccentric during the early part of the shortening history. As shown in Fig. 9, the ellipsoid may initially become slightly more prolate. Subsequent substantial shortening, however, produces a more eccentric susceptibility ellipsoid further into the field of flattening (Fig. 9).

The initial irregular motion of the susceptibility axes and the irregular change in shape of the susceptibility ellipsoid is, we believe, associated with the hourglass shape of the specimen at the early stage of shortening. We speculate that during this early shortening the ends of the cylindrical specimen spread against the steel pistons and that a locally strong magnetic fabric develops at the specimen ends. This irregular magnetic fabric is thus an artefact of the experimental method and is suppressed after 4% shortening when the bulk deformation of the specimen produces a magnetic fabric which dominates. A typical experimental result, for a test producing 27% shortening in a single event (B8514) is shown in Fig. 10a and 10b. The k_{min} axis moved toward Z (Fig 10a) and the susceptibility ellipsoid became flatter-shaped and lies further from the origin of the shape-ratio graph (Fig. 10b).

Interesting examples of transformations of original to post-deformation susceptibility ellipsoids have also been discovered. For example, in some instances where the original susceptibility ellipsoid has its k_{min} axis at large angles ($> 40°$) to Z there occur transformations initially to lower anisotropies and then with significant further strain to higher than original anisotropies. Such geometrical transformations can be considered *analogous* to the sequence of homogeneous progressive strain of ellipsoidal markers (e.g. Ramsay, 1967, pp. 204–209). However, it is not suggested that the susceptibility ellipsoid actually behaves precisely as a passive elliptical marker.

Figure 11 illustrates shape and directional changes which accompany typical experiments (B8518) and ones in which the initial ellipsoid was elongate parallel to the shortening direction (B85PF1). In experiment B8518 it was possible to use the same specimen repeatedly so that a sequence of successive anisotropies indicated the "deformation path" of susceptibility. The anisotropy becomes *progressively* greater (further from the origin) as the specimen is shortened to 4%, then to 9%, 11.5% etc. The anisotropy also moves to a more flat-shaped ellipsoid (by analogy with the T-value distribution of Fig. 4). It should be noted that the differences between the initial

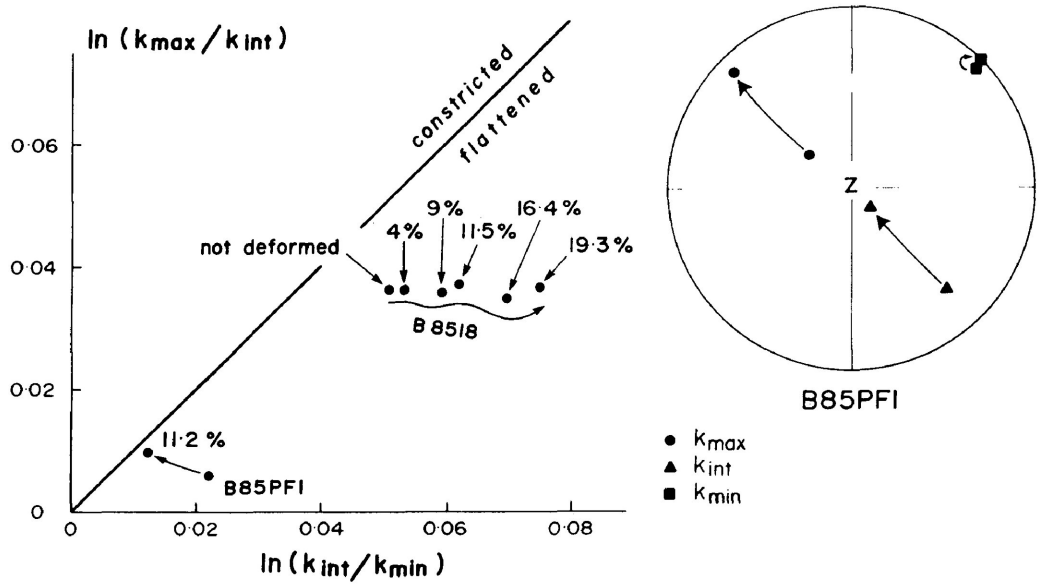

Fig. 11. Showing the changes in ratios of the principal susceptibilities, equivalent to changes in the shape of the susceptibility ellipsoid. a. In experiment B8518, the same specimen was shortened in steps by the percentages indicated. The susceptibility ellipsoid describes a path to progressively more strained, flattened shapes. b. In experiment B85PF1 a specimen was shortened by 11.2%. In this case the original susceptibility ellipsoid was inclined steeply, near to the axis of shortening (see stereonet) and the ellipsoid actually became less eccentric with advancing strain.

and final anisotropies on plots such as Figs. 11 and 13 are not proportional to the amount of shortening. They also depend strongly on the *original* orientation of the susceptibility ellipsoid.

This last point is shown well by experiment B85PF1 in which an initial susceptibility ellipsoid was inclined with its k_{max} axis at 27° to the axis of shortening (z) of the specimen (Fig. 11). The effect of an 11% shortening on this specimen is actually to reduce the anisotropy near to that position neutral between the fields of constricted and flat shapes. This emphasises the importance of the initial susceptibility in influencing the post-deformation susceptibility.

Rate of rotation of susceptibility axes with strain

In cases where the susceptibility ellipsoid has its k_{min} axis within 40° of the Z axis of the specimen the rotations of the k_{min} axes follow a consistent pattern. k_{min} rotates toward Z_y though the actual path is not known and the arrows on Figs. 9a and 10a merely act as tie-lines and are not meant to indicate actual paths.

Using a diagram showing the change in angular

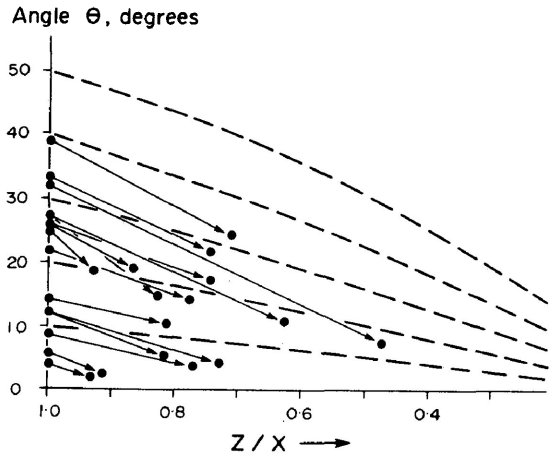

Fig. 12. The broken lines show the change in angle expected for a line rotating in homogeneous strain with ratio Z/X where $X > Z$ (Ramsay, 1967, fig. 4-6). The arrows connect the values of the angle between k_{min} and the Z-axis before shortening (left) to the values after shortening (on the right). In all cases k_{min} rotates more quickly than the hypothetical line element. *N. B.* Not all experiments can be represented in this way because some initial susceptibility ellipsoids were elongate parallel to the shortening direction. Their shape changes were thus not towards progressive eccentricity; early in the experiments they became less eccentric (this is shown in Fig. 11b).

position of k_{min} with respect to Z (θ_0 changing to θ') it is possible to show that the rotation of k_{min} exceeds that of a line element undergoing homogeneous strain which would be given by:

$$\frac{\tan \theta'}{\tan \theta_0} = \frac{Z}{X}$$

The graph in Fig. 12 shows the changes in angular position of k_{min} with the strain expressed as a ratio Z/X. In all cases the line connecting initial (θ_0) angles with final (θ') angles is steeper than the path which predicts the rotation of a line element. Susceptibility axes thus rotate faster than would be inferred from the effects of homogeneous strain on a linear element.

Changes of shape of the susceptibility ellipsoid with strain

The susceptibility ellipsoids for most of the undeformed specimens lie in the field of cigar-shaped ellipsoids (Fig. 13). In nearly all cases the effect of advancing deformation, which is of a flattening ($X = Y > Z$) character due to the symmetry of a triaxial rig, is to move the susceptibility ellipsoid,

(a) away from the origin to a more eccentric shape, and

(b) further toward or into the field of flat-shaped ellipsoids.

This confirms that the symmetry of the susceptibility ellipsoids tend to conform to that of the bulk strain ellipsoid.

Correlation between susceptibility changes and strain

If it could be shown that susceptibility anisotropy correlated with strain, it has been contended that it may be possible to calibrate the anisotropy in terms of strain. This might enable one to estimate strain from the magnetic susceptibility ellipsoid even in the absence of conventional strain markers. However, in this study as earlier (Borradaile and Mothersill 1984), it has *not* been possible to correlate the *post*-deformation susceptibility with strain.

It has, however, been possible to correlate the *change* in anisotropy of susceptibility with strain. This has only been possible of course because both the pre-deformation and post-deformation susceptibilities are known. As shown in Fig. 14 there exists a correlation between strain and the difference P' in total anisotropy before (P'_0) and after (P') deformation where:

$$\Delta P' = P' - P'_0$$

Strain has been plotted as $\ln(X/Z)$ so that a power-law relationship of the type proposed by Rathore (1979) does in fact exist with:

$$\Delta P' \propto \ln(X/Z)$$

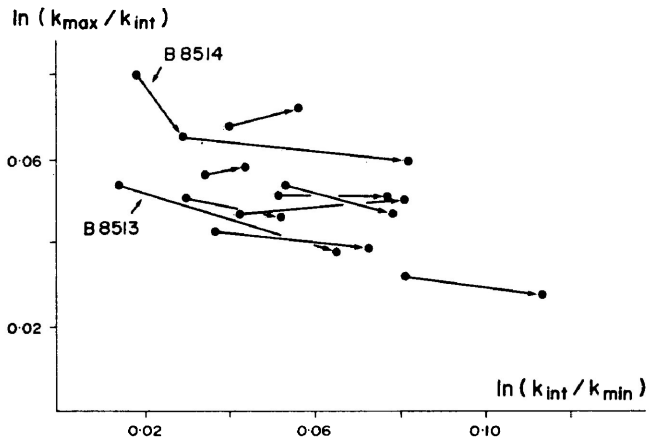

Fig. 13. Showing the change in shape of the susceptibility ellipsoid (given by the ratios of principal susceptibilities) resulting from experimental shortening. The arrows connect the initial anisotropies to the final ones. In all these cases the susceptibility ellipsoid becomes flatter, in agreement with the flattening character of the experimental deformation. *N.B.* In some experiments initially susceptibility ellipsoids were elongate parallel to the shortening direction and they became less elliptical in the early parts of the test (e.g. see Fig. 11b). These are omitted here.

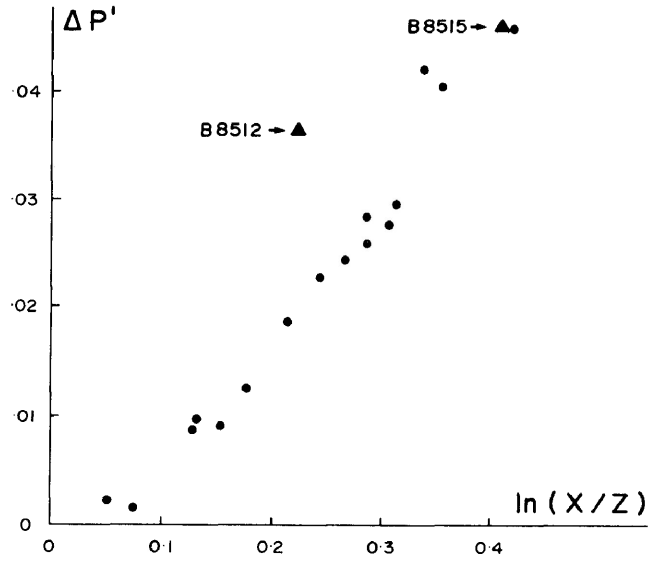

Fig. 14. The correlation between the change in the degree of anisotropy P' before and after shortening, with the logarithm of the strain ratio X/Z for all experiments. The correlation is significant at the 95% level with a coefficient of 0.973. The data of experiment B8515 were corrected for a set of visible macroscopic faults which actually produced more shortening than shown. (Only penetrative macroscopically ductile deformation is of interest here.) The data of experiment B8512 were omitted because a pore-fluid pressure was accidentally introduced in this specimen.

The correlation is significant at the 95% level and the correlation coefficient is 0.973. It should be emphasised, however, that this correlation was established using a knowledge of the anisotropy of susceptibility *before* deformation.

The regression line suggests a relationship of the form:

$$\ln \Delta P' = 0.122 \ln(X/Z) - 0.573$$

for the results of these particular experiments.

This correlation was established with the exclusion of the data for experiment B8512. This anomalous point indicates a high level of anisotropy development at quite low strain. However, in that experiment there existed a pore pressure due to accidental slow or late failure of the specimen jacket. In a later section we present results of our investigation into the effects of pore-fluid pressure.

The linear relationship of Fig. 14 only partly illustrates the dependence of the anisotropy changes on strain. For example, in special cases where the initial susceptibility ellipsoid was oriented nearly parallel to the shortening direction (Z) often the magnitude changes were non-progressive (e.g. like in Fig. 11, experiment B85PF1) and the results cannot be plotted on Fig. 14.

We have utilised the data more fully by relating all the tensor components of susceptibility to the strain tensor (the e_{ij} of Means, 1976, p. 210). We predict a relationship of the kind

$$e_{ij}k_{ij} = Mk'_{ij}$$

where k is the tensor describing the initial susceptibility and k' is the tensor describing the susceptibility after strain. The matrix M we have determined which relates these quantities for the seven best experiments in which the bulk strain was most homogeneous is:

0.066	0.001	−0.004
(±0.024)	(±0.004)	(±0.011)
−0.002	0.065	−0.010
(±0.003)	(±0.027)	(±0.014)
−0.014	−0.025	−0.175
(±0.025)	(±0.034)	(±0.071)

The quantities in parentheses are standard deviations.

The effects of pore-fluid pressure

The accidental jacket failure of experiment B8512 caused a pore-fluid pressure to develop in the specimen due to infiltration by the silicone oil used as a confining pressure medium. The fluid pressure in the specimen was sufficient to saturate the specimen but not so great as to escape to the atmosphere through the vented upper piston of the pressure vessel. This experiment produced an anomalously large change in magnetic anisotropy and we suspected that this might have been influenced by a low pore-fluid pressure. Indeed, enhancement of ductility by low fluid pressures has been noted by Rutter (1974) and Rutter and Mainprice (1978). Consequently we performed more tests using an external apparatus to apply double-distilled water at pressure through the vent of the upper piston to the deforming specimen. The pressure of the fluid was controlled manually and required constant adjustment during the experiments as the specimens changed in porosity and permeability. Nevertheless it was possible to control the fluid pressures to $\pm 10\%$ in the external apparatus.

Stress relaxation tests at fluid pressures equal to 12% and 36% of the confining pressure do show that the material is weaker at lower strain rates than the dry material (compare the slope of Fig. 15 with Fig. 6b).

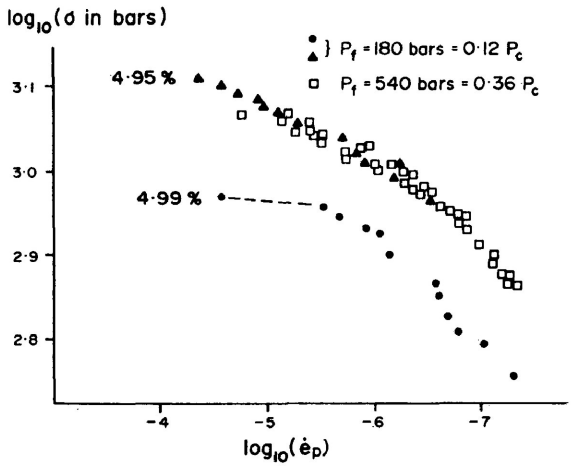

Fig. 15. Stress–relaxation tests for three different specimens (one at 4.99% strain, two at 4.95% strain). The specimens were loaded at a strain-rate of 5×10^{-6} sec^{-1} and with the pore-fluid pressures shown (12% or 36% of the confining pressure, P_c). The effect of these pore-fluid pressures is to weaken the material (compare with the dry tests shown in Fig. 6b).

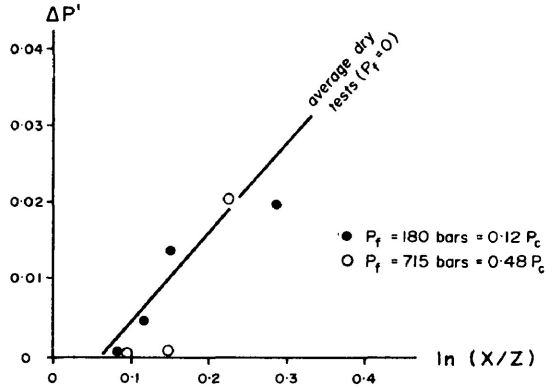

Fig. 16. The change in magnetic anisotropy degree (P') is plotted against strain ratio for seven tests with low fluid pressures. It is concluded that the effects of these pore-fluid pressures do not significantly change the relationship derived from dry samples (the straight line is taken from Fig. 14).

Nevertheless, the changes in degree of magnetic anisotropy show a similar correlation with strain as in those earlier experiments performed with zero pore-fluid pressure (Fig. 16). At the present time we believe that pore-fluid pressure has a negligible effect on the development of susceptibility anisotropy. We can offer no explanation of the anomalous anisotropy of experiment B8512.

Conclusions

Under experimental conditions:

(1) The original susceptibility behaves somewhat like an ellipsoidal strain marker in its rotations and shape changes toward the final susceptibility.

(2) The principal directions of susceptibility rotate faster than expected. There occurs a rapid alignment of k_{max} with X and k_{min} with Z at small strains (less than 20% shortening in Z).

(3) There exists a correlation between *change* in the degree of anisotropy of susceptibility ($\Delta P'$) and the bulk strain ratio (ln X/Z).

The application of these results to natural studies warrants some discussion. The experimental evidence is most applicable to the natural situation also in which the susceptibility is carried by a disseminated accessory mineral. The results may

not be applicable to situations in which matrix-forming minerals carry the susceptibility. Further, in the experiments the magnetite was the same size as the rest of the grains in the synthetic rock. Different effects might be noted where there is a large disparity in grain size.

In the experiments the principal susceptibilities satisfactorily align with the strain axes at modest strains. This is encouraging for field studies, we may predict that susceptibility will accurately indicate strain orientations at even modest strains, with k_{max} parallel to X and k_{min} parallel to Z under most circumstances. Indeed, field studies of more highly strained rocks have shown this repeatedly (Wood et al., 1976; Singh et al., 1975; Hrouda and Janák, 1976; Rathore, 1979; Hrouda, 1982; Kligfield et al., 1982; Borradaile and Tarling, 1984; Borradaile and Mothersill, 1984).

The deformation mechanisms in the samples undoubtedly involved microcracking at boundaries between the cement gel and the sand grains, rotation and other intergranular motions (particulate flow) of the sand grains. The sand grains show little evidence of cracking or plastic deformation. However, earlier work does lead us to suspect some plastic deformation of the magnetite (Müller and Siemes, 1972; Hennig-Michaeli and Siemes, 1975). Indeed, the latter could explain the rapid rotation of the principal susceptibility directions since a passive re-shaping of the magnetite grains would turn the principal directions of susceptibility more rapidly than rotation alone.

The susceptibility fabrics produced are similar in orientation to the fabrics produced in most naturally deformed regional metamorphic rocks in which other deformation mechanisms dominate. This suggests that the orientation of the susceptibility fabric may be essentially independent of *bulk* deformation mechanism where the carrier of susceptibility is a disseminated accessory mineral. An exception would be if the deformation mechanisms produced a domainal heterogeneity of the mineral carrying the susceptibility as, for example, in pressure solution (Borradaile and Tarling, 1981). This result would not of course be applicable to natural situations in which the susceptibility was chiefly carried by matrix-forming minerals such as calcite and chlorite (e.g. Owens and Bamford, 1976; Owens and Rutter, 1978; Borradaile et al., 1986). In those situations the actual deformation mechanisms and re-crystallisation processes would influence the final magnetic fabric.

In the experiments a correlation was found between the *change* in total degree of magnetic susceptibility anisotropy ($\Delta P'$) and the strain ratio (X/Z). This is not regarded as a universal law applicable to all or any natural situation. Nevertheless, it does lead us to suggest that in nature a simple relationship may exist between $\Delta P'$ and strain where the premises are valid (particularly concerning deformation mechanism and degree of dissemination and spatial distribution of the magnetic mineral). Unfortunately, this does require a knowledge of susceptibility magnitudes both before and after straining.

In the case of ductile shear zones in a single lithology this approach may be useful because one might determine the pre-strain susceptibility near the margins of a shear zone and successive post-strain susceptibility fabrics progressively towards the centre of a shear zone.

Another situation which might lend itself to analysis was suggested to us by Brian Bayly. Where one has a train of folds such that unstrained flanks alternate with strained hinge regions it may be possible to assume that fairly uniform sedimentary magnetic fabrics prevail in the flanks. These fabrics would represent the pre-strain susceptibility (k_0). The modified fabrics of the hinges would then be represented by a k' tensor. In this way one might bracket the changes in magnitude and orientation of the principal susceptibilities due to strain in the hinge regions.

Acknowledgements

Graham Borradaile is grateful to the Board of Industrial Leadership and Development (BILD) of Ontario for the grant which purchased most of the rock deformation equipment. He is also grateful to the Natural Sciences and Engineering Research Council of Canada for operating (A6861) and equipment (E5658) grants.

The triaxial rig and microprocessor control system was supplied by Earth Technology Corporation, Long Beach, CA 90807 and by CGS, 2405

Spring Creek, Austin, TX 89704. We are grateful to Drs. Donath, Fruth and Holder for advice concerning the equipment. The magnetic susceptibility instrument was supplied by Sapphire Instruments, Box 385, Ruthven, Ont. and we are grateful to Dr. Stupavsky for much advice concerning its use.

Brain Bayly provided constructive criticism of the text.

References

Borradaile, G.J., 1981. Particulate flow of rock and the formation of cleavage. Tectonophysics, 72: 77–88.

Borradaile, G.J. and Mothersill, J.S., 1984. Coaxial deformed and magnetic fabrics without simply correlated magnitudes of principal values. Phys. Earth Planet. Inter., 35: 294–300.

Borradaile, G.J. and Tarling, D.H., 1981. The influence of deformation mechanisms on magnetic fabrics in weakly deformed rocks. Tectonophysics, 77: 151–168.

Borradaile, G.J. and Tarling, D.H., 1984. Strain partitioning and magnetic fabrics in particulate flow. Can. J. Earth Sci., 21: 694–697.

Borradaile, G.J., Mothersill, J.S., Tarling, D.H. and Alford, C., 1986. Sources of susceptibility in a slate. Earth Planet. Sci. Lett., 76: 336–340.

Donath, F.A., 1970. Rock deformation apparatus and experiments for dynamic structural geology. J. Geol. Educ., 18: 3–12.

Donath, F.A. and Fruth, L.S., 1971. Dependence of strain-rate effects on deformation mechanism and rock-type. J. Geol., 79: 347–371.

Donath, F.A. and Guven, N., 1971. Data reduction for experimental rock deformation. Contrib. Geol., 10: 89–116.

Goldstein, A., 1980. Magnetic susceptibility anisotropy of mylonites from the Lake Char Mylonite Zone, Southeastern New England, Tectonophysics, 66: 197–211.

Graham, J.W., 1954. Magnetic susceptibility anisotropy, an unexploited petrofabric element. Bull. Geol. Soc. Am., 65: 1257–1258.

Graham. J.W., 1966. Significance of magnetic anisotropy in Appalachian sedimentary rocks. In: J.S. Steinhard and T.J. Smith (Editors), The Earth Beneath the Continents. Geophys. Monogr., Am. Geophys., Union, 10: 627–648.

Hamilton, N., Owens, W.H. and Rees, A.I., 1968. Laboratory experiments on the production of grain orientations in shearing sand. J. Geol., 76: 465–472.

Hennig-Michaeli, C. and Siemes, H., 1975. Zwillungsgleitung beim Magnetit. Neues Jahrb. Mineral. Abh., 123: 330–334.

Hrouda, F., 1982. Magnetic anisotropy of rocks and its application in geology and geophysics. Geophys. Surv., 5: 37–82.

Hrouda, F. and Janák, F., 1976. The changes in shape of the magnetic susceptibility ellipsoid during progressive metamorphism and deformation. Tectonophysics, 34: 135–148.

Jelínek, V., 1981. Characterization of magnetic fabrics of rocks. Tectonophysics, 79: 563–567.

Kligfield, R., Lowrie, W. and Dalziel, I.W.D., 1977. Magnetic susceptibility as a strain indicator in the Sudbury Basin, Ontario. Tectonophysics, 40: 287–308.

Kligfield, R., Owens, W.H. and Lowrie, W., 1982. Magnetic susceptibility anisotropy, strain and progressive deformation in Permian sediments from the Maritime Alps (France). Earth Planet. Sci. Lett., 55: 181–189.

Means, W.D., 1976. Stress and Strain. Springer-Verlag, Berlin, 339 pp.

Müller, P. and Siemes, H., 1972. Zur Festigkeit und Gefugeregulung von experimentell verformten Magnetiterzen. Neues Jahrb. Mineral. Abh., 117: 39–60.

Neville, A.M., 1970. Creep of Concrete: Plain, Reinforced and Pre-stressed. North-Holland Publishing Company, Amsterdam, 622 pp.

Neville, A.M., 1981. Properties of Concrete. Pitman, London, 779 pp.

Owens, W.H., 1974. Mathematical model studies on factors affecting the magnetic anisotropy of deformed rocks. Tectonophysics, 24: 115–131.

Owens, W.H. and Bamford, D., 1976. Magnetic, seismic and other anisotropic properties of rock fabrics. Philos. Trans. R. Soc. London Ser. A, 283: 55–68.

Owens, W.H. and Rutter, E.H., 1978. The development of magnetic susceptibility anisotropy through crystallographic preferred orientation in a calcite rock. Phys. Earth Planet. Inter., 16: 215–222.

Pfiffner, O.A. and Ramsay, J.G., 1982. Constraints on geological strain rates: arguments from finite strain states of naturally deformed rocks. J. Geophys. Res., 87: 311–321.

Ramsay, J.G., 1967. Folding and Fracturing of Rocks. McGraw-Hill, New York, N.Y., 568 pp.

Rathore, J.S., 1979. Magnetic susceptibility anisotropy in the Cambrian Slate Belt of North Wales and correlation with strain. Tectonophysics, 53: 83–97.

Rathore, J.S. and Henry, B., 1982. Comparison of strain and magnetic fabrics in Dalradian rocks from the southwest Highlands of Scotland. J. Struct. Geol., 4: 373–384.

Rees, A.I., 1966. The effects of depositional slopes on the anisotropy of magnetic susceptibility of laboratory deposited sands. J. Geol., 74: 856–867.

Rees, A.I., 1968. The production of preferred orientation in a concentrated dispersion of elongated and flattened grains. J. Geol., 76: 457–465.

Rees, A.I. and Woodall, W.A., 1975. The magnetic fabric of some laboratory-deposited sediments. Earth Planet. Sci. Lett., 25: 121–130.

Rutter, E.H., 1972. On the creep testing of rocks at constant stress and constant force. Int. J. Rock Mech. Min. Sci., 9: 191–195.

Rutter, E.H., 1974. The influence of temperature, strain rate and interstitial water in the experimental deformation of calcite rocks. Tectonophysics, 22: 311–334.

Rutter, E.H. and Mainprice, D.H., 1978. The effect of water on stress relaxation of faulted and unfaulted sandstone. Pure Appl. Geophys., 116: 634–654.

Rutter, E.H., Atkinson, B.K. and Mainprice, D.H., 1978. On the use of the stress relaxation testing method in studies of the mechanical behaviour of geological materials. Geophys. J. R. Astron. Soc., 55: 155–170.

Schmid, S.M., 1976. Rheological evidence for changes in the deformation mechanism of Solenhofen limestome towards low stresses. Tectonophysics, 31: T21–T28.

Schwarz, E.J., 1974. Magnetic fabrics in massive sulphide deposits. Can. J. Earth. Sci., 11: 1675–1699.

Singh, J., Anderson, D.J. and Tarling, D.H., 1975. The magnetic susceptibility anisotropy of deformed rocks from North Cornwall, England. Tectonophysics, 27: 141–153.

Stupavsky, M., 1983. Operating Manual for SI-1 magnetic susceptibility and anisotropy instrument. Sapphire Instruments, P.O. Box 385, Ruthven, Ont., 92 pp.

Wagner, J.J., Hedley, F.G., Steen, D., Tinkler, C. and Vaugnat, M., 1981. Magnetic anisotropy and fabric of some progressively deformed ophiolitic gabbros. J. Geophys. Res., 86: 307–315.

Wood, D.S., Oertel, G., Singh, J. and Bennett, M.F., 1976. Strain and anisotropy in rocks. Philos. Trans. R. Soc. London Ser. A, 283: 27–42.

Earth and Planetary Science Letters, 76 (1985/86) 336–340
Elsevier Science Publishers B.V., Amsterdam – Printed in The Netherlands

Sources of magnetic susceptibility in a slate

Graham Borradaile [1], John Mothersill [2], Don Tarling [3] and Craig Alford [1]

[1] *Geology Department, Lakehead University, Thunder Bay, Ont. P7B 5E1 (Canada)*
[2] *Principal, Royal Roads Military College, Victora, B.C. (Canada)*
[3] *Geophysics Department, School of Physics, The University, Newcastle-upon-Tyne NEL 7RU (U.K.)*

Received April 24, 1985; revised version received October 8, 1985

Magnetic susceptibility and its anisotropy in the Borrowdale Volcanic slates at Kentmere in the English Lake District are attributed largely to preferred orientation of a paramagnetic chlorite of diabantite-ripidolite composition. In units of 10^{-6} cgs/g, the principal susceptibilities for the slates are 9.61; 9.42; 8.69 and for the chlorite grains the minimum anisotropy is represented by principal susceptibilities of 11.57; 11.22 and 9.15. Because the magnetic susceptibility is carried by a tightly packed, matrix-forming mineral that has recrystallised during the deformation it is not possible to imagine simple grain rotation as being responsible for the anisotropy of susceptibility.

1. Introduction

We have been investigating the magnetic susceptibility anisotropy (MSA) of basic metavolcanic rocks, and of mylonites, and metaclastic rocks [1,2]. During the course of this work we have attempted to determine fabric anisotropies using magnetic and petrofabric methods. To some degree we have also attempted to relate magnetic fabrics to the macroscopically determined finite strains from field studies. The interpretation of the magnetic fabrics requires a knowledge of the major sources of the susceptibility in the rocks. If we are to attempt to assess the degree to which MSA related to a preferred orientation of matrix-forming phyllosilicates, we must be sure that the bulk susceptibility, or at least its anisotropy, is due to those minerals. If the susceptibility is carried by some disseminated marker mineral such as magnetite, it is also important to know this, for characteristic magnetic fabrics can develop if pressure solution operates and produces a regular domainal heterogeneity of magnetite [3]. Our attention was particularly focussed on this problem, while we were comparing magnetic fabrics of Archean metavolcanic rocks with those of the classic Borrowdale Volcanic sequence [4]. In this study we have determined susceptibilities using the SI-1 unit of Sapphire Instruments, Ruthven, Ontario described elsewhere [2].

2. Sources of susceptibility in the Borrowdale Volcanic rocks

This sequence of English Ordovician volcanic rocks has been thoroughly studied with regards to its petrology, structure, strain and magnetic properties [5–9]. The rocks are slates which experienced a single fabric-forming tectonic episode during greenschist facies regional metamorphism. The minerals present are chlorite, biotite, quartz, albite, amphibole, calcite, muscovite with traces of garnet, pyrite, magnetite, molybdenite and pentlandite.

Rock specimens were carefully partly crumbled to separate minerals while preserving their shape anisotropy as much as possible. Partly crushed samples were sieved in order to separate the mineral grains from finer dust and coarser polymineralic fragments. Desirable mineral-grain separations were trapped between 1.50 ϕ (0.353 mm) and 2.0 ϕ (0.25 mm) mesh sizes in sieves manufactured from non-ferrous materials. We are aware that not all minerals may be equally represented in this mineral-grain sample since some minerals are reduced to powder more easily. However, we have determined that the powder is not anomalously rich in magnetic minerals.

Optical examination of the separated component mineral grains of the Borrowdale Volcanic rocks indicates that magnetite is rare, as a separate

0012-821X/86/$03.50

mineral. Density and magnetic separations enabled us to estimate that such separate grains form ~ 0.001% of the rock by weight.

The susceptibility of grain-aggregates of impure magnetite that were separated from Archean metavolcanic rocks (in which separate magnetite grains are much more abundant) is given in the table of Appendix 1. If the magnetite grains in the Borrowdale volcanic rocks have susceptibilities of that order of magnitude they would account for less than 10% of the bulk susceptibility of the Borrowdale Volcanic rocks at Kentmere.

Successive separations isolated a fraction of the rock, 60–80% by weight, which accounts for about 95% of the bulk susceptibility of the Borrowdale Volcanic rocks. The susceptibility of this fraction, termed the chlorite-rich fraction and, for comparisons, the mean susceptibility of seventeen samples of Borrowdale Volcanic rock are given in Appendix 1.

X-ray diffraction indicates that the chlorite-rich fraction is composed primarily of a diabantite-ripidolite chlorite with minor contaminations (less than 10% by volume) of albite and calcite. Magnetite and other magnetic minerals could not be detected by this method in the chlorite-rich fraction.

Regarding the mineralogical sources of the susceptibility, the acquisition of isothermal remnant magnetism (IRM) indicates that micro-sized magnetite may be present in the chlorite fraction. This is the possibility which is most consistent with the petrographic observations. Further magnetite is probably produced during the heating of the chlorite-rich fraction but the fourfold increase in IRM for previously heat-treated samples still only produced a low-field susceptibility of about 0.7×10^{-6} cgs/g, as determined in the laboratory at Newcastle. Even accounting for differences in instrumentation between Lakehead and Newcastle this indicates that the ferromagnetic contribution to the susceptibility is relatively minor. It seems most likely that the magnetic properties of the chlorite-rich fraction are due to paramagnetism, presumably as an inherent property of the chlorite lattice. This effect was considered in the literature at an early stage [10]. (We wish to point out that Roy Kligfield has suggested to us previously that sheet silicates may make a significant paramagnetic contribution to the susceptibility of other rocks; personal communication to G.B. and D.T., 14-08-1981.)

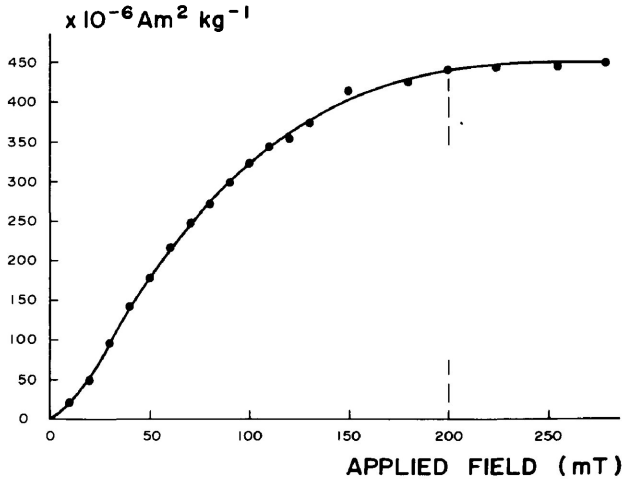

Fig. 1. Data on the acquisition of IRM.

3. Anisotropy of susceptibility of the chlorite-rich fraction

The bulk susceptibility of the Borrowdale Volcanic rocks is primarily due to the chlorite-rich fraction. Still, without some knowledge of the magnetic anisotropy of individual chlorite grains it is not easy to proceed with the analysis of any model of the development of susceptibility-anisotropy in metamorphic rocks. To attain this goal we have generated artificial fabrics using the chlorite-rich fraction from the Borrowdale Volcanic rock. Firstly, linear fabrics were produced by preparing samples in a strong magnetic field adjacent to a magnetic-separation device. The chlorite grains were allowed to settle into araldite under the influence of the strong magnetic field while being simultaneously mechanically shaken. The result was to produce a very pronounced linear fabric (L-tectonite fabric; [11]). This fabric was observed directly because araldite is transparent and the specimens were settled into the transparent plastic containers used in the magnetic susceptibility unit produced by Sapphire Instruments Incorporated. From this magnetically aligned specimen (see Fig. 2a) it was possible to determine the maximum susceptibility of the chlorite grains from the 2-direction in that figure. The directions one and three yield susceptibilities which are blends of the principal intermediate and minimum susceptibilities. A

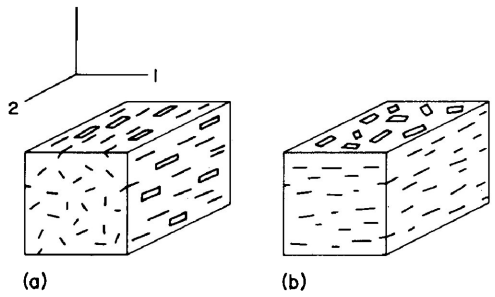

Fig. 2. Schematic representation of the fabrics synthesised from aggregates of chlorite grains. (a) represents an $L \gg S$ fabric produced by magnetic alignment. (b) represents an $S \gg L$ fabric produced by mechanical compaction. The directions *1*, *2*, *3* are used for reference purposes in the text.

correction was made for the diamagnetic contribution of the known weight of araldite.

Secondly, planar fabrics of chlorite (S-tectonite fabrics, see Fig. 2b) were produced by mechanical compaction of layers of chlorite sprinkled onto successive films of congealing araldite. Again, visual inspection permitted control of the quality of the planar fabric. From this fabric (see Fig. 2b) it is possible to determine the minimum susceptibility from the 3-direction. The 1- and 2-directions yield blends of the maximum and intermediate susceptibilities. Once more, a correction was applied for the known weight of araldite.

From our knowledge of the maximum, minimum and bulk susceptibilities it is possible to calculate the intermediate value. Unfortunately, two factors cause the principal values to be underestimated. The first of these concerns the imperfection of the fabric-generating technique. Because of the edge effects in the sample near the containers' walls, the linear fabric was not as good as that shown in Fig. 2a, nor is the planar fabric as good as 2b. Thus the maximum susceptibility will be underestimated and the minimum value overestimated, if these are associated with the shape of chlorite grains. Nevertheless, the preferred orientations of the magnetic fabrics of the fabricated specimens are qualitatively comparable to those of the natural rocks from which the chlorite was separated (Fig. 3a, b). The natural rocks actually had L-S fabrics transitional between the symmetrical fabrics generated artificially.

The second factor influencing the underestimate of the anisotropy of the chlorite grains concerns the preparation procedure. During the crum-

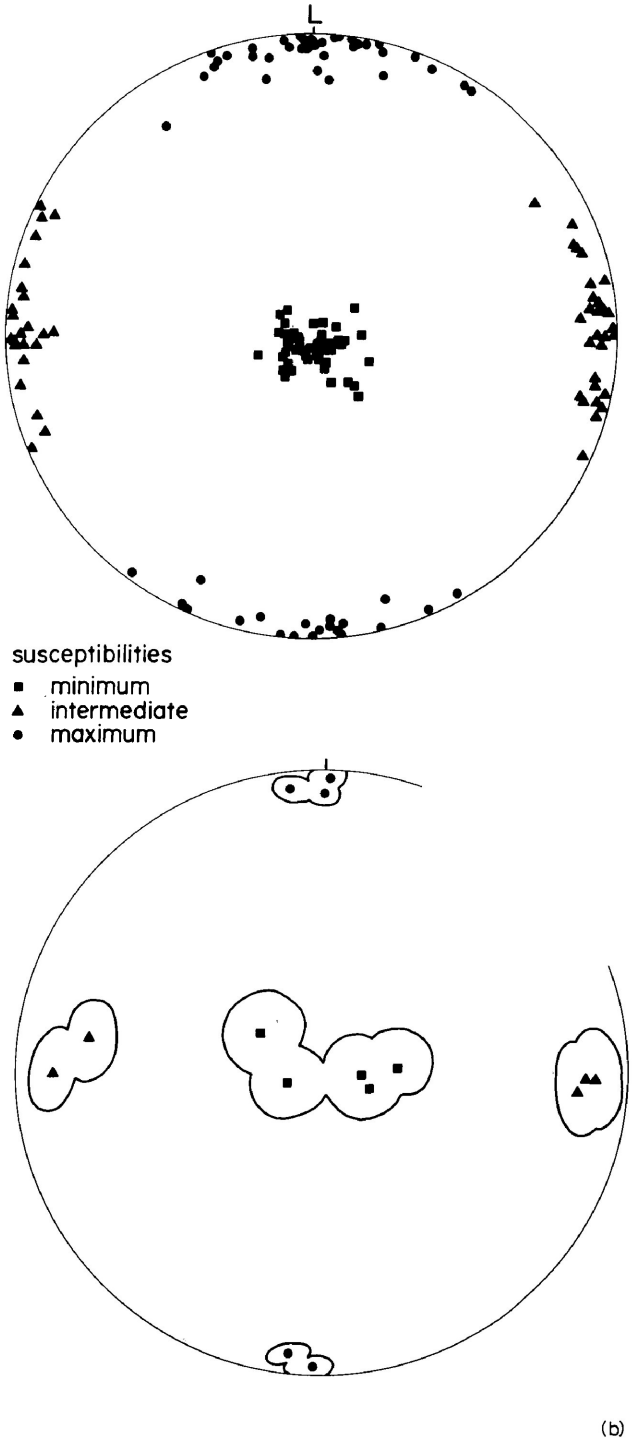

Fig. 3. (a) Principal susceptibility orientations in 23 different specimens of Borrowdale Volcanic Slate. For convenience the plane of preferred mineral orientation (= slaty cleavage) is shown horizontal and the mineral lineation (= L) is shown in a N-S direction. The specimens' volumes were 10.55 cm^3. (b) Principal susceptibilities of several synthetic chlorite aggregates aligned in the laboratory as described in the text. The contours are 95% confidence limits about the nearest principal susceptibility direction. The specimens' volumes were 8.00 cm^3.

bling of the rock the aspect ratios of the chlorite grains were certainly reduced. This may cause the maximum and intermediate principal susceptibilities to be underestimated, especially since the susceptibility appears to be a paramagnetic property of the chlorite, rather than a property of ferromagnetic inclusions.

Comparison of the anisotropies of the artificial linear and planar fabrics of the chlorite-rich fraction with the anisotropy of the whole rock is made using a T-P' diagram [12,13]. This facilitates a more symmetrical distribution of degree or shape or anisotropy (T) and magnitude of principal values (P') than the diagram commonly used to represent strain in the geological literature. Fig. 4 indicates that the bulk susceptibility of the chlorite fraction is comparable to that of the rock from which it is derived, thus confirming that chlorite is the primary source of susceptibility.

Of the two types of synthetic fabric, the planar one (CF2) has a slightly lower shape of anisotropy (T-value) than that of the whole rock (BV). This is to be expected since the laboratory fabric was not as perfect as the natural ones. Nevertheless, the calculated anisotropy for the chlorite-rich fractions

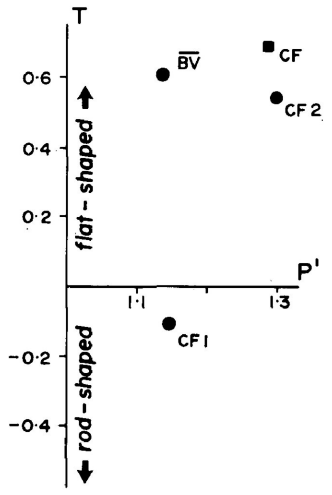

Fig. 4. A Jelinek-Hrouda diagram to illustrate shape of anisotropy (T) and total degree of anisotropy P'. $\overline{BV}$ = mean value for 17 different specimens of Borrowdale volcanic slate, data in [2]. "CF" = synthetic specimens of grain aggregates of a chlorite-rich fraction separated from the Borrowdale Volcanic slate. *1* = magnetically aligned, *2* = mechanically compacted; CF without suffix is the calculated minimum value for individual chlorite grains.

(CF) has a slightly higher T-value and a greater P'-value than that for the whole rock. This is compatible with the whole rock data because the rock is not entirely composed of chlorite, nor does its chlorite show a perfect alignment. The susceptibility anisotropy of the chlorite is approximated by the data for the chlorite-rich fraction which has principal values in the ratios 1.09 : 1.06 : 0.86.

However, the error limits would permit a nearly perfectly oblate symmetry, in which the maximum and intermediate values would be equal. The bulk susceptibility is $10.590 \pm 0.350 \times 10^{-6}$ cgs/g.

4. Remarks

The magnetic susceptibility of the slates is almost entirely due to its chlorite grains. The anisotropy of susceptibility may also be due to chlorite exclusively, but the present experimental method has prevented this from being checked. It seems to us important that the susceptibility is not due to a widely spaced, minor marker mineral but due to a matrix-forming mineral which was actively involved in metamorphism. The chlorite grains impinge upon one another in the rock and their growth overlapped with deformation. The explanation of susceptibility-anisotropy in these slates is inextricably intertwined with the explanation of the metamorphic texture of the rock. However, the association of susceptibility-anisotropy with rock-forming sheet silicates does provide encouragement to those who wish to detect cryptic fabrics or further quantify metamorphic fabrics hitherto ranked in the L-S scheme [14]. Moreover, the values that we offer as minimum estimates of the chlorite grains' magnetic anisotropy may permit numerical modelling of the same property for certain rocks and for certain deformation mechanisms.

Acknowledgements

G.B. and J.M. gratefully acknowledge the receipt of operating and equipment grants from the Natural Sciences and Engineering Research council of Canada. We thank Bill O'Reilly for advice. We are indebted to Mike Stupavsky of Sapphire Instruments, P.O. Box 385, Ruthven, Ontario N0P 2G0, for technical advice and documentation for the SI-1 AMS instrument.

Appendix 1—Principal susceptibilities

	Maximum	Intermediate	Minimum
Borrowdale Volcanic rock specimens ($\rho = 2.748$ g/cm^3)	9.612×10^{-6} (± 1.086)	9.422×10^{-6} (± 1.098)	8.686×10^{-6} (± 1.054)
Chlorite-rich fraction (magnetically aligned) (CF1)	11.640×10^{-6} (± 0.294)	10.800×10^{-6} (± 0.141)	10.165×10^{-6} (± 0.197)
Chlorite-rich fraction (mechanically aligned) (CF2)	11.497×10^{-6} (± 0.89)	10.757×10^{-6} (± 0.46)	8.925×10^{-6} (± 0.28)
Calculated chlorite grain-anisotropy (CF)	11.574×10^{-6} (± 0.38)	11.219×10^{-6} (± 0.37)	9.149×10^{-6} (± 0.30)
Magnetite (*aggregate* magnetically aligned)	10.0471×10^{-2} (± 0.005)	9.347×10^{-2} (± 0.029)	8.990×10^{-2} (± 0.006)
Araldite (hardened)	isotropic, $-2.587 \pm 0.410 \times 10^{-6}$		

All values in cgs/g (error values indicated are 95% confidence estimates).

References

1 G.J. Borradaile and D.H. Tarling, Strain partitioning and magnetic fabrics in particulate flow, Can. J. Earth Sci. 21, 694–697, 1984.

2 G.J. Borradaile and J.S. Mothersill, Coaxial deformed and magnetic fabrics without simply correlated magnitudes of principal values, Phys. Earth. Planet. Inter. 35, 294–300, 1984.

3 G.J. Borradaile and D.H. Tarling, The influence of deformation mechanisms on magnetic fabrics of weakly deformed rock, Tectonophysics 77, 151–168, 1981.

4 J.S. Rathore, The magnetic fabrics of some slates from the Borrowdale Volcanic Group in the English Lake District and their correlations with strains, Tectonophysics 67, 207–220, 1980.

5 A.M. Bell, Strain factorisations from lapilli tuff, English Lake District, J. Geol. Soc., London 138, 463–474, 1981.

6 D.G. Helm and A.W.B. Siddans, Deformation of a slaty, lapillar tuff in the English Lake District, discussion, Geol. Soc. Am. Bull. 82, 523–531, 1971.

7 J.F.N. Green, The geological structure of the Lake District, Proc. Geol. Assoc. London 31, 109–126, 1920.

8 G.H. Mitchell, The succession and structure of the Borrowdale Volcanic Series of Troutbeck, Kentmere and the western part of the Longsleddale, Q.J. Geol. Soc. London 96, 301–319, 1929.

9 G. Oertel, Deformation of a slaty, lapillar tuff in the Lake District, England, Geol. Soc. Am. Bull. 81, 1172–1187, 1970.

10 M.D. Fuller, Magnetic anisotropy and paleomagnetism, J. Geophys. Res. 68, 293–309, 1963.

11 D. Flinn, On the symmetry principle and the deformation ellipsoid, Geol. Mag. 102, 36–45, 1965.

12 V. Jelínek, Characterization of magnetic fabrics of rocks, Tectonophysics 79, T63–T67, 1981.

13 F. Hrouda, Magnetic anisotropy of rocks and its application in Geology and Geophysics, Geophys. Surv. 5, 37–82, 1982.

14 W.M. Schwerdtner, P.J. Bennett and J.W. Jones, Application of L-S fabric scheme to structural mapping and paleostrain analysis, Can. J. Earth Sci. 14, 1021–1032, 1977.

Physics of the Earth and Planetary Interiors, 48 (1987) 161–166
Elsevier Science Publishers B.V., Amsterdam – Printed in The Netherlands

Anisotropy of magnetic susceptibility of some metamorphic minerals

G. Borradaile, W. Keeler [1], C. Alford and P. Sarvas

Geology Department and Physics [1] Department, Lakehead University, Thunder Bay, Ontario, P7B 5E1 (Canada)

(Received July 15, 1986; revision accepted October 13, 1986)

Borradaile, G., Keeler, W., Alford, C. and Sarvas, P., 1987. Anisotropy of magnetic susceptibility of some metamorphic minerals. Phys. Earth Planet. Inter., 48: 161–166.

The anisotropy of susceptibility of metamorphic rocks can be due to paramagnetic rock-forming silicates such as amphiboles, chlorites and micas. It is not always necessary to invoke fabrics of separate grains of iron oxide to explain the anisotropy. Minimum estimates of lattice anisotropies of typical samples of silicates have maximum-to-minimum ratios of 1.1–1.7. Since the magnetic anisotropies of most metamorphic rocks are less than this, these minerals can control the anisotropy of susceptibility because their preferred crystallographic orientations are usually very strong in comparison with the preferred dimensional orientation of magnetite and because they are more abundant than magnetite.

1. Introduction

There is now considerable interest in the use of anisotropy of susceptibility in studying metamorphic rocks, their fabrics and even their strain (Owens and Bamford, 1976; Hrouda, 1982; Tarling, 1983). Unfortunately, for metamorphic rocks, data is lacking on the contribution from typical, natural examples of rock-forming minerals to the susceptibility and its anisotropy. This is because large single crystals of many common metamorphic species are very rare, especially those of slates and schists which are, by definition, fine-grained.

Our approach is to separate grains of individual minerals from natural metamorphic rocks. Grains a few millimetres long of a single mineral species from a given rock are then reassembled in an aggregate with a strong preferred crystallographic orientation. If the preferred orientation of the aggregate were perfect it would be possible to determine accurately the anisotropy of the natural grains. It is not possible to orientate the grains perfectly but we do provide a close, minimum estimate of the anisotropy in this way. Each of the minerals for which data are tabulated is taken from a different metamorphic rock.

It would be useful to have such data for chemically pure minerals. However, metamorphic grains are naturally impure and, in any case, our purpose is to appreciate the magnetic susceptibility and anisotropy of typical natural metamorphic rock-forming grains. These form the matrices of metamorphic rocks and we shall show that they can contribute to the magnetic susceptibility and fabric of the whole rock.

Of course we have separated other distinct mineral grains from those we consider but since we must preserve the grain-shapes of the minerals, to aid in their alignment, they have not been reduced to a powder. Therefore, they must contain impurities as inclusions. If such inclusions influence the magnetic properties of the host grains, this does not disturb us. It is our intention to investigate how those typical, impure metamorphic grains contribute to the overall metamorphic fabric of the rock. For example, in a hypothetical

0031-9201/87/$03.50

chlorite schist there may be separate grains of magnetite. The question arises, 'Does the magnetite cause the susceptibility anisotropy of the rock?' Whilst a fraction of 1% of magnetite may contribute much to the bulk susceptibility, it is difficult to know whether the fabric of the magnetite or the fabric of the less magnetic but more numerous and more anisotropic chlorite flakes controls the magnetic anisotropy of the schist. Thus we need knowledge of the susceptibility anisotropy of typical chlorite grains with any inclusions that they might contain. Even with the minimum values of anisotropy determined by our methods we can go some way to evaluating the role of matrix minerals.

2. Analytical methods

Chiefly, we have used a standard induction coil instrument for the determination of susceptibility. This is a Sapphire Instruments SI-1 unit (Stupavsky, 1983). It consists of a sensing coil and attached control and data-acquisition circuitry. The comparison of the inductances of the coil with and without a sample present is used to compare the susceptibility of the specimen parallel to the coil axis with that of a standard. The instrument is regularly calibrated using MnO_2 as a standard which has a susceptibility of 3.29×10^{-4} SI units/g (Weast and Astle, 1978). Using specially designed holders, we position granular MnO_2 in the coil so as to occupy the same volume, the same shape of space and the same location as the material whose susceptibility is to be determined by comparison. This required standards of between 20 and 160 g of MnO_2 for the specimens used in the present study.

Results obtained using this single-coil instrument were supported by measurements made with an inductive bridge assembled by W. Keeler. The latter uses a lock-in amplifier as a detector and, because of its phase sensitivity, the sample signal can be separated into electrical conduction and susceptibility components. The bridge can distinguish between diamagnetic and paramagnetic/ferrimagnetic response and was thus used to confirm the sign and magnitude of the signals determined by the single-coil instrument. This was especially useful with minerals such as talc and calcite, which have very feeble magnetic responses.

The anisotropies of individual species of rock-forming minerals are sometimes difficult to determine in conventional coil instruments. This is because large (c. 10 cm^3) single crystals are normally required and these must be shaped so as to minimise any contribution of specimen shape to anisotropy. Many common rock-forming metamorphic minerals are rarely available in sufficiently large crystals so we have extended a recently developed technique (Borradaile et al., 1986).

This involves the use of grains of the mineral in question that have been separated from metamorphic rocks. The separation procedure involves picking, flaking and gently crushing the rock to yield the grains. With sufficient care it is possible to do this while preserving most of the metamorphic grain-shapes. Grains of other mineral species were removed from these fragments by gravity-separation procedures in heavy liquids and by magnetic separation methods. The chosen grains were then washed and further hand-picked under a binocular microscope to remove any remaining foreign grains. In this way we obtained essentially monomineralic aggregates.

Compositions of sub-samples were confirmed by X-ray diffraction and the grains were then physically aligned and cemented with araldite into transparent cubical plastic containers, gradually, until the box was filled. The boxes have a volume of 8 cm^3. Grains were aligned with their long axes parallel to a reference direction marked on the box and their intermediate axes were aligned in a common plane with the longest axes. Thus the cubical specimens contained very strong preferred orientations of the mineral. In the case of some micas and one chlorite it was possible to obtain large flakes, each of which was trimmed to stack neatly in the box. For one chlorite sample, a small fragment of monomineralic schist with extremely strong preferred mineral orientations was machined and fitted directly into the box.

3. Results

The anisotropy of susceptibility of the cubical samples relates to the anisotropy of susceptibility of the mineral lattices and any microscopic lattice-controlled inclusions in these typical samples. In the case of the aggregates of small grains, the anisotropy is underestimated because it is not possible to obtain a perfect crystallographic alignment of those grains. Nevertheless, the alignments are much better than in most natural metamorphic rocks.

3.1. Minerals with moderate susceptibility

The metamorphic rock-forming silicates that fall into this category possess mean susceptibilities of $> 10^{-4}$ SI units/cm^3. Data for these paramagnetic silicates, each from a different metamorphic rock, are recorded in Table I, together with information for metamorphic grains of magnetite for comparison. The values tabulated have been corrected for the susceptibility contribution of the plastic specimen containers and for any significant amounts of araldite cement if that was used.

The anisotropies are presented as normalised principal values such that the product of these three values is unity. The ratios of the principal susceptibilities are thus more readily apparent from the numbers k_{max}, k_{int} and k_{min} (Table I). Actual principal values in SI units per unit volume are obtained by multiplying a normalised value by the mean (or bulk) susceptibility which is also

TABLE I

Susceptibility data for common minerals of different metamorphic rocks and for magnetite

Mineral	k_{min}	k_{int}	k_{max}	SG	Mean susceptibility SI/cm^3 $\times 10^{-6}$	Mass of sample used
	(±95% limits)				(±s.d.)	(g)
Actinolite (1)	0.947	0.982	1.076	2.90	3560.4	8.10
	(0.005)	(0.007)	(0.01)		(8.9)	
Actinolite (2)	0.899	1.027	1.083	3.42	6506.0	12.79
	(0.002)	(0.002)	(0.003)		(19.1)	
Hornblende (1)	0.809	0.917	1.347	3.28	8919.0	21.00
	(0.002)	(0.001)	(0.001)		(11.0)	
Crocidolite	0.958	0.992	1.052	3.44 [a]	332.5	9.60
	(0.03)	(0.03)	(0.03)		(8.2)	
Glaucophane	0.908	1.006	1.094	3.17	787.1	5.76
	(0.013)	(0.016)	(0.01)		(43.8)	
Chlorite (1)	0.864	1.060	1.093	2.76	358.4	11.01
(diabantite-ripidolite)	(0.028)	(0.035)	(0.035)		(53.7)	
Chlorite (2)	0.734	1.058	1.287	2.80 [a]	68.8	3.11
(leuchtenbergite)	(0.2)	(0.25)	(0.24)		(23.0)	
Chlorite (3) solid [b]	0.866	1.023	1.128	2.99	1553.6	12.94
	(0.01)	(0.01)	(0.01)		(184.0)	
Chlorite (4)	0.921	1.020	1.063	2.76	371.9	6.44
(Thuringite)	(0.02)	(0.02)	(0.02)		(8.0)	
Biotite (1) (large sheets)	0.812	1.106	1.114	2.94	1234.6	6.08
	(0.01)	(0.02)	(0.03)		(6.5)	
Biotite (2) (large sheets)	0.832	1.095	1.098	3.03	1183.4	9.62
	(0.01)	(0.01)	(0.01)		(170.0)	
Phlogopite (large sheets)	0.838	1.091	1.098	2.80	1178.2	10.21
	(0.01)	(0.01)	(0.01)		(6.5)	
Muscovite (large sheets)	0.820	1.052	1.159	2.82	165.0	5.21
	(0.07)	(0.004)	(0.09)		(17.3)	
Magnetite	0.951	0.989	1.063	5.17	5841000	25.0
	(0.001)	(0.001)	(0.001)		(40000)	

[a] These densities were taken from published values.

[b] This was an unseparated, polygranular, solid sample of highly oriented schist.

given. We use the geometric mean of the principal susceptibilities as the mean value. In the determinations, known masses were used so that densities had also to be determined for the mineral grains to permit values to be presented on a volume basis.

The anisotropies of these minerals are plotted on a 'Flinn' diagram with k_{max}/k_{int} vs. k_{int}/k_{min} (Fig. 1). In general the anisotropies are reasonably high for the matrix-forming silicates, and greater than for metamorphic magnetite. The magnetic anisotropy of detrital magnetite, also shown in this figure, is more extreme than for metamorphic grains of magnetite but the determination is also less precise. However, even this sample of detrital magnetite is less magnetically anisotropic than most of the silicates. It is also worth noting that the detrital magnetite is from a very immature fluvial sediment and its grain-shape may be less rounded than detrital grains from more extensively abraded sediment that has been further transported.

The error bars give some measure of the reproducibility of the anisotropy determination of the

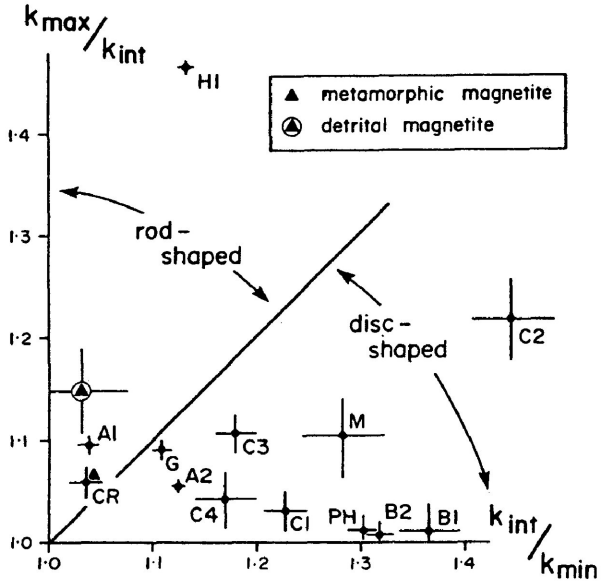

Fig. 1. 'Flinn' plot of the ratios of principal susceptibilities for the moderately susceptible paramagnetic metamorphic minerals and for magnetite from metamorphic and from detrital sedimentary rocks. The minerals are identified by their initial letters in Table I.

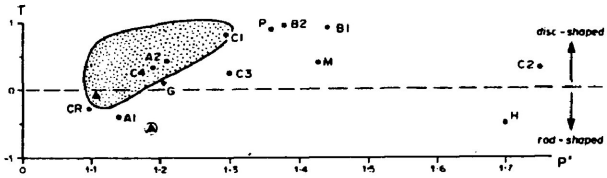

Fig. 2. Sense of anisotropy (T) vs. degree of anisotropy (P') for the minerals determined (indicated by their initial letters, see Table I). The field outlined indicates the main range for metamorphic rocks presented in Hrouda (1982). The triangle represents metamorphic magnetite from a large number of different rocks and the triangle inside a circle represents detrital magnetite from a very immature sediment.

synthesised aggregates. How closely these relate to the true anisotropies of the lattices depends on the success of the aligning procedure, which can be judged only qualitatively. The chief factors influencing the alignment procedure are the shape and size of the grains in question. We believe that the anisotropy determinations that are closest to the true values are for biotite, phlogopite and muscovite. The worst approximations to the true anisotropy are for hornblende and glaucophane. The chlorites, actinolite and crocidolite would be intermediate between these extremes in the degree to which they approach the true anisotropy. However, we emphasise that it is not possible to exaggerate the anisotropy in our procedure—all the estimates of anisotropy are minimum estimates.

The anisotropies are plotted also on a Hrouda–Jelinek diagram (Fig. 2) of P' vs. T where

$$P' = \exp\left(\sqrt{\left[2\left((a-k)^2 + (b-k)^2 + (c-k)^2\right)\right]}\right)$$

$$T = 2((b-c)/(a-c)) - 1$$

In these equations a, b and c are the natural logarithms of the principal susceptibilities in descending order and k is the logarithm of the mean susceptibility. This type of more modern and useful representation distinguishes degree (P') from sense (T) of anisotropy more successfully than the conventional Flinn plot.

3.2. *Minerals with low susceptibility*

A large proportion (30–60%) of the volume of many slates and schists is occupied by minerals

that have low susceptibility ($< 10^{-5}$ SI units/cm^3) e.g. Hrouda (1986). The instruments designed to deal routinely with the anisotropy of metamorphic rocks, like our SI-1 meter, are not capable of determining the anisotropy of very weakly susceptible materials. Nevertheless, we attempted this to compare the relative contributions of weakly susceptible materials with the overall rock susceptibility.

The noise level of our SI-1 meter is equivalent to a susceptibility difference of about 1.25×10^{-6} SI units under favourable circumstances. For the strongly susceptible materials, which were discussed in the previous section, this presented no problems for the biggest specimen sizes that can be turned inside the coil to determine susceptibility in different directions. The typical specimens occupied volumes of 8 cm^3 representing 10–25 g of material.

However, the weak magnetic responses of minerals such as quartz, feldspar and calcite require such large specimens to produce a measurable signal that we are unable to orient that size of specimen within the coil in any required direction. For these materials we utilised the full coil volume of 140 cm^3 and compared sample signals with the signal from the amount of MnO_2 standard required to fill that space. In this way we were able to determine the bulk or mean susceptibilities of randomly oriented powders of the minerals by comparison with the same volume of MnO_2 powder.

The results for the weakly magnetic matrix-forming minerals are presented in Table II. The most disappointing result is the low susceptibility of pure calcite.

Calcite and calcareous rocks are important in geomechanical analysis because the mineral is amenable to petrofabric analysis and it is useful in experimental work because it deforms relatively easily (Owens and Rutter, 1978; Friedman et al., 1981). Using a chemically pure calcite powder (Fisher Chemical Corporation), we were able to fix a diamagnetic value of about -13.8×10^{-6} SI units/cm^3. While we are unable to determine the anisotropy at this level, Voigt and Kinoshita (1907) reported a moderate anisotropy from 12 measurements on two small (0.036 cm^3) specimens of single crystals. They reported two principal values for this uniaxial mineral of:

$$-13.83(\pm \text{s.d. } 0.004) \text{ and } -12.39(\pm \text{s.d. } 0.010)$$

In various studies of four marbles, a chalk rock and natural vein calcite, we have recorded larger susceptibilities. In some cases we have been able to detect reproducible anisotropies even with the SI-1 meter using samples of 11 cm^3. However, in all these instances we have been able to confirm the presence of natural impurities upon subsequently destroying the samples. For example, one marble, from Vermont, when dissolved yielded an insoluble residue of 2% weight chlorite and 2% weight muscovite. We believe that such impurities may override the magnetic anisotropy of the calcite's tectonic fabric.

4. Discussion

It is well known that small amounts of magnetite or other iron oxides can cause most of the susceptibility of many rocks including metamorphic rocks. Indeed in some rocks, especially ig-

TABLE II

Weakly susceptible minerals. Mean susceptibilities in units of 10^{-6} SI units per cm^3

	Mean susceptibility	Standard deviation	Number of measurements	Sample size(g)	Specific gravity
Plagioclase (Oligoclase)	−2.78	0.34	10	212.5	2.650
Quartz	−9.29	1.26	20	166.1	2.654
Calcite	−13.8	0.34	30	83.6	2.715
Talc	+5.36	0.82	20	162.1	2.750

neous ones, there is even a correlation between the volume of magnetite and the mean susceptibility of the rock (Balsey and Buddington, 1958). Nevertheless in most metamorphic rocks iron oxides are present only in traces as accessory minerals or can also be absent. Although small amounts of magnetite considerably raise the mean susceptibility, paramagnetic and diamagnetic silicates form the bulk of most metamorphic rocks. While their mean susceptibilities are low (see Tables I and II) the anisotropies of many common paramagnetic silicates are high (Figs. 1 and 2) and since they can form a major portion of the rock they may dominate the anisotropy of magnetic susceptibility in some instances (e.g., Borradaile et al., 1986). This is possible in most mature meta-sedimentary rocks such as pelitic slates, schists and phyllites where micas dominate the susceptibility fabric. Similarly, amphiboles and chlorite may control the anisotropy of many greenschists, amphibolites and blueschists. The minerals whose anisotropies are tabulated represent the common, natural examples of metamorphic minerals that are expected to have moderately high susceptibilities on the basis of known compositions.

The potential for the contribution of moderately susceptible paramagnetic silicates to rock anisotropy is reviewed in Fig. 2. The anisotropies for our minerals are compared with determinations for a variety of metamorphic rocks by the Czechoslavakian group (Hrouda, 1982, fig. 17). This graph shows that the anisotropies of such minerals are much higher than that of most metamorphic rocks so that it may be inferred that these silicates can dominate the *anisotropy* of susceptibility, even if minor traces of magnetite are present. Furthermore, we should consider the relative degrees of preferred crystallographic orientation of the silicates versus the preferred dimensional orientation of magnetite in metamorphic rocks since these are the factors that influence susceptibility anisotropy (Owens and Bamford, 1976). The preferred dimensional orientation of magnetite is normally low, so that the mineral's magnetic fabric anisotropy will rarely be appreciated to its fullest extent. In contrast, the preferred orientation of the lattices of the silicates illustrated in Table I and Figs. 1 and 2 is normally extremely high. This is because metamorphic processes are very effective in producing a near-saturation alignment of such crystal lattices. Thus the magnetic anisotropies of these silicates, *underestimated* in Figs. 1 and 2, will be appreciated to their fullest extent in the overall magnetic fabric of the rock.

Acknowledgements

G. Borradaile thanks N.S.E.R.C. for the support through grant A6861 and W. Keeler for support through grant A6710. We thank Dr. Mike Stupavsky (Sapphire Instruments, P.O. Box 385, Ruthven, Ontario) and Dr. Don Tarling, Newcastle, U.K., for much advice and technical support over the years. We thank two anonymous referees for very helpful reviews.

References

Balsey, J.R. and Buddington, A.F., 1958. Iron–titanium oxide minerals, and aero-magnetic anomalies of the Adirondack area, New York. Econ. Geol., 53: 777–805.

Borradaile, G.J., Mothersill, J.S., Tarling, D. and Alford, C.A., 1986. Sources of magnetic susceptibility in a slate. Earth Planet. Sci. Lett., 76: 336–340.

Friedman, M. and Higgs, N.G., 1981. Calcite fabrics in experimental shear-zones. In: N.L. Carter et al. (Editors), Mechanical Behaviour of Crustal Rocks. Geophysical Monograph, 24, pp. 11–27.

Hrouda, F., 1982. Magnetic anisotropy of rocks and its application in geology and geophysics. Geophys. Surv., 5: 37–82.

Hrouda, F. 1986. The effect of quartz magnetic anisotropy of quartzite. Studia Geophys. Geod., 30: 39–45.

Owens, W.H. and Bamford, D., 1976. Magnetic, seismic and other anisotropic properties of rock fabrics. Philos. Trans. R. Soc. London, A283: 55–68.

Owens, W.H. and Rutter, E.H., 1978. The development of magnetic susceptibility anisotropy through crystallographic preferred orientation in a calcite rock. Phys. Earth Planet. Inter., 16: 215–222.

Stupavsky, M., 1983. SI-1 Magnetic Susceptibility Instrument Handbook. Sapphire Instruments, P.O. Box 385, Ruthven, Ont., Canada, 92 pp.

Tarling, D., 1983. Paleomagnetism. Chapman and Hall, London and New York, 379 pp.

Voigt, W. and Kinoshita, S., 1907. Bestimmung absoluter Werte von Magnetisierungszahlen, insbesondere fur Kristalle. Ann. Phys., 24: 492–514.

Weast, R.C. and Astle, M.J. (Editors), 1978. CRC Handbook of Chemistry and Physics. CRC Press Inc., Palm Beach, FL, 59th ed.